AD NUMBER
ADB003396
LIMITATION CHANGES

TO:

Approved for public release; distribution is unlimited.

FROM:

Distribution authorized to U.S. Gov't. agencies only; Test and Evaluation; OCT 1973. Other requests shall be referred to Air Force Aero Propulsion Lab., Wright-Patterson AFB, OH 45433.

AUTHORITY

AFAPL per DTIC form 55

AFAPL-TR-73-100

SHORT PULSE SWITCH FOR AIRBORNE HIGH POWER SUPPLIED

WESTINGHOUSE ELECTRIC CORPORATION

OCTOBER 1973

DD
APR 28 1975

TECHNICAL REPORT AFAPL—TR—73—100

FINAL REPORT FOR PERIOD JUNE 1972 — FEBRUARY 1973

AIR FORCE AERO PROPULSION LABORATORY
AIR FORCE SYSTEMS COMMAND
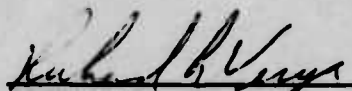WRIGHT—PATTERSON AIR FORCE BASE, OHIO 45433

NOTICE

When Government drawings, specifications, or other data are used for any purpose other than in connection with a definitely related Government procurement operation, the United States Government thereby incurs no responsibility nor any obligation whatsoever; and the fact that the government may have formulated, furnished, or in any way supplied the said drawings, specifications, or other data, is not to be regarded by implication or otherwise as in any manner licensing the holder or any other person or corporation, or conveying any rights or permission to manufacture, use, or sell any patented invention that may in any way be related thereto.
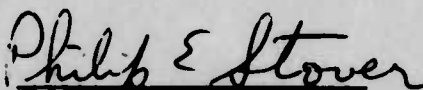
This report contains the results of an effort to develop a switch to be used with the inductive energy storage and which will conduct 20,000 amperes and hold off 100,000 volts after opening. The work was performed in the Aerospace Power Division of the Air Force Aero-Propulsion Laboratory, Air Force Systems Command, Wright-Patterson AFB, Ohio under Project 3145, Task 314532, and Work Unit 31453210. The effort was conducted by Mr. Richard L. Verga (AFAPL/POD-1) during the period June 1972 through February 1973.

Distribution Limited to U.S. Government Agencies only; Test and Evaluation; October 1973. Other requests for this document must be referred to AF Aero-Propulsion Laboratory (AFAPL/POD-1) WPAFB OH 45433.

This technical report has been reviewed and is approved for publication.

RICHARD L. VERGA
Project Engineer

FOR THE COMMANDER

PHILIP E. STOVER
Chief
Power Distribution Branch

REPORT DOCUMENTATION PAGE		READ INSTRUCTIONS BEFORE COMPLETING FORM
1. REPORT NUMBER AFAPL-TR-73-100	2. GOVT ACCESSION NO.	3. RECIPIENT'S CATALOG NUMBER
4. TITLE (and Subtitle) Short Pulse Switches for Airborne High Power Supplies		5. TYPE OF REPORT & PERIOD COVERED Final Report Jun 1972 - Feb 1973
		6. PERFORMING ORG. REPORT NUMBER
7. AUTHOR(s) D. Mergerian		8. CONTRACT OR GRANT NUMBER(s) F33615-72-C-2099
9. PERFORMING ORGANIZATION NAME AND ADDRESS Westinghouse Electric Corporation Baltimore, Maryland 21203		10. PROGRAM ELEMENT, PROJECT, TASK AREA & WORK UNIT NUMBERS Project 3145, Task 314532 Work Unit 31453210
11. CONTROLLING OFFICE NAME AND ADDRESS AF Aero-Propulsion Laboratory Wright-Patterson AFB OH 45433		12. REPORT DATE Oct 1973
		13. NUMBER OF PAGES 259
14. MONITORING AGENCY NAME & ADDRESS(if different from Controlling Office)		15. SECURITY CLASS. (of this report) UNCLASSIFIED
		15a. DECLASSIFICATION DOWNGRADING SCHEDULE

16. DISTRIBUTION STATEMENT (of this Report)

Distribution limited to U.S. Government Agencies only; Test and Evaluation; Oct 1973. Other requests for this document must be referred to Air Force Aero-Propulsion Laboratory (AFAPL/POD-1), Wright-Patterson AFB OH 45433.

17. DISTRIBUTION STATEMENT (of the abstract entered in Block 20, if different from Report)

18. SUPPLEMENTARY NOTES

19. KEY WORDS (Continue on reverse side if necessary and identify by block number)

20. ABSTRACT (Continue on reverse side if necessary and identify by block number)

A switch is designed which is capable of conducting 20,000 amperes and of holding off 100,000 volts after opening. This switch is to be employed in switching the energy from a 1 Mjoule superconducting coil. The switch element is a vacuum interrupter which is driven by a hydraulic actuation mechanism which can open ten pounds of contacts through a distance of 0.5 inch in 2 msec. Upon separation of the contacts, a 20,000 ampere arc is formed which must be extinguished by a commutation circuit. The commutation circuit consists of a pulse forming network which produces a 20,000 ampere bucking current which is

DD FORM 1473 EDITION OF 1 NOV 65 IS OBSOLETE

applied for 2 microseconds. This 2 microsecond pulse continues to supply current
to the energy storage coil once the vacuum interrupter arc has been extinguished,
thus, acting to delay the rise of voltage generated by the coil and to permit the
interrupter to partially recover its voltage stand-off capability. The use of a
specific contact material and contact geometry to insure against the formation of
anode hot spots and to permit a useful lifetime in excess of 50,000 cycles is
described. The entire switch system including the vacuum interrupter, the
hydraulic actuation mechanism and the commutator circuit has a total weight of
115 pounds.

Table of Contents

List of Illustrations

vi

1. INTRODUCTION AND SUMMARY

This report summarizes the work performed during the initial phase of a two-phase program to design, build, and test a Short Pulse Switch for Airborne High Power Supplies. This program was performed by the Systems Development Division of the Westinghouse Electric Corporation for the United States Air Force Systems Command, Air Force Aero Propulsion Laboratory, Wright Patterson Air Force Base under contract number F33615-72-C-2099 over a period extending from June 1, 1972 to February 28, 1973.

The primary goal of the first phase program was the design of a switch for subsequent fabrication and testing during the second phase of the program. In addition to the primary design effort, the program included experimental testing, theoretical analyses, and computer simulations which would both validate the design and generate data required in formulation of the design.

The program was broken down into three specific areas which were of prime significance in meeting the design goals set forth in the statement of work. These areas are:

- Vacuum Interrupter Technology
- Commutator Circuit Analysis
- Actuation Mechanism Studies

Under the first of these areas, Westinghouse relied heavily upon its long proven expertise and experience in vacuum switch design and fabrication. This experience was utilized in carrying out a detailed experimental

1

study program to yield the data required to establish the design parameters. Included in this series of tests were:

- Voltage Recovery Measurements
- Anode Spot Formation Studies
- Contact Erosion Measurements
- Contact Resistance Measurements

The results derived from these studies were incorporated into a comprehensive theoretical analysis of the transient thermal behavior of the vacuum interrupter contacts under repetitive arcing conditions corresponding to 60 seconds of operation at maximum current of 20,000 amperes at a 5 pulse/sec repetition rate without external cooling. The data were also analyzed to determine the expected voltage recovery rate of the vacuum interrupter which will be fabricated during Phase II. On the basis of these figures, the Phase I design utilizes only a 2_μsec current zero condition before the switch is asked to hold off the voltage generated by the storage coil. In addition, the coil can be allowed to rise in voltage at some rate between 5 and 10 kV/μsec. These very rapid recovery rates and voltage rise times allow a commutator circuit to be supplied without a significant weight penalty and, at the same time, reduce the capacitance which the storage coil itself must have in parallel with it to reduce the voltage rise time.

In order to achieve the required 50,000 cycle lifetime of the device, it was necessary to totally design out the possibility of forming an anode hot spot. Such hot spots, if allowed to form on the anode of a vacuum interrupter, result in rapid erosion of the anode surface and would radically limit the lifetime of the contacts. The Phase I design was established so as to eliminate the formation of such spots, and this is substantiated by the

2

experimental investigations of anode spot formation rates as well as by the transient thermal analysis which indicates a large margin of safety between the maximum temperature the anode will attain and the temperature at which hot spots have been observed to be initiated.

A commutator circuit has been designed which extinguishes the arc and provides 2 μsec of zero current during which time the switch begins to recover. In addition, a hydraulic actuation mechanism has been designed which opens and closes the switch contacts. Computer simulations have been performed on both of these components to insure that they will perform as required in the proposed application.

In summary, the Phase I design developed by Westinghouse is shown, in the body of this report, to be capable of meeting or surpassing each of the design goals set forth in the statement of work. The overall system weight including the commutation circuitry is shown to be only 115 pounds. The Phase II effort will be involved with the fabrication of the device and its testing. This Phase II testing effort will be of the utmost importance, since it will constitute the first such testing of a DC vacuum interrupter at these current and voltage values, and will be necessary to validate any extrapolations made on the basis of tests performed on smaller devices at lower current and voltage levels.

Section 2 of this report describes the design approach utilized during the Phase I program while Section 3 gives a detailed technical discussion which brings forth the reasoning behind this design approach and stresses the soundness of the design.

There are also three appendices which present the detailed

3

theoretical analyses of the transient thermal study, the commutator design, and the hydraulic actuation system.

2. WESTINGHOUSE APPROACH TO SHORT PULSE SWITCH DESIGN

The Short Pulse Switch for Airborne High Power Supplies Program has as its goal the design and development of a switch capable of conducting 20,000 amperes, withstanding 100,000 volts within 40 microseconds of opening, and operating at a repetition rate of five pulses per second with flexibility to allow operation at somewhat higher repetition rates at correspondingly lower current levels. The switch must be small and lightweight and must operate reliably for 50,000 cycles. All of these design goals can be met utilizing the vacuum interrupter, actuator, and commutator designed by Westinghouse during Phase I of this program.

2.1 BASIC DESIGN PHILOSOPHY

Westinghouse has relied heavily upon its long experience in the design, development, and manufacture of vacuum interrupters in arriving at a design which fulfills the above stated requirements. In addition, existing commercially available vacuum interrupter components have been utilized both to take advantage of their proven reliability and to significantly reduce development and future manufacturing costs. Where necessary, modifications have been made to these components in order to upgrade vacuum interrupter technology to the point that the above goals can be satisfied.

In order to insure 50,000 cycle operation, it is necessary that the formation of an anode hot spot must be avoided, since this leads to catastrophic erosion of the anode. As a result, the vacuum interrupter contacts

5

were designed with a four-inch diameter flat contact area and the contact separation was held to only 0.5 inch. These figures are well below the anode spot formation thresholds at 20,000 amperes. In fact, the estimated current required to initiate an anode hot spot in contacts of this geometry is in excess of 25,000 amperes. The contact material is CLR, chosen on the basis of its superior erosion resistance characteristics and voltage recovery characteristics. CLR is a Westinghouse proprietary material utilized in our current vacuum interrupter product line.

In order to insure highly reliable lightweight actuation of the switch contacts, a hydraulic actuation mechanism has been designed which weighs only 15 pounds and which can operate at either 5 or 20 pulses per second. This mechanism can be built to operate at repetition rates as high as 50 pulses per second with only minor modifications.

Finally, by suitable selection of contact material, diameter and separation, combined with current Westinghouse vacuum interrupter technology, a vacuum interrupter with extremely rapid voltage recovery characteristics, well in excess of 2,500 volts per microsecond, can be fabricated. As a result of these recovery measurements, the interrupter is capable of withstanding the 100,000 volt maximum potential in well under the 40 microseconds set as a design goal for this program, and may be capable of achieving this standoff voltage in less than 20 microseconds. Since a long voltage buildup time reduces the overall efficiency of the energy storage coil and further implies a significant weight penalty in the form of capacitance required across the coil to limit the rate of voltage rise, reducing this time is of the utmost importance. The voltage recovery tests have indicated that it is possible to reduce the commutation time to two microseconds or less, implying a further

6

significant decrease in capacitive storage in the commutator. The Westinghouse design requires 0.4 μF of capacitance in the commutator circuit to supply the 2 μsec commutation time. This capacitance operates at one polarity during commutation and at the opposite polarity during the voltage buildup from the storage coil. This capacitance value is, therefore, utilized twice per cycle, since it both stores the commutation energy and also acts to limit the rate of voltage buildup from the coil. In fact, utilizing a 0.4 μF capacitor weighing 40 pounds in the commutator network allows the coil manufacturer to utilize 80 pounds less capacitance across the coil, in limiting this voltage risetime. This permits the utilization of a commutator circuit which will weigh less than 75 pounds, and combined with the 15 pound hydraulic mechanism and 25 pound vacuum interrupter, will yield a total switching system weight of less than 115 pounds.

All of the modifications outlined above will be incorporated into an existing Westinghouse vacuum interrupter bottle, and will be coupled with an existing high speed bellows, developed by the Metal Bellows Corporation for Ontario Hydroelectric, Ltd. of Canada, to provide a switch unit capable of meeting or surpassing all of the design goals of the present program. Figure 1. shows a schematic illustration of the vacuum interrupter system Westinghouse has developed during the Phase I effort.

2.2 TESTING PERFORMED TO ESTABLISH FEASIBILITY OF DESIGN CONCEPT

In order to establish confidence in the overall switch designed during Phase I, as well as to generate data required to formulate this design, a comprehensive program of experimental testing coupled with theoretical analyses and computer simulations has been conducted. The experimental effort

HYDRAULIC ACTUATOR

PILOT STAGE

POWER STAGE

METAL BELLOWS &
GUIDE BUSHINGS

CERAMIC BOTTLE

MOVING CONTACT

STATIONARY CONTACT

4.50

6.00

1.50 DIA

3.50 DIA
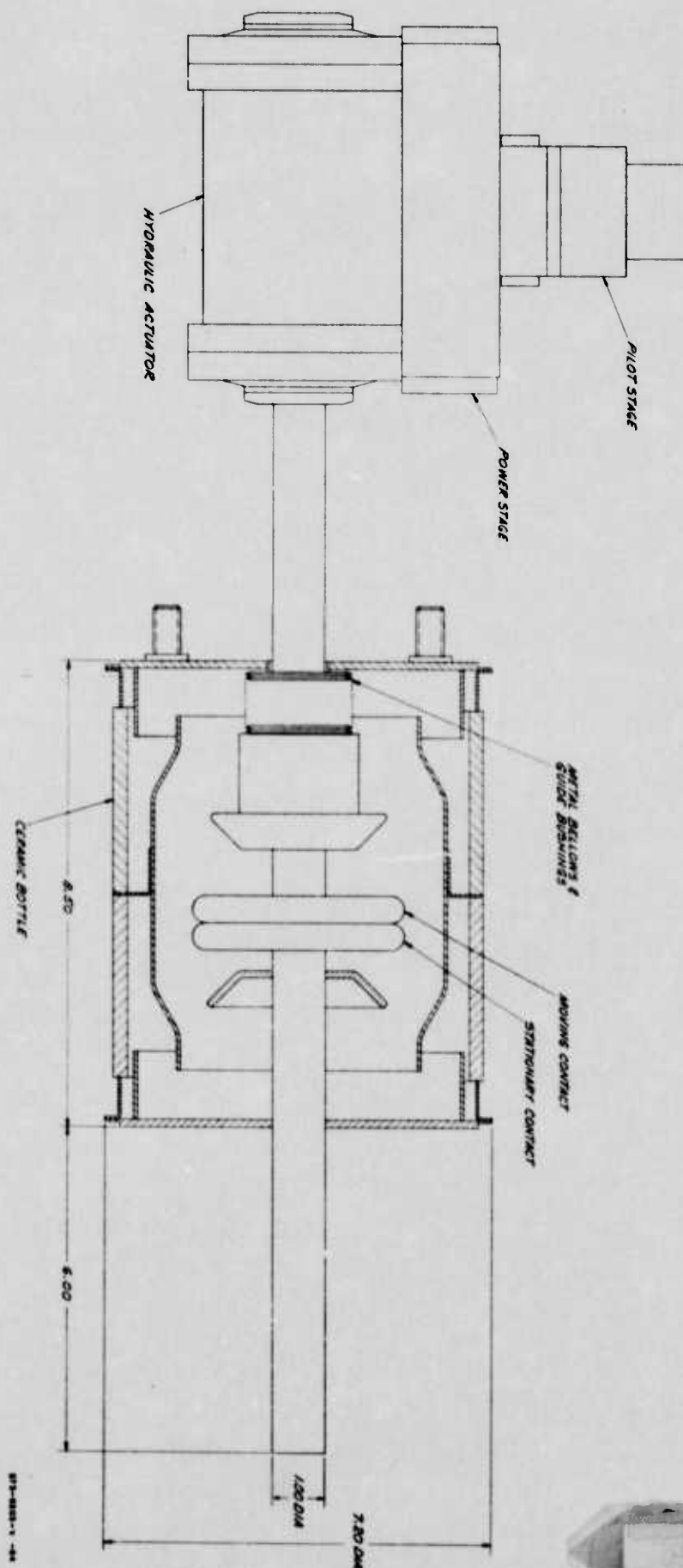
Figure 1. Conceptual Drawing of Short Pulse Switch

9

has been devoted to a comprehensive study of contact materials. The anode spot formation tendencies of vacuum interrupter contact materials, their erosion characteristics, their contact resistance as a function of various parameters such as temperature, current, and the force applied in holding the contacts together, have been covered in the experimental studies. In addition, measurements have been made on the voltage recovery of CLR contacts in small vacuum interrupters. The experimental results indicate that the voltage recovery rate of the interrupter should exceed 5 kV/μsec, that operation with an arc duration of 2 μsec should cause no anode spot formation, and that gross electrode erosion through 50,000 cycles of operation should amount to only about 1 millimeter. The theoretical analyses and computer simulations have been carried out to obtain the transient thermal behavior of the contacts during repetitive switching cycles, the dynamics of the hydraulic actuation mechanism, and the electrical characteristics of the commutating circuit required to extinguish the 20,000 ampere arc formed when the contacts are first opened. The thermal analysis indicates that the maximum temperature attained by any portion of the switch occurs at the outer edge of the front surface of the anode. With a pessimistically high arc voltage of 40 V, the instantaneous value of this temperature is only 900°K after the 300th arc when operating at 20,000 amperes and a 5 pulse/sec repetition rate. This temperature is well below the 1356°K melting point of copper, the lowest melting constituent of CLR, and insures the anode spot free performance of the contacts without the use of cooling. Detailed discussions of both these experimental tests and the theoretical analyses and computer simulations are presented in Section 3 and in Appendices A, B, and C.

Briefly, the most significant results obtained by the experimental

11

and theoretical analyses that were carried out during the vacuum interrupter switch design are as follows:

- The vacuum interrupter switch is capable of withstanding a voltage buildup of well over 2.5 kV/usec after arc extinction,

- The anode and cathode plate dimensions and maximum separation distance are such that anode spot formation will not occur,

- External cooling of the switch is not required, since the maximum temperatures reached by the components after 300 cycles are substantially below critical values.

2.3 RESULTS OF DESIGN STUDY

As a result of the Phase I design effort coupled with the experimental and theoretical studies mentioned above, Westinghouse has designed a short pulse switch with the following characteristics:

- 20,000 ampere current capability

- 100,000 volt hold-off

- 60 seconds of operation at 20,000 amperes and 5 pulse/sec repetition rate

- operation without external cooling

- capable of operation at repetition rates up to 50 pulses/sec at correspondingly lower current levels

- switch mechanism (less commutator) weight of 40 pounds—compared to 70 pound goal of contract

- total switch system weight of 115 pounds

- 40 pound commutator capacitance is also used to save 80 pounds of capacitance across the storage coil.

12

3. TECHINCAL DISCUSSION

The results of the techni cal effort during Phase I of the Short Pulse
Switch Program, which were summarized briefly in the preceding Section, are
presented in detail in this Section. Successful arrival at a design for a
switch system capable of meeting all of the requirements specified in the State-
ment of Work reouired that concurrent design efforts be conducted in each of
three major sub-system areas:

     (1) The Switching Element

     (2) The Commutation Network

     (3) The Switch Actuation Mechanism

In each case, an in-depth analysis has been carried out to determine the crit-
ical constraints which the system requirements place on that sub-system and to
identify the approach most likely to offer successful satisfaction of these
constraints at a minimum cost in overall system weight and with sufficiently
high reliability to allow the system to operate without failure for the required
lifetime of ≥ 50,000 operations at maximum loading. The design of the switching
element, a vacuum interrupter (VI), was supported wherever possible by detailed
experimental studies. In all cases where experimental verification of predicted
sub-system performance was not feasible during Phase I, computer simulations
were utilized to establish design confidence.

The sub-system design studies are presented in the following paragraphs.
Section 3.1 gives the results of the VI design effort. The commutator network
design analysis and its results are given in Section 3.2. The actuation analysis
which resulted in the design of a hydraulic actuator system, is presented in
Section 3.3.

13

3.1 VACUUM INTERRUPTER DESIGN

The switching element for the Short Pulse Switch must satisfy the following requirements:

- A current carrying capability in the closed position in excess of 20,000 A.
- A voltage standoff capability in excess of 100 kV in the open position.
- A recovery time from initial current zero to full voltage stand-off capability of less than 40 µsec.
- An energy loss per cycle of less than 5000 J.
- A capability of operating at a frequency of at least 5 pulses per second under maximum loading for 60 seconds.
- An accumulated lifetime capability of at least 50,000 full cycles of operation.
- A total weight, including the weight of the switch actuation mechanism, of less than 70 pounds.
- Airborne operation capability at altitudes of 50,000 feet or more.

In its proposal to conduct this program, Westinghouse showed that a VI is the switching element which holds the greatest promise of being developed to the point where it meets these requirements. In particular, Westinghouse proposed to base its design around the WL 23231 interrupter, the most reliable high current, high voltage VI on the commercial market, and suggested several design modifications to upgrade the performance capabilities of the WL 23231. These modifications and their intended purpose include:

(1) The use of 4-inch diameter by 1-inch thick, flat-faced electrodes in place of the rather complicated electrode geometry employed

14

in the commercial AC device. The larger electrodes should
withstand the effects of the repeated 20,000 A arcs with a
minimum of erosion, thereby promoting a longer life expectancy.

(2) An increase in the outer diameter of the electrode stems to
$1\frac{1}{2}$-inch and in the stem protrusion from the bottle to 6 inches
The extended length was proposed for the purposes of allowing
greater external sleeve contact surface area to minimize contact
heat generation and of providing space for incorporation of
coolant flow inlet and outlet lines.

(3) Incorporation of cooling channels through the electrode stems
and into the electrode plates in order to allow a circulating
coolant to carry away the heat generated in the high current arcs.

(4) Utilization of an actuation mechanism which fully opens the
VI in 2 m sec rather than the 8 to 10 msec required in commer-
cially available VI's. This modification, which is also
dictated by the specified charge-discharge times for the system,
should significantly decrease the arc heating and erosion of
the electrodes, but it also greatly increases the transient
g-forces imposed upon the bellows and could require an improved
bellows design.

In addition, the possibility of replacing the electrode material. CLR, utilized
in Westinghouse AC VI's was left open on the theory that. although CLR is
clearly the best AC VI material available today, other materials might display
superior performance in a DC interrupter.

The principal thrust of the Phase I VI design effort has consisted
of theoretical analyses supported by experimental tests on small VI's to

substantiate that these design modifications will result in a VI which satisfies the requirements of the program. It has been concluded from these studies that all of the performance requirements can be met through incorporation of these proposed modifications and that, indeed, the cooling system will not be necessary to successful operation of the switch for 300 cycles under maximum loading. In addition, it has been concluded that the stem diameter can be decreased to 1 inch without causing thermal runaway problems. This decrease in the diameter of the stem on the movable electrode will allow utilization of an already existing bellows which is expected to be capable of 50,000 cycles of operation without rupture. The stem diameter on the other electrode can also be decreased in order to effect a decrease in system weight. The performance features expected of the VI designed during Phase I include:

- Voltage standoff capability well in excess of 100 kV.

- Recovery after extinction of a 20,000 A arc to 100 kV in less than 40 μsec and possibly less than 20 μsec.

- Energy loss of ~ 2 kJ per cycle at full loading including 2msec of switch-opening arc at 20,000 A.

- Overall contact erosion depth of only 1mm after 50,000 operations, a depth well under the 6.35 mm allowed for in the bellows design and the actuator design.

- Switch weight of 25 pounds for the VI and 40 pounds for the VI and its hydraulic actuator.

The design analyses and verification leading to these expectations are summarized in the paragraphs which follow. Section 3.1.1 presents the results of contact material investigations which led to the choice of CLR

16

as the material to be used in both electrodes and to verification that the VI will not be subject to the destructive erosion associated with the formation of anode hot spots. The voltage recovery test results and supporting analysis are given in Section 3.1.2. The thermal analysis is discussed in Section 3.1.3, VI lifetime considerations are covered in Section 3.1.4, and Section 3.1.5 presents a treatment of the bellows to be utilized in the VI.

3.1.1   Electrode Material Investigations

The arc which burns in a VI when a circuit is broken under voltage load is actually a low pressure metal vapor arc. The initial vapor is provided by the explosion of the electrode material in the tiny areas last remaining in contact before the electrodes separate completely. As this vapor is lost to condensation on the electrodes and to escape from the interelectrode space, it must be replenished in order that a space charge neutralized plasma be maintained. As long as the interelectrode spacing is not too great, this replenishment is provided by evaporation at local hot spots on the cathode and the arc therefore burns at a voltage and system pressure which are characteristic of the cathode material. The evaporation of metal from the hot spots causes erosion of the cathode, but these spots move more or less randomly across the cathode face causing a smooth, gradual overall erosion. The rate at which erosion occurs for various cathode materials has been studied by numerous workers and seen to be a constant for each material. In particular, Rondeel[*] has shown that CLR exhibits one of the lowest erosion rates of materials which are

---

[*] W. G. J. Rondeel, "Electrode Erosion and Energy Balance of a Metal Vapor Arc", Thesis, Norwegian Institute of Technology, Trondheim (1971).

17

known to give stable arcing conditions, a value corresponding to 30 μgram loss per coulomb of arc current or approximately 1 atom for each 20 arc electrons. Because of this and its low arc voltage ($\sim$ 20 V - see below), the decision was made to stay with CLR as the cathode material.

Gradual cathode erosion does little to limit the life of a VI. The key to extended lifetime is the prevention of anode erosion because of the manner in which anode erosion occurs. Although the anode is heated strongly by the arc current at all times, little or no erosion takes place until an anode hot spot forms. When this happens, the arc energy is non-uniformly deposited into this hot spot, and this causes gross melting and excessive erosion in the area of the hot spot.

The sequence of events in anode spot formation (ASF) has been studied by Kimblin[*] by means of high speed motion pictures of the arcing electrodes. Kimblin observed that as long as the electrode separation is small (actually less than about half the anode diameter), the vapor released by the cathode is sufficient to fill the interelectrode space uniformly and to maintain a low arc voltage. As the separation increases, more vapor escapes from this space and, at some critical spacing for any given arc current, a depletion layer forms in front of the anode face. This results in a sudden increase of the arc voltage (often to more than 100 V) and much more rapid heating of the anode. The incrased rate of heating continues until an area on the face becomes sufficiently hot to start producing vapor which, in turn, destroys the depletion layer above this area. This provides the arc with a

[*] C. W. Kimblin, "Anode Voltage Drop and Anode Spot Formation in DC Vacuum Arcs", Journal Applied Physics, Vol. 40, (1969) p. 1744.

lower voltage path to this area, and the arc constricts until all of the current is delivered to this area. Once this happens, the arc remains constricted until it is extinguished and gross melting and splattering of this area occurs especially if the arc is maintained for any appreciable duration.

The proposed electrode spacing to diameter ratio of 1/8 should provide a high safety margin for prevention of ASF, and further margin should be provided by the arcing time of only 2 msec. Nevertheless, the possibility of further militating against ASF by the use of a different anode material was investigated. Rich, et al.[*] studied the propensity of materials to form anode spots and found that this tendency can be correlated with the thermal properties of the materials. They showed that, among common materials, W has the greatest resistance to ASF. In addition to this, W has higher electrical and thermal conductivities than CLR so that the decision was made to test W as an anode material for our application.

Comparative tests were carried out at the Westinghouse Research Laboratories on small VI's equipped with 3/4-inch diameter CLR-CLR and CLR-W electrode combinations. Tests of the contact resistance between electrodes at various currents, temperatures, and contact pressures showed that the CLR-W combination consistently exhibited contact resistances lower by 1 to 3 $\mu \Omega$ than the CLR-CLR combination. The contact resistance for CLR-CLR electrodes of 1.5 inch diameter was, however, less than 4 $\mu \Omega$ at a contact pressure of 100 to 400 pounds, so that the advantage of using W for reducing contact resistance is quite small.

---

[*] J. A. Rich, L. E. Prescott, and J. D. Cobine, "Anode Phenomena in Metal Vapor Arcs at High Currents," J. Appl. Phys, Vol. 42 (1971) p. 587.

Detailed studies were performed of the ASF behavior of 3/4-inch W and CLR anodes, and of the material behavior once a spot formed, in the apparatus previously utilized by Kimblin for such studies. The experiments were carried out over the current range from 100 A to 4,000 A. with high speed motion pictures recording the time sequence of events as the anode was separated from a 1.25-inch diameter CLR cathode. The ion current to the chamber walls and the arc voltage across the electrodes were also monitored in synchronism with the movies. Two sets of runs were made for each material with

(1) manual contact separation to a spacing of about 1-inch in ~ 130 msec, and

(2) automatic opening to 0.75-inch in 30 msec.

Figure 2. shows a schematic of the experimental chamber, while Figure 3. shows the sequence of experimental events. Some of the more important results of these studies are summarized below.

The threshold current for anode spot formation on CLR at 1-inch separation was found to be 600 A and at 0.75-inch it was 800 A. As the current was increased, the separation necessary to give an anode spot decreased, as did the time. Representative data for CLR are given in Figures 4. through 6. for currents of 700 A, 1100 A, and 3000 A, respectively; the first two of these were taken with manual contact opening, while the third utilized the automatic contact separator. The figures indicate the time and spacing at which ASF occurred, the voltage during the arc, and the ion currents to the chamber walls. It can be seen that both the voltage and the ion currents show discontinuities at the time of spot formation. It is notable that, in every case, the arc current remained below 30 V until an anode

20
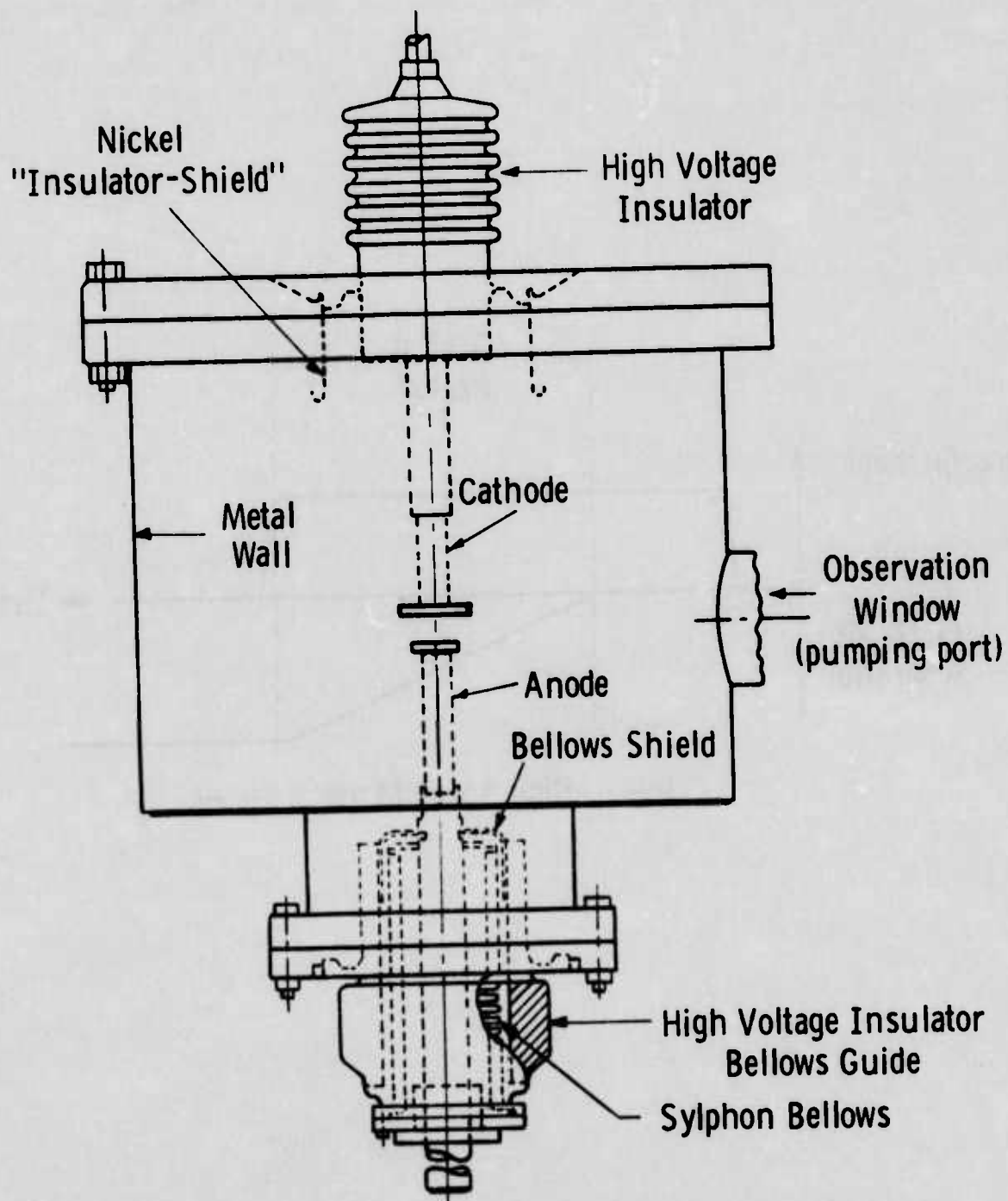
Figure 2. Experimental Metal-Walled Arc Chamber for ASF Studies.
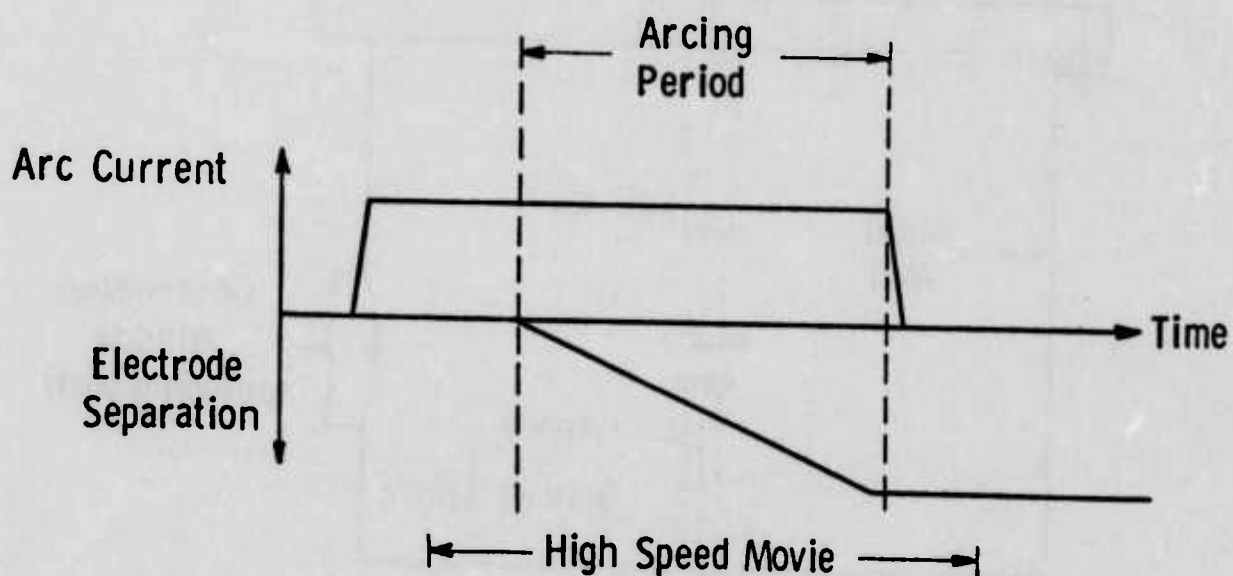
Figure 3.   Experimental Sequence and Technique for Photographing
DV Vacuum Arcs During Electrode Separation.

← Arc Voltage
Baseline

← Electrode Spacing Baseline

← Ion Current
Baseline

↑ Spot Forms

(a) 700 A
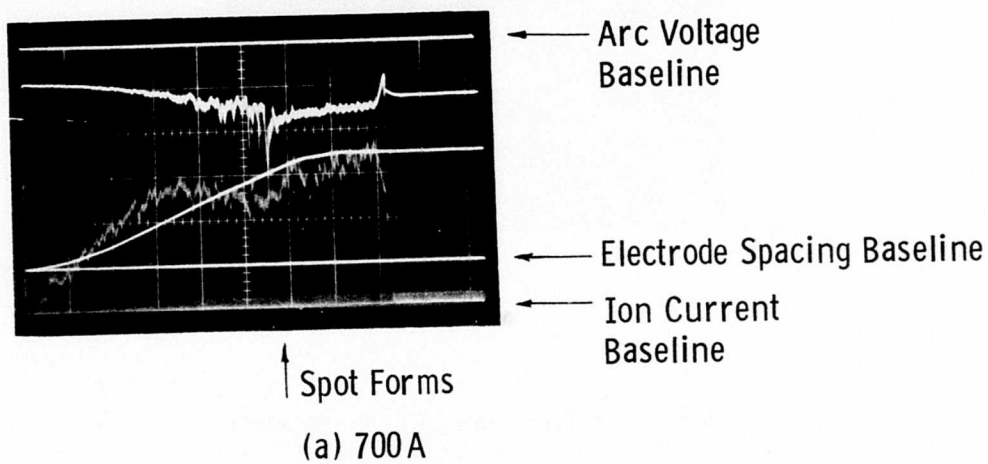
t = 20 msec/div

Upper Trace (Arc Voltage) = 20 V/div

Mid Trace (Electrode Spacing) ≅ 0.4 μi/div

Lower Trace (Ion Current) = 20 A/div

Figure 4.   Record of ASF on CLR at 700 A.

23
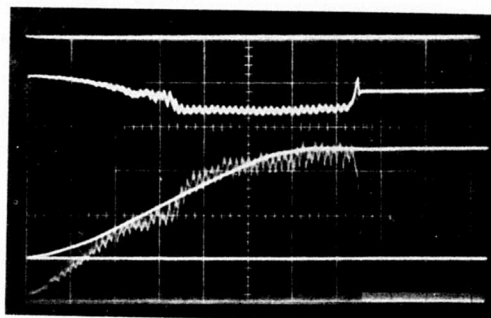
↑ Spot Forms

Lower Trace (Ion Current) = 50 A/div

Figure 5.   Record of ASF on CLR at 1100 A.
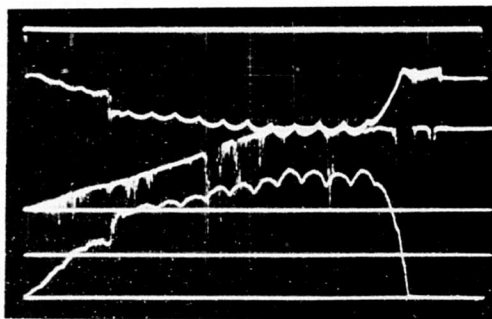
↑ Spot Forms

t = 5 msec/div

Lower Trace (Ion Current) = 200 A/div

Figure 6.   Record of ASF on CLR at 3000 A

spot formed; this is especially important in the case of the 3000 A arc where the arc current density is 4.3 times higher than for a 20,000 A arc to a 4-inch anode. Also notable is the fact that the 3000 A arc did not cause ASF until 9 msec after it began.

Figures 7. and 8. show the ion current to the chamber walls before and after ASF. These show clearly that there is a definite increase at the time of ASF in agreement with Kimblin's model which predicts rapid evaporation of material from the anode spot.

The motion pictures showed that, at the time of ASF, the CLR anode surface and adjacent plasma became highly luminous. When low current arcs were extinguished, no residual anode luminosity could be seen after the last cathode spot went dark, but when higher current arcs were employed, the anode glowed red for several tens of milliseconds.

Visual inspection after each ASF showed evidence of fresh melting of the anode surface, but the anode shape remained unchanged even after many arcs at 3000 to 4000 A. This is in marked contrast to Kimblin's earlier results for Cu where gross distortion was observed often after a single high current ASF.

The results for W showed that the 1-inch ASF threshold was 640 A, an increase of 40 A over that for CLR. At 1700 A and 1/4-inch spacing, no anode spot formed on W for times of up to 150 msec, while CLR showed intermittent ASF at these same values. Thus, W exhibits a slightly higher ASF threshold.

More important, however, is the different behavior of W when ASF occurred. Many highly luminous particles were seen to be thrown away from the anode surface, thus indicating rapid and gross erosion. It is likely

25
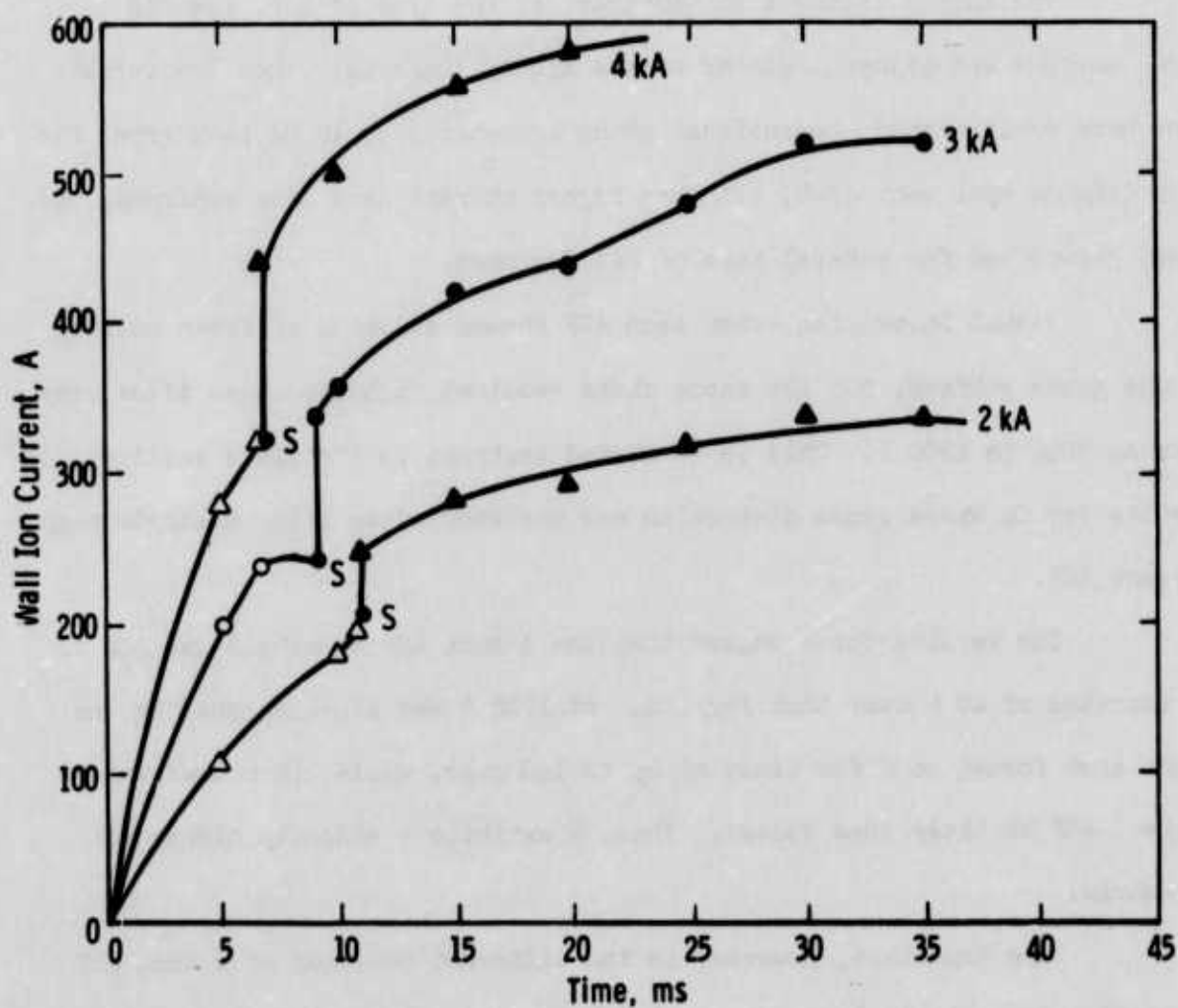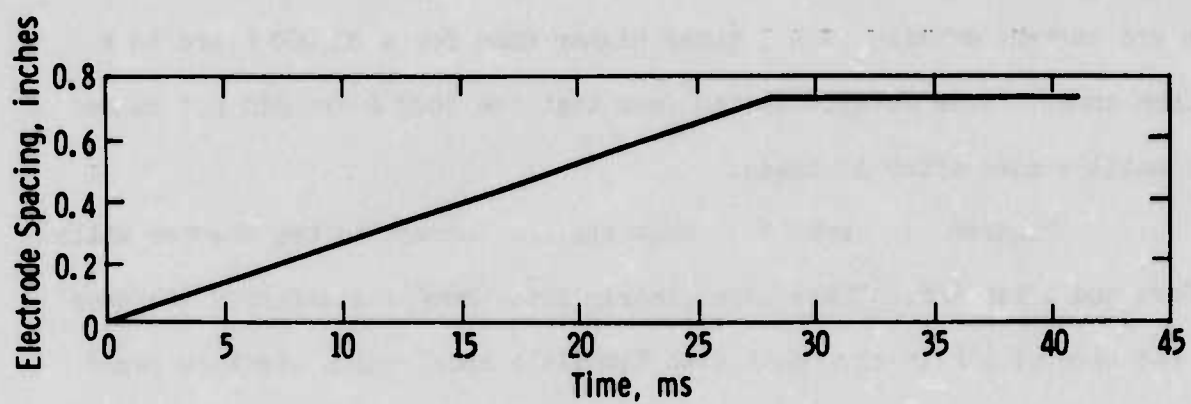
Figure 7.   Ion Current Traces for CIR at 2, 3, and 4 kA and Electrode Spacing

26
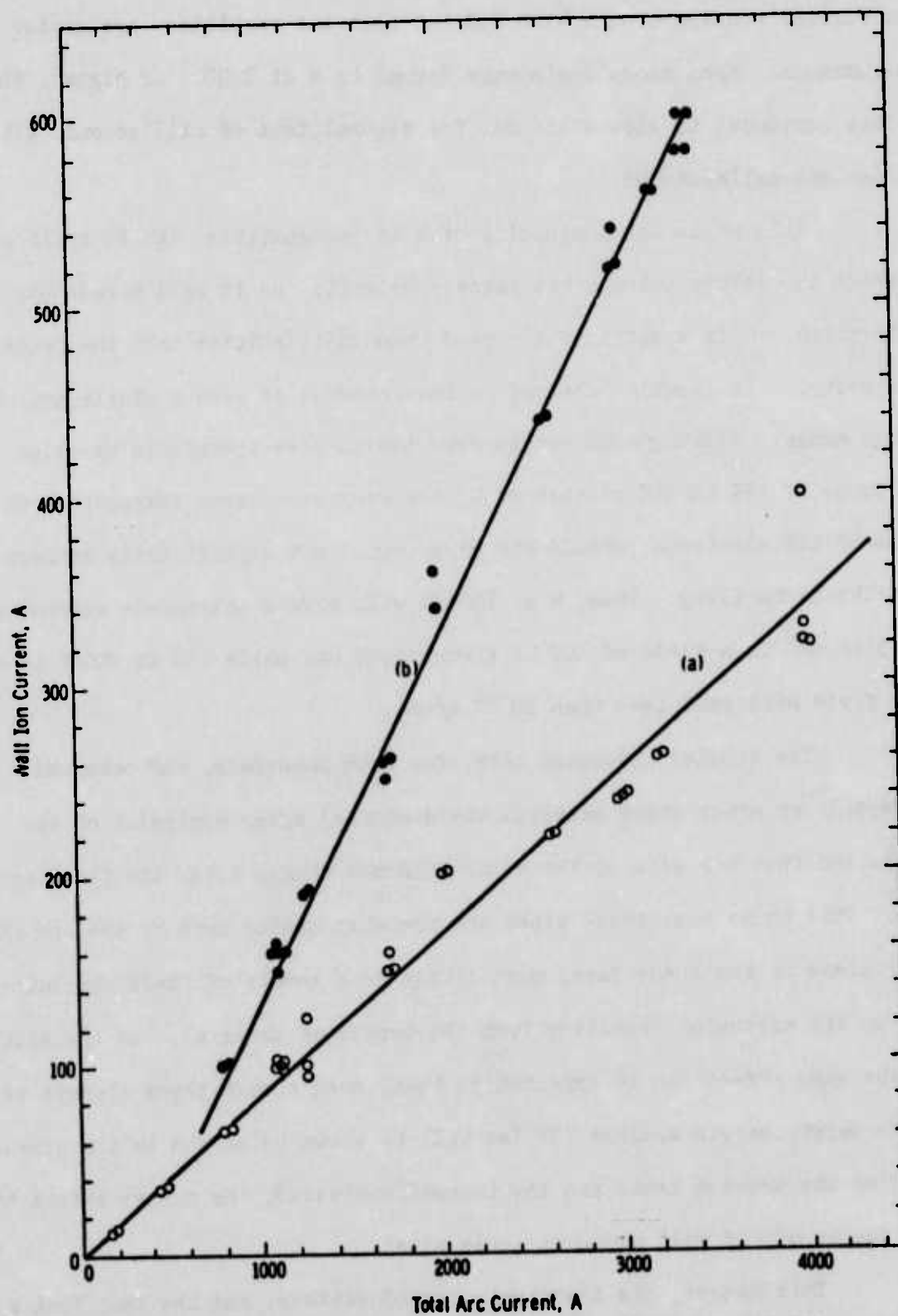
Figure 8.   Maximum Observed Ion Current for CLR (a) Prior to ASF
(Open Points) and (b) Following ASF (Solid Points).

that similar erosion occurs with CLR but that the particles are cooler and non-luminous. When anode spots were formed on W at 1700 A or higher, the surface continued to glow white hot for several tens of milliseconds after the arc was extinguished.

This white hot luminosity of W is incompatible with VI applications in which the return voltage has reverse polarity, as it will have in the expected application. W is a sufficiently good thermionic emitter that the probability of a restrike is greatly enhanced by the presence of even a single hot spot on the anode. Although CLR can be expected to give thermionic emission in the range of 15% to 20% of that of W, the very much lower temperature of the post-ASF CLR electrode, should ASF occur, will not significantly enhance the restrike probability. Thus, W at 1500°K will give a thermionic current of ~ 0.5 mA/cm^2 in a field of 100 kV across 1.27 cm, while CLR at 800°K in the same field will emit less than 10^{-14} A/cm^2.

The studies indicated that, for both materials, ASF occurred preferably at sites where material was deposited after explosion of the bridge and that the site of the bridge did not change after the first explosion. This shows that these sites are probably heated more by the arc than other areas on the anode face, most likely as a result of field concentration at the protusion resulting from the deposited material. In the actual VI, the same effect can be expected so that, even though there appears to be a wide safety margin against ASF (as will be shown below and in the discussions of the erosion tests and the thermal analysis), the danger exists that some degree of ASF will occur at these sites.

This danger, the thermionic considerations, and the fact that W is a brittle material which is difficult to work argue against the use of W

as the anode material and in favor of CLR. Such a decision is strengthened by the highly satisfactory performance of CLR in the erosion and voltage recovery tests to be discussed later.

Certain other points should be made concerning these ASF studies. The threshold of 800Å for CLR at 0.75-inch separation translates to a threshold current of 22,800 A for a 4-inch diameter electrode at the same spacing. At a spacing of only ½-inch, the threshold should be considerably higher, so that ASF should not occur no matter what the arc duration is. This same conclusion was reached by Kimblin through a comparative analysis of CLR data with Cu data of Kimblin[*] and of Rich, et al.[**] which led to a predicted threshold current of 24,500 to 32,500 A for ASF on a 4-inch CLR anode at ½-inch separation.

Referring back to Figures 3.1.3 through 3.1.5, the threshold conditions for ASF were

(1) 700 A, t = 110 msec, $\bar{V}$ arc ~ 23 V

(2) 1100 A, t = 70 msec, $\bar{V}$ arc ~ 22 V

(3) 3000 A, t = 9 msec, $\bar{V}$ arc ~ 23 V.

From these data, the surface temperatures of the anode at the time of ASF can be estimated using the formula for surface temperature of a semi-infinite slab with an energy input to the surface of F_o Joules/cm^2-sec[***]

$$T(o, t) = \frac{2 F_o}{A} \left(\frac{\alpha t}{\pi} \right)^{\frac{1}{2}} , \qquad (3.1-1)$$

---

[*] Kimblin, op cit.

[**] Rich, Prescott, and Cobine, op cit.

[***] H. S. Carslaw and J. C. Jaeger, Conduction of Heat in Solids, Second Edition, (Oxford: Clarendon Press, 1959) P. 75.

where $\hbar$ = thermal conductivity = 1.23 J/cm-°K-sec for CLR,

and α = thermal diffusivity = 0.3334 cm^{-2} sec^{-1} for CLR.

Assuming that 90% of the arc current is carried by electrons and utilizing a value of 4.5 for the work function of CLR, Eq. (3.3-1) gives values of approximately 1390°K, 1550°K, and 1600°K for the surface temperatures in the three cases. All of these temperatures are higher than the melting point of copper, the lowest melting component of CLR. Hence, it can be concluded that melting of the surface occurs prior to the formation of the anode spot and that the danger of ASF is practically nonexistent until the surface temperature approaches the melting point of the anode material.

Finally, it is worth noting again that the pre-ASF arc voltage for CLR never reached 30 V, not even at current densities 4 to 6 times higher than those expected in the VI, and were usually less than 25 V. For a value of 25 V and a work function of 4.5, the arc energy deposition into the anode face (assuming all current is carried by electrons) will be of the order of

$$E \approx 30 \times 20,000 \times 0.002 = 1200 \text{ J/cycle.}$$

Other losses include approximately 50 J/cycle into a contact resistance of 2 $\mu\Omega$ and approximately 400 J/cycle I^2R losses in the stems for a total of approximately 1650 J/cycle. Of this total, ~ 1225 J are deposited directly into the anode face.

3.1.2 Voltage Recovery

It was pointed out in the proposal that CLR is known to exhibit significantly more rapid recovery to full standoff voltage than Cu-Bi in high-current AC switches. Its recovery in DC switching had not, however, previously been determined, and it was necessary to conduct measurements of

30

the DC recovery rate during Phase I. Because rapid switching of DC currents in the range of interest to this program would require the use of a commutating circuit equivalent to that which was to be designed during Phase I, it was necessary to conduct these tests on smaller devices at lower currents and to attempt to show theoretically how these results should scale upward.

A small VI equipped with 3/4-inch butt CLR contacts was chosen for these measurements. Its voltage standoff capability at a spacing of $\frac{1}{4}$-inch between contacts was determined to be approximately 50 kV prior to the tests. The recovery experiments were carried out using equipment previously utilized in measurements of the DC recovery of high pressure SF_6 circuit breakers by Perkins and Frost[*] at the Westinghouse Research Laboratories.

The apparatus is shown schematically in Figure 9. A square wave current is produced by discharging capacitor C_1 through the inductor resistor combination $L-R_1$, the isolating switches, and the test breakers. The $L-R_1$ combination maintains the current approximately constant for about 1/2 of the unmodified discharge time constant $(R_1 + R_{ne}) C_1$, after which the current is crowbarred to zero, by diversion through SW3, in about 1 μsec. A pre-ionization current from C_2 allows the test VI and SW1 and SW2 to be fully opened before the square wave current is initiated. The C_3, R_3 combination is used to apply a recovery voltage through SW4 at any desired time, t_R, after current zero. The sequence of events is shown schematically in Figure 10.

For the tests, current of 1000 A was applied for a duration of 400 μsec and a gap spacing of 3/8-inch was utilized. This current value

---

[*] J. F. Perkins and L. S. Frost, "Dielectric Recovery and Predicted AC Performance of Blown SF_6 Arcs," IEEE Trans. Power Apparatus and Systems, PAS-91, (1972) p. 368.
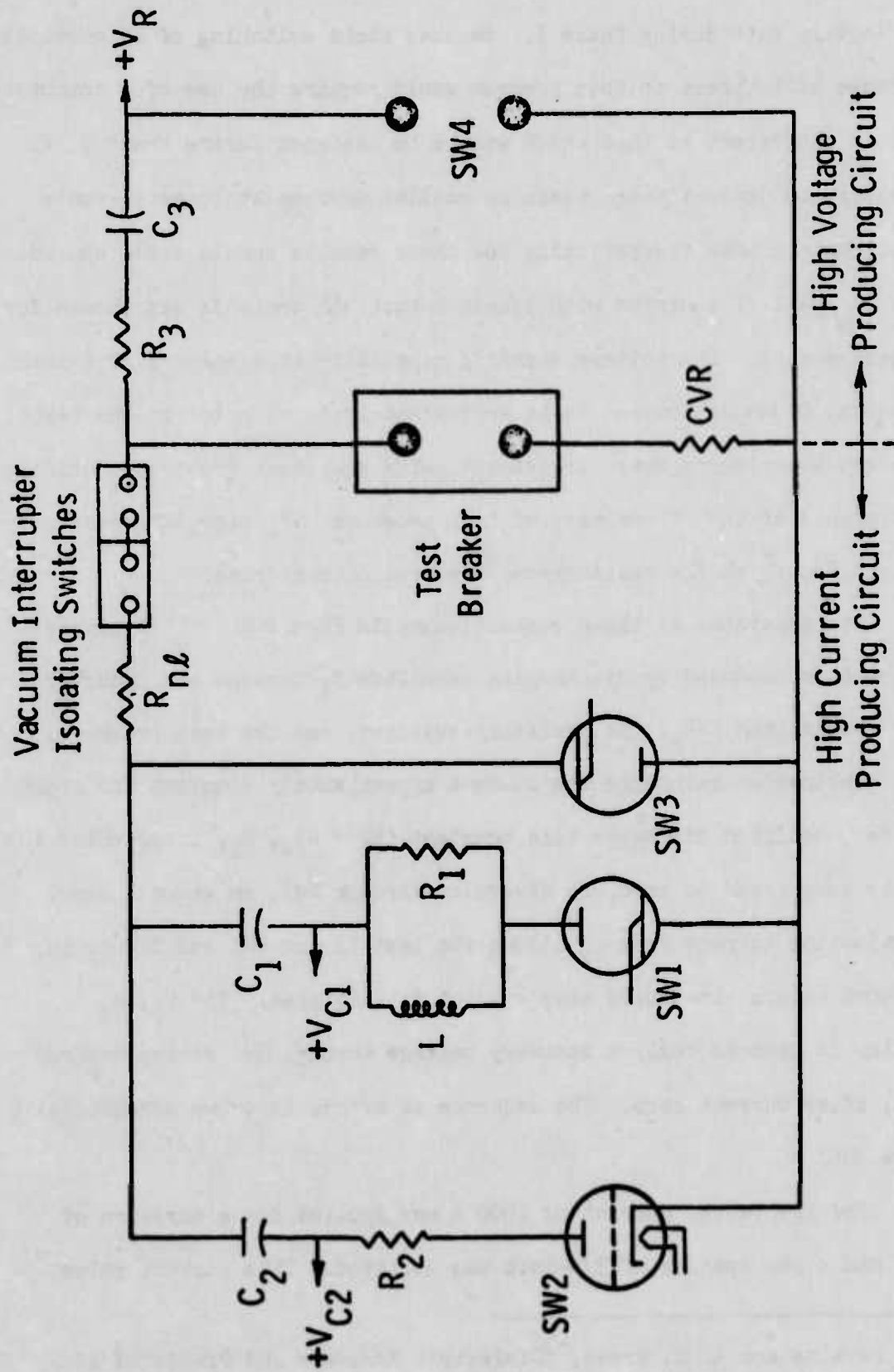
Figure 9. Schematic of Test Circuit for Recovery Voltage Measurements.
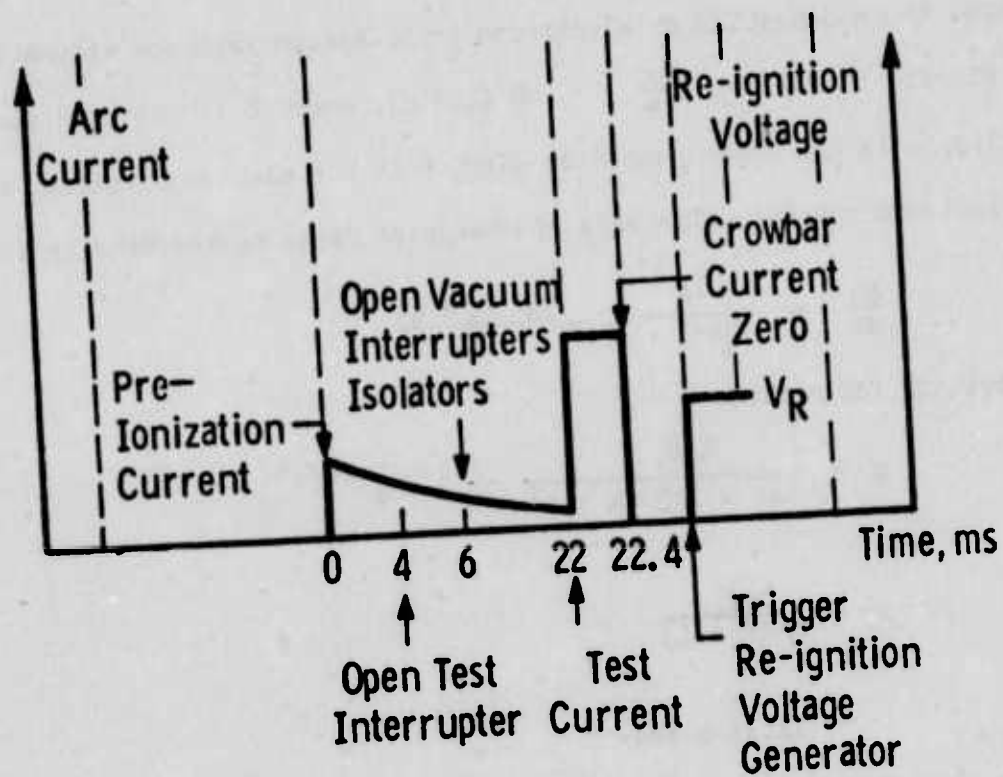
Figure 10. Sequence of Operations in Recovery Voltage Tests.

33

scales to 28,500 A for 4-inch diameter electrodes. That the duration is sufficient to allow an equilibrium vapor density to be established can be shown by the following analysis[*]. The rate at which vapor comes off the cathode during arcing is given by $I\beta/e$, where β is the number of vapor atoms produced per arc electron and e is the electronic charge. The rate of loss of vapor to condensation on electrodes or to escape from the volume is given, from kinetic theory, by $\frac{n\bar{c}}{4} \cdot 2\pi R (L + R)$, where $\bar{c}$ is the mean vapor atom velocity, n is the vapor number density, R is the electrode radius, and L is the electrode spacing. The rate of change of vapor number density is

$$\frac{dn}{dt} = \frac{I\beta}{\pi R^2 L \cdot e} - \frac{n\bar{c}(L+R)}{2RL} \tag{3.1-2}$$

and, solving for n gives

$$n = \frac{4I\beta}{ec \cdot 2\pi R (R + L)} \left(1 - e^{-t/\tau'} \right) \tag{3.1-3}$$

where

$$\tau' = \frac{2RL}{\bar{c}(R+L)}$$

$$= 11.15 \; \mu \; sec$$

for the electrode spacing and radius in these tests and for an assumed vapor temperature of 2000 K. With this value of τ', it can be seen that the exponential term in Eq. (3.1-3) is vanishingly small so that equilibrium has been reached in a time short compared to 400μsec.

The arc time and current are, however, insufficient to cause any significant heating of the anode surface. As a result, it was decided that application of reverse polarity recovery voltages would give recovery rates that would be too high because there would be no possibility of a restrike caused by overheated metal. On the other hand, the cathode hot spots are

[*] C. W. Kimblin, "Dielectric Recovery and Shield-Currents in Vacuum-Arc Interrupters," IEEE Trans. Power Apparatus and Systems, PAS-90 (1971) p. 1261.

present in a density somewhat greater than that expected in the actual VI (the anode spot studies showed that each CLR cathode hot spot emits ~ 50 A so that in this case there will be ~ 20 hot spots on the 3/4-inch cathode while a corresponding area in the the actual VI will have only ~ 14 spots). Ecker's cathode hot spot theory[*] predicts that these spots will have temperatures of the order of 4000°K. Recovery tests with the same polarity should, therefore, more clearly demonstrate the effects, if any, of hot metal on the recovery, and it was decided to perform the tests using only the same polarity.

The results of recovery measurements on CLR with the same polarity are shown in Figure 11. The data points correspond to 10 to 20 tests at each voltage and represent a 50% to 75% probability of successful recovery. The dashed curve is drawn on the basis of Kimblin's observation that 5 to 10 kV separates 0% recovery probability from 100% recovery probability[**] and represents the estimated 100% recovery probability curve for this device. For comparison, Kimblin's 100% recovery data for 1-inch diameter Cu electrodes after switching 930 A are presented in the same figure. It can be seen that the CLR recovery begins after ~ 2 μsec and reaches 35 to 40 kV in the next 7 μsec; by constrast, the Cu electrodes at 1.3 cm spacing did not reach 40 kV until after ~ 23 μsec, despite an earlier initial recovery. The CLR thus recovered at a rate of > 5 kV/μsec after an initial 2 μsec delay.

Kimblin also measured recovery rates for the same Cu electrodes with reversed polarity and the results are depicted in Figure 12, which also shows the same polarity results again for comparison. The very much faster

---

[*] G. Ecker, Zeitschrift Für Natürforschung, 26a, (1971) p. 935.

[**] Kimblin, IEEE Transactions, op.cit.
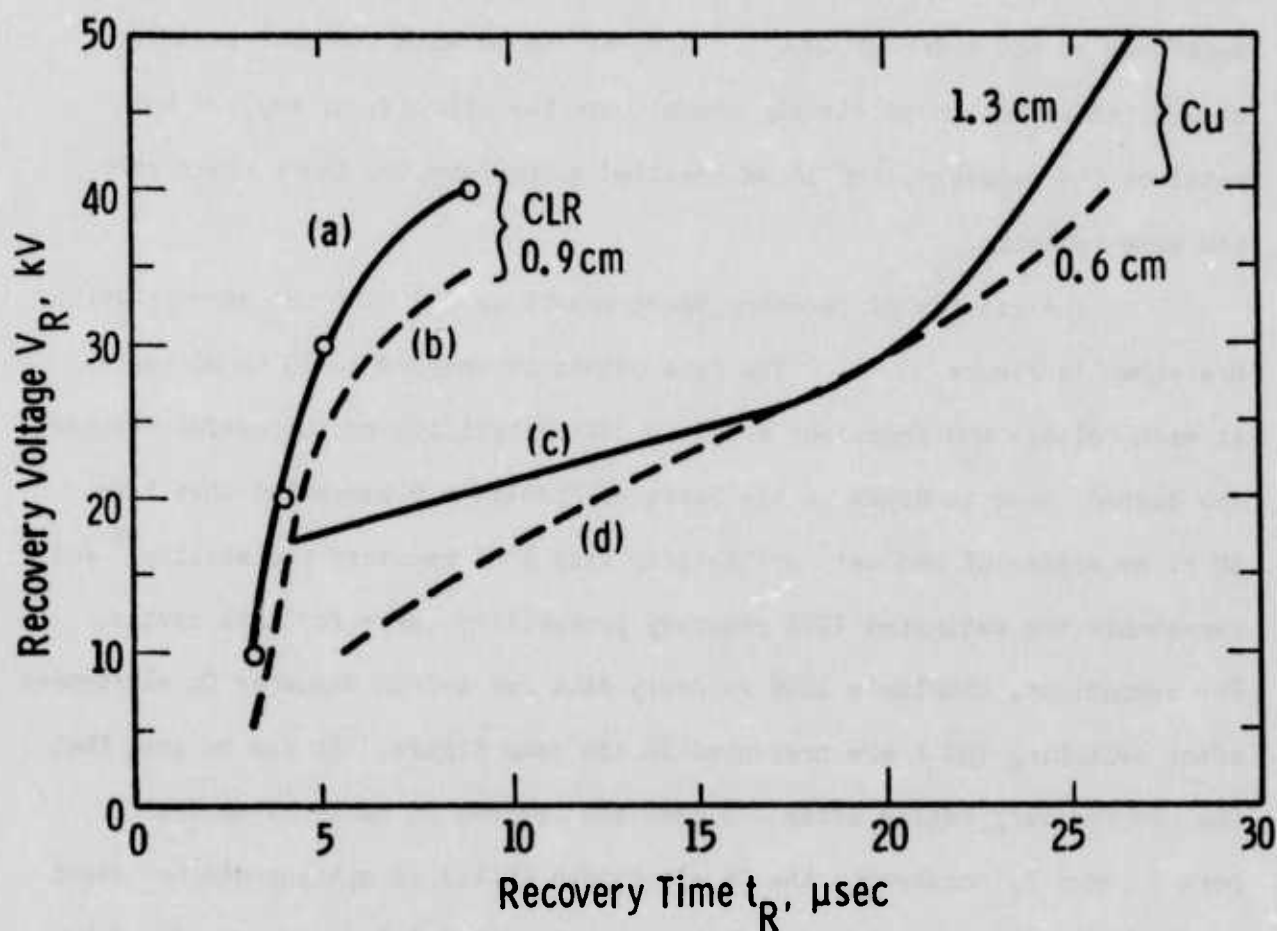
Curves (a) and (b) are for 3/4-inch CLR at 3/8-inch spacing:
(a) is measured 50 to 75% recovery probability, (b) is esti-
mated 100% recovery probability. Curves (c) and (d) are
measured 100% curves for 1-inch copper at ½ and ¼-inch spacings.

Figure 11.   Recovery Voltage Characteristics of CLR and Cu.
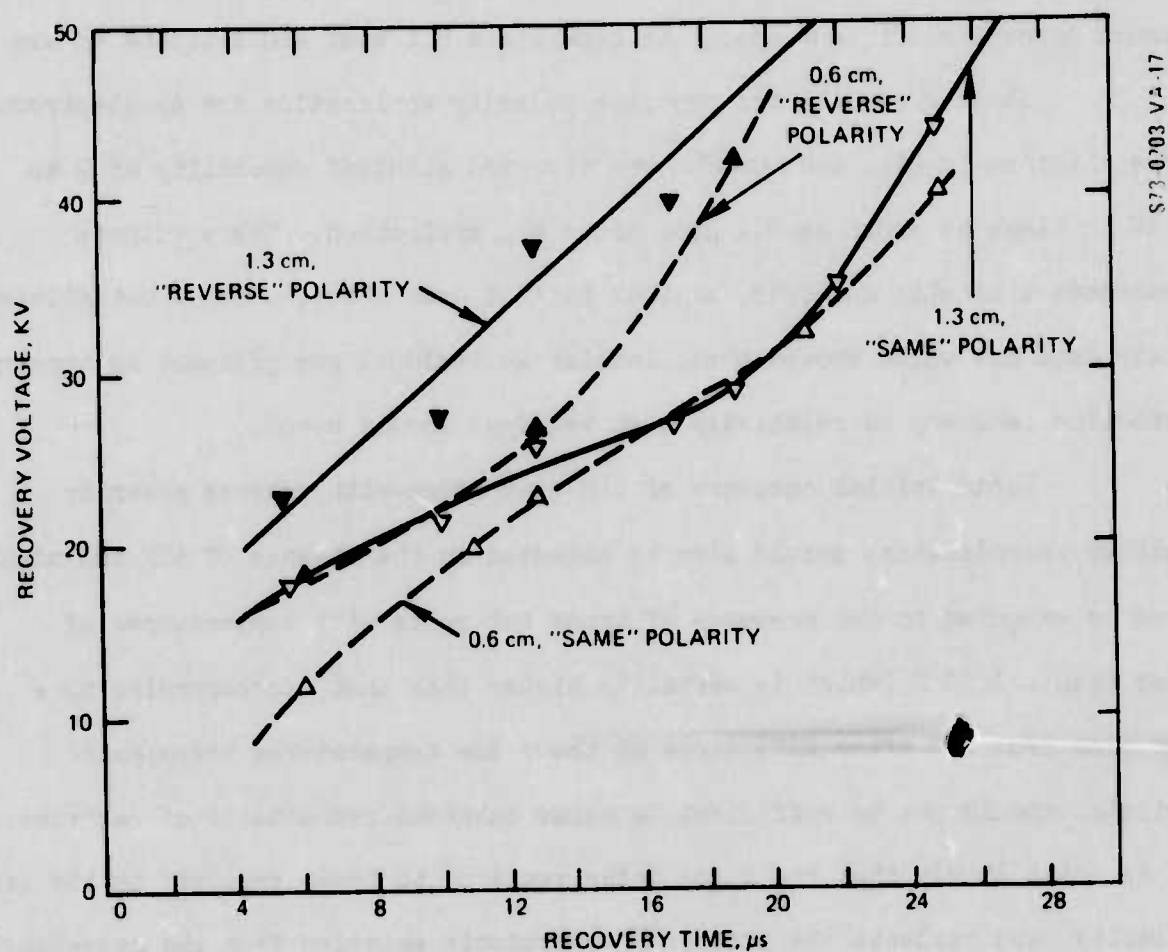
Figure 12.   Recovery Voltages of Cu for "Same" and "Reversed" Polarity.

opposite polarity recovery and the apparent instantaneous recovery to ~ 10 kV
are explained by Kimblin as showing that there were no local hot spots on
the arcing anode which could feed a restriking arc while the remanent hot
spots on the arcing cathode can feed a restrike. Application of reverse
voltage merely sweeps out the ions left between the electrodes and these
cannot deposit sufficient energy to generate a hot spot and initiate an arc.

Similar results for opposite polarity application for Ag electrodes
were obtained by Rich and Farrall,[*] who observed standoff capability of 2 to
4 kV in times as short as 0.1 μsec after arc extinction. These authors
presented a kinetic analysis, similar to that used above, which substantiated
their data and which showed that, insofar as residual gas pressure is concerned,
zero-time recovery to relatively high voltages should occur.

Rapid initial recovery of CLR electrodes with reverse polarity
voltage reapplication should also be expected in the absence of ASF and might
even be expected in the presence of anode hot spots with temperatures of
less than ~ 1500 K (which is certainly higher than that corresponding to a
red glow from CLR after ASF) since at these low temperatures thermionic
emission should not be sufficient to cause enhanced probability of restrike.
It is quite likely that the 2μsec delay required to begin recovery in the same
polarity case reflects the effects of thermionic emission from the exceedingly
hot cathode spots until they cool below some critical temperature. We
expect, therefore, to obtain an immediate onset of recovery with CLR in
reversed polarity and a subsequent recovery rate at least as great as the
> 5 kV/μsec recovery seen in the experimental tests.

---

[*] J. A. Rich and G. A. Farrall, "Vacuum Arc Recovery Phenomena," IEEE
Proceedings, 52, (1964) p. 1293.

Several other approaches were taken to substantiate this expectation. Voshall[*] extended the Rich-Farrall analysis to allow calculation of recovery rates for VI's at any current switching level. Applying the same recovery criterion to CLR as Voshall used to predict successfully the recoveries of Cu and Ag electrodes, i.e., a mean free path in the residual gas equal to twice the electrode spacing indicates that the 4-inch CLR electrodes at $\frac{1}{2}$-inch spacing should recover to 100 kV in 12 to 16 μsec; using a more conservative critical gas density 2.5 times lower gives an expected recovery time of ~ 30 μsec.

That residual gas density should present no problem to recovery can be shown further by comparison to Kimblin's copper experiments cited above. Under the conditions of Kimblin's experiments, the residual gas density after 20 μsec, when the 1.3 cm gap withstood 50 kV, was calculated to be approximately 1.5×10^{15} cm^{-3}. Applying the same analysis to the 4-inch CLR electrodes at $\frac{1}{2}$-inch separation gives a gas density of 1.2×10^{15} cm^{-3} at the instant of current extinction and $< 0.5 \times 10^{15}$ cm^{-3} 20 μsec later. Thus, the initial density, owing to the slower CLR erosion ($\beta \approx 0.05$ as compared to 0.18 for Cu), will be lower than that at which Cu electrodes withstood 50 kV and the residual density at 20 μsec will be three times lower. On the basis of this comparison, 100 kV holdoff should be possible in less than 20 μsec, perhaps in a time as short as 10 μsec.

In summary, experimental tests on a small-scale CLR-equipped VI showed recovery at a rate of > 5 kV/μsec after a 2 μsec initial recovery delay which probably results from residual cathode hot spot emission upon

---

[*] R. E. Voshall, "Current Interruption Ability of Vacuum Switches", IEEE Trans. Power Apparatus and Systems, PAS-91, (1972) p. 1219.

same polarity voltage application. Several different analytical approaches to scaling of there results indicate that a recovery rate to 100 kV of at least 5 kV/μsec can be expected in the large device. Moreover, they show that for reversed polarity voltage application, in the absence of gross ASF, the recovery will begin instantaneously and will easily reach 100 kV in less than 20 μsec.

Despite the fact that recovery is expected to begin instantaneously, the commutator circuit has been designed to yield a 2 μsec delay before the coil reaction voltage begins to rise. This not only produces an added safety margin insofar as switch recovery is concerned, but as will be shown in Section 3.2, it will provide this margin at a net weight saving to the entire system.

3.1.3   Thermal Analysis

Because of the high power dissipation expected in the arc, it was proposed that forced convective cooling of both electrodes be incorporated in the VI, and a very conservative steady-state thermal analysis was presented to show that, even at arc voltage drops of 100 V, such cooling would be feasible. It was noted, however, that addition of coolant device to the movable electrode would create added complexity, so that it was proposed that the feasibility of cooling only the stationary electrode be investigated during Phase I.

A similar steady-state analysis was conducted early in the program, and this indicated that convective cooling of the anode alone would be sufficient to maintain a mean electrode face temperature of 300 to 360°C. This analysis assumed a heat input of 4 kJ/cycle to allow for relatively

high arc powers and high contact resistance losses. As in the previous
estimate, no allowance was made for the thermal inertia of the VI components,
so that the treatment was again highly conservative. The cooling system
required to maintain these temperatures was predicted to be one which pumps
30 gallons of coolant per minute at a head pressure in excess of 100 psi.
Although such a system is relatively simple to design and fabricate, it
increases the system complexity and adds more than 25 pounds to the overall
weight.

When the much more optimistic values of arc voltage and contact
resistance became available and showed that an energy input of only about
1700 J/cycle could be expected, it was decided to perform a transient thermal
analysis to determine the rate at which the system increases in temperature
and the number of cycles of continuous operation to which the VI can be
subjected without requiring a cooling system.

The approach taken in this dynamic thermal analysis is described
in detail in Appendix A, which also lists the computer programs utilized
for calculating the temperatures of the systems both with and without coolant
and gives sample temperature print-outs at a variety of operation times.

The only assumptions made in performing these analyses, together
with their justifications, were:

(1) All of the arc energy goes into the anode and is deposited
uniformly over the face. Because of their much lower
velocities, the ions can carry only a tiny fraction of the arc
current, and the ASF studies showed that the plasma is always
uniform and diffuse in the absence of anode spots.

(2) For the uncooled case, the ends of the stems are maintained

41

at 300°K but that no other heat transfer from the system occurs. In view of the $10\frac{1}{2}$-inch distance of the ends from the electrode faces, the contribution of cooled ends to lowering the electrode temperatures is minimal. In addition, maintenance of good electrical contact to the stems will require that they be held at moderate temperatures.

(3) The temperature coefficient of the electrical conductivity of CLR is the same as that of Cu. Since the conductivity variations with temperature of most metals are similar to, and frequently less than that of Cu, this assumption seems justified.

The physical properties of CLR used in the analysis are those measured at the Westinghouse Electronic Tube Division and are $\rho = 8.1$ g/cm^3, resistivity $= 7 \times 10^{-6}$ Ω-cm, and $\text{\Lambda} = 1.23$ J/cm-°k-sec. In order to keep the analysis conservative, the arc energy deposition rate was taken to be 1600 J/cycle ($= 1/3$ higher than expected) and the contact resistance heating was taken to be twice that expected ($R_c = 4$ μΩ rather than 2 μΩ); the energy input per cycle to the face of the anode was thus taken to be 1650 J rather than the 1225 J estimated previously. Because of the desirability of using a 1-inch stem diameter to mate with the bellows chosen for the VI, the calculation was performed for this stem diameter on both ends.

Several checks were performed to establish confidence in the calculations. The most significant of these is described on page A-9 of Appendix A; it showed that the mesh calculation predicts a peak surface temperature at the end of an arc within 1.5°K of that predicted by exact analysis. The temperature profile proceeding into the anode plate was estimated to

correspond to an energy input of approximately 1700 J in the first cycle in very good agreement with the arc energy and contact resistance heat inputs. Finally, the I^2R losses in the Cu stems should increase their temperature by approximately 0.5°K per cycle at the beginning of switch operation, and this value again checks closely with the calculated data. Thus, a rather high level of confidence can be placed in the validity of the thermal analysis. Detailed results of the computation are given in Appendix A.

The analysis predicts that the peak anode surface temperature at the end of the 300th cycle will be 719°K and that, at the moment of arc extinction, this value will be 901°K for the system without cooling. In view of the ASF data presented earlier, which indicate that a temperature of the order of 1400 to 1600°K is necessary before an anode spot begins to form, this indicates that the uncooled switch will have a safety margin of 500 to 700°K after the 300th cycle, even with a 34% overestimate of the heat input per cycle. Thus, cooling should not be necessary.

The removal of the need for a cooling system decreases the overall weight of the system by about 25 pounds. The changes in the VI electrode design, i.e., the use of solid stems 1-inch in diameter and solid plates 4-inches in diameter by 1-inch thick, gives the following weight tally for the VI:

Weight of bottle and end plates	-	12 pounds
Weight of electrode plates	-	7.7 pounds
Weight of electrode stems	-	4.9 pounds
Total VI weight	-	24.6 pounds

This value was rounded off to 25 pounds in Section 3.1.

More limited calculations were performed for the cooled anode case.

These are also described in Appendix A. Extrapolation of the results to 300
cycles gives an expected temperature of 580°K after the 8 msec post-arc
quiescent period. The peak temperature at arc extinction should, therefore,
be approximately 760°K. This would seem to indicate that a cooling system
increases the safety margin by only about 140°K or about 20 to 30%. The
added weight and system complexity hardly justify such a small increase in
safety margin.

This conclusion is further strengthened when it is considered
that, should something happen at the face which could promote ASF during
any given cycle, the cooling system can do nothing to prevent ASF. That is,
the coolant is separated from the face by $\frac{1}{2}$-inch of metal and thermal trans-
port through the metal during a 2 msec arc is negligible.

3.1.4   VI Lifetime Considerations

Several phenomena can limit the lifetime of a VI, the most impor-
tant being gross erosion due to ASF, but this has already been considered.

Many VI's are observed to fail when a catastrophic arc occurs
to the shield and perforates it. The inside of the container then becomes
coated with metal and the device no longer holds any appreciable voltage.
Arcs to the shield can be avoided by so designing the electrode profile that
the fields between the electrodes are always greater than the fields between
either electrode and the shield. With electrode plates of 1-inch thickness,
it is expected that gentle rounding of the outer edges together with the
smooth evaporation of CLR during arcing should be sufficient to ensure low
fields between the electrodes and the shield, but this should be investigated
further.

44

In the event that something more than gentle rounding is required, analyses have been carried out to specify other electrode geometries. These analyses show that the use of a Bruce profile or of a 90° Rogowski profile would necessitate very large increases in the diameter of the VI bottle. A 120° Rogowski profile, calculated according to the formulas given by Cobine[*], would necessitate an increase in the electrode diameter to about 5.1-inch. This diameter could be accommodated in an 8-inch diameter VI bottle which Westinghouse has recently added to its VI product line. The weight increase resulting from use of this bottle would be less than 2 pounds and, since thin-walled metal could be used to add the Rogowski profile to the outer edges of the electrodes, the overall weight increase would be only about 2 pounds.

It was suggested in our proposal that arc confinement or dispersal techniques be investigated as means of controlling the energy dissipation during arcing. Fins are often used in large VI's to promote arc dispersal and it is generally agreed that such fins increase the switching capability of a given electrode assembly by 30% to 40%. The ASF studies described in Section 3.1.1, however, indicate that dispersal is unnecessary to switching large currents as long as the arc duration and energy dissipation are mini-mized. It is felt, therefore, that incorporation of fins to aid in dispersing the arc is unnecessary. Similarly, arc confinement appears to be unnecessary for the relatively narrow separation of $\frac{1}{2}$-inch for 4-inch electrodes.

Long-term erosion studies were performed on a small VI with 3/4-inch CLR contacts. The contacts were opened to a separation of 0.18 inch in 3 msec while drawing an arc current which fell from 680 A to 325 A during the opening

---

[*] J. D. Cobine, Gaseous Conductors, Theory and Engineering Applications, (New York: Dover, 1958) pp 177-181.

process; pulsed pancake coils were utilized to effect the opening. The total charge passed through the interrupter in each cycle of operation was ~ 2.8 coul, or approximately twice the charge which would have passed if the experiment were a direct scale model of the actual operation of the large VI. In addition, more than half of the total charge passed at electrode separations considerably greater than the 0.094 inch which would correspond to the same L/R as in the larger device. Thus, each cycle of operation corresponded to two or more cycles of the larger device insofar as cathode erosion is concerned and to considerably more severe treatment insofar as the probability of ASF is concerned.

The test was carried through 3500 cycles, or the equivalent of about 7000 cycles in the large VI. The cathode erosion rate was monitored by measuring changes in the separation between a fixed point on the movable electrode stem and a fixed point on the bottle. The results are shown in Figure 13, where it can be seen that the data clearly indicate that the fixed point on the cathode stem moved away from the anode , i.e., the electrodes appeared to grow by 0.022 cm rather than shrink. It was decided to open the bottle for inspection.

Before opening, the voltage holdoff capability was measured to be 60 kV reliably. Prior to the tests, the holdoff was initially 45 kV and it grew to 55 kV after five voltage applications. Thus, the long term voltage standoff capability of the device shows a definite increase during these erosion tests.

The surfaces of the anode and cathode are shown in Figures 14. and 15., respectively. The photographs reveal that the apparent electrode growth resulted from transport of molten material from the cathode to the

46
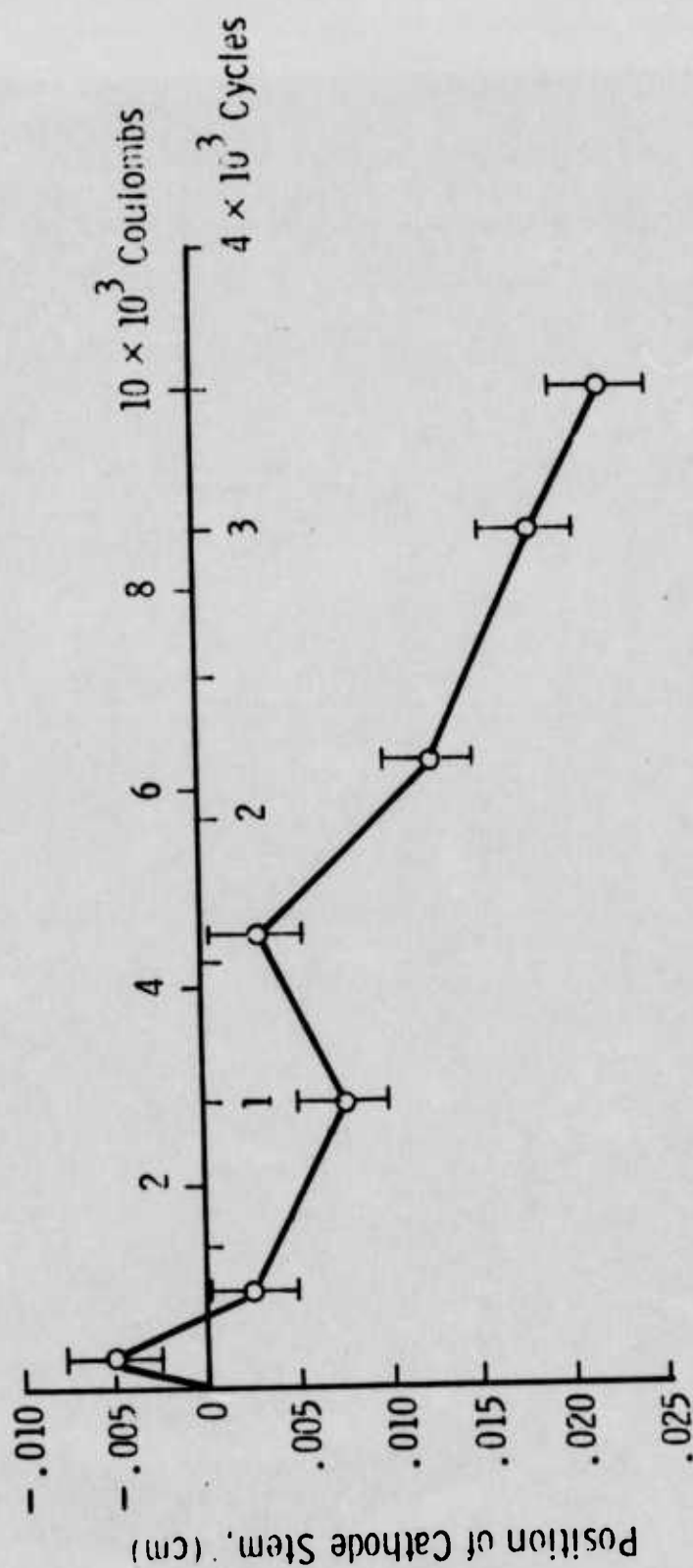
Figure 13. Position of Cathode Stem Relative to Anode Stem Vs. Number of Arcing Cycles and Total Charge.
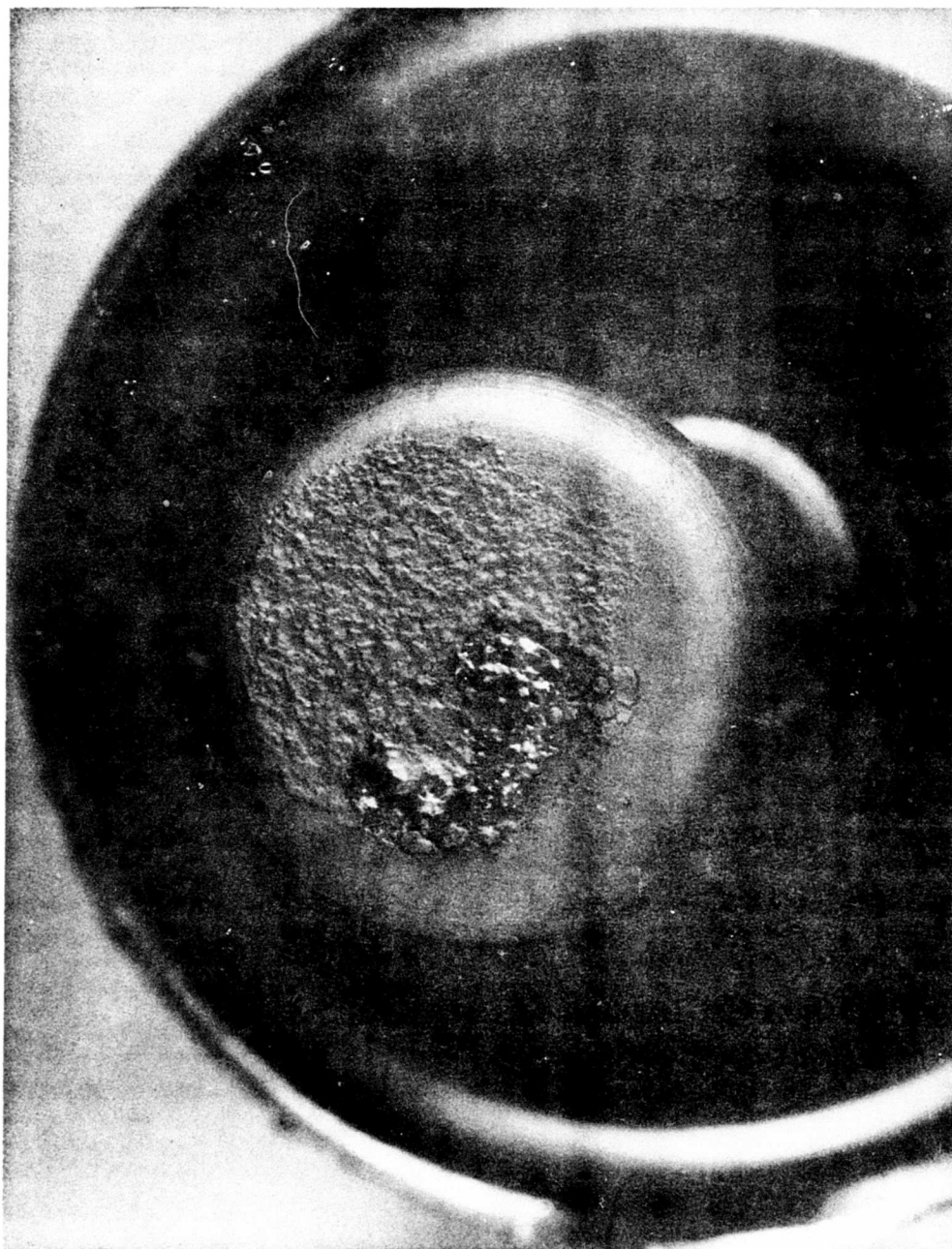
Figure 14.   Anode Face After 3500 Arcing Cycles.

48
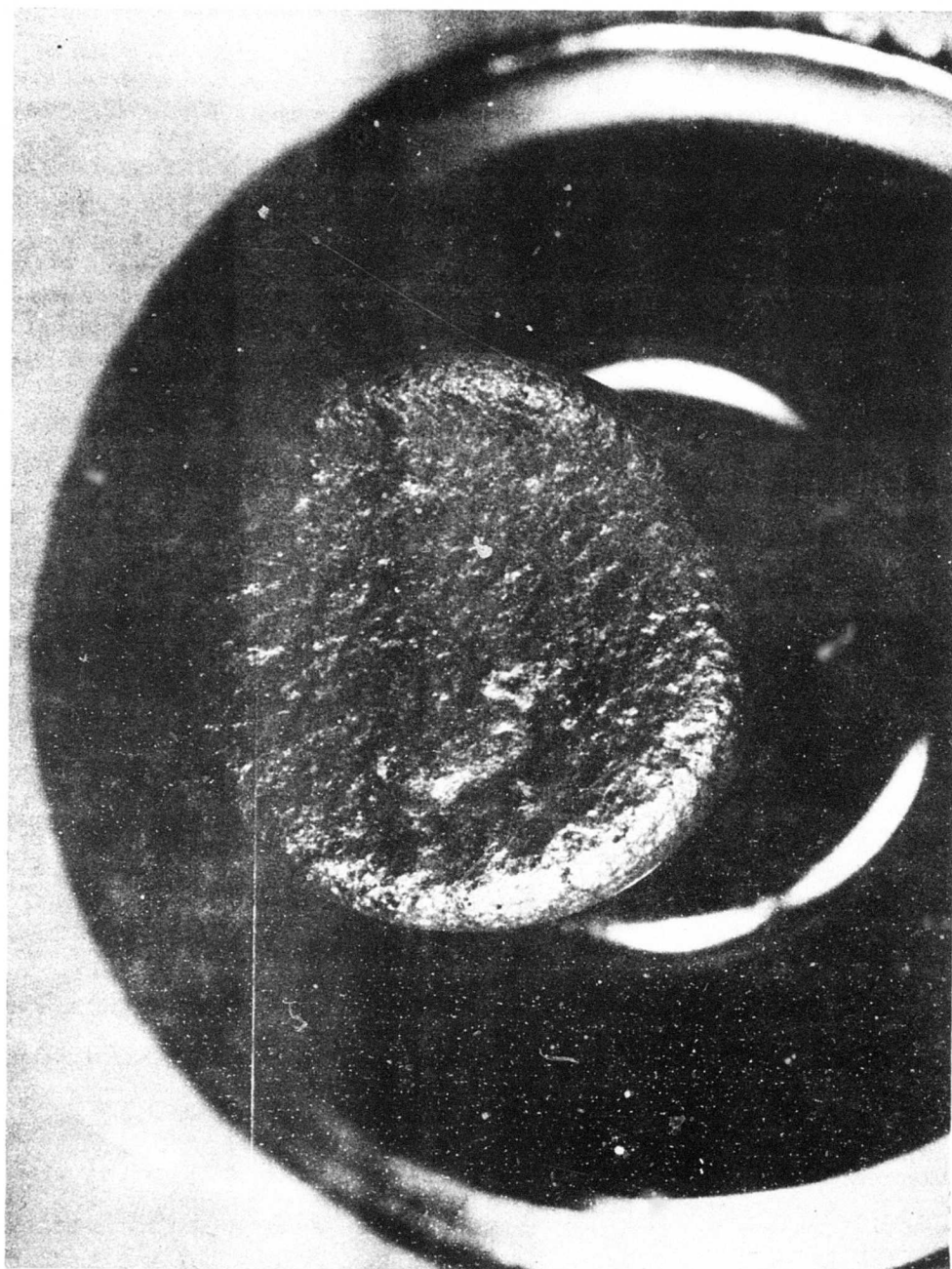
Figure 15.   Cathode Face After 3500 Arcing Cycles.

anode, as indicated by the presence of a rise on the anode and a mating crater on the cathode. This probably occurred as a result of repeated bridge explosions at the same sites, an effect also seen in the ASF studies. There is no evidence that an anode spot formed at any time during the experiments. The voltage standoff tests indicate that no deleterious effect results from this continued localized bridge explosion effect.

Slow erosion elsewhere on the cathode is evidenced by the gentle pitting of the face. The average cathode erosion depth was estimated by measuring the difference in thickness of the anode and cathode plates. The cathode thickness decreased by 0.18 ± 0.07 mm during the 3500 cycles, giving an erosion rate of 43 ± 17 μg/Coul in reasonable agreement with the Rondeel data of 30 μg/Coul cited earlier. As a result of these measurements, the large VI is expected to experience an erosion of 1.1 ± 0.45 mm during 50,000 cycles of operation. This is well within the limits of adjustment of actuator travel (6.35 mm) designed into the actuation mechanism and should present no serious danger to the VI lifetime.

It appears, therefore, that the basic components of the VI should be capable of providing a 50,000 cycle lifetime.

3.1.5   Bellows Coupling

The bellows coupling is expected to be supplied by Metal Bellows Corp., and to be developed in conjunction with Westinghouse if development becomes necessary. Specialists at Metal Bellows feel that the welded diaphragm bellows recently designed for Ontario Hydroelectric should be acceptable for our application at a maximum velocity of 40 feet per sec and a stroke of one-half inch. This bellows has been designed and developed for a lifetime

50

of 10,000 cycles, for a one-inch travel at 30 feet per second and is presently undergoing testing at Ontario Hydroelectric. Because of an extended strike at Ontario Hydro., no test results are yet available. Preliminary tests had previously been conducted by Ontario Hydroelectric on a bellows best suited to their application but selected off the shelf so that design data could be accumulated. It failed after 70 cycles of moving one inch at 30 feet per second.

The method utilized by Metal Bellows to design high speed bellows is an empirical approach. A preliminary design is subjected to tests in its intended application. High speed motion pictures are then taken to determine instantaneous deflection of each convolution of the bellows. A computer analysis is then performed to determine the static stress condition. Then using existing stress/cycle curves for the material, they can predict operating life. This procedure was used in designing the bellows now under test at Ontario Hydroelectric. A similar approach would be required for the Short Pulse switch bellows if the present Ontario Hydroelectric bellows proves inadequate for our application.

To date in the development of high speed bellows by Metal Bellows, the weld has not been a problem. Any potential failures are expected in the diaphragm immediately adjacent to the weld in either of the first three or four convolutions. This is corrected by altering the diaphragm configuration immediately adjacent to the weld as depicted in Figure 16.

The bellows expected to be utilized in the VI is illustrated in Figure 17. The diaphragm thickness varies so that a graduated spring rate is obtained. Each end uses the thicker material for approximately three or four convolutions, to provide the higher spring rate. The varied spring rate distributes stresses uniformly throughout the stroke.

51

DIAPHRAGM

DIAPHRAGM

I D OF BELLOWS

O D OF BELLOWS
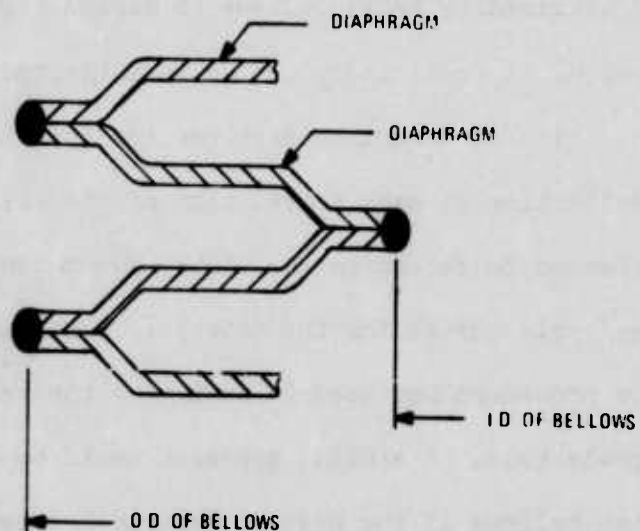
TWO DIAPHRAGMS METAL ARC WELDED CIRCUMFERENTIALLY
MAKE-UP ONE CONVOLUTION TWO CONVOLUTIONS ARE SHOWN

S73 0203 VA 54

**Figure 16.   Alteration in Diaphragm Configuration
to Increase Bellows Strength.**

52
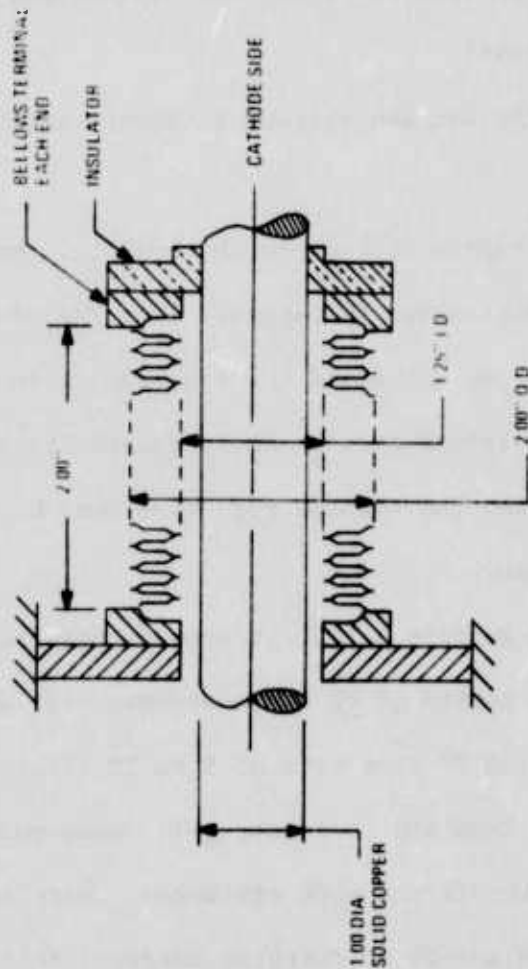
BELLOWS CONFIGURATION

CONTOUR NESTING RIPPLE, VARIED THK 010" 005"
NO OF CONVOLUTIONS 37
MAT'L AM 350 PRECIPITATION HARDENING STN STL

S73 0203 VA 53

BELLOWS TERMINAL
EACH END

INSULATOR

CATHODE SIDE

2 00" OD

1 25" ID

2 00"

1 00 DIA
SOLID COPPER

Figure 17.   Configuration of Bellows to be Utilized in VI.

53

3.2 Commutator Circuit

3.2.1 Fundamental Requirements of Commutator Circuit

During the opening of the vacuum interrupter contacts, an arc carrying 20,000 amperes is formed. This arc continues to supply current to the cryogenic coil, and the coil does not sense the switch opening. It is the commutator circuit which must:

1) Extinguish the arc and thereby interrupt the current supply to the coil.

2) Continue to supply current to the coil for the length of time required for the vacuum interrupter to recover, from the newly extinguished arc, to the point where it can withstand the required voltage buildup.

Since the vacuum interrupter standoff capability depends upon the value of the applied voltage, the voltage rise-time must be sufficiently long to prevent restriking an arc.

As discussed in Section 3.1.2 it appears that the vacuum interrupter, after a dispersion period of ≤ 2 microseconds, will withstand a reapplied voltage rising to 100 KV at a rate of 5 to 10 KV/µsec.

The voltage rise from the cryogenic coil, upon current interruption, is given as 2.5 KV/µsec in the work statement. With an ideal coil (no stray capacity) of 5 mH and 20 kA charging current, this limitation of the voltage rise requires that either the coil manufacturer incorporate a capacitance of approximately 8 µF into the coil or that the circuit designer provide such a capacitance across the coil.

This capacitance requirement follows from the voltage build-up equation:

$$L \frac{di}{dt} + \frac{1}{C} \int idt + iR = 0$$

54

where L is the coil inductance 0.005H and C is the capacitance associated with the coil. The circuit resistance, R, is unknown, but very small, and can be neglected. Solving the equation yields

$$100,000 \text{ Volts} = \frac{1}{C} \int i\, dt = \frac{20,000 \text{ amps}}{C \cdot \omega} \sin \frac{t}{\sqrt{LC}}$$

$$5 = \sqrt{\frac{L}{C}} \sin \frac{40 \cdot 10^{-6}}{\sqrt{LC}}$$

The equation cannot be solved explicitly for C, but yields

C = 7.9464 μF,

the resonant frequency

f_{res} = 798 Hz,

and for a rise time of 40 μsec,

ωt = 11.5°.

At this small angle, the voltage rise is very close to linear.

The energy stored by this capacitor is

$$E = \frac{C}{2} \cdot v^2 = \frac{8}{2} \cdot 100^2 = 40k \text{ joule}$$

and its weight at 50j/lb

$$W = \frac{40,000}{50} = 800 \text{ lbs}$$

Its weight, thus, is quite significant.

If the circuit resistance, R, were included, a slight attenuation and a slight decrease in frequency would occur. Hence the value of C could be reduced correspondingly.

More significant, however, are the experimental voltage recovery results. If the full scale experiments of the second phase confirm these results, it may be possible to allow a voltage rise of up to 10 kV/μsec and a reduction of the capacitor by a factor of four to 2μF and 200 pounds.

The voltage rise so far considered is produced by the collapse of the field of the cryogenic coil. It should be noted that another voltage rise is produced by the internal reactance of the generator. This voltage rise will occur on the other contact of the circuit breaker with opposite polarity and will increase the potential across the circuit breaker. The necessary data are not on hand to determine the magnitude of this voltage rise. However, should this rise prove significant, it appears that it will be necessary to eliminate it by a triggered shunting branch so as to protect the generator against dielectric breakdown. Since this is a generator problem, it is not included in the present circuit analysis.

A variety of circuits have been conceived and analyzed for their ability to provide the conditions for current interruption as outlined above with a minimum of weight, power consumption and complexity. The more significant ones are discussed in the next section.

3.2.2   Basic Circuit Alternatives

The cryogenic coil can be connected either in a shunt or in a series connection to the load, as shown in Figure 18. a and b, respectively.

In the shunt coil circuit, the switch interrupts the current from the power source to the storage coil, and the coil is allowed to discharge directly into the load. Since the power source unavoidably is inductive, a surge voltage will develop across it and will appear on the left switch electrode with polarity opposite that of the right electrode as mentioned above.

In the series coil circuit, the load is inserted into the main circuit by opening the switch. The load, representing a high impedance, will

56
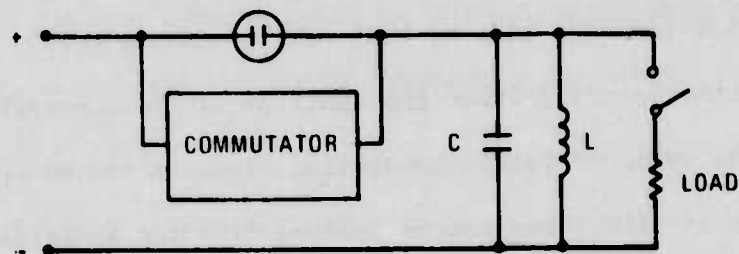
SHUNT COIL

A
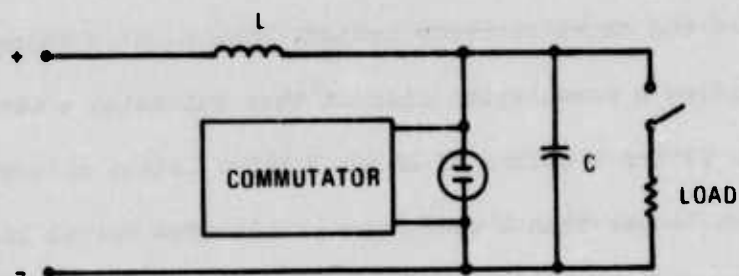
SERIES COIL

B

S73-0203-VA-62

Figure 18. Alternate Circuits for Coil and VI.

57

cause a reduction of the current at a rate such that the voltage developed
in the inductance, $L \frac{di}{dt}$, equals the voltage drop across the load. The
current decay as seen by the power source is slower than in the former case,
and the voltage surge in the power source is correspondingly less. Secondly,
this energy is not lost but adds to that of the storage coil.

In either configuration the function of the commutator circuit is
essentially the same, and basic commutating circuits can be applied to either.
With constraints of the power source removed from the analysis, the shunt
coil circuit lends itself more easily to computer simulation. The results
of various commutator circuit analyses are given in the following discussion.

The rate of voltage rise after current interruption, as specified
for the coil and load circuit, is 2.5 kV/µsec. As discussed above in
Section 3.2.1, this voltage rise is less then the capability of the vacuum
interrupter after the short recovery period. The problem therefore reduces
to that of providing a commutation circuit that maintains a zero current
condition in the VI for a period of about 2 µsec. Since this period is
expected to be no longer than 2 µsec, the problem reduces to basically two
different approaches which may be taken to provide the current zero time,
namely:

1) An auxiliary (or commutating) circuit which drives a current
through the VI of magnitude equal to the main circuit current and of opposite
polarity. In this case the net current in the VI goes to zero, the arc
extinguishes, and the interrupter recovery begins.

2) An auxiliary voltage is applied to the input electrode of the
switch and drives it negative at a rate equal to the voltage buildup due to
the storage coil, i.e., 2.5 kV/µsec. This voltage is applied for a duration

58

of 2 μsec, and during this time there is zero voltage across the interrupter so that the arc extinguishes and recovery begins.

The two approaches accomplish the same result, i.e., they both extinguish the arc and provide 2 μsec before the switch is subjected to the voltage generated by the storage coil. A choice may be made between the two approaches based upon weight, circuit complexity and energy loss considerations.

3.2.3 Commutator Circuit Analysis

The basic commutator circuit could consist of a damped L-C circuit which passes a bucking current, slightly greater than the arc current, through the vacuum interrupter. This would create one or more transitions through a net zero current and would extinguish the arc. Continued application of this bucking current which oscillates around zero would also provide a recovery period to the switch before it would be subjected to the voltage generated by the storage coil.[x]

Since the actual extinction of the arc and absence of vapor formation occurs at zero current, a more efficient commutation and voltage withholding capability will be provided by a more extended zero current condition. Hence, a pulse-forming network is preferable over a plain L-C circuit and permits a subsequent faster reapplication of voltage, as required in the present application.

During the course of this program a number of commutator circuits were subjected to digital computer analysis and analog circuit measurements.

---

[x]Greenwood, A.N., Lee, T.H., Theory and Application of the Commutation Principle for HVDC Circuit Brakers, Transactions Paper IEEE Power Engineering Society, 1972.

Thus the switch current and reoccurence of voltage were plotted. To meet

the time schedule, this work was initiated at the beginning of the program

simultaneously with the development of the vacuum interrupter and the

actuator. Since these studies were initiated prior to the availability of

the experimental results generated during the course of this program, these

analyses covered quite extended periods of commutation and voltage rise.

Recent voltage recovery measurements have greatly reduced the anticipated

commutation time, and have produced a corresponding decrease in the commu-

tator energy storage requirements. The commutator circuit to be utilized

in the Westinghouse design is discussed below, whereas the earlier analysis

is included in Appendix B.

The basic commutator and VI circuit is given in Figure 3.2.2a,

where a pulse forming network (PFN), of internal impedance Z_0, provides an

essentially square pulse. R is a matching resistor and L is the cryogenic

coil. After firing the commutator gap, but before extinction of the arc,

its equivalent circuit is as shown in Figure 3.2.2b. The impedance in the

arc is small and the gap more closely represents a constant voltage drop of

about 30 volts which is insignificant compared with the voltage of the PFN

and can therefore be neglected. The network is matched, i.e., $R = Z_0$.

After extinction of the arc, the VI represents an open circuit,

and the equivalent circuit of the network is as shown in Figure 3.2.2c.

The load for the cryogenic coil is not connected until the voltage reaches

100 kV, and is therefore not included in the figure. Limitation of the

voltage rise to 2.5 kV/μsec, or some other suitable value, requires a cap-

acitance, C , of some suitable value, which is included in the equivalent

circuit.

60
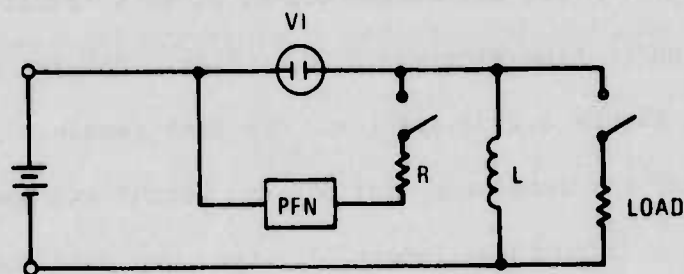
A
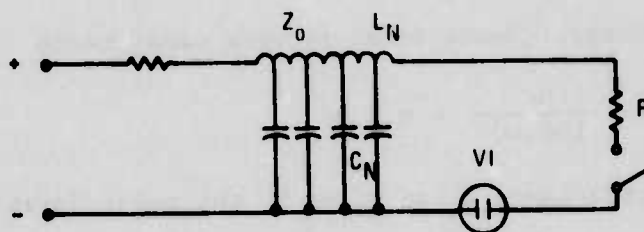
B
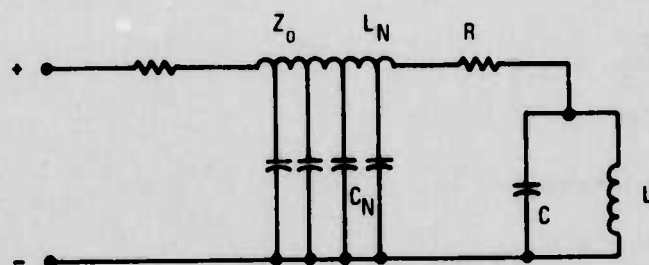
C

S73-0203-VA-61

Figure 19. Basic Commutator and VI Circuit

Based upon the analysis of experimental voltage recovery measurements it appears that arc extinction occurs after a fraction of a microsecond, during which time Figure 3.2.2b applies. For the remainder of the pulse ($\sim2\mu$sec), Figure 3.2.2c applies. The task remaining, then, is to determine the value of the components for minimum weight and power loss.

With a given pulse length of 2 μsec and coil charging current of 20 kA, the network charge is given by

$$Q = i \times \tau = 20,000 \times 2 \times 10^{-6} = 0.04 \text{ Coul.}$$

Since the network must withstand 100 kV during the time the cryocoil is giving off its energy, the smallest PFN weight is attained by designing it for a 100 kV charge voltage. Hence total network capacitance

$$C_N = \frac{Q}{V} = \frac{0.04}{100,000} = 0.4 \ \mu F$$

The network total inductance L_N is given by the pulse duration

$$\tau = 2\sqrt{L_N C_N}$$

$$L_N = \frac{\tau^2}{4C} = \frac{2^2 \cdot 10^{-12}}{4 \cdot 0.4 \cdot 10^{-6}} = 2.5 \ \mu H$$

The network impedance

$$Z_O = \sqrt{\frac{L_N}{C_N}} = 2.5 \ \Omega$$

and for matched condition

$$R = Z_O = 2.5 \ \Omega$$

Since the ohmic resistance of the cryocoil is small, it can be neglected. Furthermore, the coil was being charged from the source with 20,000A prior to the extinction of the arc, and immediately after extinction it is being charged with 20,000A from the PFN for the remainder of its pulse (approxi-

mately 2 μsec). During this period the coil senses no change, and no surge is developed.

As soon as the pulse is terminated, the charging current goes to zero, and the coil will develop a voltage given by $V = -L \frac{di}{dt}$. This voltage is applied across a circuit consisting of two parallel branches, namely, the capacitance C and the series combination of R and Z_0. The PFN represents a short transmission line. As the voltage V appears on C, the same voltage will divide between R and Z_0. The voltage pulse will travel to the far end of the line in one microsecond and then be reflected. The voltage increase on the input to the line will therefore always be one half of the increase on C and will reach the full increase 2 μsec later. As the voltage, therefore, rises on C, the voltage on the PFN will lag by 2 μsec. This lag, however, is insignificant, and the reoccurence of voltage on the VI can be calculated with adequate accuracy by considering C and C_N in parallel.

As discussed in Section 3.1.2 the voltage recovery measurements made during this program indicate that, after an initial VI recovery period of ≤ 2 sec, a voltage buildup of approximately 6 kV/μsec can be tolerated without danger of restriking an arc. Accordingly, it appears safe to allow a reduction of C from 8 μF (as required to give 2.5 kV/μsec) to 3 μF. With these assumptions and using the formulas derived in Section 3.2.1, the time needed to reach 100 kV is given by

$$V = i \sqrt{\frac{L}{C+C_N}} \sin \frac{t}{\sqrt{L(C+C_N)}}$$

$$t = \sqrt{L(C+C_N)} \ \text{arc} \sin \left(\frac{V}{i} \sqrt{\frac{C+C_N}{L}} \right)$$

63

$$t = \sqrt{0.005 \cdot 3,4 \cdot 10^{-6}} \quad \text{arc sin} \left(\frac{100,000}{20,000} \sqrt{\frac{3.4 \cdot 10^{-6}}{0.005}} \right)$$

$t = 17$ μsec

The total time from extinction of the arc, thus, is

$t = 2 + 17 = 19$ μsec

The voltage build-up on the capacitor (and the cryocoil) is sinusoidal, but the angle corresponding to 17 μsec is only 7.5^{o}. Therefore the voltage build-up for all practical purposes is linear.

It is noted that the PFN capacitance C_N first is charged to 100 kV in one direction. By discharging its 0.04 Coulombs into the cryocoil, it delays its back-surge for 2 μsec. Thereafter it is charged to the opposite polarity by the back-surge and now contributes with its full capacity value to reduce the rate of voltage rise. In the absence of the PFN, C would have to be 3.8 μF in order to slow down the voltage rise to 100 kV at 19 μsec. Therefore, C_N may be considered as contributing with twice its value.

The current pulse from the PFN need not be perfectly square. If some ripple is present on this pulse, it will provide several transitions through zero without associated re-occurrence of high voltages. Furthermore, after extinction of the arc, the ripple on the pulse will not cause a re-action from the cryocoil because the reactance of the capacitor C is only a few milli-ohms at the ripple frequency. This reactance is in series with the load resistor R of the PFN, and the ripple current is thus attenuated by a factor of 250 or more. The PFN may thus consist of four capacitors each 0.1 μF tapped to the appropriate points on the 2.5 μH coil.

Based on our preliminary results, a voltage re-occurrence rate of about 5 kV/μsec or 19 μsec to reach 100 kV appears conservative but safe for initial Phase II design considerations. When the full scale model of the VI has been manufactured, it will be tested to determine if an even faster voltage rise can be permitted. If so, a further savings on the weight and size of the capacitance of the cryocoil will be allowed.

The commutator circuit discussed above comes under the type a, or current cancelation method, of the preceeding section. Several circuits of type b, or voltage compensating method, have also been analyzed. Since the present results on the VI indicate that a much faster voltage rise than 2.5 kV/μsec is permissible, the latter method becomes less favorable. Further pursuit of that approach, therefore, appears unwarranted.

3.2.4   Commutator Circuit Switch

The problem of switching in the commutation circuit has been investigated. The triggered vacuum gap produced by General Electric for crowbar service will not hold up for the present requirement, according to representatives of this company.

Ignitrons, which are mercury pool devices, apparently have the highest Coulomb rating for this type of device. However, since they require close temperature control, the maintenance of a vertical position, and probably a connection of two in series, to withstand the voltage, simultaneous triggering problems are anticipated, and they are ruled out for the present application.

Another alternative is to use a gas gap, which operates over approximately 3 to 1 voltage range. In order to reduce erosion, a tungsten-copper matrix may be added to the electrodes.

65

This material increases capabilities in gas gaps, but cannot be used in vacuum gaps because of out-gassing during operation.

The vacuum gap GP-74B-120 produced by EG&G has a rating of 120 kV and has been tested at 60 kA peak. Reliable firing of the gap can be obtained with anode voltage as low as 2 kV. Although tests conducted on the gap have exceeded the requirements for commutator service, life expectancy may be somewhat short. Based on a 10 µsec commutation at 20 kA and 300 shots per minute, representatives of the company estimate 10^4 reliable discharge cycles and degradation thereafter. With the present reduction of commutation period to 2 µsec and recharge at reduced current value, this device may perform reliably for a total of 50,000 operations. If experience should prove differently, it is an inexpensive item that can be easily replaced at scheduled maintenance.

3.2.5   Commutator Circuit Weight Breakdown

The weight of the commutator circuit is a function of the commutation time required for the vacuum interrupter to recover. The experimental results discussed in Section 3.1 indicate that a recovery time of 2 µsec is more than sufficient for the interrupter to withstand a voltage rise of the order of 5 kV/µsec. Based upon this figure for the commutation time, a 0.4 µF capacitance weighing 40 pounds will be required for energy storage. Assuming that the aircraft on which the switch assembly is mounted will provide the basic power source at 400 cycles, the following weight breakdown can be made for the commutator:

Capacitors	40 lbs
Transformer	20 lbs

Rectifier   10 lbs

Vacuum Gap Switch   5 lbs

Total Commutator Circuit Weight - 75 lbs

3.2.6   Commutator Circuit Summary

The commutator circuit designed by Westinghouse will extinguish
the 20,000 ampere arc by passing an equivalent bucking current through the
vacuum interrupter. The circuit will then continue to supply 20,000 amperes
to the cryogenic storage coil for an additional period of 2 μsec in order to
allow the interrupter to begin to recover its voltage hold-off capability.
This circuit will consist of a pulse forming network as shown in Figure 19.
The network is matched with a 2.5 ohm matching resistor R which matches the
internal impedance Z_o of the PFN. We have assumed here that the impedance
of the arc is small, and have neglected it. The total inductance of the
network is 2.5 μH. It should be noted in summary, that the 0.4 μF capacitor
employed in the pulse forming network serves two purposes. The primary pur-
pose of this capacitance is to store the energy to extinguish the arc and
to hold off the voltage buildup for 2 μsec. The secondary service performed
by this capacitance is to limit the rate of rise of voltage from the storage
coil after the commutator current has dropped to zero. It accomplishes this
secondary purpose by being charged to reverse polarity by the back-surge
from the coil, and it thereby reduces the capacitance required in parallel
across the coil from 3.8 μF to 3.0 μF. This results in a weight reduction
of 40 pounds.

3.3   ACTUATION MECHANISM

3.3.1   Introduction

The mechanism selected to drive the contacts must be capable of opening the switch in two milliseconds or less in order to permit the device to operate without cooling, and to maintain a suitable margin of safety which will insure against the formation of anode hot spots. Once the switch has been opened, the arc can be extinguished and the coil can be discharged into the load in less than one millisecond, leaving up to seven milliseconds to again close the contacts. Techniques which were considered include:

- Spring drives
- Hydraulic actuators
- Magnetic actuators
- Flywheels
- Electric motors

Of these possible techniques, flywheels and electric motors were ruled out because either of these would require the use of a clutch which would be subjected to excessive forces and would necessitate a considerable advance over the present state-of-the-art in clutch design and fabrication.

The feasibility of utilizing a magnetic technique was considered, and it was found that there are at present two electromagnetic techniques which have been successfully utilized in opening vacuum interrupters in times of the order of two milliseconds. The first of these was developed at the University of Waterloo, Ontario, Canada for Ontario Hydroelectric, Ltd., while the second has been developed at the Westinghouse R&D Center in Pittsburgh, Pennsylvania. The Canadian scheme utilizes the repulsive forces set up between a current-carrying coil and a disk carrying induced eddy

68

currents and has moved a one pound switch mechanism 1/4-inch in one milli-second. The Westinghouse technique passes current through two closely-spaced pancake coils and has opened a three pound switch a distance of 3/8-inch in two milliseconds. The existing coils can generate a repulsive force in excess of 4000 pounds.

Of the two, the Westinghouse mechanism promises to be the more efficient. To date, however, an efficiency of only about 10% has been achieved. Since as much as 400 joules may be required to open the contacts, even an increase in efficiency to 20% would require storage of up to 2000 joules, requiring of the order of 40 pounds of capacitors. This weight was deemed excessive in comparison to that required for a hydraulic mechanism.

The two remaining techniques, namely hydraulic and spring mecha-nisms, were judged to be most promising and were more closely analyzed dur-ing the course of the program. The results of these studies, along with the reasoning behind the selection of the hydraulic mechanism as the actuation means for the Short Pulse Switch are given in Sections 3.3.2, 3.3.3 and in Appendix C of this report.

3.3.2   Spring Mechanism

A cam and spring operated actuator concept was conceived and in-vestigated in some detail during the course of the program. This concept embodies a motor driven cam to store energy in a coil spring which is then tripped to open the switch. Other springs act to stop the moving contact mass and to store enough of the switch-opening energy to return the contacts to a closed position. A schematic of the conceived device is shown in Figure 20.   The closing spring is sized to store enough energy and apply enough force to reclose the contacts in the seven millisecond closing time allotted. A third spring, the holding spring of Figure 3.3.1, aids in stopping

69

MECHANICAL ACTUATOR FOR
SHORT PULSE SWITCH
(SHOWN CLOSED)

HOLDING SPRING

MOVING
CARRIAGE

OPENING DRIVE
SPRING

CARRIAGE TABS

FIXED TABS

RETURN SPRING

FOLLOWER

CAM
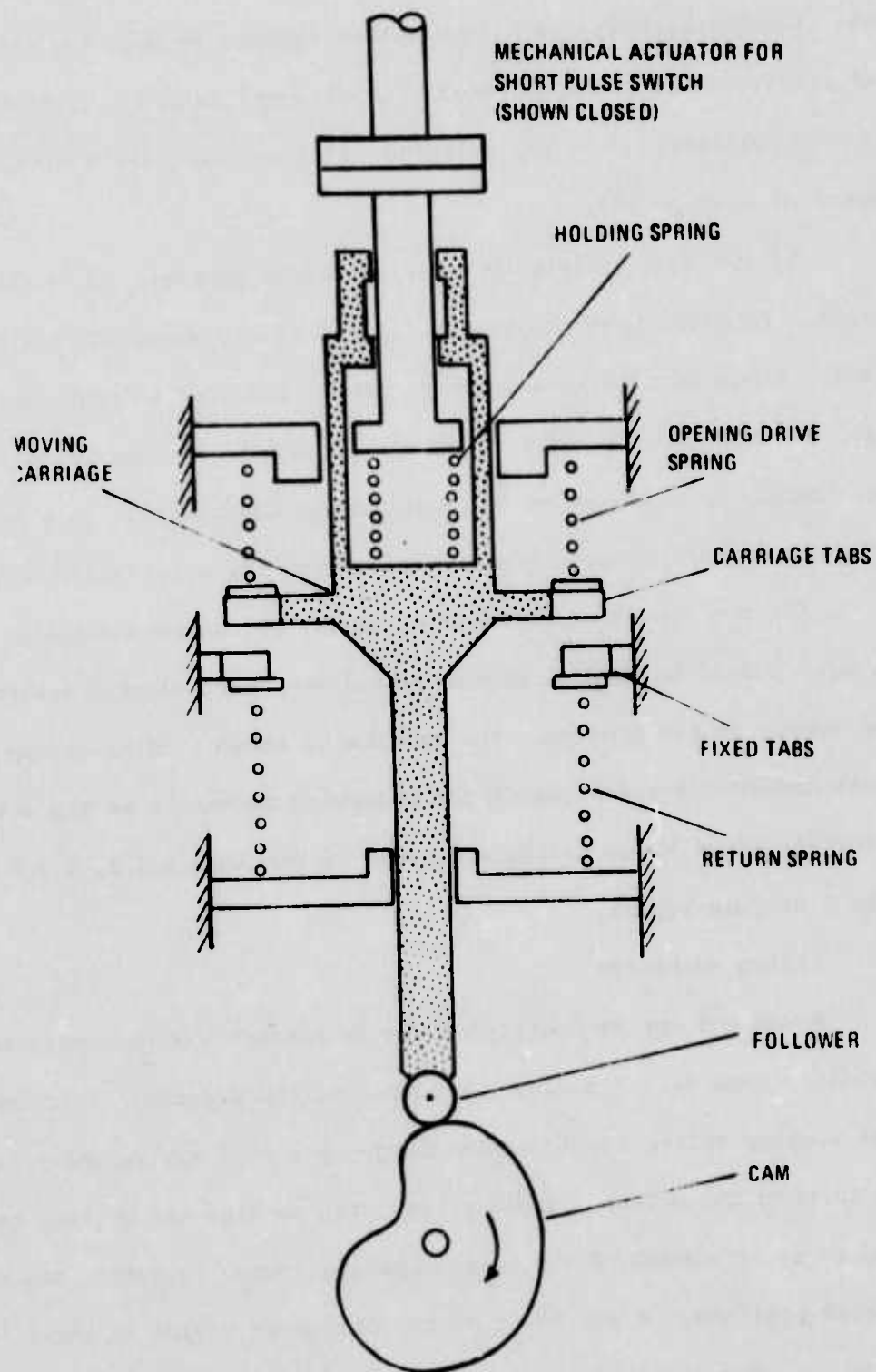
S73-0203-VB-63

Figure 20.   Schematic of Spring Actuation Mechanism.

the contact during opening and acts to set the contact closure pressure at the desired level to maintain closure during high current conduction. The cam can be so designed as to continually compress and impart potential energy to the opening spring during most of the 190 milliseconds that the contacts are closed.

When the cam follower falls over the brink of the cam, the opening spring accelerates it downward, but the contacts do not open until the moving carriage strikes the rear portion of the contact assembly (or some other impact mechanism), at which point the spring motion is arrested. This allows the mass of the spring and carriage to accelerate for a longer period of time than the desired switch opening time and this, in turn, allows a reasonably sized spring to be used.

Calculations indicate that an opening spring weighing about twelve pounts can, with an average force of about 1200 pounds, accelerate ten pounds of weight, including four pounds of its own weight, to about 300 inches per second in one inch of travel. Upon striking the impact mechanisms, it can impart a velocity of approximately 250 in/sec after a very short acceleration time. While slightly higher forces and speeds may be necessary, these calculations indicate probable feasibility. In fact, the opening spring in this example is subjected to about the same load as, and travels a shorter distance than, a typical automobile spring.

While this concept does appear feasible, it became apparent during the course of the hydraulic actuation analysis, which was conducted concurrently, that the latter was even more promising. Due to the light weight and proven high reliability performance of such hydraulic mechanisms a decision was reached to drop the spring mechanism and to utilize the hydraulic mechanism as the switch actuator.

71

3.3.3 Hydraulic Actuation Mechanism

3.3.3.1 Introduction

A hydraulic actuation mechanism has the advantage of being highly efficient so that the large driving forces necessary to open the contacts in two milliseconds can be provided without paying a high penalty in weight and volume. The particular actuation mechanism selected to operate the contacts will be capable of opening the contacts to the full 0.5 inch separation in 1.85 milliseconds at either 5 or 20 pulses per second. In addition, with minor modifications this mechanism can be made to operate at repetition rates as high as 50 pulses per second. The weight of the hydraulic mechanism will be shown in Appendix C-5 to be under 15 pounds.

The following guidelines will be employed in fabricating this device:

  (1) An open loop binary switching valve will be used to avoid the stability problems encountered in high bandwidth closed loop systems. The opening time of 2 milliseconds implies a closed loop bandwidth on the order of 1000 radians/second. This would be a risky task with the high flow rates involved.

  (2) The seal problems will be greatly minimized using the following policies developed as a result of over 20 years experience in high performance, high pressure airborne hydraulic systems:

  (a) A minimum number of elastometric seals is attained using close-fit, clearance seals on internal parts wherever feasible.

  (b) There are no high pressure dynamic seals. The internal dynamic seals are designed per (a) and

72

the external dynamic seal is operated at return
pressure. This low pressure external dynamic seal
is attained by providing a clearance seal between
the high pressure cavity and the o-ring. (See
Figure 21.

(c) The pilot stage will be a jet pipe servovalve.
This servovalve is a two stage valve with a jet
pipe first stage and spool valve second stage.
Westinghouse has extensive experience with this
component and its reliability is well proven.
The reason for a servovalve as opposed to a
solenoidvalve is that the predictability of
operation from stroke to stroke is far greater
with the servovalve.

(d) Spool valves will be used instead of poppet valves.
While a poppet valve offers more orifice conduc-
tance per inch of poppet travel, it also suffers
from a lack of predictability due to "a peculiar
kind of unsymmetrical 'stiction' which in effect
introduces a highly variable lag in operation."[1]

The function of the actuation mechanism is to hold the contactors
together with a 400 lb force while current is flowing through the switch,
and upon command separate the contactors to a distance of 0.5 inches in an
elapsed time of 2 milliseconds. The acceleration force required to achieve

[1] Pg. 243, "Fluid Power Control", Blackburn, Reethof, Shearer, Technology
Press of M.I.T. and John Wiley and Sons, Inc., New York & London.

73
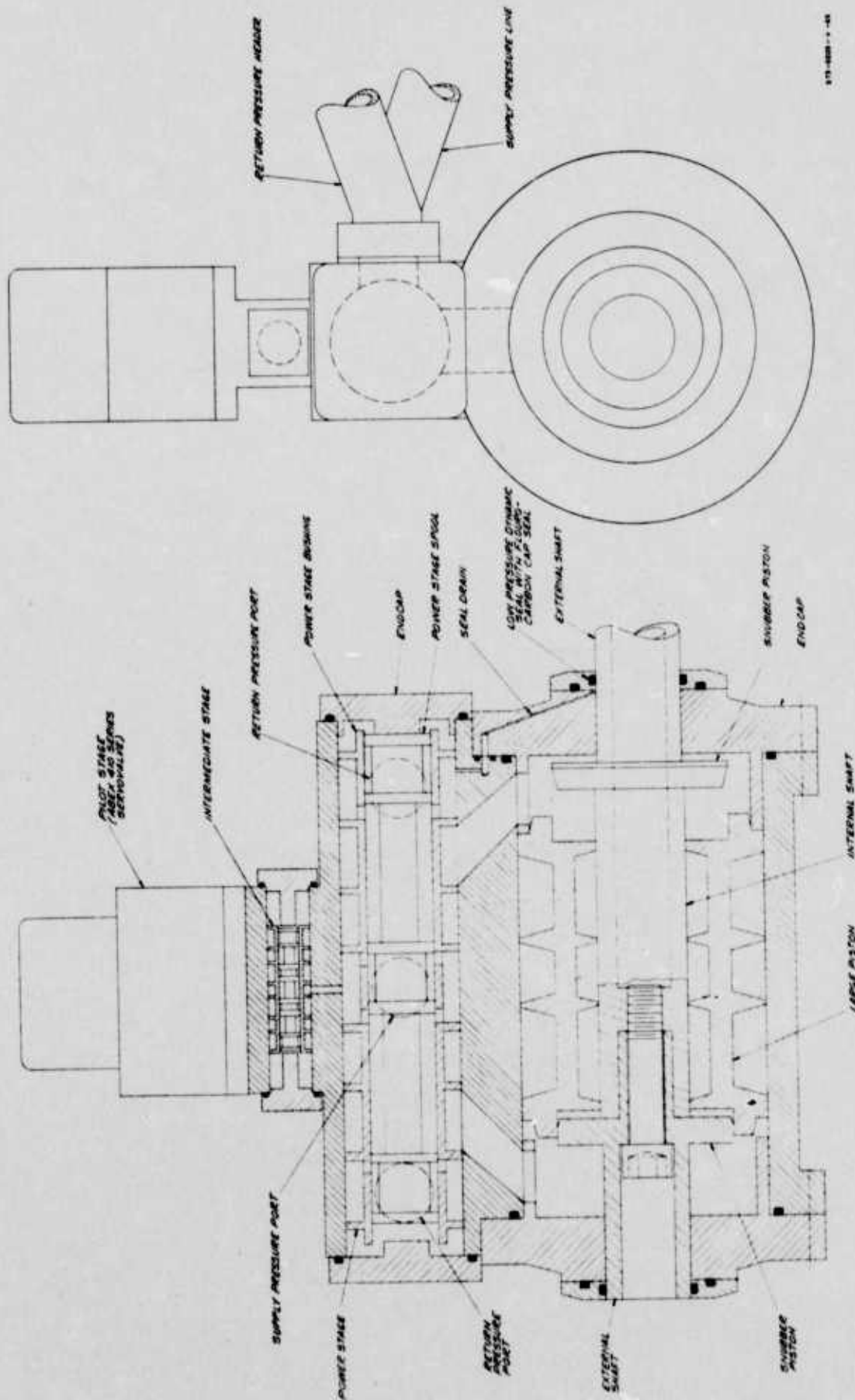
Figure 21. Short Pulse Switch Hydraulic Actuator.

75

this separation in the required time is in the order of 15,000 lbs. The

application of these two widely different force levels is achieved in a

binary switching valve-actuator by using a staged actuation piston. The

400 lb force piston is carried inside the 15,000 lbs force piston. There are

"squish" volumes at all ends of piston travel to minimize shock loading. The

"squish" volume is obtained by configuring the pistons so that a volume of

fluid is trapped and pumped through a leakage path as the piston nears its

end of travel. The damping obtained from this protects the parts as well as

preventing the contactors from flying apart when they close.

The basic advantages of the staged piston arrangement are:

1. Power consumption is minimized since the big piston

   moves only through a short stroke while the small one

   covers most of the travel.

2. A binary-open loop actuator can be used. A rise time

   of 2 millisec implies a closed loop bandwidth of the

   order of 1000 rad/sec. There are many spool valve

   instability problems encountered over that frequency

   range. The bad effects on performance are avoided

   completely by an open loop system.

3. Electrode wear compensation is easily built into

   the arrangement.

The disadvantages of additional sealing and complexity due to the

presence of the extra piston are not significant. The sealing problems are

minimized through the use of clearance seals in the piston. That is: the

parts are matched to a very close tolerance so that leakage is minimal and

no elastomer is required. This is a technique which has been proven over

the past 20 years. There is additional complexity for manufacture; however,

all the surfaces to be close matched are cylindrical and the machining pro-

blems are straightforward. Precision actuators and spool valves of this

type have been mass produced for airborne hydraulic systems for over 20 years.

Schematics of the valve-actuator are shown in Figure 21.

22. The materials to be used are yet to be chosen. For the actuator and

spool valves, a hard, stable material like tool steel is most desirable from

a machining standpoint; however, a hard stainless steel such as 440C stain-

less may be needed for corrosion resistance. The impact characteristics must

also be considered in the choice. The weight estimate of 15 lb (per Appendix

C-5.2) is based on the assumption that the entire valve-actuator assembly is

steel. This permits the bushings of the intermediate and power stages to be

installed with no internal elastomer seals. The seal is obtained by an

interference fit between the bushing and the housing. An alternative

method is to use aluminum for the housing and use internal static seals.

This alternative method permits a lighter weight design. Thus the 15 lb

based on a steel housing is pessimistic.

3.3.3.2 Design and Analysis of The Actuation Mechanism

A design and analysis of the actuation mechanism was performed.

The design information is shown in Appendices C1 and C2. The analysis by

digital computation is shown in Appendices C3 and C4 for an actuator opera-

ting at 5 pulses per second and also at 20 pulses per second.

The design was based on incompressible flow with an additional

lag time added to account for compressibility. This is only an approximation

but the results corresponded reasonably well to the detailed analysis which

included compressibility effects. The switch opening time is the Δt be-

78

PILOT
STAGE

INTERMEDIATE
STAGE

POWER
STAGE

S73-0203-/A-1
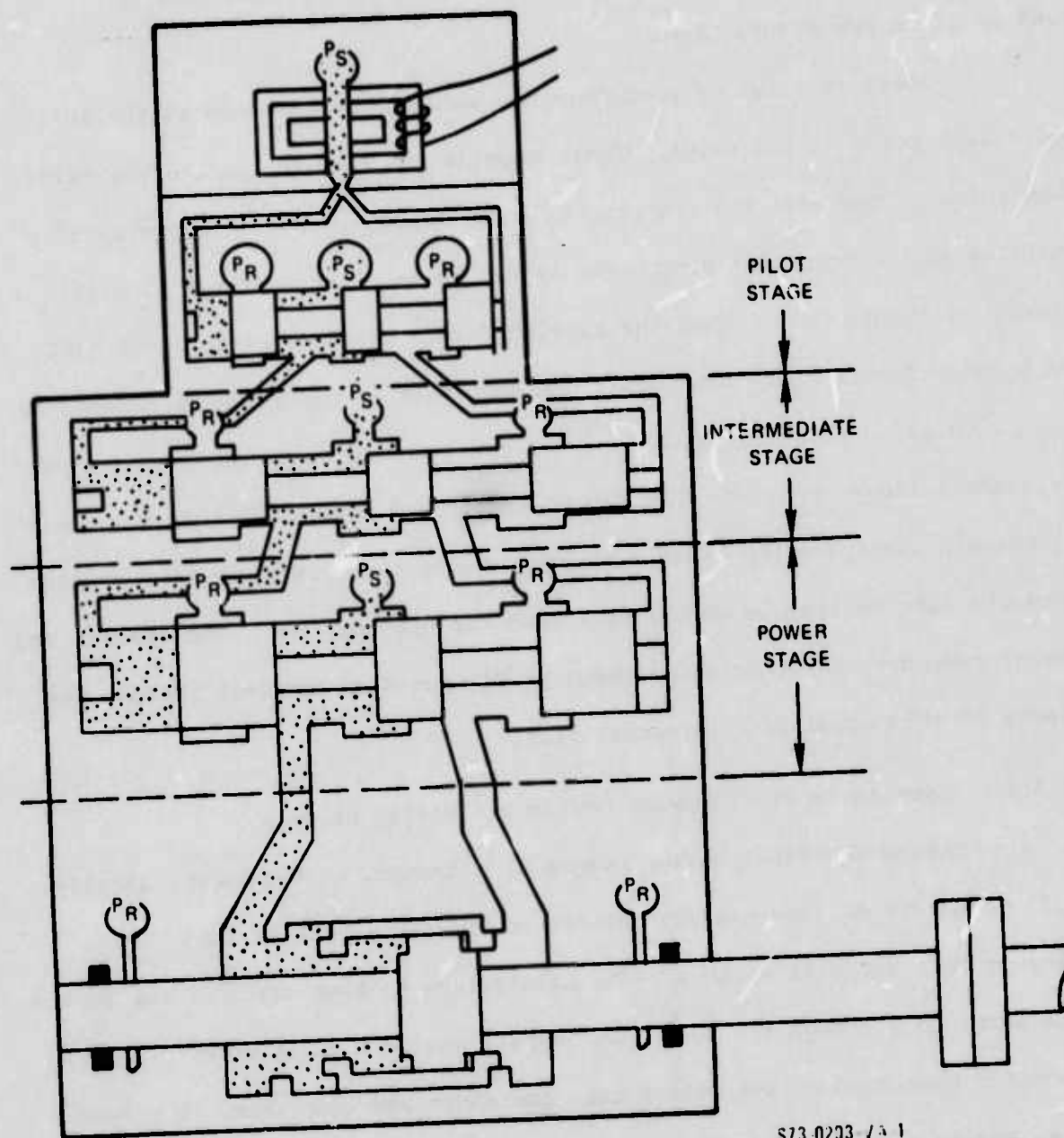
Figure 22.   Detailed Schematic of Hydraulic Actuator (Switch Shown Closed).

79

ginning when the power spool crosses center and ending when the small piston
(which is connected to the contact) clears .5". The opening time is
1.85 millisec per Figure C-10.

There is a set of high response accumulators located at the inlet
and outlet ports of the valve. These provide the flow to operate the valve
each pulse. They have the property that the supply pressure is continually
dropping as the actuation progresses as can be seen in the first 10 milli-
seconds of Figure C-18. Thus the closing forces are reduced to about half
the opening forces since the supply pressure seen by the valve is reduced to
about 2500 psi. This is favorable since the lower closing forces will reduce
the overall impact problems when the contacts meet and insure that the squish
volumes can dissipate the kinetic energy. There is no response time problem
since the closing time is much longer than the opening time. The opening and
closing response characteristics shown in Figures C-10 and C-11 include the
effects of this accumulator pressure drop.

3.3.3.3   Comments On The Hardware Design and Design Process

During the final design stages of a system, some changes, usually
small, occur due to problems encountered in the mechanical design. The
policy on this job will be to use the simulations to keep track of any impact
on performance a change may have. An overall analog simulation will be used
to monitor operation of the switch over the short and long term. The feed
system analog simulator is already operational.

Since the rate of stress application is high, the impact properties
of available materials will be carefully considered in the final design. The
simulations will be expanded in the detail of the trapped fluid volumes to
provide accurate structural loading information. The rapid motions

80

of this mechanism will generate considerable acoustical noise and this area will be examined to insure that the noise is minimized to make the lab environment as comfortable as possible.

The high response accumulator design will exploit the knowledge gained in the bellows design. Each accumulator will consist of a radial arrangement of bellows in a cylinder. Each bellows will contain a trapped volume of gas. The high response is obtained since the bellows have little mass and there is little fluid restriction through the accumulator.

In summary, the design effort will be a closely controlled effort exploiting the latest techniques available. The hardware details will be incorporated into an overall analog simulation to insure the performance requirements are met for both short and long bursts of pulsing the switch.

3.3.3.4 Conclusions

A satisfactory hydraulic actuation mechanism can be built and used in this application. The conclusions of this Phase I effort with regard to the actuation mechanism are:

1) Opening time requirements can be met.

2) Simplicity of design is achieved using basic, widely employed types of hydraulic components and techniques. This insures high reliability.

3) The contact acceleration force (15,000 lbs) and the contact holding forces (400 lbs) can be adjusted to considerably different values during the design phase with no significant impact on cost or schedule.

4) The damping required to minimize impact forces and prevent rebound of the contacts can be easily incorporated in this design.

81

5) Allowance for contact wear is easily attained.

6) The actuation mechanism will be small and light weight.

7) The mechanism uses a minimum of hydraulic power to
    complete the task. The use of two pistons with two
    different strokes permits optimum distribution of
    energy into acceleration and displacement of the
    contacts.

8) In an airborne application, aircraft hydraulic power
    operating a hydraulic transformer can be used to
    operate the actuation mechanism.

9) The actuation unit can operate at the high electrical
    potential, and the hydraulic power supply at ground
    potential. The insulation is attained by a length
    of hydraulic hose.

10) The supply pressure will be 9500 psi and the return
    pressure 100 psi. The flow rate is 48 cis at 20 pps.
    The leakage flows add approximately another 2 cis.
    Thus approximately 34 hydraulic horsepower are needed.

APPENDIX A

TIME DEPENDENT HEAT FLOW ANALYSIS OF THE ELECTRODES

A.1   Statement of The Problem and Boundary Values

This appendix summarizes the work that was necessary to determine the temperature of the electrodes of the switch as a function of time and position with and without cooling the anode. The bulk of our discussion concerns the solid (uncooled) electrodes in which case the temperature was determined for 300 cycles of operation of the switch. The alterations necessary to include cooling in the analysis appear later in the appendix.

The idea was to solve the heat equation in the electrodes for the following three distinct cases which, collectively, constitute one cycle of operation of the switch.

Case (1): $0 \leq$ time ≤ 190 msecs

The electrodes are in contact and current is flowing according to the rule $I(t) = (2 \times 10^4 \text{ amps}) t/.19$ secs.

Case (2): 190 msecs $\leq$ time ≤ 192 msecs

The electrodes are separated and an arc is sustained at the peak current of 2×10^4 amps. The arc voltage is assumed to be 40 volts.

Case (3): 192 msecs $<$ time ≤ 200 msecs

The electrodes remain separated and the current is zero.

The general expression for the heat equation is

$$c \rho \frac{\partial u}{\partial t} = \nabla \cdot (k \nabla u) + S(u) \tag{A.1}$$

where u is temperature, and S is a heat generation term. When cylindrical symmetry is imposed, Eq. (A.1) becomes

$$c \rho \frac{\partial u}{\partial t} = \frac{\partial k}{\partial r} \frac{\partial u}{\partial r} + \frac{\partial k}{\partial Z} \frac{\partial u}{\partial Z} + \frac{k}{r} \frac{\partial u}{\partial r} \left(r \frac{\partial u}{\partial r} \right) + k \frac{\partial^2 u}{\partial_Z^2} + S(u). \tag{A.2}$$

We solve this equation where the thermal conductivity k is considered radially constant. The detailed equations with boundary conditions as we have solved them are listed next.

$$C_i(u) \rho_i \frac{\partial u}{\partial t}$$

$$= \frac{\partial k_i}{\partial Z} \frac{\partial u}{\partial Z} + k_i(u) \left(\frac{1}{r} \frac{\partial u}{\partial r} + \frac{\partial^2 u}{\partial_r^2} \right) + \frac{\partial^2 u}{\partial_Z^2} + S_i(u) \tag{A.3}_i$$

where i = 1 refers to the plate in the sketch below and i = Z labels the rod.

Eq. $(A.3)_1$ is solved in the domain

$$D_1 = \left\{ (r,Z,t) : 0 \le r \le r_1, 0 \le Z \le a, t \ge 0 \right\}$$

and Eq. $(A.3)_2$ in the domain

$$D_2 = \left\{ (r,Z,t) : 0 \le r \le r_2, a \le Z \le b, t \ge 0 \right\} .$$

$$\left. \begin{array}{l} u(r,Z,0) = f_1(r,Z) \quad (0 \le r \le r_1, 0 \le Z \le a) \\[2mm] u(r,Z,0) = f_2(r,Z) \quad (0 \le r \le r_2, a \le Z \le b) \end{array} \right\}$$
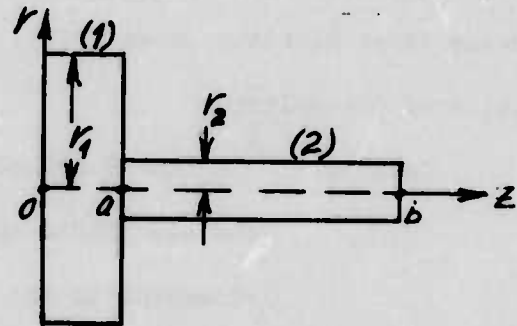
(Initial Conditions) (A.4)

$$\left. \begin{array}{l} u(r,a-,t) = u(r,a+,t) \qquad (0 \le r \le r_2, t \ge 0) \\[3mm] k_1 \dfrac{\partial u(r,a-,t)}{\partial Z} = k_2 \dfrac{\partial u(r,a+,t)}{\partial Z} \quad (0 \le r \le r_2, t \ge 0) \end{array} \right\}$$

(Connecting Relations at the Interface between Regions (1) and (2)) (A.5)

$$\frac{\partial u(r_1,Z,t)}{\partial r} = 0 \qquad (0\leq Z \leq a, t\geq 0)$$

$$\frac{\partial u(r,a,t)}{\partial Z} = 0 \qquad (r_2 \leq r \leq r_1, t\geq 0)$$

(Insulating Boundary Conditions) (A.6)

$$\frac{\partial u(r_2,Z,t)}{\partial r} = 0 \qquad (a\leq Z \leq b, t\geq 0)$$

$$u(r,b,t) = u_0 \quad (0\leq r \leq r_2, t\geq 0) \qquad \text{(End Condition)} \qquad (A.7)$$

Conditions at Electrode Faces:

(ε indexes the electrode: $\varepsilon = 1$ corresponds to the anode and $\varepsilon = 2$ to the cathode. This index frequently appears as a superscript.)

Case (1): ($0\leq t \leq .19$ secs.)

$$-k_1^\varepsilon \frac{\partial u}{\partial Z} = q^\varepsilon$$

where

$$q^\varepsilon = \frac{I^2(t)R_C}{\text{Area}} \cdot \left\{ \frac{(2-\varepsilon)u^{3-\varepsilon}}{u^\varepsilon + u^{3-\varepsilon}} + \frac{(\varepsilon - Du^\varepsilon)}{u^\varepsilon + u^{3-\varepsilon}} \right\} - \left(\frac{k_1^\varepsilon}{2} \frac{\partial u^\varepsilon}{\partial Z} + \frac{k_1^{3-\varepsilon}}{2} \frac{\partial u^{3-\varepsilon}}{\partial Z} \right) \qquad (A.6)$$

It is assumed that the anode lies on the positive side of the Z-axis; the convention u^ε means $u^1 = u(r,0+,t)$ and $u^2 = u(r,0-,t)$. R_C is contact resistance between the electrodes when they are closed.

Case (2): ($.19$ secs $\leq t \leq .192$ secs)

$$-k_1^1 \frac{\partial u^1}{\partial Z} = q^1, \quad \frac{\partial u^2}{\partial Z} = 0$$

where $q^1 = J(t) \cdot \Delta V = \dfrac{I(t)\Delta V}{\text{Area}}$ (A.7)

and ΔV represents the arc potential.

Case (3): ($.192 < $ secs $< t \leq .2$ secs)

$$\frac{\partial u}{\partial Z} = 0.$$

Some general comments on the boundary and initial conditions are in order. The term $S_i(u)$ in Eq. (A.3)$_i$ accounts for heating the electrodes by current flow. For Cases (1) and (2) its values is $J_i^2(r,Z,t)/k_{e,i}$ where $k_{e,i}$ is the electrical conductivity of material i. S_i is zero for Case (3). The initial conditions in the first cycle are specified by $f_1 = f_2 = u_0$ where $u_0 = 300^\circ K$; in each succeeding cycle f_1 and f_2 are defined by the temperature field determined by the previous cycle. Cooling by radiative transfer has a negligible effect on the temperature field, and this fact justifies our use of insulating boundary conditions. The time rate of energy per unit area that flows into a medium is given by q. In Eq.(A.6) q is represented by two terms; the first term expresses heating caused by the presence of contact resistance and the factor enclosed in curly buckets weights the flow of this heat into the electrodes in a fashion that depends on the electrode temperatures. The second term in Eq.(A.6) accounts for heat flow between electrodes when they are in contact in the first case of each cycle. Initially this term is zero but in succeeding cycles the anode becomes hotter than the cathode and a net flow of heat occurs between the electrodes, and this term becomes increasingly important. The expression for q in Eq.(A.7) is by far the largest source of heat in the system. It has been expressed in terms of electron flow; Eq.(A.7) express the heat input to the anode caused by a stream of electrons of current density J that give up their energy at the anode surface. There is some ion flow when the arc is sustained but that effect has been neglected here.

The thermal quantities and transport coefficients are considered temperature dependent. The cgs systems of units has been employed in the calculations, and temperatures are expressed in $^\circ K$. The plate thicknesses are

86

1 inch each and their diameters are 4 inches. The rod diameters are 1 inch
each and their lengths are 10 inches. Both electrode plates are assumed to
be CLR and the rods are copper. These dimensions are simply input parameters
in the computer programs, and these programs can accommodate four distinct
materials for electrode plates and rods.

For the sake of computational convenience all the quantities in-
volved have been recast in dimensionless form. To do this we use $\langle \dot{g}_0 \rangle$ to
represent the mean $(g_0(CLR)+g_0(Cu))/2$ of a physical quantity g whose value
at room temperature is g_0. X_0 is a characteristic distance taken to be
.04 cm in these calculations; u_0 is $300^\circ K$. The transformations are

$$ t = \frac{\langle k_0 \rangle}{\langle c_0 \rangle \langle \rho_0 \rangle x_0^2} \, t, $$

$$ \zeta = Z/X_0 $$

and

$$ \xi = r/X_0. $$

The functional form of specific heat and thermal conductivity are, respec-
tively, expressed as $\mathcal{T}$ and K. Dimensionless temperature is w.

A.2   Numerical Analysis

It was supposed that temperature variations along the axial direc-
tion would be more rapid than in the radial direction. For this reason an
implicit-type finite difference method was applied in the Z-direction and an
explicit-type was reserved for the radial displacements in an attempt to
solve the heat equation. The difference equation in dimensionless variables
is given as

$$\mathcal{T}_\mu \frac{(w_{i,j,n}) \ (i-1)\Delta\xi}{\Delta} \ [w_{i,j,n+1} - w_{i,j,n}]$$

$$= \frac{\Delta\xi(i-1)}{(\Delta\zeta_\mu)^2} \left\{ K_\mu(w_{i,j+1,n}) - K_\mu(w_{i,j,n}) \right\} \ [w_{i,j+1,n+1} - w_{i,j,n+1}]$$

$$+ \frac{K_\mu(w_{i,j,n})}{\Delta\xi} \ [w_{i+1,j,n} - w_{i,j,n}]$$

$$+ \frac{(i-1)K_\mu(w_{i,j,n})}{\Delta\xi} \ [w_{i-1,j,n} - 2w_{i,j,n} + w_{i+1,j,n}]$$

$$+ \frac{(i-1)\Delta\xi K_\mu(w_{i,j,n})}{(\Delta\zeta_\mu)^2} \ [w_{i,j-1,n+1} - 2w_{i,j,n+1} + w_{i,j+1,n+1}]$$

$$+ \overline{S}_\mu(w_{i,j,n}) \ (i-1)\Delta\xi. \tag{A.8}$$

In this equation μ indexes the medium (1) or (2) and $\overline{S}_\mu$ is the dimensionless counterpart of S_μ. The radial and axial displacements are indexed by i and j, respectively; n indexes the time increment. Eqs. (A.8) must be solved for $w_{i,j-1,n+1}$, $w_{i,j+1,n+1}$, and $w_{i,j,n+1}$. The coefficients of these quantities are listed in the tridiagonal matrix on the next page.

$$
\begin{bmatrix} \cdots V_{i,j} \cdots \end{bmatrix} = \begin{bmatrix} \cdots W_{i,j} \cdots \end{bmatrix} \begin{bmatrix} \ddots & & \\ & [C] & \\ & & \ddots \end{bmatrix}
$$

(A.9)

A-7

Eq. (A.9) has been solved for each time increment. Non-linearities are introduced into the problem by allowing the thermal properties to be time dependent. This poses no real difficulty as Eqs. (A.8) indicate; these functions are evaluated at the local temperature determined in the previous cycle. Such approximations are plausible because these functions are slowly varying with temperature.

Forward differences have been evaluated throughout this analysis. A typical boundary condition

$$\frac{\partial w}{\partial \zeta}\Big|_a = -G \tag{A.14}$$

has been incorporated as follows: Expanding the temperature about "a",
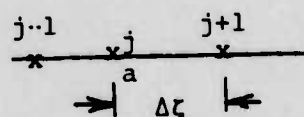
$$w(\zeta) = w(a) + \frac{\partial w}{\partial \zeta}\Big|_a \cdot \Delta \zeta$$

$$+ \frac{1}{2}\frac{\partial^2 w}{\partial \zeta 2}\Big|_a \cdot (\Delta \zeta)^2 + 0\ ((\Delta \zeta)^3)$$

$$\frac{\partial^2 w}{\partial \zeta^2}\Big|_a = \frac{2}{(\Delta \zeta)^2}\ [w(\zeta) - w(a) + G\ \Delta \zeta] + 0\ (\Delta \zeta) \tag{A.15}$$

Eq. (A.15) replaces the next to the last term in Eqs. (A.8); when it was appropriate the first differences in Eqs. (A.8) were replaced by -G. Similar expressions to these were used for boundary conditions expressed by radial derivatives.

The modus operandi for numerical calculations follows: The first time interval (Case (1)) is divided into 20 equal intervals of length $\Delta t_1 = 9.5$ msecs each. In the remaining time intervals increments of length

90

$\Delta t_2 = 1$ msec each Δt_2 are used. After time Δt_1 the initial temperature u_0 is used and Eq. (A.9) is solved for the temperature mesh on the anode. Maintaining the use of u_0, a similar temperature calculation is performed for the cathode. In the next time interval the initial temperature field is now replaced by the one just computed. The calculation proceeds in this fashion to determine the temperature field after a given number of cycles. For a time interval n (n≤20), the rms current given by

$$I_{rms}(n) = \frac{I_{max} \Delta t_1}{.19} \left(\frac{3n^2 - 3n + 1}{3} \right)^{1/2} \tag{A.16}$$

is used in the calculation.

In the study of solid electrodes a mesh, as indicated in Figure A-2, is used where JM = 21, JM2 = 31, IM2 = 3 and IM = 9. The x's in this figure indicate the reference points for temperatures appearing in Tables A-1 through A-12. Also Figure A-3 illustrates how the maximum temperature of the electrodes vary with the number of cycles for 0 to 300 cycles.

An important phase of the calculation for solid electrodes was checked against a justifiable theoretical result. From Carslaw and Yeager's text (Conduction of Heat In Solids, Oxford, 1959), page 75, the temperature at the surface of a semi-infinite solid is

$$u(t) = \frac{2J\Delta V}{k} \left(\frac{\alpha t}{\P} \right)^{1/2} + u_0 \tag{A.17}$$

where k is the medium's thermal conductivity, α is its diffusivity and u_0 its initial temperature. This equation supposes the material to be subject to a constant flux of power $J\Delta V$ for t secs. Our machine program was compared to this result for the following case. Assuming the electrode is copper, the temperature of the surface element of thickness $\Delta \zeta$ is determined in a time $\Delta t = 2$ msec. Similarly, the temperatures of surface elements were com-

puted for element thickness of $2\Delta\zeta/3$, $\Delta\zeta/2$ and $2\Delta\zeta/5$. A second degree least square fit of temperature vs. incremental thickness was established and extrapolated to thickness 0. The temperature at that point was $434.1^{\circ}K$ where $J = 2x10^4$ amp/$(2.54)^2$ cm^2 and $\Delta V = 40$ volts. For these physical parameters Eq. (A.17) gives the value $u(\Delta t) = 435.6^{\circ}K$.

The mesh of points for which the cooled anode calculations were performed appears in Figure A-4. In this calculation the integers used to define the mesh sizes are

$$(IM,IM2,JM,JM2) = (17,5,21,31) \tag{A.18}$$

and the indices used to determine the interface between solid and liquid media are

$$(IF1,IF2,JF1,JF2) = (3,15,6,16). \tag{A.19}$$

The x's in Figure A-4 indicate the positions for which temperature are tabulated in Tables A-13 through A-17. The heat flow across the interface between solid and coolant is determined by

$$-k \frac{\partial u}{\partial n} = h (u-u_f) \tag{A.20}$$

where u_f is fluid temperature, h is the heat transfer coefficient, k is the thermal conductivity of the solid medium and $\partial/\partial n$ indicates a normal derivitive. Eq. (A.20) was used in the nth time increment where u indicates the temperature in the $(n-1)^{th}$ time increment for a specific coordinate (i,j). The increase in fluid temperature was estimated at the end of each cycle. If $t = .2$ secs, the length of a cycle, the temperature change of the fluid is given by

$$\Delta u_f = (\rho_f C_f v_f)^{-1} [t \cdot h \sum_{k} (u_k - u_f^o) \Delta a_k - H_C] \tag{A.21}$$

where $H = t \cdot h \sum_{k}(u_k - u_f^o)\, \Delta a_k$ was the heat added to the fluid inside the

metal; the sum in this expression involves

a local temperature assumed to be reasonably

constant over an area Δa_k.
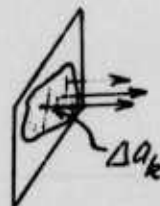
The areas used in this calculation are indicated in Figure A-4 by (1), (2),

(3) and (4). Two calculations were performed for $H = H_c$. We have included

in Tables A-13 through A-17 the physically more interesting case where

$H_c = 0$, for a system with one gallon of coolant.

The curves in Figure A-5 illustrate the maximum temperatures for

cooled and uncooled anodes as functions of the number of cycles of operation.

The curve for the cooled anode was quadratically fit in the region of 20 to

50 cycles and this result was extrapolated (dashed curve) to 300 cycles using

a (1,1) Pade' approximant. This extrapolation can be justified reasonably

well from a physical standpoint.

The main programs for these calculations are listed at the end of

this section. SW2 refers to the calculations for solid electrodes and

SWFLOW to those for a cooled anode. A program flow chart appears on the next

page. Each tape in this procedure contains the I's and J's depicting mesh

sizes, overall electrode dimensions, maximum temperatures, and complete tem-

perature fields for the anode and the cathode. SWITCHIN is a short program

used to define an initial data tape, and EHJPLOT (or FLWPLOT in the cooled

electrode case) is used to plot the results appearing in the tables at the

end of this section.

93

PROGRAM FLOW
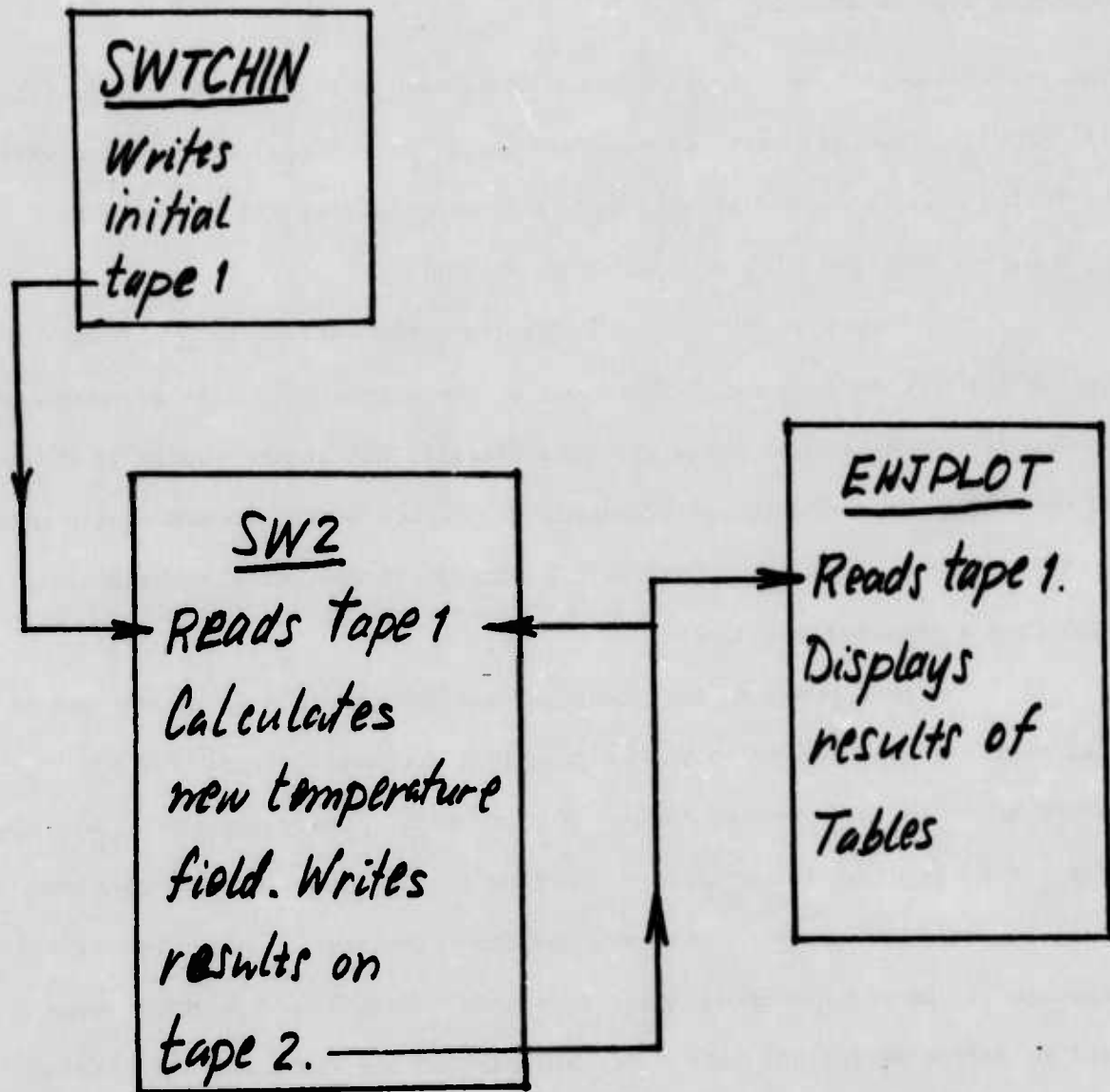
Figure A-1

Figure A-2

Figure A-3

700

600

500

400

300

°K

max. temp. of anode

max. temp. of cathode

0   100   200   300

no. of cycles

96
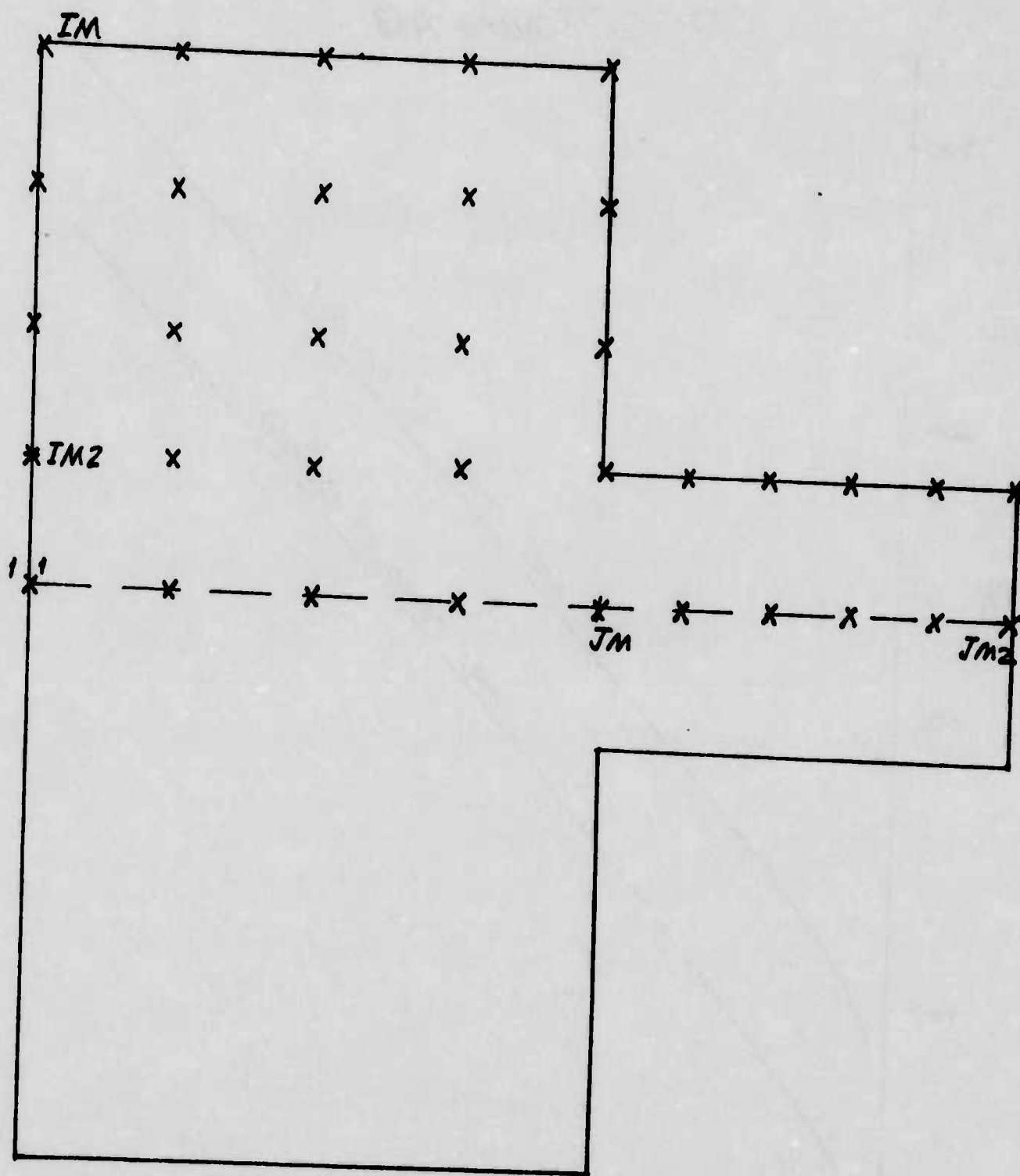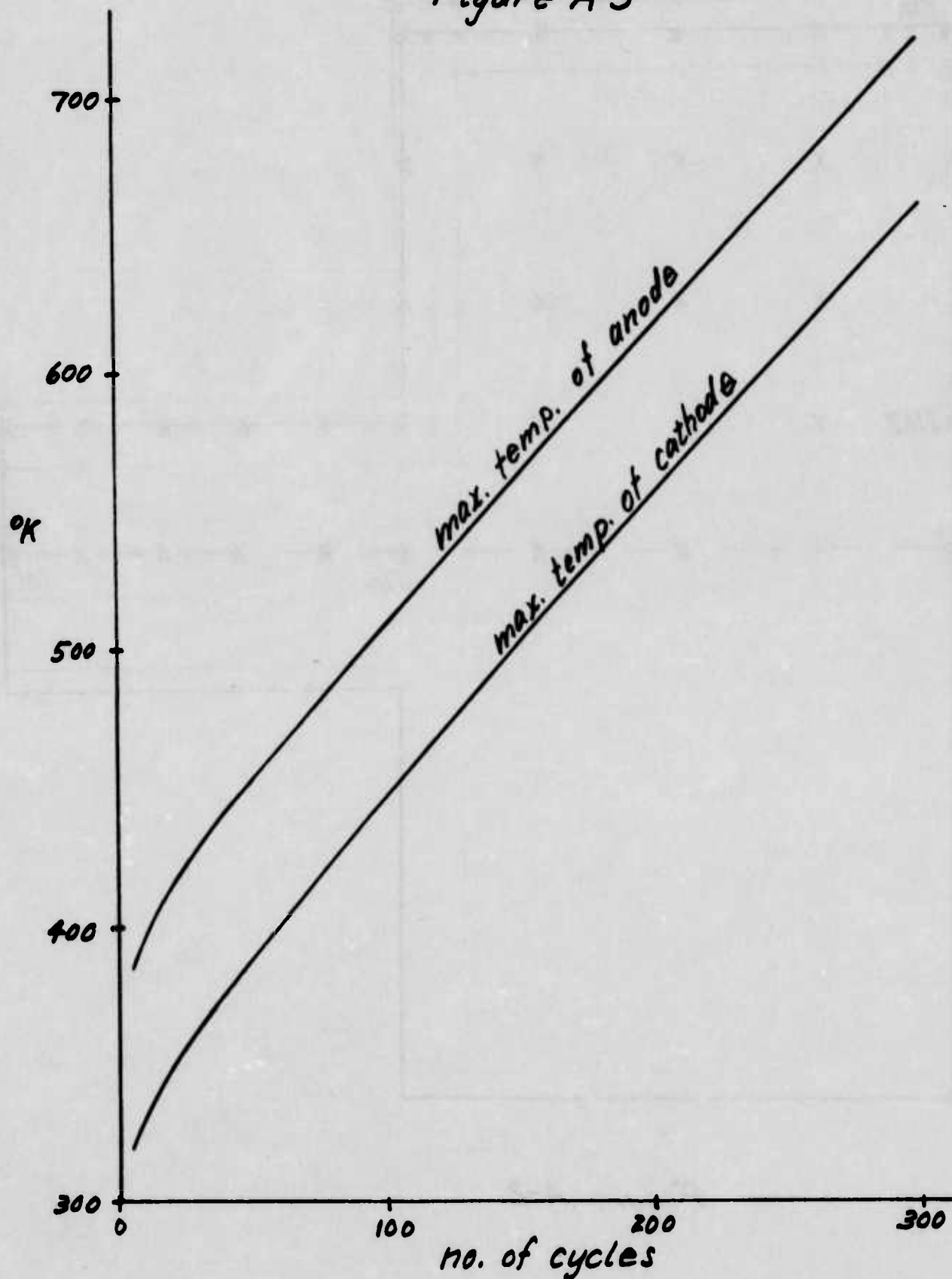
Figure A-4

Figure A-5

98

```
SWITCH DIMENSIONS FOLLOW
PLATE AND ROD RADII (CMS)=    5.08    1.27
PLATE THICKNESS AND ROD LENGTH (CMS)=    2.54  25.40
NUMBER OF CYCLES IS    5
PLATE TEMPS LISTED NEXT FOR
THE ANODE
MAX ANODE TEMP IS    384.0
        384.0        310.3        302.1        300.3        300.1
        384.0        310.3        302.1        300.3        300.1
        384.0        310.3        302.1        300.3        300.1
        384.0        310.3        302.2        300.5        300.9
        384.0        310.3        302.2        300.6        301.2

ROD TEMPS LISTED NEXT FOR
THE ANODE
        300.9        302.4        302.4        302.4        302.4        300.0
        301.2        302.4        302.4        302.4        302.4        300.0


PLATE TEMPS LISTED NEXT FOR
THE CATHODE
MAX CATHODE TEMP IS    318.2
        318.2        306.6        301.2        300.2        300.1
        318.2        306.6        301.2        300.2        300.1
        318.2        306.6        301.2        300.2        300.1
        318.2        306.6        301.2        300.4        300.9
        318.2        306.6        301.3        300.4        301.2

ROD TEMPS LISTED NEXT FOR
THE CATHODE
        300.9        302.4        302.4        302.4        302.4        300.0
        301.2        302.4        302.4        302.4        302.4        300.0
```

Table A-1

99

```
SWITCH DIMENSIONS FOLLOW
PLATE AND ROD RADII (CMS)=    5.08   1.27
PLATE THICKNESS AND ROD LENGTH (CMS)=   2.54   25.40
NUMBER OF CYCLES IS   10
PLATE TEMPS LISTED NEXT FOR
THE ANODE
MAX ANODE TEMP IS    396.7
        396.7      321.5      308.3      302.7      301.3
        396.7      321.5      308.3      302.7      301.3
        396.7      321.5      308.3      302.8      301.4
        396.7      321.5      308.4      303.0      302.1
        396.7      321.5      308.4      303.1      302.3

ROD TEMPS LISTED NEXT FOR
THE ANODE
        302.1      304.8      304.9      304.9      304.8      300.0
        302.3      304.8      304.9      304.9      304.8      300.0


PLATE TEMPS LISTED NEXT FOR
THE CATHODE
MAX CATHODE TEMP IS    330.7
        330.7      315.8      305.7      301.8      300.8
        330.7      315.8      305.7      301.8      300.8
        330.7      315.8      305.8      301.8      300.9
        330.7      315.8      305.9      302.1      301.8
        330.7      315.9      305.9      302.3      302.1

ROD TEMPS LISTED NEXT FOR
THE CATHODE
        301.8      304.8      304.9      304.9      304.8      300.0
        302.1      304.8      304.9      304.9      304.8      300.0
```

Table A-2

```
SWITCH DIMENSIONS FOLLOW
PLATE AND ROD RADII (CMS)=   5.08    1.27
PLATE THICKNESS AND ROD LENGTH (CMS)=   2.54   25.40
NUMBER OF CYCLES IS   15
PLATE TEMPS LISTED NEXT FOR
THE ANODE
MAX ANODE TEMP IS    406.3
      406.2      330.5     314.8     306.9      304.5
      406.2      330.5     314.8     306.9      304.5
      406.3      330.5     314.9     306.9      304.6
      406.3      330.5     315.0     307.1      304.7
      406.3      330.6     315.0     307.1      304.7

ROD TEMPS LISTED NEXT FOR
THE ANODE
      304.7      307.2     307.3     307.3      307.1     300.0
      304.7      307.2     307.3     307.3      307.1     300.0


PLATE TEMPS LISTED NEXT FOR
THE CATHODE
MAX CATHODE TEMP IS    340.3
      340.2      323.8     311.1     304.9      303.1
      340.2      323.9     311.1     304.9      303.1
      340.3      323.9     311.2     305.0      303.2
      340.3      323.9     311.3     305.3      303.7
      340.3      323.9     311.3     305.4      303.9

ROD TEMPS LISTED NEXT FOR
THE CATHODE
      303.7      307.2     307.3     307.3      307.1     300.0
      303.9      307.2     307.3     307.3      307.1     300.0
```

Table A-3

101

SWITCH DIMENSIONS FOLLOW
PLATE AND ROD RADII (CMS)=   5.08   1.27
PLATE THICKNESS AND ROD LENGTH (CMS)=   2.54 25.40
NUMBER OF CYCLES IS 20
PLATE TEMPS LISTED NEXT FOR
THE ANODE
MAX ANODE TEMP IS   414.3

414.2	338.3	321.3	312.0	309.0
414.3	338.3	321.4	312.0	309.0
414.3	338.3	321.4	312.0	309.1
414.3	338.4	321.4	312.0	308.6
414.3	338.4	321.4	311.9	308.4

ROD TEMPS LISTED NEXT FOR
THE ANODE

308.6	309.5	309.7	309.7	309.3	300.0
308.4	309.5	309.7	309.7	309.3	300.0

PLATE TEMPS LISTED NEXT FOR
THE CATHODE
MAX CATHODE TEMP IS   348.4

348.3	331.0	316.7	309.0	306.7
348.3	331.0	316.7	309.1	306.7
348.3	331.1	316.8	309.1	306.8
348.4	331.1	316.9	309.2	306.8
348.4	331.2	316.9	309.3	306.8

ROD TEMPS LISTED NEXT FOR
THE CATHODE

306.8	309.5	309.7	309.7	309.3	300.0
306.8	309.5	309.7	309.7	309.3	300.0

Table A-4

```
SWITCH DIMENSIONS FOLLOW
PLATE AND ROD RADII (CMS)=   5.08    1.27
PLATE THICKNESS AND ROD LENGTH (CMS)=    2.54  25.40
NUMBER OF CYCLES IS   30
PLATE TEMPS LISTED NEXT FOR
THE ANODE
MAX ANODE TEMP IS    428.1
      428.0      352.2      334.1      323.6      320.1
      428.1      352.2      334.1      323.6      320.1
      428.1      352.2      334.1      323.5      320.0
      428.1      352.2      334.0      323.0      318.6
      428.1      352.2      333.9      322.8      318.0

ROD TEMPS LISTED NEXT FOR
THE ANODE
      318.6      314.3      314.5      314.5      313.4      300.0
      318.0      314.3      314.5      314.5      313.4      300.0


PLATE TEMPS LISTED NEXT FOR
THE CATHODE
MAX CATHODE TEMP IS    362.3
      362.2      344.0      328.1      318.9      315.9
      362.3      344.1      328.1      318.9      315.9
      362.3      344.1      328.1      318.9      315.9
      362.3      344.1      328.1      318.7      315.1
      362.3      344.1      328.1      318.6      314.8

ROD TEMPS LISTED NEXT FOR
THE CATHODE
      315.1      314.2      314.5      314.5      313.4      300.0
      314.8      314.2      314.5      314.5      313.4      300.0
```

Table A-5

SWITCH DIMENSIONS FOLLOW
PLATE AND ROD RADII (CMS)= 5.08 1.27
PLATE THICKNESS AND ROD LENGTH (CMS)= 2.54 25.40
NUMBER OF CYCLES IS 40
PLATE TEMPS LISTED NEXT FOR
THE ANODE
MAX ANODE TEMP IS 440.5

440.5	365.0	346.7	335.7	332.1
440.5	365.0	346.6	335.7	332.1
440.5	364.9	346.5	335.5	331.9
440.4	364.8	346.2	334.7	329.7
440.4	364.8	346.1	334.3	328.8

ROD TEMPS LISTED NEXT FOR
THE ANODE

329.7	319.5	319.4	319.3	317.3	300.0
328.8	319.5	319.4	319.3	317.3	300.0

PLATE TEMPS LISTED NEXT FOR
THE CATHODE
MAX CATHODE TEMP IS 374.9

374.9	356.2	339.5	329.7	326.5
374.9	356.2	339.5	329.7	326.5
374.9	356.2	339.5	329.6	326.4
374.8	356.1	339.3	329.1	324.9
374.8	356.1	339.2	328.8	324.3

ROD TEMPS LISTED NEXT FOR
THE CATHODE

324.9	319.1	319.3	319.3	317.3	300.0
324.3	319.1	319.3	319.3	317.3	300.0

Table A-6

SWITCH DIMENSIONS FOLLOW
PLATE AND ROD RADII (CMS)= 5.08 1.27
PLATE THICKNESS AND ROD LENGTH (CMS)= 2.54 25.40
NUMBER OF CYCLES IS 50
PLATE TEMPS LISTED NEXT FOR
THE ANODE
MAX ANODE TEMP IS 452.5

452.5	377.3	359.0	348.0	344.3
452.4	377.3	358.9	347.9	344.3
452.4	377.2	358.7	347.6	343.9
452.2	376.9	358.3	346.5	341.1
452.2	376.9	358.1	346.0	340.1

ROD TEMPS LISTED NEXT FOR
THE ANODE

341.1	325.1	324.2	324.0	320.9	300.0
340.1	325.1	324.2	324.0	320.9	300.0

PLATE TEMPS LISTED NEXT FOR
THE CATHODE
MAX CATHODE TEMP IS 387.0

387.0	368.0	351.0	341.0	337.6
387.0	368.0	351.0	340.9	337.6
386.9	367.9	350.9	340.7	337.3
386.8	367.8	350.5	339.9	335.2
386.7	367.7	350.4	339.5	334.4

ROD TEMPS LISTED NEXT FOR
THE CATHODE

335.2	324.3	324.2	324.0	320.9	300.0
334.4	324.3	324.2	324.0	320.9	300.0

Table A-7
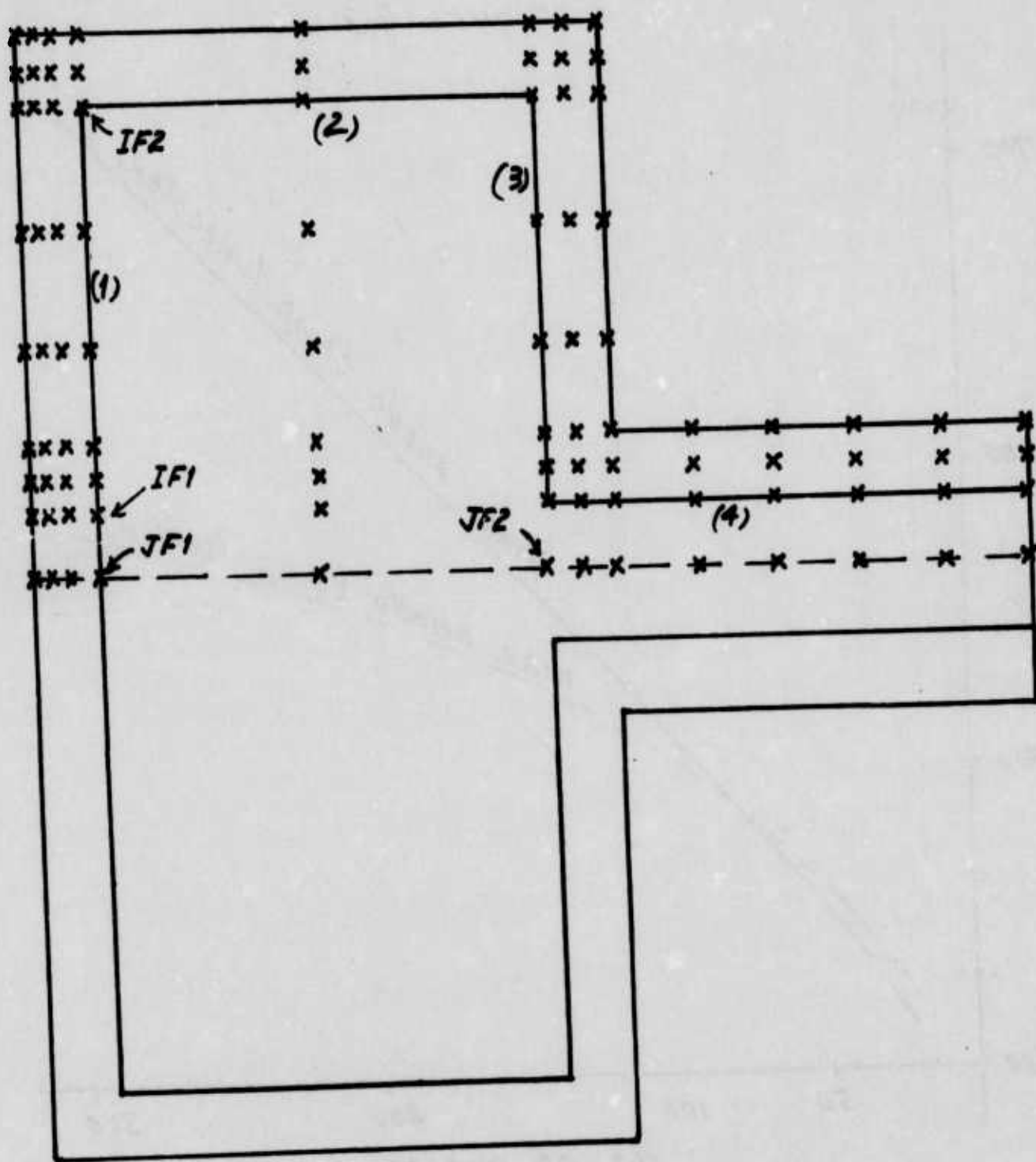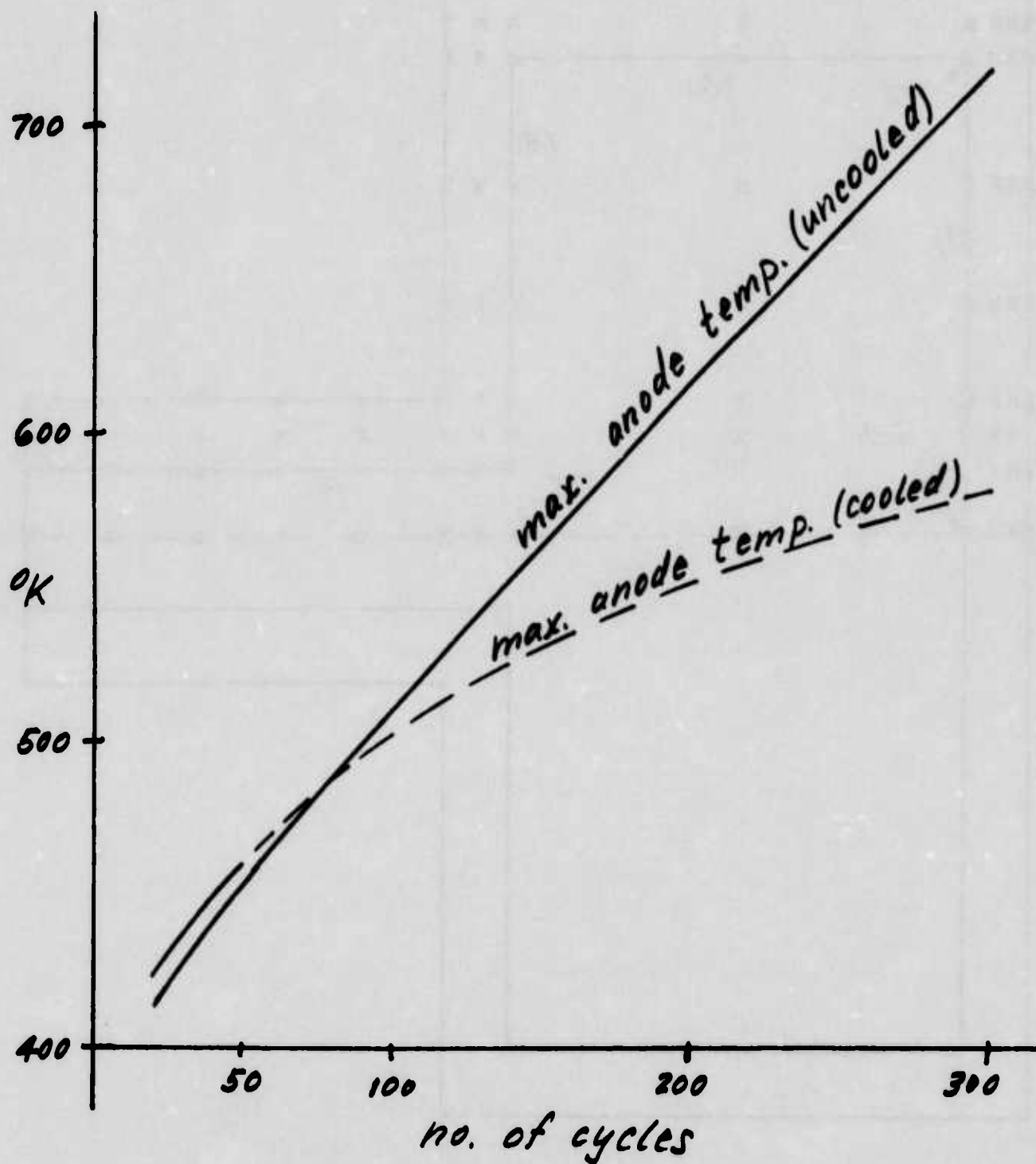
SWITCH DIMENSIONS FOLLOW
PLATE AND ROD RADII (CMS)= 5.08   1.27
PLATE THICKNESS AND ROD LENGTH (CMS)=   2.54   25.40
NUMBER OF CYCLES IS 100
PLATE TEMPS LISTED NEXT FOR
THE ANODE
MAX ANODE TEMP IS   509.6

509.6	436.1	418.1	407.3	403.7
509.5	436.0	417.9	407.1	403.5
509.1	435.6	417.4	406.4	402.7
508.7	435.0	416.4	404.4	398.3
508.6	434.8	416.1	403.7	396.8

ROD TEMPS LISTED NEXT FOR
THE ANODE

398.3	360.6	351.7	348.3	337.5	300.0
396.8	360.6	351.7	348.3	337.5	300.0

PLATE TEMPS LISTED NEXT FOR
THE CATHODE
MAX CATHODE TEMP IS   445.2

445.2	425.6	408.0	397.6	394.1
445.1	425.5	407.9	397.4	393.9
444.7	425.1	407.5	396.8	393.2
444.3	424.6	406.6	395.1	389.4
444.2	424.4	406.3	394.4	388.1

ROD TEMPS LISTED NEXT FOR
THE CATHODE

389.4	357.9	351.1	348.2	337.5	300.0
388.1	357.9	351.1	348.2	337.5	300.0

Table A-8

SWITCH DIMENSIONS FOLLOW
PLATE AND ROD RADII (CMS)= 5.08 1.27
PLATE THICKNESS AND ROD LENGTH (CMS)= 2.54 25.40
NUMBER OF CYCLES IS 150
PLATE TEMPS LISTED NEXT FOR
THE ANODE
MAX ANODE TEMP IS 564.4

564.4	492.2	474.3	463.6	460.1
564.2	492.0	474.1	463.4	459.8
563.8	491.5	473.4	462.5	456.8
563.2	490.8	472.2	460.1	453.6
563.0	490.5	471.8	459.2	451.8

ROD TEMPS LISTED NEXT FOR
THE ANODE

453.6	402.2	382.7	372.3	351.9	300.0
451.8	402.2	382.7	372.3	351.9	300.0

PLATE TEMPS LISTED NEXT FOR
THE CATHODE
MAX CATHODE TEMP IS 501.2

501.2	481.3	463.7	453.1	449.6
501.0	481.2	463.5	452.9	449.4
500.6	480.6	462.8	452.1	448.4
500.0	479.9	461.7	449.9	443.7
499.8	479.7	461.3	449.0	442.0

ROD TEMPS LISTED NEXT FOR
THE CATHODE

443.7	397.8	381.3	372.0	351.8	300.0
442.0	397.8	381.3	372.0	351.8	300.0

Table A-9

SWITCH DIMENSIONS FOLLOW
PLATE AND ROD RADII (CMS)=   5.08   1.27
PLATE THICKNESS AND ROD LENGTH (CMS)=   2.54   25.40
NUMBER OF CYCLES IS 200
PLATE TEMPS LISTED NEXT FOR
THE ANODE
MAX ANODE TEMP IS   617.5

617.5	546.4	528.6	517.9	514.3
617.3	546.2	528.4	517.6	514.1
616.8	545.6	527.6	516.6	512.9
616.1	544.8	526.2	514.0	507.3
615.9	544.5	525.7	513.0	505.3

ROD TEMPS LISTED NEXT FOR
THE ANODE

507.3	446.5	416.6	396.7	365.3	300.0
505.3	446.5	416.6	396.7	365.3	300.0

PLATE TEMPS LISTED NEXT FOR
THE CATHODE
MAX CATHODE TEMP IS   555.4

555.4	535.4	517.7	507.1	503.6
555.2	535.2	517.5	506.9	503.3
554.7	534.6	516.7	505.9	502.2
554.0	533.8	515.4	503.4	497.0
553.8	533.6	515.0	502.5	495.1

ROD TEMPS LISTED NEXT FOR
THE CATHODE

497.0	441.0	414.3	396.0	365.2	300.0
495.1	441.0	414.3	396.0	365.2	300.0

Table A-10

108

SWITCH DIMENSIONS FOLLOW
PLATE AND ROD RADII (CMS)=   5.08   1.27
PLATE THICKNESS AND ROD LENGTH (CMS)=   2.54   25.40
NUMBER OF CYCLES IS 250
PLATE TEMPS LISTED NEXT FOR
THE ANODE
MAX ANODE TEMP IS   669.0

669.0	599.0	581.2	570.5	566.9
668.8	598.8	580.9	570.2	566.6
668.3	598.1	580.1	569.1	565.4
667.6	597.2	578.6	566.4	559.6
667.4	596.9	578.2	565.4	557.6

ROD TEMPS LISTED NEXT FOR
THE ANODE

559.6	492.2	452.4	421.9	378.7	300.0
557.6	492.2	452.4	421.9	378.7	300.0

PLATE TEMPS LISTED NEXT FOR
THE CATHODE
MAX CATHODE TEMP IS   608.0

608.0	587.9	570.2	559.6	556.1
607.8	587.7	570.0	559.4	555.8
607.3	587.1	569.2	558.3	554.6
606.5	586.2	567.8	555.7	549.1
606.3	586.0	567.3	554.7	547.2

ROD TEMPS LISTED NEXT FOR
THE CATHODE

549.1	485.9	449.4	420.7	378.3	300.0
547.2	485.9	449.4	420.7	378.3	300.0

Table A-11

109

```
SWITCH DIMENSIONS FOLLOW
PLATE AND ROD RADII (CMS)=   5.08   1.27
PLATE THICKNESS AND ROD LENGTH (CMS)=   2.54  25.40
NUMBER OF CYCLES IS 300
PLATE TEMPS LISTED NEXT FOR
THE ANODE
MAX ANODE TEMP IS   719.2
        719.2      650.1      632.3      621.6      618.1
        719.0      649.9      632.0      621.3      617.8
        718.4      649.2      631.2      620.2      616.5
        717.7      648.3      629.7      617.5      610.7
        717.5      648.0      629.2      616.4      608.6

ROD TEMPS LISTED NEXT FOR
THE ANODE
        610.7      538.6      489.6      448.0      392.2      300.0
        608.6      538.6      489.6      448.0      392.2      300.0


PLATE TEMPS LISTED NEXT FOR
THE CATHODE
MAX CATHODE TEMP IS   659.3
        659.3      639.0      621.3      610.7      607.2
        659.1      638.8      621.1      610.5      606.9
        658.4      638.2      620.3      609.4      605.7
        657.7      637.3      618.8      606.7      600.1
        657.5      637.0      618.4      605.7      598.1

ROD TEMPS LISTED NEXT FOR
THE CATHODE
        600.1      531.6      485.8      446.2      391.6      300.0
        598.1      531.6      485.8      446.2      391.6      300.0
```

Table A-12

110

SWITCH DIMENSIONS FOLLOW
PLATE AND ROD RADII (CMS)=   5.08   1.27
PLATE THICKNESS AND ROD LENGTH (CMS)=   2.54   25.40
NUMBER OF CYCLES IS   10
PLATE TEMPS LISTED NEXT FOR
THE ANODE
MAX ANODE TEMP IS   402.0
FLUID TEMP=   300.3

398.3	346.9	330.6	323.2	309.5	303.9	303.0	302.6
398.5	347.1	330.9	323.4	309.4	303.8	303.0	302.6
399.1	347.8	331.8	324.0	308.9	303.6	302.8	302.5
401.4	350.5	336.0	331.1	300.3	302.8	302.9	303.0
402.0	351.1	336.7	331.8	300.3	306.6	306.9	307.1
401.9	351.1	336.7	331.7	300.3	313.7	314.0	311.1
401.9	351.1	336.7	331.7	300.3	314.8	314.9	311.1
401.9	351.1	336.6	331.7	300.3	314.4	314.6	310.9
401.9	351.1	336.6	331.7	300.3	300.3	300.3	300.3

ROD TEMPS LISTED NEXT FOR
THE ANODE

311.1	307.9	307.9	307.9	307.8	300.0
311.1	307.9	307.8	307.8	307.7	300.0
310.9	307.8	307.7	307.7	307.6	300.0
300.3	300.3	300.3	300.3	300.3	300.0

PLATE TEMPS LISTED NEXT FOR
THE CATHODE
MAX CATHODE TEMP IS   334.1

331.9	329.8	322.9	316.3	305.9	301.8	301.2	300.8
332.0	329.9	323.0	316.3	305.9	301.8	301.2	300.8
332.3	330.2	323.2	316.4	305.9	301.8	301.2	300.8
333.7	331.4	323.9	316.8	306.0	301.8	301.2	300.8
334.1	331.7	324.1	317.0	306.0	301.9	301.2	300.9
334.1	331.7	324.1	317.0	306.1	302.1	301.5	301.5
334.1	331.7	324.1	317.0	306.1	302.2	301.7	301.8
334.1	331.7	324.1	317.0	306.2	302.2	301.8	301.9
334.1	331.7	324.1	317.0	306.2	302.3	301.8	302.0

ROD TEMPS LISTED NEXT FOR
THE CATHODE

301.5	304.8	304.9	304.9	304.8	300.0
301.8	304.8	304.9	304.9	304.8	300.0
301.9	304.8	304.9	304.9	304.8	300.0
302.0	304.8	304.9	304.9	304.8	300.0

Table A-13

111

```
SWITCH DIMENSIONS FOLLOW
PLATE AND ROD RADII (CMS)=    5.08    1.27
PLATE THICKNESS AND ROD LENGTH (CMS)=    2.54   25.40
NUMBER OF CYCLES IS   20
PLATE TEMPS LISTED NEXT FOR
THE ANODE
MAX ANODE TEMP IS    422.0
FLUID TEMP=  301.2
    416.9    365.8    349.2    340.5    322.2    312.4    310.5    309.5
    417.1    366.0    349.3    340.5    321.8    312.1    310.3    309.3
    417.7    366.7    350.1    340.7    320.5    311.0    309.4    308.7
    420.5    369.9    354.6    347.8    301.2    306.8    307.1    307.2
    421.8    371.2    356.0    349.1    301.2    311.2    311.8    312.1
    421.9    371.3    356.2    349.2    301.2    319.2    319.8    316.9
    422.0    371.3    356.2    349.2    301.2    320.3    320.7    317.0
    422.0    371.3    356.2    349.2    301.2    319.7    320.1    316.7
    422.0    371.3    356.2    349.2    301.2    301.2    301.2    301.2

ROD TEMPS LISTED NEXT FOR
THE ANODE
    316.9    314.5    314.3    314.3    313.7    300.0
    317.0    314.4    314.2    314.2    313.7    300.0
    316.7    314.2    314.0    314.0    313.5    300.0
    301.2    301.2    301.2    301.2    301.2    300.0

PLATE TEMPS LISTED NEXT FOR
THE CATHODE
MAX CATHODE TEMP IS    354.5
    350.7    348.5    340.7    332.7    317.6    309.5    307.9    307.0
    350.9    348.6    340.8    332.7    317.6    309.5    307.9    307.0
    351.3    349.0    341.1    332.9    317.7    309.5    307.9    307.0
    353.2    350.7    342.3    333.7    318.0    309.7    308.0    307.1
    354.3    351.7    343.1    334.4    318.4    309.9    308.2    307.2
    354.4    351.9    343.3    334.6    318.5    309.9    308.2    307.2
    354.4    351.9    343.3    334.6    318.5    310.0    308.2    307.2
    354.5    351.9    343.3    334.6    318.5    310.0    308.2    307.1
    354.5    351.9    343.3    334.6    318.6    310.0    308.2    307.1

ROD TEMPS LISTED NEXT FOR
THE CATHODE
    307.2    309.6    309.8    309.8    309.4    300.0
    307.2    309.6    309.8    309.8    309.4    300.0
    307.1    309.6    309.8    309.8    309.4    300.0
    307.1    309.6    309.8    309.8    309.4    300.0
```

Table A-14

```
SWITCH DIMENSIONS FOLLOW
PLATE AND ROD RADII (CMS)=    5.08    1.27
PLATE THICKNESS AND ROD LENGTH (CMS)=    2.54   25.40
NUMBER OF CYCLES IS   30
PLATE TEMPS LISTED NEXT FOR
THE ANODE
MAX ANODE TEMP IS    435.0
FLUID TEMP=  302.4
    430.3    379.2    362.2    352.9    332.5    321.0    318.6    317.4
    430.4    379.4    362.3    352.7    331.9    320.5    318.2    317.0
    430.9    379.9    362.8    352.5    330.1    318.8    316.6    315.9
    433.3    382.6    366.7    358.6    302.4    311.6    312.1    312.4
    434.7    384.0    368.1    359.9    302.4    315.1    315.8    316.2
    434.9    384.3    368.4    360.2    302.4    323.1    323.8    321.1
    435.0    384.3    368.4    360.2    302.4    324.1    324.7    321.2
    435.0    384.4    368.5    360.2    302.4    323.4    324.0    320.8
    435.0    384.4    368.5    360.2    302.4    302.4    302.4    302.4

ROD TEMPS LISTED NEXT FOR
THE ANODE
    321.1      320.0      319.7      319.7      318.4      300.0
    321.2      319.9      319.6      319.6      318.3      300.0
    320.8      319.6      319.3      319.3      318.1      300.0
    302.4      302.4      302.4      302.4      302.4      300.0


PLATE TEMPS LISTED NEXT FOR
THE CATHODE
MAX CATHODE TEMP IS    368.4
    364.6    362.4    354.6    346.2    329.7    320.0    318.0    316.9
    364.8    362.5    354.7    346.3    329.7    320.1    318.0    316.9
    365.1    362.9    354.9    346.5    329.8    320.1    318.1    316.9
    366.8    364.4    356.1    347.3    330.2    320.3    318.2    317.1
    368.1    365.6    357.1    348.2    330.7    320.6    318.5    317.3
    368.4    365.9    357.4    348.4    330.9    320.5    318.2    316.7
    368.4    365.9    357.4    348.5    330.9    320.4    318.0    316.3
    368.4    366.0    357.4    348.5    330.9    320.4    317.9    316.1
    368.4    366.0    357.5    348.5    330.9    320.3    317.9    316.0

ROD TEMPS LISTED NEXT FOR
THE CATHODE
    316.7      314.4      314.8      314.8      313.7      300.0
    316.3      314.4      314.8      314.8      313.7      300.0
    316.1      314.4      314.8      314.8      313.7      300.0
    316.0      314.4      314.8      314.8      313.7      300.0
```

Table A-15

SWITCH DIMENSIONS FOLLOW
PLATE AND ROD RADII (CMS)= 5.08 1.27
PLATE THICKNESS AND ROD LENGTH (CMS)= 2.54 25.40
NUMBER OF CYCLES IS 40
PLATE TEMPS LISTED NEXT FOR
THE ANODE
MAX ANODE TEMP IS 445.0
FLUID TEMP= 303.9

441.0	390.0	372.7	362.8	341.1	328.7	326.1	324.8
441.1	390.1	372.7	362.5	340.4	328.0	325.5	324.2
441.4	390.5	372.9	362.0	338.1	325.8	323.7	322.7
443.4	392.7	376.1	367.1	303.9	316.4	317.2	317.6
444.6	393.9	377.4	368.2	303.9	318.8	319.7	320.2
444.9	394.2	377.7	368.5	303.9	326.5	327.4	324.8
445.0	394.3	377.7	368.5	303.9	327.4	328.2	324.9
445.0	394.3	377.7	368.5	303.9	326.6	327.4	324.4
445.0	394.3	377.7	368.5	303.9	303.9	303.9	303.9

ROD TEMPS LISTED NEXT FOR
THE ANODE

324.8	324.6	324.4	324.2	322.2	300.0
324.9	324.5	324.2	324.1	322.1	300.0
324.4	324.2	323.9	323.7	321.8	300.0
303.9	303.9	303.9	303.9	303.9	300.0

PLATE TEMPS LISTED NEXT FOR
THE CATHODE
MAX CATHODE TEMP IS 379.5

376.2	374.1	366.4	358.1	341.5	331.4	329.3	328.1
376.2	374.1	366.5	358.2	341.5	331.5	329.3	328.1
376.5	374.4	366.7	358.3	341.6	331.5	329.4	328.2
377.9	375.7	367.7	359.1	342.0	331.7	329.6	328.3
379.1	376.8	368.6	359.9	342.5	332.0	329.7	328.5
379.4	377.1	368.9	360.2	342.5	331.7	329.2	327.4
379.4	377.1	368.9	360.2	342.5	331.6	329.0	326.9
379.4	377.1	369.0	360.2	342.5	331.5	328.8	326.6
379.5	377.1	369.0	360.2	342.5	331.4	328.7	326.4

ROD TEMPS LISTED NEXT FOR
THE CATHODE

327.4	319.6	319.8	319.8	317.7	300.0
326.9	319.6	319.8	319.8	317.7	300.0
326.6	319.6	319.8	319.8	317.7	300.0
326.4	319.6	319.8	319.8	317.7	300.0

Table A-16

SWITCH DIMENSIONS FOLLOW
PLATE AND ROD RADII (CMS)= 5.08 1.27
PLATE THICKNESS AND ROD LENGTH (CMS)= 2.54 25.40
NUMBER OF CYCLES IS 50
PLATE TEMPS LISTED NEXT FOR
THE ANODE
MAX ANODE TEMP IS 453.5
FLUID TEMP= 305.6

450.4	399.4	381.7	371.3	348.6	335.5	332.8	331.4
450.4	399.4	381.6	370.9	347.7	334.7	332.1	330.8
450.6	399.6	381.6	370.1	345.1	332.2	330.0	329.0
452.2	401.4	384.2	374.4	305.6	321.1	322.0	322.5
453.2	402.4	385.3	375.4	305.6	322.5	323.4	324.0
453.5	402.7	385.5	375.6	305.6	329.8	330.8	328.4
453.5	402.7	385.5	375.6	305.6	330.7	331.6	328.4
453.5	402.7	385.6	375.6	305.6	329.8	330.6	327.9
453.5	402.7	385.6	375.6	305.6	305.6	305.6	305.6

ROD TEMPS LISTED NEXT FOR
THE ANODE

328.4	328.7	328.4	328.2	325.4	300.0
328.4	328.5	328.3	328.1	325.2	300.0
327.9	328.1	327.9	327.7	324.9	300.0
305.6	305.6	305.6	305.6	305.6	300.0

PLATE TEMPS LISTED NEXT FOR
THE CATHODE
MAX CATHODE TEMP IS 388.9

386.3	384.3	377.0	369.0	352.7	342.8	340.7	339.5
386.3	384.4	377.1	369.0	352.7	342.8	340.7	339.5
386.5	384.5	377.2	369.1	352.8	342.9	340.7	339.6
387.7	385.6	378.0	369.8	353.1	343.1	340.9	339.7
388.6	386.5	378.8	370.4	353.5	343.2	341.0	339.8
388.9	386.7	379.0	370.6	353.5	342.8	340.3	338.4
388.9	386.8	379.1	370.7	353.5	342.6	340.0	337.7
388.9	386.8	379.1	370.7	353.5	342.4	339.7	337.3
388.9	386.8	379.1	370.7	353.4	342.4	339.6	337.1

ROD TEMPS LISTED NEXT FOR
THE CATHODE

338.4	325.3	324.9	324.7	321.5	300.0
337.7	325.3	324.9	324.7	321.5	300.0
337.3	325.3	324.9	324.7	321.5	300.0
337.1	325.3	324.9	384.7	381.5	300.0

Table A-17

115

```
100      PROGRAM SW2(INPUT,OUTPUT,TAPE1,TAPE2)
110      COMMON/TDMI/CM1(1000),C(1000),C1(1000),V(1000)
120      COMMON/BLK1/AMP(500),AREA1,AREA2,
121+     UO,XO,NTIM,THKAV
130      COMMON/BLK2/WANODE(1000),WCATHD(1000),DZ,I1
135      COMMON/BLK3/DELT,THKA1,THKC1
140      DIMENSION W(1000),WAND(1000),WCAT(1000)
150      DATA NO/2HNO/
200C     ------------------------------------------------
210C     STATEMENT FUNCTIONS
220      CAPPA1(V,KE)=THKA1/THKAV
230      CAPPA2(V,KE)=THKA2/THKAV
240      CAPP1P(V,KE)=THKA1/THKAAV
250      CAPP2P(V,KE)=THKA2/THKAAV
260      SIGMA1(V,KE)=RHOA1*(4.24+.75*(V-1.))*1.E+6/(RHOAV*SHAV)
270      SIGMA2(V,KE)=RHOA2*(3.849+.315*(V-1.))*1.E+6/(RHOAV*SHAV)
280      IS(IR,JZ)=(IR-1)*JM2+JZ
290      ISP(IR,JZ)=IM2*JM2+(IR-IM2-1)*JM+JZ
291C     ------------------------------------------------
292C     TAPES READ AND PARAMETERS DEFINED:
293      REWIND 1
294      READ(1,83)NCYC,IM,IM2,JM,JM2,MTOT
295   83 FORMAT(6I5)
296      READ(1,84)UMAXA,UMAXC
297   84 FORMAT(2E23.14)
298      READ(1,85)RAD1,RAD2,PLNGTH,RLNGTH
299      READ(1,85)DELR,DELZ1,DELZ2,DELT
300   85 FORMAT(4E15.5)
301      DO 86 M=1,MTOT
302   86 READ(1,87)WANODE(M),WCATHD(M)
303   87 FORMAT(2E23.14)
304      REWIND 1
305      UO=300.
307      RHOA1=8.08
308      RHOA2=8.96
309      RHOC1=8.08
310      RHOC2=8.96
311      RHOAV=.25*(RHOA1+RHOA2+RHOC1+RHOC2)
312      SHA1=4.24E+6
313      SHA2=3.849E+6
314      SHC1=4.24E+6
315      SHC2=3.849E+6
316      SHAV=.25*(SHA1+SHA2+SHC1+SHC2)
320      SPHT=3.849E+6
331      THKA1=1.18E+7
332      THKA2=3.908E+7
334      THKC1=1.18E+7
336      THKC2=3.908E+7
337      THKAV=.25*(THKA1+THKA2+THKC1+THKC2)
338      THKAAV=.5*(THKA1+THKA2)
339      THKCAV=.5*(THKC1+THKC2)
340      XO=.04
343      AMPMAX=2.E+4
```

116

```
346    DTT=.0095
348    DO 120 N=1,20
350    XN=FLOAT(N)
352    XNSQ=XN*XN
354    120   AMP(N)=AMPMAX*DTT*SQRT(XNSQ-XN+1./3.)/.19
356    AMP(21)=AMPMAX
358    AMP(22)=AMPMAX
360    DO 124 N=23,30
362    124   AMP(N)=0.
375    DTAU=THKAV*DELT/(SHAV*RHOAV*XO*XO)
376    DTAU1=DTAU
377    DTAU2=DTAU
410    PI=2.*ASIN(1.)
420    AREA1=PI*RAD1*RAD1
430    AREA2=PI*RAD2*RAD2
470    DXI=DELR/XO
560    DZ=DELZ1/XO
570    DZSQ=DZ*DZ
580    DZ2=DELZ2/XO
590    DZ2SQ=DZ2*DZ2
600    MTOT=IM2*JM2+(IM-IM2)*JM
620    JM1M=JM-1
630    JM1P=JM+1
640    JM21M=JM2-1
650    JM21P=JM2+1
660    IM1M=IM-1
670    IM1P=IM+1
680    IM21M=IM2-1
690    IM21P=IM2+1
700    WO=1.
760C   ----------------------------------------------------
800C   MAIN CALCULATION OF TEMPERATURE BEGINS NOW:
802    KCYC=1
804    4   CONTINUE
810    6   NTIM=1
820    7   KE=1
825    IF(NTIM.LE.20)DTAU=9.5*DTAU1
826    IF(NTIM.GT.20)DTAU=DTAU2
830    8   CONTINUE
840    IF(KE.EQ.1)GO TO 9
850    GO TO 11
860    9   DO 10 M=1,MTOT
870    10   W(M)=WANODE(M)
880    GO TO 13
890    11   DO 12 M=1,MTOT
900    12   W(M)=WCATHD(M)
910    13   CONTINUE
920C   ----------------------------------------------------
930C   2 .LE. I .LE. IM-1 IN FIRST I LOOP:
940C   ALSO 1 .LE. J .LE. JM-1 IN THIS LOOP:
950    DO 17 I=2,IM1M
960C   J=1
970    I1=(I-1)*JM2+1
975    IF(I.GT.IM2)I1=IM2*JM2+(I-IM2-1)*JM+1
```

117

```
980    I2=I1+1
990    CM1(I1)=0.
1000   W1=W(I1)
1010   SIG=SIGMA1(W1,KE)
1020   CAP=CAPPA1(W1,KE)
1030   SUM1=SIG*(I-1.)*DXI/DTAU
1040   SUM2=2.*(I-1.)*DXI*CAP/DZSQ
1050   W2=W(I2)
1060   CAP2=CAPPA1(W2,KE)
1070   FAC=-DXI*(I-1.)/DZ
1080   C(I1)=SUM1+SUM2
1090   C1(I1)=-SUM2
1100   V1=SIG*(I-1.)*DXI*W1/DTAU
1110   IP1=IS(I+1,1)
1116   IF(I.GE.IM2)IP1=ISP(I+1,1)
1120   IM1=IS(I-1,1)
1125   IF(I.GT.IM21P)IM1=ISP(I-1,1)
1130   WP1=W(IP1)
1140   WM1=W(IM1)
1150   V2=CAP*(WP1-W1)/DXI
1160   V3=(I-1.)*CAP*(WM1-2.*W1+WP1)/DXI
1170   VS=S1(W1,KE)*(I-1.)*DXI
1180   VBDRY=FAC*(CAP2-3.*CAP)*G(W1,KE)
1200   V(I1)=V1+V2+V3+VS+VBDRY
1210   DO 16 J=2,JM1M
1220   I1=IS(I,J)
1225   IF(I.GT.IM2)I1=ISP(I,J)
1230   I2=IS(I+1,J)
1235   IF(I.GE.IM2)I2=ISP(I+1,J)
1240   I3=I1+1
1250   I4=IS(I-1,J)
1255   IF(I.GT.IM21P)I4=ISP(I-1,J)
1260   I5=I1-1
1270   W1=W(I1)
1280   W2=W(I2)
1290   W3=W(I3)
1300   W4=W(I4)
1310   W5=W(I5)
1320   SIG=SIGMA1(W1,KE)
1330   CAP=CAPPA1(W1,KE)
1340   CAP2=CAPPA1(W3,KE)
1350   FAC1=DXI*(I-1.)/DZSQ
1360   FAC2=CAP/DXI
1370   CM1(I1)=-FAC1*CAP
1380   SUM1=SIG*(I-1.)*DXI/DTAU
1390   SUM2=FAC1*(CAP2+CAP)
1400   C(I1)=SUM1+SUM2
1410   C1(I1)=CM1(I1)
1420   V1=SUM1*W1
1430   V2=FAC2*(W2-W1)
1440   V3=(I-1.)*FAC2*(W4-2.*W1+W2)
1450   VS=S1(W1,KE)*(I-1.)*DXI
1460 16  V(I1)=V1+V2+V3+VS
1465 17   CONTINUE
```

118

```
1470C   --------------------------------------------------
1472C   2 .LE. I .LE. IM2 AND J=JM NEXT:
1475    DO 19 I=2,IM2
1480    I1=IS(I,JM)
1490    I2=IS(I+1,JM)
1500    I3=IS(I,JM+1)
1510    I4=IS(I-1,JM)
1520    I5=IS(I,JM-1)
1530    W1=W(I1)
1540    W2=W(I2)
1550    W3=W(I3)
1560    W4=W(I4)
1570    W5=W(I5)
1580    CAP1=CAPPA1(W1,KE)
1590    CAP11=CAPPA1(W5,KE)
1600    CAP2=CAPPA2(W1,KE)
1610    CAP22=CAPPA2(W3,KE)
1620    SIG1=SIGMA1(W1,KE)
1630    SIG2=SIGMA2(W1,KE)
1640    CAPP1=CAPP1P(W1,KE)
1650    CAPP2=CAPP2P(W1,KE)
1660    ANUM1C=CAPP1*DZ
1670    DENC1=DXI*(I-1.)*(3.*CAP1-CAP11)
1680    FAC1C=ANUM1C/DENC1
1690    ANUM2C=CAPP2*DZ2
1700    DEN2C=DXI*(I-1.)*(3.*CAP2-CAP22)
1710    FAC2C=ANUM2C/DEN2C
1720    AA=(I-1.)*DXI/DTAU
1730    BB=AA*SIG1
1740    CC=AA*SIG2
1750    DD=CAP1/DZSQ
1760    EE=CAP2/DZ2SQ
1770    SUM1=AA*(FAC1C*SIG1+FAC2C*SIG2)
1780    SUM2=2.*(I-1.)*DXI*(FAC1C*DD+FAC2C*EE)
1790    C(I1)=SUM1+SUM2
1800    CM1(I1)=-FAC1C*2.*(I-1.)*DXI*DD
1810    C1(I1)=-FAC2C*2.*(I-1.)*DXI*EE
1820    V1=(FAC1C*BB+FAC2C*CC)*W1
1830    V2=(W2-W1)*(FAC1C*CAP1+FAC2C*CAP2)/DXI
1840    FAC=(W4-2.*W1+W2)*(I-1.)/DXI
1850    FACC=FAC1C*CAP1+FAC2C*CAP2
1860    V3=FAC*FACC
1870    VS=(I-1.)*DXI*(FAC1C*S1(W1,KE)+FAC2C*S2(W1,KE))
1872 19 V(I1)=V1+V2+V3+VS
1875C   --------------------------------------------------
1878C   2 .LE. I .LE. IM2 AND JM+1 .LE. J .LE. JM2-1 NEXT:
1880    DO 25 I=2,IM2
1885    DO 25 J=JM1P,JM21M
1890    I1=IS(I,J)
1900    I2=IS(I+1,J)
1910    I3=IS(I,J+1)
1920    I4=IS(I-1,J)
1930    I5=IS(I,J-1)
1940    W1=W(I1)
1950    W2=W(I2)
```

119

```
1960    W3=W(I3)
1970    W4=W(I4)
1980    W5=W(I5)
1990    SIG=SIGMA2(W1,KE)
2000    CAP=CAPPA2(W1,KE)
2010    CAPP=CAPPA2(W3,KE)
2015    IF(I.EQ.IM2)GO TO 21
2020    AA=(I-1.)*DXI/DZ2SQ
2030    BB=(I-1.)*SIG*DXI/DTAU
2040    CC=CAP/DXI
2050    CM1(I1)=-AA*CAP
2060    C(I1)=BB+AA*(CAPP+CAP)
2070    C1(I1)=-AA*CAPP
2080    V1=BB*W1
2090    V2=CC*(W2-W1)
2100    V3=(I-1.)*CC*(W4-2.*W1+W2)
2110    VS=S2(W1,KE)*(I-1.)*DXI
2120    V(I1)=V1+V2+V3+VS
2130    GO TO 23
2140 21 AA=DXI/DZ2SQ
2150    BB=SIG*DXI/DTAU
2160    CC=CAP/DXI
2170    CM1(I1)=-AA*CAP
2180    C(I1)=BB+AA*(CAPP+CAP)
2190    C1(I1)=-AA*CAPP
2200    V1=BB*W1
2210    V2=2.*CC*(W4-W1)
2220    VS=S2(W1,KE)*DXI
2230    V(I1)=V1+V2+VS
2240 23 CONTINUE
2250 25 CONTINUE
2260C   -------------------------------------------------
2270C   2 .LE. I .LE. IM2 AND J=JM2 NEXT:
2280    DO 28 I=2,IM2
2290    I1=IS(I,JM2)
2300    CM1(I1)=0.
2310    C(I1)=1.
2320    C1(I1)=0.
2330 28 V(I1)=WO
2340C   -------------------------------------------------
2350C   IM2+1 .LE. I .LE. IM AND J=JM NEXT:
2360    DO 36 I=IM21P,IM
2370    I1=ISP(I,JM)
2380    I2=I1-1
2390    I3=ISP(I-1,JM)
2395    I4=ISP(I+1,JM)
2400    IF(I.LE.IM21P)I3=IS(IM2,JM)
2410    W1=W(I1)
2420    W2=W(I2)
2430    W3=W(I3)
2435    W4=W(I4)
2440    SIG=SIGMA1(W1,KE)
2450    CAP=CAPPA1(W1,KE)
2460    AA=DXI/DZSQ
```

120

```
2470    BB=SIG*DXI/DTAU
2480    CC=CAP/DXI
2490    IF(I.EQ.IM)GO TO 32
2500    C1(I1)=0.
2510    CM1(I1)=-2.*(I-1.)*AA*CAP
2520    C(I1)=(I-1.)*BB+2.*(I-1.)*AA*CAP
2530    V1=(I-1.)*BB*W1
2540    V2=CC*(W4-W1)
2550    V3=(I-1.)*CC*(W3-2.*W1+W4)
2560    VS=S1(W1,KE)*(I-1.)*DXI
2570    V(I1)=V1+V2+V3+VS
2580    GO TO 33
2590  32 C1(I1)=0.
2600    CM1(I1)=-2.*AA*CAP
2610    C(I1)=BB+2.*AA*CAP
2620    V1=BB*W1
2630    V2=2.*CC*(W3-W1)
2640    VS=S1(W1,KE)*DXI
2650    V(I1)=V1+V2+VS
2660  33  CONTINUE
2670  36  CONTINUE
2680C  ----------------------------------------------------------
2690C   I=IM AND 1 .LE. J .LE. JM-1 AT LAST
2700    DO 45 J=1,JM1M
2710    I1=ISP(IM,J)
2720    I2=I1+1
2730    I3=ISP(IM-1,J)
2740    W1=W(I1)
2750    W2=W(I2)
2760    W3=W(I3)
2780    SIG=SIGMA1(W1,KE)
2790    CAP=CAPPA1(W1,KE)
2800    CAPP=CAPPA1(W2,KE)
2810    AA=DXI/DZSQ
2820    BB=SIG*DXI/DTAU
2830    CC=CAP/DXI
2840    IF(J.EQ.1)GO TO 40
2850    CM1(I1)=-AA*CAP
2860    C(I1)=BB+AA*(CAPP+CAP)
2870    C1(I1)=-AA*CAPP
2880    V1=BB*W1
2890    V2=2.*CC*(W3-W1)
2900    VS=S1(W1,KE)*DXI
2910    V(I1)=V1+V2+VS
2915    GO TO 42
2920  40  CM1(I1)=0.
2930    C(I1)=BB+2.*AA*CAP
2940    C1(I1)=-2.*AA*CAP
2950    V1=BB*W1
2960    V2=-AA*(CAPP-CAP)*G(W1,KE)*DZ
2970    V3=2.*CC*(W3-W1)+2.*AA*DZ*CAP*G(W1,KE)
2980    VS=S1(W1,KE)*DXI
2990    V(I1)=V1+V2+V3+VS
2995  42  CONTINUE
```

121

```
2998    45  CONTINUE
4000C   ------------------------------------------------------------
4010     IF(KE.EQ.1)GO TO 60
4020     GO TO 62
4025    60  CALL TDMATI(WAND,JM21P,MTOT)
4030     GO TO 66
4040    62  CALL TDMATI(WCAT,JM21P,MTOT)
4050     DO 64 M=JM21P,MTOT
4060     WANODE(M)=WAND(M)
4070    64  WCATHD(M)=WCAT(M)
4072     DO 65 J=1,JM2
4074     JM2J=JM2+J
4076     WANODE(J)=WANODE(JM2J)
4078    65  WCATHD(J)=WCATHD(JM2J)
4080    66  KE=KE+1
4090     IF(KE.LT.3)GO TO 8
4100     NTIM=NTIM+1
4110     IF(NTIM.GE.31)GO TO 68
4120     GO TO 7
4130    68  KCYC=KCYC+1
4140     IF(KCYC.LE.50)GO TO 4
4150     MCYC=NCYC+KCYC-1
4160     REWIND 2
4170     WRITE(2,83)MCYC,IM,IM2,JM,JM2,MTOT
4180     WMAXC=0.
4190     DO 70 M=1,MTOT
4195     IF(WANODE(M).GE.WMAXA)WMAXA=WANODE(M)
4200     IF(WCATHD(M).GE.WMAXC)WMAXC=WCATHD(M)
4210    70  CONTINUE
4220     UMAXA=UO*WMAXA
4225     UMAXC=UO*WMAXC
4230     WRITE(2,84)UMAXA,UMAXC
4235     WRITE(2,85)RAD1,RAD2,PLNGTH,RLNGTH
4238     WRITE(2,85)DELR,DELZ1,DELZ2,DELT
4240     DO 72 M=1,MTOT
4250    72  WRITE(2,87)WANODE(M),WCATHD(M)
4260     REWIND 2
4480     END
4500C   ------------------------------------------------------------
4510C   ------------------------------------------------------------
5000     FUNCTION S1(W,KE)
5010     COMMON/BLK1/AMP(500),AREA1,AREA2,
5011+UO,XO,NTIM,THKAV
5020     EK(Y,KK)=1.E+6/(7.+1.29*(Y-1.))
5030     FAC1=AMP(NTIM)*AMP(NTIM)/(AREA1*AREA1*EK(W,KE))
5040     FAC2=XO*XO*1.E+7/(THKAV*UO)
5050     S1=FAC1*FAC2
5060     RETURN
5070     END
5080C   ------------------------------------------------------------
5090C   ------------------------------------------------------------
5100     FUNCTION S2(W,KE)
5110     COMMON/BLK1/AMP(500),AREA1,AREA2,
5111+    UO,XO,NTIM,THKAV
5120     EK(Y,KK)=1.E+6/(1.647+1.29*(Y-1.))
```

122

```
5130      FAC1=AMP(NTIM)*AMP(NTIM)/(AREA2*AREA2*EK(W,KE))
5140      FAC2=XO*XO*1.E+7/(THKAV*UO)
5150      S2=FAC1*FAC2
5160      RETURN
5170      END
5180C     ----------------------------------------------------------
5190C     ----------------------------------------------------------
5300      FUNCTION G(W,KE)
5310      CAP(V,K)=1.*(2-K)+1.*(K-1)
5320      TH(K)=THKA1
5325      COMMON/BLK2/WA(1000),WC(1000),DZ,I1
5330      COMMON/BLK1/AMP(500),AREA1,AREA2,
5340+     UO,XO,NTIM,THKAV
5342      COMMON/BLK3/DELT,THKA1,THKC1
5345      W1=WA(I1)
5346      W2=WC(I1)
5350      RC=4.E-6
5360      DELV=40.
5380      TIMV=9.5*NTIM*DELT
5385      IF(NTIM.GT.20)TIMV=.19+(NTIM-20)*DELT
5450      IF(TIMV.LE..19)GO TO 8
5460      GO TO 10
5470    8 ANUM=AMP(NTIM)*AMP(NTIM)*XO*1.E+7*RC
5472      DEN=AREA1*UO*TH(KE)*CAP(W,KE)
5474      HEAT=ANUM/DEN
5476      FACA=.5+.5*(W2-W1)/(W2+W1)
5478      FACC=.5-.5*(W2-W1)/(W2+W1)
5480      G1=HEAT*(FACA*(2-KE)+FACC*(KE-1))
5482      TOP=TH(KE)*W1-TH(KE)*W2
5484      BOT=2.*DZ*TH(KE)*CAP(W,KE)
5486      G2=TOP/BOT
5487      L=3-2*KE
5488      G=G1-G2*L
5520      RETURN
5530   10  CONTINUE
5540      IF(TIMV.LE..192)GO TO 12
5550      GO TO 14
5560   12  FAC=AMP(NTIM)*DELV*XO*1.E+7
5570      DEN=AREA1*UO*TH(KE)*CAP(W,KE)
5580      G=(2-KE)*FAC/DEN
5590      RETURN
5600   14  G=0.
5700      RETURN
5710      END
5720C     ----------------------------------------------------------
5730C     ----------------------------------------------------------
9000      SUBROUTINE TDMATI(U,K1,KMAX)
9010      DIMENSION U(1000),GAM(1000),BETA(1000)
9020      COMMON/TDMI/A(1000),B(1000),C(1000),D(1000)
9030      BETA(K1)=B(K1)
9040      GAM(K1)=D(K1)/BETA(K1)
9050      K1P=K1+1
9060      DO 10 K=K1P,KMAX
9070      BETA(K)=B(K)-A(K)*C(K-1)/BETA(K-1)
```

123

```
9080    10    GAM(K)=(D(K)-A(K)*GAM(K-1))/BETA(K)
9090          U(KMAX)=GAM(KMAX)
9100          KMAXM=KMAX-1
9110          DO 20 L=K1,KMAXM
9120          K=KMAX+K1-L-1
9130    20    U(K)=GAM(K)-C(K)*U(K+1)/BETA(K)
9140          RETURN
9150          END
```

```
100     PROGRAM SWFLOW(INPUT,OUTPUT,TAPE1,TAPE2)
110     COMMON/TDM1/CM1(1000),C(1000),C1(1000),V(1000)
120     COMMON/BLK1/AMP(500),AREA1,AREA2,
121+    UO,XO,NTIM,THKAV
130     COMMON/BLK2/WANODE(1000),WCATHD(1000),DZ,I1
135     COMMON/BLK3/DELT,THKA1,THKC1
136     COMMON/BLK6/R10,R10SQ,R20,R20SQ,H,WF,D
138     COMMON/BLX5/IF1,IF2,JF1,JF2,IM,IM2,JM,JM2,DELR,I,J
140     DIMENSION W(1000),WAND(1000),WCAT(1000)
150     DATA NO/2HNO/
200C    ------------------------------------------------------
210C    STATEMENT FUNCTIONS
220     CAPPA1(V,KE)=THKA1/THKAV
230     CAPPA2(V,KE)=THKA2/THKAV
240     CAPP1P(V,KE)=THKA1/THKAAV
250     CAPP2P(V,KE)=THKA2/THKAAV
260     SIGMA1(V,KE)=RHOA1*(4.24+.75*(V-1.))*1.E+6/(RHOAV*SHAV)
270     SIGMA2(V,KE)=RHOA2*(3.849+.315*(V-1.))*1.E+6/(RHOAV*SHAV)
280     IS(IR,JZ)=(IR-1)*JM2+JZ
290     ISP(IR,JZ)=IM2*JM2+(IR-IM2-1)*JM+JZ
291C    ------------------------------------------------------
292C    TAPES READ AND PARAMETERS DEFINED:
293     REWIND 1
294     READ(1,83)NCYC,IM,IM2,JM,JM2,MTOT
295  83  FORMAT(6I5)
296     READ(1,84)UMAXA,UMAXC,WF
297  84  FORMAT(3E23.14)
298     READ(1,85)RAD1,RAD2,PLNGTH,RLNGTH
299     READ(1,85)DELR,DELZ1,DELZ2,DELT
300  85  FORMAT(4E15.5)
301     DO 86 M=1,MTOT
302  86  READ(1,87)WANODE(M),WCATHD(M)
303  87  FORMAT(2E23.14)
304     REWIND 1
305     UO=300.
307     RHOA1=8.08
308     RHOA2=8.96
309     RHOC1=8.08
310     RHOC2=8.96
311     RHOAV=.25*(RHOA1+RHOA2+RHOC1+RHOC2)
312     SHA1=4.24E+6
313     SHA2=3.849E+6
314     SHC1=4.24E+6
315     SHC2=3.849E+6
316     SHAV=.25*(SHA1+SHA2+SHC1+SHC2)
320     SPHT=3.849E+6
331     THKA1=1.18E+7
332     THKA2=3.908E+7
334     THKC1=1.18E+7
336     THKC2=3.908E+7
337     THKAV=.25*(THKA1+THKA2+THKC1+THKC2)
338     THKAAV=.5*(THKA1+THKA2)
339     THKCAV=.5*(THKC1+THKC2)
340     XO=.04
```

125

```
343     AMPMAX=2.E+4
346     DTT=.0095
348     DO 120 N=1,20
350     XN=FLOAT(N)
352     XNSQ=XN*XN
354  120  AMP(N)=AMPMAX*DTT*SQRT(XNSQ-XN+1./3.)/.19
356     AMP(21)=AMPMAX
358     AMP(22)=AMPMAX
360     DO 124 N=23,30
362  124  AMP(N)=0.
375     DTAU=THKAV*DELT/(SHAV*RHOAV*XO*XO)
376     DTAU1=DTAU
377     DTAU2=DTAU
410     PI=2.*ASIN(1.)
420     AREA1=PI*RAD1*RAD1
430     AREA2=PI*RAD2*RAD2
440     JF1=6
445     JF2=16
450     IF1=3
455     IF2=15
458     D=.635
460     R10=RAD1-D
461     H=.7E+7
462     R20=RAD2-D
464     R10SQ=R10*R10
466     R20SQ=R20*R20
468     SPF=1.268E+7
469     VOLF=3785.4   SRHOF=1.451
470     DXI=DELR/XO
560     DZ=DELZ1/XO
570     DZSQ=DZ*DZ
580     DZ2=DELZ2/XO
590     DZ2SQ=DZ2*DZ2
600     MTOT=IM2*JM2+(IM-IM2)*JM
620     JM1M=JM-1
630     JM1P=JM+1
640     JM21M=JM2-1
650     JM21P=JM2+1
660     IM1M=IM-1
670     IM1P=IM+1
680     IM21M=IM2-1
690     IM21P=IM2+1
700     WO=1.
760C    -------------------------------------------------
800C    MAIN CALCULATION OF TEMPERATURE BEGINS NOW:
802     KCYC=1
804  4  CONTINUE
805     IX1=ISP(8,JF1)   $IX2=ISP(IF2,11)
806     IX3=ISP(9,JF2)   $IX4=IS(IF1,26)
807     HX1=PI*R10SQ*(WANODE(IX1)-WF)
808     HX2=2.*PI*R10*(PLNGTH-2.*D)*(WANODE(IX2)-WF)
809     HX3=PI*(R10SQ-R20SQ)*(WANODE(IX3)-WF)
810     HX4=2.*PI*R20*(RLNGTH+D)*(WANODE(IX4)-WF)
811     HX=HX1+HX2+HX3+HX4
812     HX=.2*H*HX
```

126

```
813     DENWF=RHOF*SPF*VOL,
814     DELWF=HX/DENWF
815     WF=WF+DELWF
817   6  NTIM=1
820   7   KE=1
825     IF(NTIM.LE.20)DTAU=9.5*DTAU1
826     IF(NTIM.GT.20)DTAU=DTAU2
830   8  CONTINUE
840     IF(KE.EQ.1)GO TO 9
850     GO TO 11
860   9  DO 10 M=1,MTOT
870   10  W(M)=WANODE(M)
880     GO TO 13
890   11  DO 12 M=1,MTOT
900   12  W(M)=WCATHD(M)
910   13  CONTINUE
920C    ----------------------------------------------------
930C    2 .LE. 1 .LE. IM-1 IN FIRST I LOOP:
940C    ALSO 1 .LE. J .LE. JM-1 IN THIS LOOP:
950     DO 15 I=2,IM1M
960C    J=1
970     I1=(I-1)*JM2+1
975     IF(I.GT.IM2)I1=IM2*JM2+(I-IM2-1)*JM+1
980     I2=I1+1
990     CM1(I1)=0.
1000    W1=W(I1)
1010    SIG=SIGMA1(W1,KE)
1020    CAP=CAPPA1(W1,KE)
1030    SUM1=SIG*(I-1.)*DXI/DTAU
1040    SUM2=2.*(I-1.)*DXI*CAP/DZSQ
1050    W2=W(I2)
1060    CAP2=CAPPA1(W2,KE)
1070    FAC=-DXI*(I-1.)/DZ
1080    C(I1)=SUM1+SUM2
1090    C1(I1)=-SUM2
1100    V1=SIG*(I-1.)*DXI*W1/DTAU
1110    IP1=IS(I+1,1)
1116    IF(I.GE.IM2)IP1=ISP(I+1,1)
1120    IM1=IS(I-1,1)
1125    IF(I.GT.IM21P)IM1=ISP(I-1,1)
1130    WP1=W(IP1)
1140    WM1=W(IM1)
1150    V2=CAP*(WP1-V1)/DXI
1160    V3=(I-1.)*CAP*(WM1-2.*W1+WP1)/DXI
1170    VS=S1(W1,KE)*(I-1.)*DXI
1180    VBDRY=FAC*(CAP2-3.*CAP)*G(W1,KE)
1200    V(I1)=V1+V2+V3+VS+VBDRY
1202    15  CONTINUE
1204    DO 17 I=2,IM1M
1210    DO 16 J=2,JM1M
1220    I1=IS(I,J)
1225    IF(I.GT.IM2)I1=ISP(I,J)
1230    I2=IS(I+1,J)
1235    IF(I.GE.IM2)I2=ISP(I+1,J)
1240    I3=I1+1
```

127

```
1250      I4=IS(I-1,J)
1255      IF(I.GT.IM21P)I4=ISP(I-1,J)
1260      I5=I1-1
1270      W1=W(I1)
1280      W2=W(I2)
1290      W3=W(I3)
1300      W4=W(I4)
1310      W5=W(I5)
1320      SIG=SIGMA1(W1,KE)
1330      CAP=CAPPA1(W1,KE)
1340      CAP2=CAPPA1(W3,KE)
1350      FAC1=DXI*(I-1.)/DZSQ
1360      FAC2=CAP/DXI
1370      CM1(I1)=-FAC1*CAP
1380      SUM1=SIG*(I-1.)*DXI/DTAU
1390      SUM2=FAC1*(CAP2+CAP)
1400      C(I1)=SUM1+SUM2
1410      C1(I1)=CM1(I1)
1411      V1=SUM1*W1
1412      V2=FAC2*(W2-W1)
1413      V3=(I-1.)*FAC2*(W4-2.*W1+W2)
1414      VS=S1(W1,KE)*(I-1.)*DXI
1415      VF=0.
1416      IF(KE.EQ.2)GO TO 16
1417      IF(I.LT.IF2.AND.J.EQ.JF1)GO TO 133
1418      GO TO 135
1419  133 C(I1)=SUM1+2.*FAC1*CAP
1420      C1(I1)=0.
1421      CM1(I1)=-2.*FAC1*CAP
1422      CAPS=CAPPA1(W5,KE)
1423      VF=HE(W1,CAP)*DZ*FAC1*(3.*CAP-CAPS)
1424  135 CONTINUE
1425      IF(I.EQ.IF2.AND.JF1.LT.J.AND.J.LT.JF2)GO TO 137
1426      GO TO 143
1427  137 V3=0.
1428      VF=2.*(I-1.)*FAC2*(W2-W1+DXI*HE(W1,CAP))
1429  143 CONTINUE
1430      IF((I.LT.IF2.AND.JF1.LT.J.AND.J.LT.JF2).OR.
1431+     (I.LT.IF1.AND.JF2.LE.J))GO TO 145
1432      GO TO 147
1433  145 C(I1)=1.  SCM1(I1)=0.  SC1(I1)=0.
1434      VF=VF-V1-V2-V3-VS
1435  147 CONTINUE
1436      IF(IF1.LT.I.AND.I.LT.IF2.AND.J.EQ.JF2)GO TO 153
1437      GO TO 155
1438  153 CM1(I1)=0.
1439      C1(I1)=-2.*FAC1*CAP
1440      C(I1)=SUM1+2.*FAC1*CAP
1441      VF=HE(W1,CAP)*DZ*FAC1*(3.*CAP-CAP2)
1442  155 CONTINUE
1443      IF(I.EQ.IF1.AND.J.EQ.JF2)GO TO 163
1444      GO TO 165
1445  163 C1(I1)=C1(I1)-FAC1*CAP
1446      CM1(I1)=0.
1447      VF=(I-1.)*FAC2*(W2-W4+2.*DXI*(1.+DXI/DZ)*HE(W1,CAP))
1448  165 CONTINUE
```

128

```
1449      IF(I.EQ.IF1.AND.JF2.LT.J)GO TO 173
1450      GO TO 175
1451      173   VF=(I-1.)*FAC2*(W2-W4+2.*DXI*HE(W1,CAP))
1452      175   CONTINUE
1460      16    V(I1)=V1+V2+V3+VS+VF
1465      17    CONTINUE
1470C     --------------------------- ------------------
1472C     2 .LE. I .LE. IM2 AND J=JM NEXT:
1475      DO 19 I=2,IM2
1480      I1=IS(I,JM)
1490      I2=IS(I+1,JM)
1500      I3=IS(I,JM+1)
1510      I4=IS(I-1,JM)
1520      I5=IS(I,JM-1)
1530      W1=W(I1)
1540      W2=W(I2)
1550      W3=W(I3)
1560      W4=W(I4)
1570      W5=W(I5)
1580      CAP1=CAPPA1(W1,KE)
1590      CAP11=CAPPA1(W5,KE)
1600      CAP2=CAPPA2(W1,KE)
1610      CAP22=CAPPA2(W3,KE)
1620      SIG1=SIGMA1(W1,KE)
1630      SIG2=SIGMA2(W1,KE)
1640      CAPP1=CAPP1P(W1,KE)
1650      CAPP2=CAPP2P(W1,KE)
1660      ANUM1C=CAPP1*DZ
1670      DENC1=DXI*(I-1.)*(3.*CAP1-CAP11)
1680      FAC1C=ANUM1C/DENC1
1690      ANUM2C=CAPP2*DZ2
1700      DEN2C=DXI*(I-1.)*(3.*CAP2-CAP22)
1710      FAC2C=ANUM2C/DEN2C
1720      AA=(I-1.)*DXI/DTAU
1730      BB=AA*SIG1
1740      CC=AA*SIG2
1750      DD=CAP1/DZSQ
1760      EE=CAP2/DZ2SQ
1770      SUM1=AA*(FAC1C*SIG1+FAC2C*SIG2)
1780      SUM2=2.*(I-1.)*DXI*(FAC1C*DD+FAC2C*EE)
1790      C(I1)=SUM1+SUM2
1800      CM1(I1)=-FAC1C*2.*(I-1.)*DXI*DD
1810      C1(I1)=-FAC2C*2.*(I-1.)*DXI*EE
1820      V1=(FAC1C*BB+FAC2C*CC)*W1
1830      V2=(W2-W1)*(FAC1C*CAP1+FAC2C*CAPP2)/DX1
1840      FAC=(W4-2.*W1+W2)*(I-1.)/DXI
1850      FACC=FAC1C*CAP1+FAC2C*CAP2
1860      V3=FAC*FACC
1865      VS=(I-1.)*DXI*(FAC1C*S1(W1,KE)+FAC2C*S2(W1,KE))
1867      VF=0.
1868      IF(KE.EQ.2)GO TO 19
1870      VS=(I-1.)*DXI*(FAC1C*S1(W1,KE)+FAC2C*S2(W1,KE))
1871      IF(I.EQ.IF1)GO TO 183
1872      GO TO 185
1873      183   CAPAV=.5*(CAP1+CAP2)
```

129

```
1874     VF1=(I-1.)*(FAC1C*CAP1+FAC2C*CAP2)
1875     VF2=W2-W4+2.*DXI*HE(W1,CAPAV)
1876     VF=VF1*VF2/DXI
1877  165  CONTINUE
1878     IF(I.LT.IF1)GO TO 193
1879     GO TO 195
1880  193  CM1(I1)=0.
1881     C1(I1)=0.
1882     C(I1)=1.
1883     VF=VF-V1-V2-V3-VS
1884  195  CONTINUE
1885  19   V(I1)=V1+V2+V3+VS+VF
1886C    --------------------------------------------------------
1887C    2 .LE. I .LE. IM2 AND JM+1 .LE. J .LE. JM2-1 NEXT:
1888     DO 25 I=2,IM2
1889     DO 25 J=JM1P,JM21M
1890     I1=IS(I,J)
1900     I2=IS(I+1,J)
1910     I3=IS(I,J+1)
1920     I4=IS(I-1,J)
1930     I5=IS(I,J-1)
1940     W1=W(I1)
1950     W2=W(I2)
1960     W3=W(I3)
1970     W4=W(I4)
1980     W5=W(I5)
1990     SIG=SIGMA2(W1,KE)
2000     CAP=CAPPA2(W1,KE)
2010     CAPP=CAPPA2(W3,KE)
2015     IF(I.EQ.IM2)GO TO 21
2020     AA=(I-1.)*DXI/DZ2SQ
2030     BB=(I-1.)*SIG*DXI/DTAU
2040     CC=CAP/DXI
2050     CM1(I1)=-AA*CAP
2060     C(I1)=BB+AA*(CAPP+CAP)
2070     C1(I1)=-AA*CAPP
2080     V1=BB*W1
2090     V2=CC*(W2-W1)
2100     V3=(I-1.)*CC*(W4-2.*W1+W2)
2110     VS=S2(W1,KE)*(I-1.)*DXI
2120     VF=0.
2130     GO TO 201
2140  21   AA=DXI/DZ2SQ
2150     BB=SIG*DXI/DTAU
2160     CC=CAP/DXI
2170     CM1(I1)=-AA*CAP
2180     C(I1)=BB+AA*(CAPP+CAP)
2190     C1(I1)=-AA*CAPP
2200     V1=BB*W1
2210     V2=2.*CC*(W4-W1)
2215     V3=0.
2220     VS=S2(W1,KE)*DXI
2221     VF=0.
2222  201  CONTINUE
```

130

```
2223      IF(KE.EQ.2)GO TO 215
2225      IF(I.EQ.IF1)GO TO 203
2227      GO TO 205
2230  203 VF=(I-1.)*CC*(W2-W4+2.*DXI*HE(W1,CAP))
2232  205 CONTINUE
2234      IF(I.LT.IF1)GO TO 213
2236      GO TO 215
2238  213 CM1(I1)=0.
2240      C1(I1)=0.
2242      C(I1)=1.
2244      VF=WF-V1-V2-V3-VS
2246  215 V(I1)=V1+V2+V3+VS+VF
2248  23  CONTINUE
2250  25  CONTINUE
2260C    --------------------------------------------------
2270C    2 .LE. I .LE. IM2 AND J=JM2 NEXT:
2280      DO 28 I=2,IM2
2290      I1=IS(I,JM2)
2300      CM1(I1)=0.
2310      C(I1)=1.
2320      C1(I1)=0.
2330  28  V(I1)=WO
2340C    --------------------------------------------------
2350C    IM2+1 .LE. I .LE. IM AND J=JM NEXT:
2360      DO 36 I=IM21P,IM
2370      I1=ISP(I,JM)
2380      I2=I1-1
2390      I3=ISP(I-1,JM)
2395      I4=ISP(I+1,JM)
2400      IF(I.LE.IM21P)I3=IS(IM2,JM)
2410      W1=W(I1)
2420      W2=W(I2)
2430      W3=W(I3)
2435      W4=W(I4)
2440      SIG=SIGMA1(W1,KE)
2450      CAP=CAPPA1(W1,KE)
2460      AA=DXI/DZSQ
2470      BB=SIG*DXI/DTAU
2480      CC=CAP/DXI
2490      IF(I.EQ.IM)GO TO 32
2500      C1(I1)=0.
2510      CM1(I1)=-2.*(I-1.)*AA*CAP
2520      C(I1)=(I-1.)*BB+2.*(I-1.)*AA*CAP
2530      V1=(I-1.)*BB*W1
2540      V2=CC*(W4-W1)
2550      V3=(I-1.)*CC*(W3-2.*W1+W4)
2560      VS=S1(W1,KE)*(I-1.)*DXI
2570      V(I1)=V1+V2+V3+VS
2580      GO TO 33
2590  32  C1(I1)=0.
2600      CM1(I1)=-2.*AA*CAP
2610      C(I1)=BB+2.*AA*CAP
2620      V1=BB*W1
2630      V2=2.*CC*(W3-W1)
2640      VS=S1(W1,KE)*DXI
```

131

```
2650      V(I1)=V1+V2+VS
2660   33  CONTINUE
2670   36  CONTINUE
2680C   --------------------------------------------------------
2690C   I=IM AND 1 .LE. J .LE. JM-1 AT LAST
2700      DO 45 J=1,JM1M
2710      I1=ISP(IM,J)
2720      I2=I1+1
2730      I3=ISP(IM-1,J)
2740      W1=W(I1)
2750      W2=W(I2)
2760      W3=W(I3)
2780      SIG=SIGMA1(W1,KE)
2790      CAP=CAPPA1(W1,KE)
2800      CAPP=CAPPA1(W2,KE)
2810      AA=DXI/DZSQ
2820      BB=SIG*DXI/DTAU
2830      CC=CAP/DXI
2840      IF(J.EQ.1)GO TO 40
2850      CM1(I1)=-AA*CAP
2860      C(I1)=BB+AA*(CAPP+CAP)
2870      C1(I1)=-AA*CAPP
2880      V1=BB*W1
2890      V2=2.*CC*(W3-W1)
2900      VS=S1(W1,KE)*DXI
2910      V(I1)=V1+V2+VS
2915      GO TO 42
2920   40  CM1(I1)=0.
2930      C(I1)=BB+2.*AA*CAP
2940      C1(I1)=-2.*AA*CAP
2950      V1=BB*W1
2960      V2=-AA*(CAPP-CAP)*G(W1,KE)*DZ
2970      V3=2.*CC*(W3-W1)+2.*AA*DZ*CAP*G(W1,KE)
2980      VS=S1(W1,KE)*DXI
2990      V(I1)=V1+V2+V3+VS
2995   42  CONTINUE
2998   45  CONTINUE
4000C   --------------------------------------------------------
4010      IF(KE.EQ.1)GO TO 60
4020      GO TO 62
4025   60  CALL TDMATI(WAND,JM21P,MTOT)
4030      GO TO 66
4040   62  CALL TDMATI(WCAT,JM21P,MTOT)
4050      DO 64 M=JM21P,MTOT
4060      WANODE(M)=WAND(M)
4070   64  WCATHD(M)=WCAT(M)
4072      DO 65 J=1,JM2
4074      JM2J=JM2+J
4076      WANODE(J)=WANODE(JM2J)
4078   65  WCATHD(J)=WCATHD(JM2J)
4080   66  KE=KE+1
4090      IF(KE.LT.3)GO TO 8
4100      NTIM=NTIM+1
4110      IF(NTIM.GE.31)GO TO 68
4120      GO TO 7
```

132

```
4130   68  KCYC=KCYC+1
4140       IF(KCYC.LE.10)GO TO 4
4150       MCYC=NCYC+KCYC-1
4160       REWIND 2
4170       WRITE(2,83)MCYC,IM,IM2,JM,JM2,MTOT
4180       WMAXC=0.
4190       DO 70 M=1,MTOT
4195       IF(WANODE(M).GE.WMAXA)WMAXA=WANODE(M)
4200       IF(WCATHD(M).GE.WMAXC)WMAXC=WCATHD(M)
4210   70  CONTINUE
4220       UMAXA=UO*WMAXA
4225       UMAXC=UO*WMAXC
4230       WRITE(2,84)UMAXA,UMAXC,WF
4235       WRITE(2,85)RAD1,RAD2,PLNGTH,RLNGTH
4238       WRITE(2,85)DELR,DELZ1,DELZ2,DELT
4240       DO 72 M=1,MTOT
4250   72  WRITE(2,87)WANODE(M),WCATHD(M)
4260       REWIND 2
4480       END
4500C  ------------------------------------------------------
4510C  ------------------------------------------------------
5000       FUNCTION S1(W,KE)
5005       COMMON/BLK5/IF1,IF2,JF1,JF2,IM,IM2,JM,JM2,DELR,I,J
5010       COMMON/BLK1/AMP(500),AREA1,AREA2,
5011+      UO,XO,NTIM,THKAV
5015       COMMON/BLK6/R1O,R1OSQ,R2O,R2OSQ,H,WF,D
5020       EK(Y,KK)=1.E+6/(7.+1.29*(Y-1.))
5021       IF(KE.EQ.2)GO TO 150
5022       PI=2.*ASIN(1.)
5026       CURD=0.
5027       IF(I.LT.IF2.AND.J.LE.JF1)GO TO 2
5028       GO TO 4
5029   2   CURD=DELR*(I-1.)*AMP(NTIM)/(2.*D*AREA1)
5030       GO TO 100
5032   4   CONTINUE
5034       IF(I.GE.IF2.AND.J.LT.JF2)GO TO 6
5036       GO TO 8
5038   6   CONTINUE
5040       R1=(IM-1)*DELR
5044       R1SQ=R1*R1
5046       DEN=PI*(R1SQ-R1OSQ)
5048       CURD=AMP(NTIM)/DEN
5050       GO TO 100
5052   8   CONTINUE
5054       IF(I.GT.IM2.AND.J.GE.JF2)GO TO 10
5056       GO TO 12
5058   10  FAC1=FLOAT(IM2-1)/(I-1.)
5060       FAC2=AMP(NTIM)/(2.*PI*(IM2-1.)*DELR*D)
5062       CURD=FAC1*FAC2
5064       GO TO 100
5066   12  CONTINUE
5068       IF(IF1.LE.I.AND.I.LE.IM2.AND.JF2.LE.J)GO TO 14
5069       GO TO 100
5070   14  R2O=(IF1-1.)*DELR
5074       R2OSQ=R2O*R2O
```

133

```
5076      R2=(IM2-1.)*DELR
5078      R2SQ=R2*R2
5080      DEN=PI*(R2SQ-R2OSQ)
5082      CURD=AMP(NTIM)/DEN
5084  100   FACC=XO*XO*1.E+7/(EK(W,KE)*THKAV*UO)
5086      S1=CURD*CURD*FACC
5088      RETURN
5090  150   FAC1=AMP(NTIM)*AMP(NTIM)/(AREA1*AREA1*EK(W,KE))
5092      FAC2=XO*XO*1.E+7/(THKAV*UO)
5094      S1=FAC1*FAC2
5095     .RETURN
5096      END
5098C     --------------------------------------------------------
5099C     --------------------------------------------------------
5100      FUNCTION S2(W,KE)
5105      COMMON/BLK5/IF1,IF2,JF1,JF2,IM,IM2,JM,JM2,DELR,I,J
5110      COMMON/BLK1/AMP(500),AREA1,AREA2,
5111+     UO,XO,NTIM,THKAV
5115      COMMON/BLK6/R1O,R1OSQ,R2O,R2OSQ,H,WF,D
5120      EK(Y,KK)=1.E+6/(1.647+1.29*(Y-1.))
5121      IF(KE.EQ.2)GO TO 150
5122      PI=2.*ASIN(1.)
5126      CURD=0.
5127      IF(IF1.LE.I.AND.I.LE.IM2)GO TO 14
5130      GO TO 100
5132   14  CONTINUE
5136      R2=(IM2-1.)*DELR
5138      R2SQ=R2*R2
5140      DEN=PI*(R2SQ-R2OSQ)
5142      CURD=AMP(NTIM)/DEN
5144  100   FACC=XO*XO*1.E+7/(EK(W,KE)*THKAV*UO)
5146      S2=CURD*CURD*FACC
5148      RETURN
5150  150   FAC1=AMP(NTIM)*AMP(NTIM)/(AREA2*AREA2*EK(W,KE))
5155      FAC2=XO*XO*1.E+7/(THKAV*UO)
5160      S2=FAC1*FAC2
5165      RETURN
5170      END
5180C     --------------------------------------------------------
5190C     --------------------------------------------------------
5300      FUNCTION G(W,KE)
5325      COMMON/BLK2/WA(1000),WC(1000),DZ,II
5330      COMMON/BLK1/AMP(500),AREA1,AREA2,
5340+     UO,XO,NTIM,THKAV
5342      COMMON/BLK3/DELT,THKA1,THKC1
5343      CAP(V,K)=1.*(2-K)+1.*(K-1)
5344      TH(K)=THKA1
5345      W1=WA(II)
5346      W2=WC(II)
5350      RC=4.E-6
5360      DELV=40.
5380      TIMV=9.5*NTIM*DELT
5385      IF(NTIM.GT.20)TIMV=.19+(NTIM-20)*DELT
5450      IF(TIMV.LE..19)GO TO 8
5460      GO TO 10
```

134

```
5470   8  ANUM=AMP(NTIM)*AMP(NTIM)*XO*1.E+7*RC
5472      DEN=AREA1*UO*TH(KE)*CAP(W,KE)
5474      HEAT=ANUM/DEN
5476      FACA=.5+.5*(W2-W1)/(W2+W1)
5478      FACC=.5-.5*(W2-W1)/(W2+W1)
5480      G1=HEAT*(FACA*(2-KE)+FACC*(KE-1))
5482      TOP=TH(KE)*W1-TH(KE)*W2
5484      BOT=2.*DZ*TH(KE)*CAP(W,KE)
5486      G2=TOP/BOT
5487      L=3-2*KE
5488      G=G1-G2*L
5520      RETURN
5530   10  CONTINUE
5540      IF(TIMV.LE..192)GO TO 12
5550      GO TO 14
5560   12  FAC=AMP(NTIM)*DELV*XO*1.E+7
5570      DEN=AREA1*UO*TH(KE)*CAP(W,KE)
5580      G=(2-KE)*FAC/DEN
5590      RETURN
5600   14  G=0.
5700      RETURN
5710      END
5720C  ------------------------------------------------------
5730C  ------------------------------------------------------
5800      FUNCTION HE(WW,CC)
5810      COMMON/BLK5/IF1,IF2,JF1,JF2,IM,IM2,JM,JM2,DELR,I,J
5850      COMMON/BLK6/R10,R10SQ,R20,R20SQ,H,WF,D
5870      XO=.04
5880      THKAV=2.544E+7
5890      PROD=H*XO/THKAV
5895      PROD=-PROD
5900      IF(WW.LE.WF)GO TO 2
5910      GO TO 3
5920   2  HE=0.
5930      RETURN
5940   3  HE=PROD*(WW-WF)/CC
5950      IF(J.GT.JF1)HE=.5*HE
5960      RETURN
5970      END
5980C  ------------------------------------------------------
5990C  ------------------------------------------------------
9000      SUBROUTINE TDMATI(U,K1,KMAX)
9010      DIMENSION U(1000),GAM(1000),BETA(1000)
9020      COMMON/TDMI/A(1000),B(1000),C(1000),D(1000)
9030      BETA(K1)=B(K1)
9040      GAM(K1)=D(K1)/BETA(K1)
9050      K1P=K1+1
9060      DO 10 K=K1P,KMAX
9070      BETA(K)=B(K)-A(K)*C(K-1)/BETA(K-1)
9080   10  GAM(K)=(D(K)-A(K)*GAM(K-1))/BETA(K)
9090      U(KMAX)=GAM(KMAX)
9100      KMAXM=KMAX-1
9110      DO 20 L=K1,KMAXM
9120      K=KMAX+K1-L-1
9130   20  U(K)=GAM(K)-C(K)*U(K+1)/BETA(K)
9140      RETURN
9150      END
```

135

APPENDIX B

COMMUTATOR CIRCUIT ANALYSIS

B-1 Commutator Circuit Requirements

The initial commutator analysis was based on the assumption of a much larger commutation period being needed than that later realized in our VI development. Computer programs were, therefore, set up for analysis of circuits wherein the commutator contributed a major part in slowing down the voltage rise to 2-5 kV/μsec or 100 kV in 40 μseconds.

Basically, the function of the commutator is to extinguish the arc in the VI, although by suitable design it subsequently will contribute some to the other function. Controlling the voltage rise to acceptable limits, however, is the function of the overall circuit, which includes the power source, energy storage element (coil), load, and switch.

Nevertheless, the computer programs as carried out provide very useful information about the overall behavior of the complete circuits from switch opening to application of the load.

Although the coil and load circuit fundamentally require a capacitance of approximately 8 μF to constrain the voltage rise to 2.5 kV/μsec, the analyses were performed with this capacitance reduced to 4 μF giving the commutator the extra burden of constraining the voltage rise.

The programs start with simple damped L-C circuits and expand to multisection pulse forming networks. All of these are aimed at providing a long arc extinction period (greater than 10 μsec) and to constrain the voltage rise to less than 100 kV in 40 μsec. Both digital and analog computer

137

programs were developed simultaneously and each has particular advantages.

B-2 Digital Computer Analysis

Figures B1 through B4 summarize the results of a single section network with a load resistor of 2.6 Ω. Unfortunately the load resistor matches the circuit only during the very short period where the arc impedance can be considered negligible. No exact expression is available for the impedance of the arc, but as an approximation the relation

$$R_{SW} = \frac{E}{I}\ (1 + t^3) = \frac{500V}{20,000A}\ (1 + t^3) = 0.025\ (1 + t^3)\ \text{ohms}$$

has been used, where t is expressed in μsecs.

Figure B1 shows the VI current I_{SW} for two combinations of L and C and Z_o of $\approx$ 2.5 ohms. Note the time for I_{SW} reversal in each case. Figure B3, which is for a compressed time scale and expanded I_{SW} scale, shows that the current reverses again before damping to zero.

Figure B2 shows that the commutator current I_{COM} remains much higher than I_{SW} throughout the transient. This means that the voltage source E must be able to tolerate this transient in addition to supplying the current to charge the storage coil initially. This surge into the voltage source E, however, is based on the time function given for R_{SW}. In reality it may be assumed that the VI interrupts during this time.

Figure B4 shows how the storage coil and vacuum interrupter voltage varies with time. The average rate of rise of voltage in each case is approximately 3 kV/μsec. However, the lower frequency L-C combination delays the start of voltage rise by nearly 2 to 1 and would appear preferable. Again, the cost is twice as much stored energy in the capacitor

139

SINGLE SECTION NETWORK

$$R_{SW} = \frac{E}{I_0} (1 + t^3)$$

I_{SW}

I_{COIL}

V_{SW}

E

C1

L

2.6Ω

V_{COIL}

4μf

5mh

I_{COM}

I_{COIL}

C = 4μf, L = 27μh

C = 2μf, L = 12.5μh

I_{SW} KA

t·μs
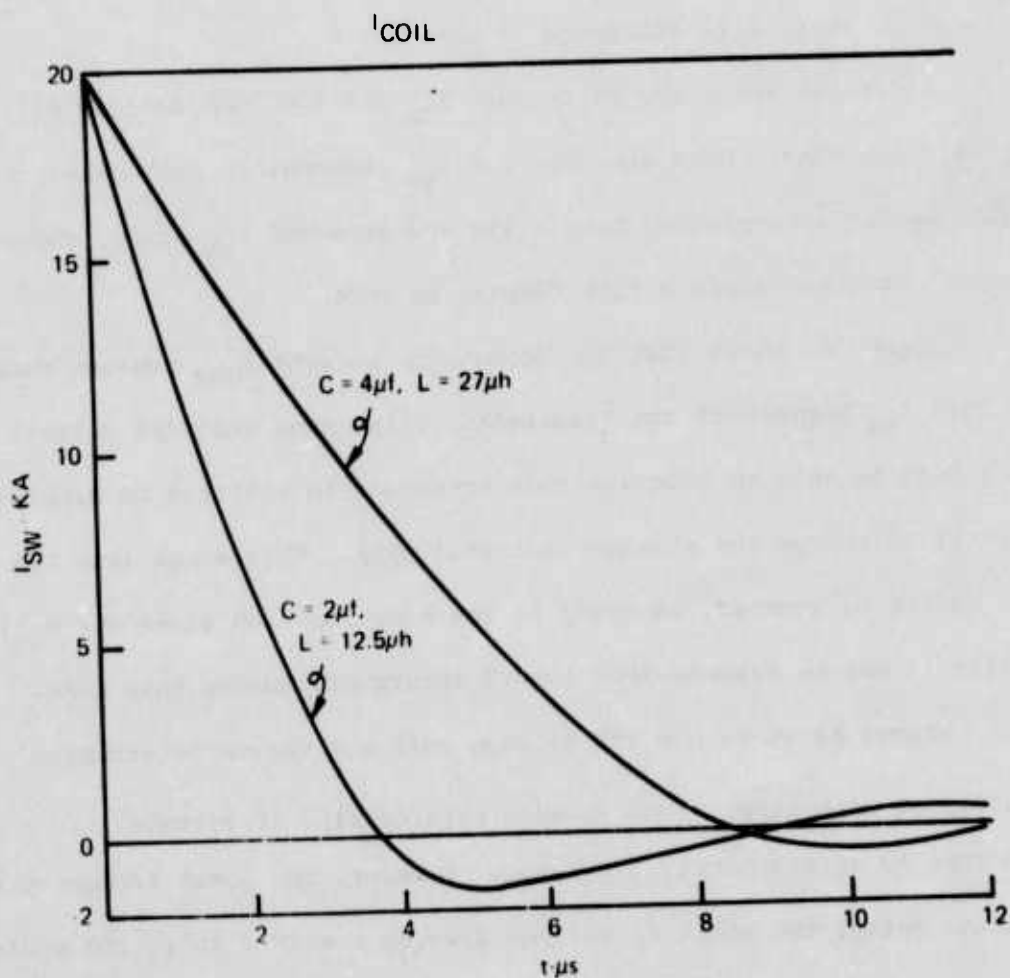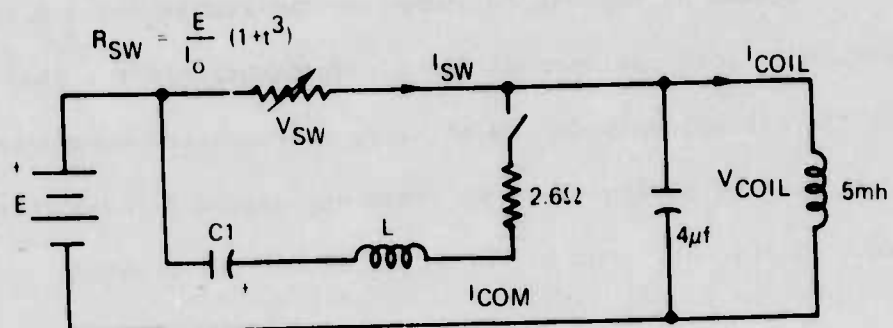
S73-0203-VA-18

Figure B-1. Single section network, switch current vs. time.

140
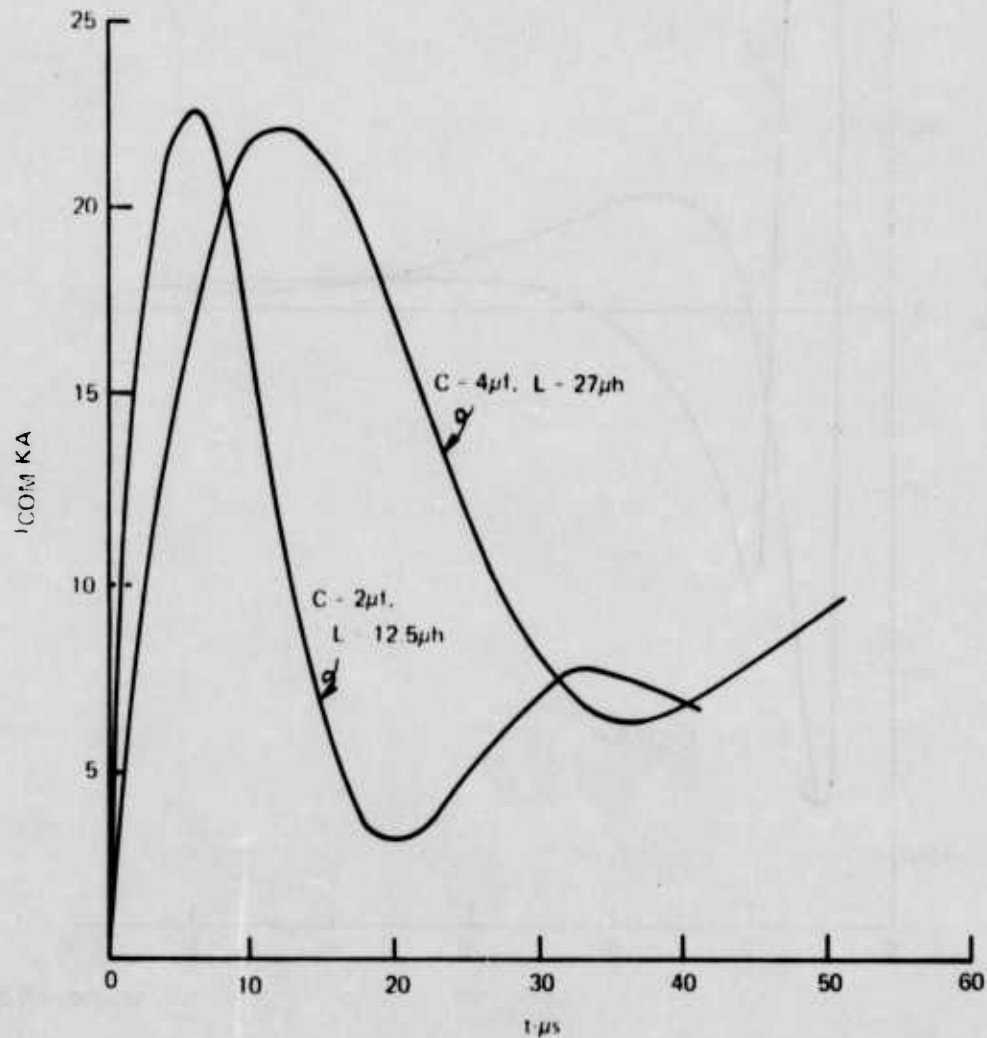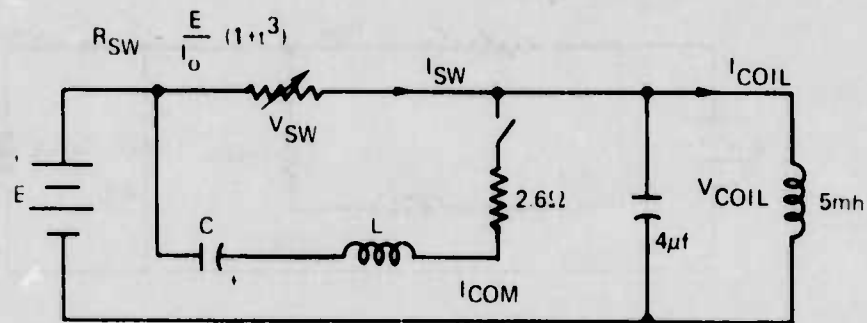
SINGLE SECTION NETWORK

Figure B-2. Single section network commutator current vs time.

S73-0203-VA-19

141
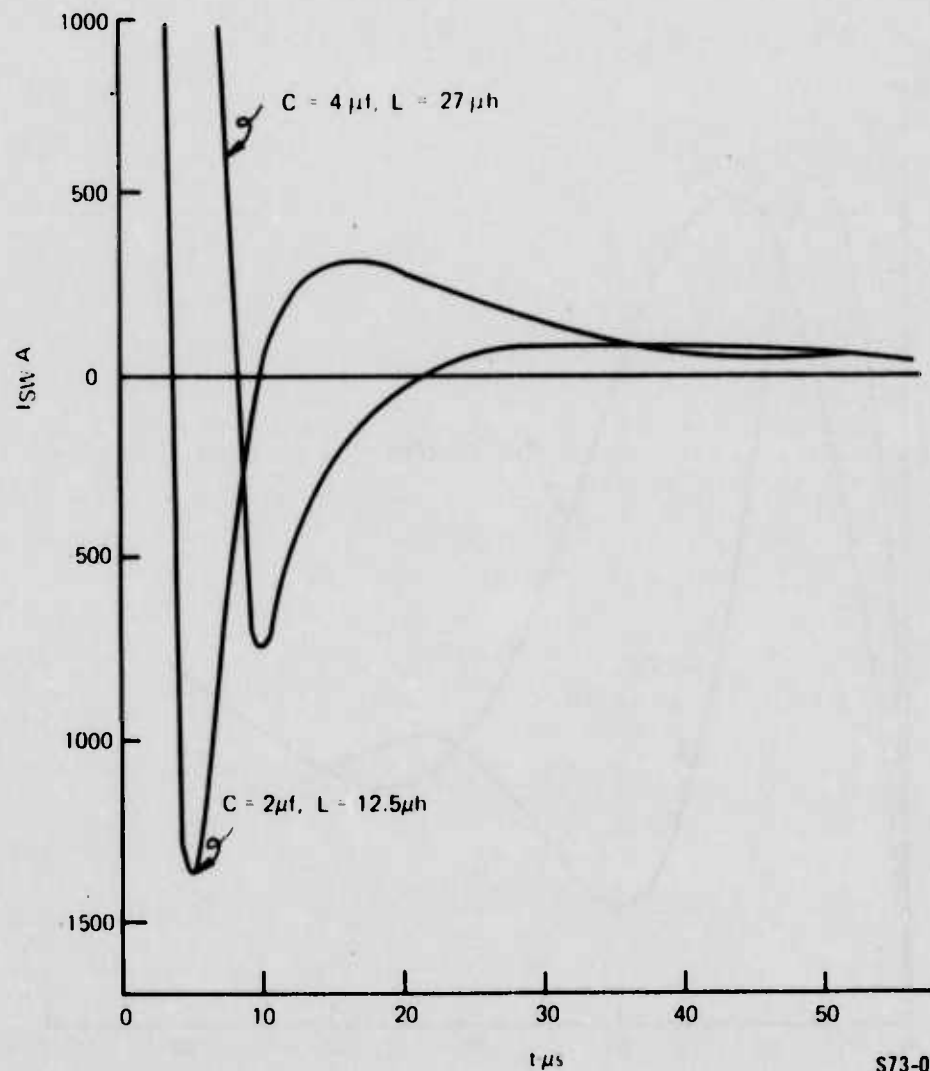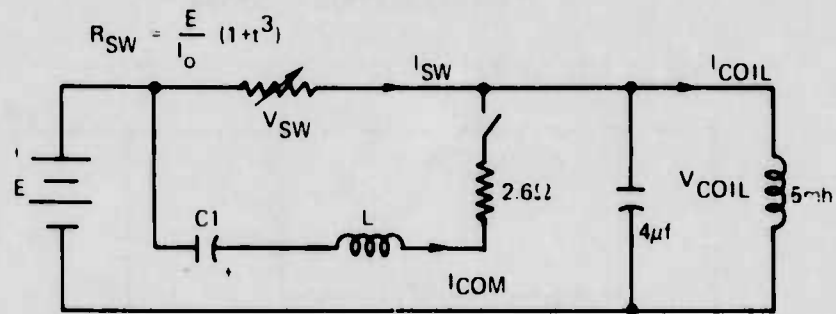
SINGLE SECTION NETWORK

Figure B-3. Single section network switch current vs time (compressed scale).

S73-0203-VA-20

SINGLE SECTION NETWORK
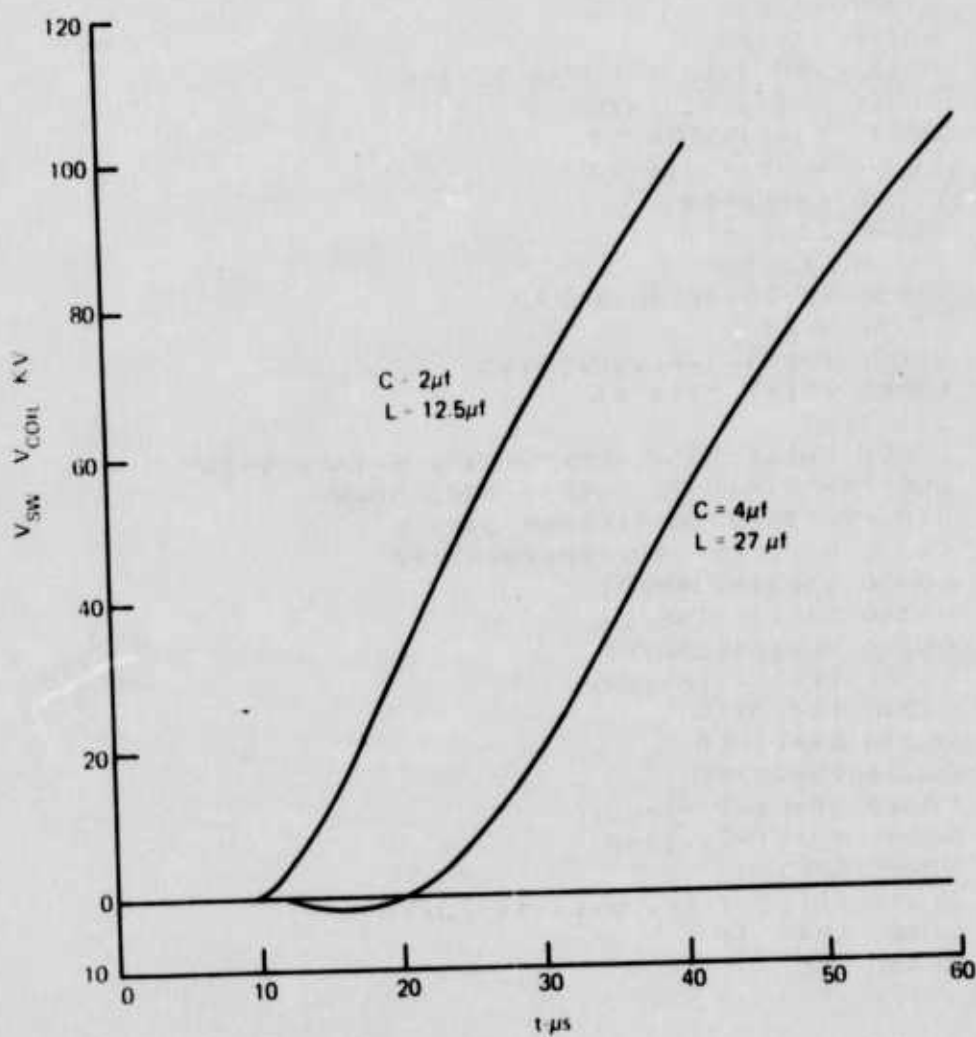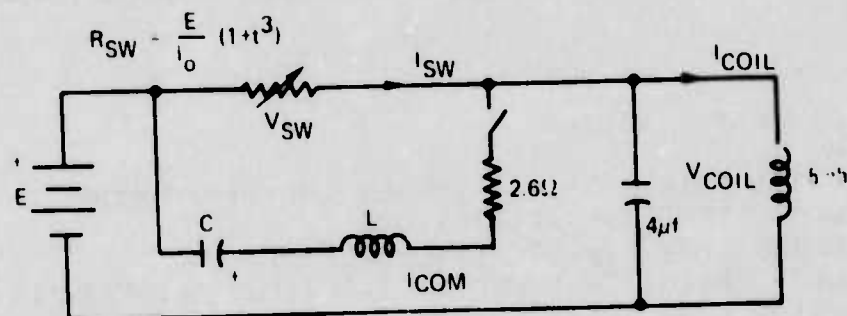
S73-0203-VA-21

Figure B-4.   Single section network switch and coil voltages vs time.

Single Section Network Commutator Computer Program

```
PROGRAM    VACSW2

00100 PRINT  "T","RO","V-L1","I-SW","V-SW"
00110 READ  R,L1,C1,L2,C2,H
00120 DATA  2.6,27E-6,4E-6,5E-3,4E-6
00130 PRINT  "R="R,"C1="C1,"L1="L1,"C2="C2,"L2="L2
00140 DATA  1E-7
00150 I2=2E4
00160 RO=500/I2
00170 K=1E18
00180 V1=1E5
00190 FOR T=0 TO 20E-6 STEP H
00200   V1=V1-I1*H/C1
00210   I1=I1+V2*H/L1
00220   V2=V1-I1*R-V3
00240   I4=I2+I3
00245   I5=I1-I4
246  V3=I5*RO
00250 IF  I5=>0 THEN 270
00260 NEXT T
00270 PRINT  T,RO,V2,I5,V3
00280 PRINT  "V1="V1
285  T0=T
00290 PRINT  "T","RO","V-L1","I-SW","V-SW"
300  FOR T1=T0 TO 500E-6 STEP 50*H
310  FOR T=T1 TO T1+50*H STEP H
00320   RO=500*(1+(T-T0)*3*K)/I2
00330   V1=V1-I1*H/C1
00340   I1=I1+V2*H/L1
00350   V0=V0+I3*H/C2
00360   I2=I2+V0*H/L2
00370   I3=I4-I2
00374   I4=I1-I5
00376   I5=V3/RO
00380   V2=V1-I1*R-V0
00390   V3=V1-V2-I1*R
00400 NEXT T
00410 PRINT  T,RO,V2,I1-I2-I3,V3
00420 NEXT T1
00430 END
```

Table B-1

144

$$\frac{4 \times 10^{-6} \times 10^{10}}{2} = 20 \text{ kilojoules}$$

Although the voltage rise is slightly steeper than the specified rate of 2.5 kV/µsec, the arc extinguishes, and the VI recovers, shortly after the I_{SW} transition through zero. The curves of Figure B4 will, therefore, lie entirely below the VI voltage recovery curves.

Figures B5 through B8 show corresponding transient shapes for a two-section network. Note the differences between Figures B3 and B7 for the interrupter current I_{SW}. Compare the 4µf, 27 µH transient of Figure B3 with the 20 µsec pulse of Figure B7. (The total capacitance is approximately equal for these cases.) Note that in Figure B3 the interrupter current is changing rapidly up to about 15 µsecs after the commutator cycle is initiated. In this case the vacuum interrupter may not open since the current is still high ($\approx$ 250A). In Figure B7 the 20 µsec pulse, high current, rapidly changing portion is completed in about 7.5 µsecs. Then for 7.5 µsecs the rate of change of current and the magnitude are both low. This should be the condition which will permit complete deionization. The pulse shapes shown are far from optimum, but do indicate the possibility of some shaping of both the current amplitude and rate of change to suit the ultimate switch behavior better than for the single section network.

The results thus far indicate that commutation networks with more sections to reduce pulse top ripple should be an advantage in minimizing current variation during interruption. This should be possible without increasing the total capacitance required.

145

TWO SECTION NETWORK

$$R_{SW} = \frac{E}{I_o}(1+t^3)$$

I_{SW} I_{COIL}

V_{SW}

E   L2   2.6Ω V_{COIL} 5 mh

C1   L1   4μf

C2

τ	C1 μf	C2 μf	C_T μf
40	6.2	4.1	10.3
20	3.1	2	5.1
10	1.55	1	2.55

I_{SW} KA

$\tau = 40\mu s$

$\tau = 20\mu s$

$\tau = 10\mu s$

t μs
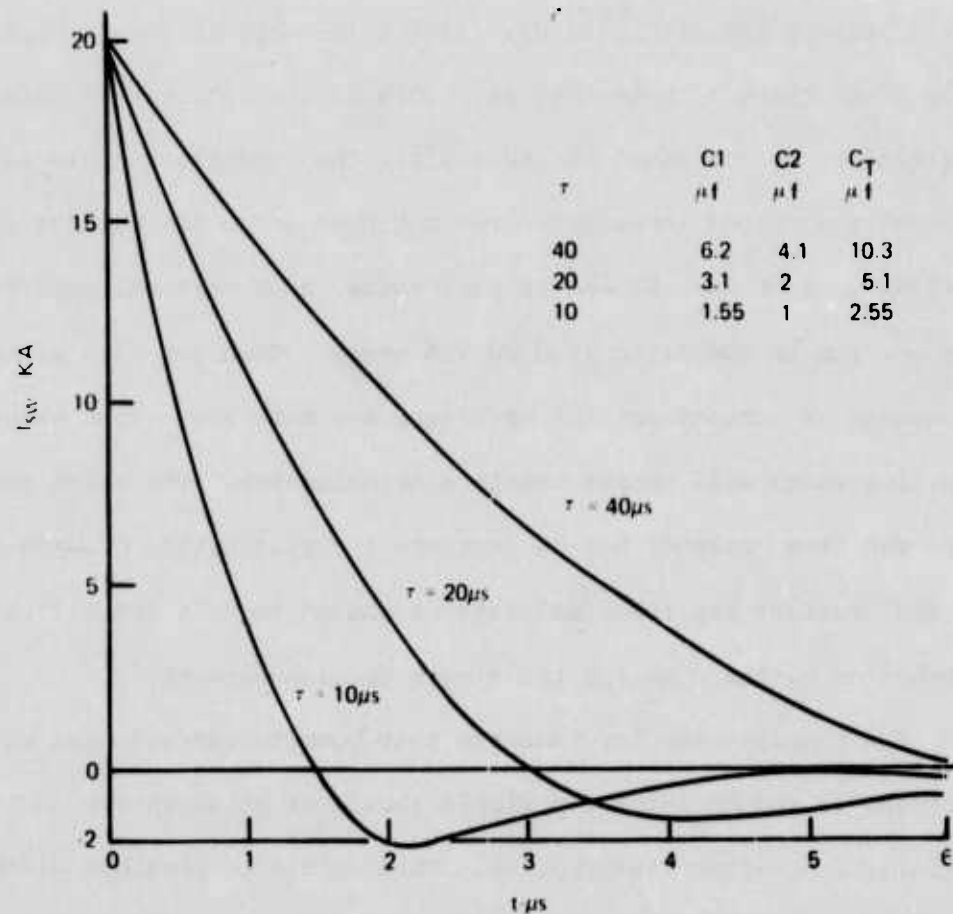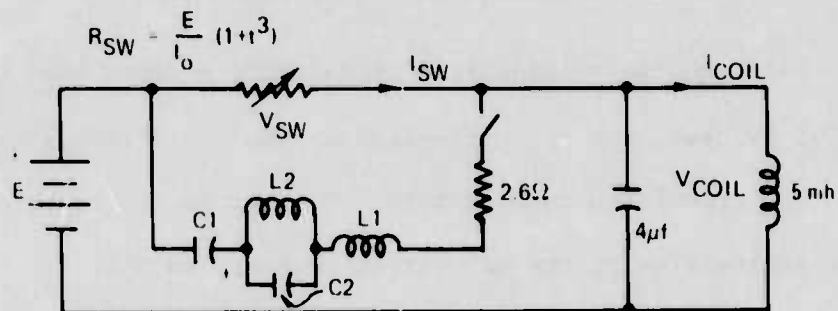
S73-0203-VA-22

Figure B-5. Two-section network switch current vs time.

146

TWO SECTION NETWORK

$$R_{SW} = \frac{E}{I_o} (1+t^3)$$

V_{SW}

I_{COIL}

E

C1

L2

L1

2.6Ω

V_{COIL}

5 mh

4μf

C2

25

20

15

$I_{COM} \cdot KA$

10

5

0   10   20   30   40   50   60

$t \cdot \mu s$
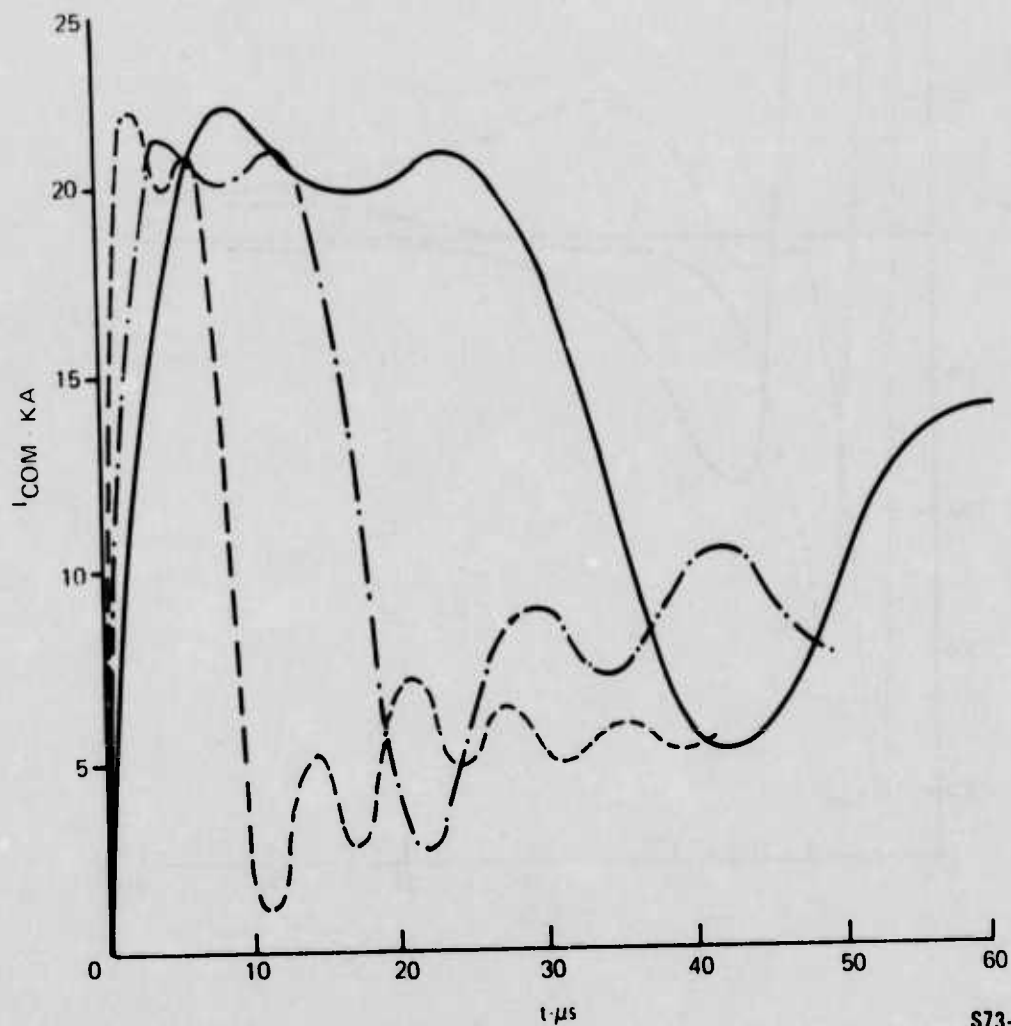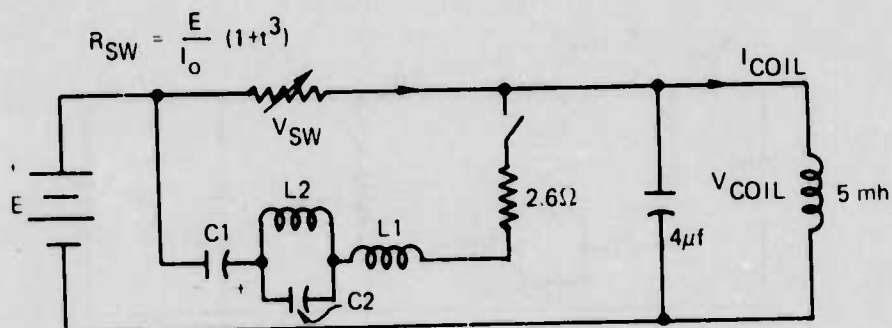
S73-0203-VA-23

Figure B-6.   Two-section network commutator current vs time.

147

TWO SECTION NETWORK
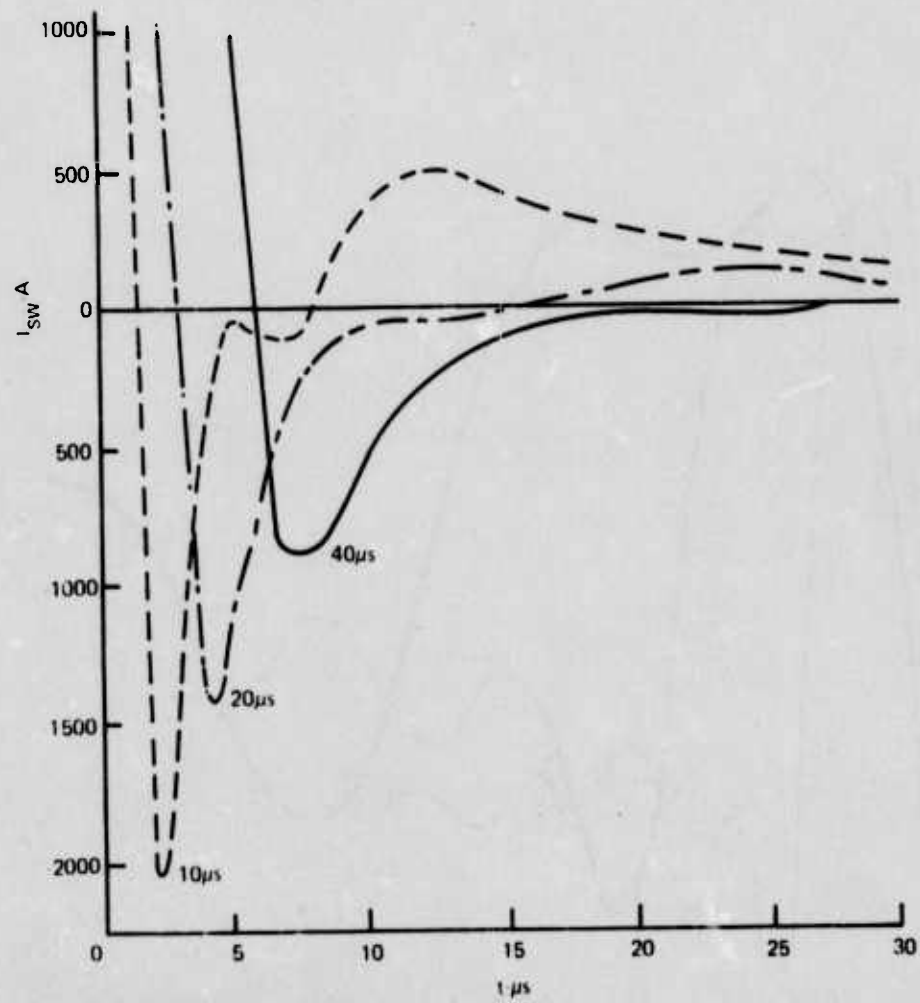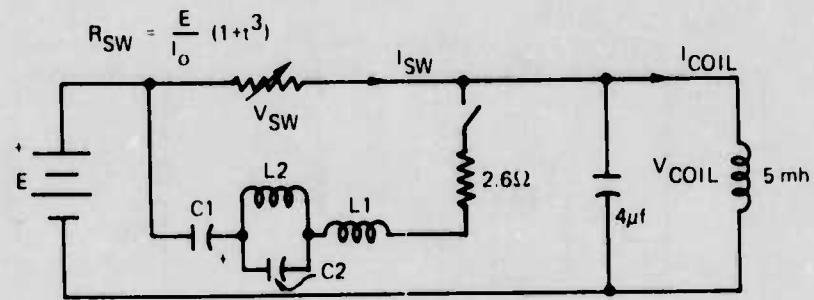
S73-0203-VA-24

Figure B-7. Two-section network switch current vs time (compressed scale).

148

TWO SECTION NETWORK
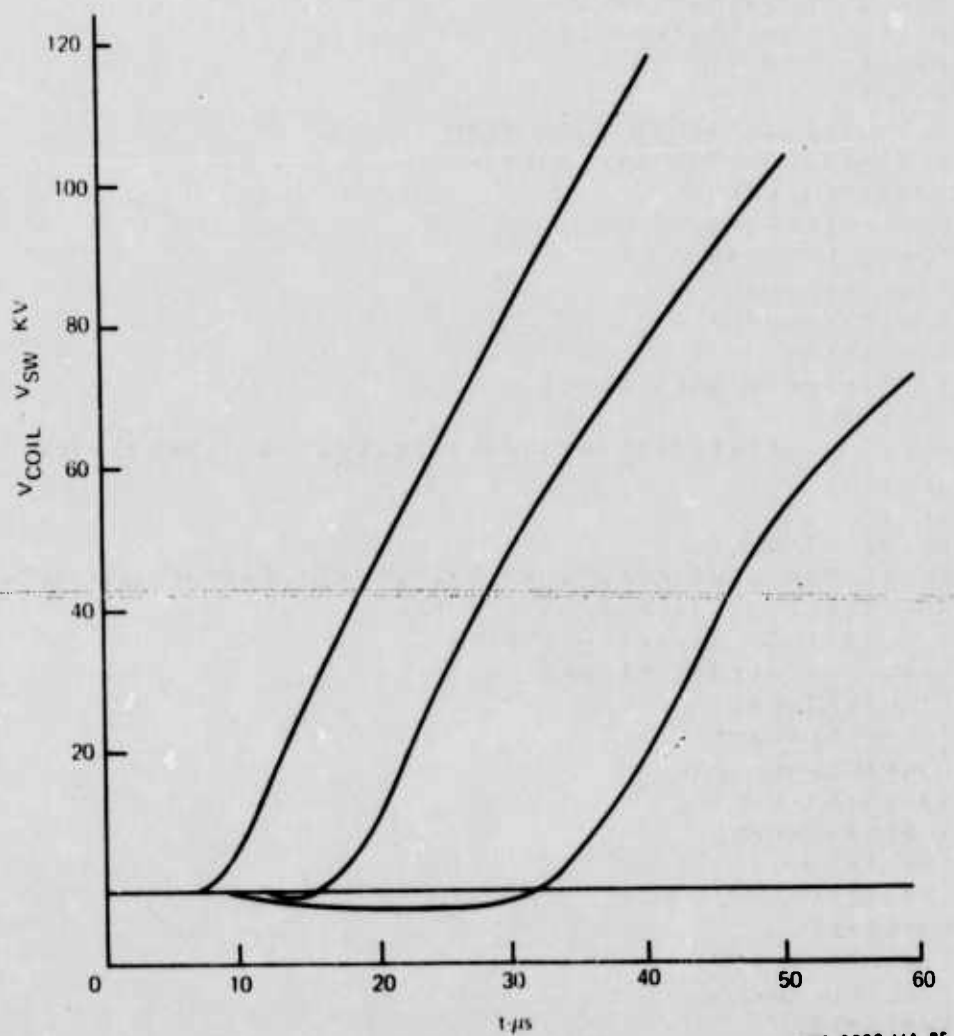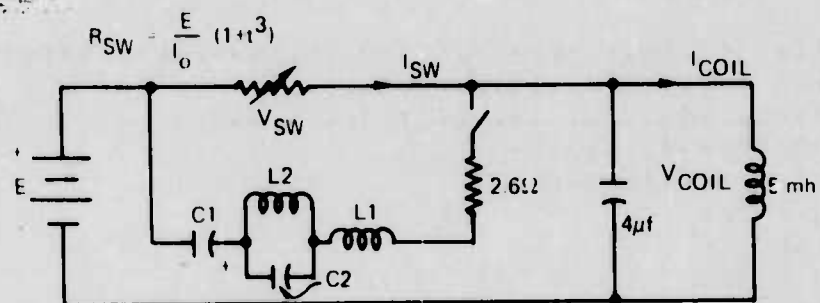
Figure B-8. Two-section network switch and coil voltages vs time

S73-0203-VA-25

149

```
PROGRAM   SWITCH

00100  PRINT "I-MICROSECS.","I-COM.","I-COIL.","V-COIL.","V-C1"
00110  READ A,F,G,D,H,B,T,Z,R,C3,L5,16
00120  DATA .387,.256,.19,.6666,1003,2.6
00130  DATA 6CF-6,8.5,1F-8
00140  DATA 4F-6,5F-3,2F4
00150  C1=F*T/2
00160  C2=F*T/2
00170  L1=G*T*Z
00180  L2=D*T*Z
00190  V1=B
00200  PRINT "B=",B,"Z=",Z,"T=",T
00210  PRINT "C1=",C1,"C2=",C2
00220  PRINT "L1=",L1,"L2=",L2
00230  PRINT "C3=",C3
00240  F=1F15
00250  FOR T1=0 TO 2CF-6 STEP 5C*R
00260  FOR T=T1 TO T1+5C*R STEP R
00270  V1=V1-11*R/C1
00280  V2=V2+12*R/C2
00290  V3=V1-V2-11*R
00300  11=11+V3*R/L1
00310  13=13+V2*R/L2
00320  12=11-13
00330  IF 11-16=>0 THEN 00370
00340  NEXT T
00350  PRINT T*1F6,INT(1F4*11)/1F4,16,V6,INT(1F4*V1)/1F4
00360  NEXT T1
00370  TC=T
00380  PRINT "TC=",TC
00390  PRINT "I-MICROSECS.","I-COM.","I-SW.","V-COIL/SW.","I-COIL"
00400  FOR T1=TC TO 1CCF-6 STEP 1CC*R
00410  FOR T=T1 TO T1+1CC*R STEP R
00420  16=.C25*C1+(T-TC)*3*R2
00430  V1=V1-11*R/C1
00440  V2=V2+12*R/C2
00450  V3=V1-V2-V6-11*R
00460  11=11+V3*R/L1
00470  13=13+V2*R/L2
00480  12=11-13
00490  15=V7/16
00500  17=11-15
00510  V6=V6+14*R/C3
00520  17=17+V6*R/L5
00530  14=17-16
00540  V7=V1-V2-V3-11*R
00550  NEXT T
00560  PRINT T*1F6,INT(1CC*11)/1CC,INT(1CC*15)/1CC,INT(1CC*V6)/1CC,
00570  PRINT INT(1CC*16)/1CC
00580  NEXT T1
00590  END
```

Table B-2

An investigation of a 5-section 1.25 ohm, 20µ sec Type C network was performed. This network is not ideal from a pulse-top ripple point of view, but is easier to compute than the flatter-topped Type E which involves mutual coupling between inductors.

Figure B9 shows the initial portion of the VI current for two values of initial network voltage. The 51 kV transient is similar to that for the 20 µsec, 2-section network (Figure B5) except that, since the pulse rise time is shorter, the current zero occurs earlier. The 47 kV transient may be advantageous since the current, and hence the voltage across the VI never reverses.

Figure B10 shows the commutator current (I_{COM}) pulse shape. Note that the post-pulse reflections are worse than for the single and 2-section networks because the mismatch to the lower impedance network is worse after the VI opens. The effect of these reflections is seen in Figure B12 in the steeper rise in coil voltage in the interval between 18 and 30 µsec.

Figure B11 shows the VI current (I_{SW}) on an expanded scale. Note that for the 51 kV transient the current reverses twice, as it does for the simpler networks. For the 47 kV transient the current never reverses. In both cases the amplitude of the ripple after about 5 µsecs is only slightly less than for the simpler networks. It is possible to reduce this ripple considerably with the Type E network so as to have a more precise control of VI current during interruption.

The computer program utilized in generating these results is shown in Table B3.

151

5-SECTION NETWORK

$$R_{SW} = \frac{E}{I_o}(1 + t^3)$$

C1 = 6.27μf
C3 = 0.531μf
C5 = 0.105μf
C9 = 0.0096μf

L1 = 6.46μh
L3 = 8.48μh
L5 = 15.42μh
L7 = 46.18μh
L9 = 523.5μh

47 KV

51 KV

I_{SW} KA

t μs
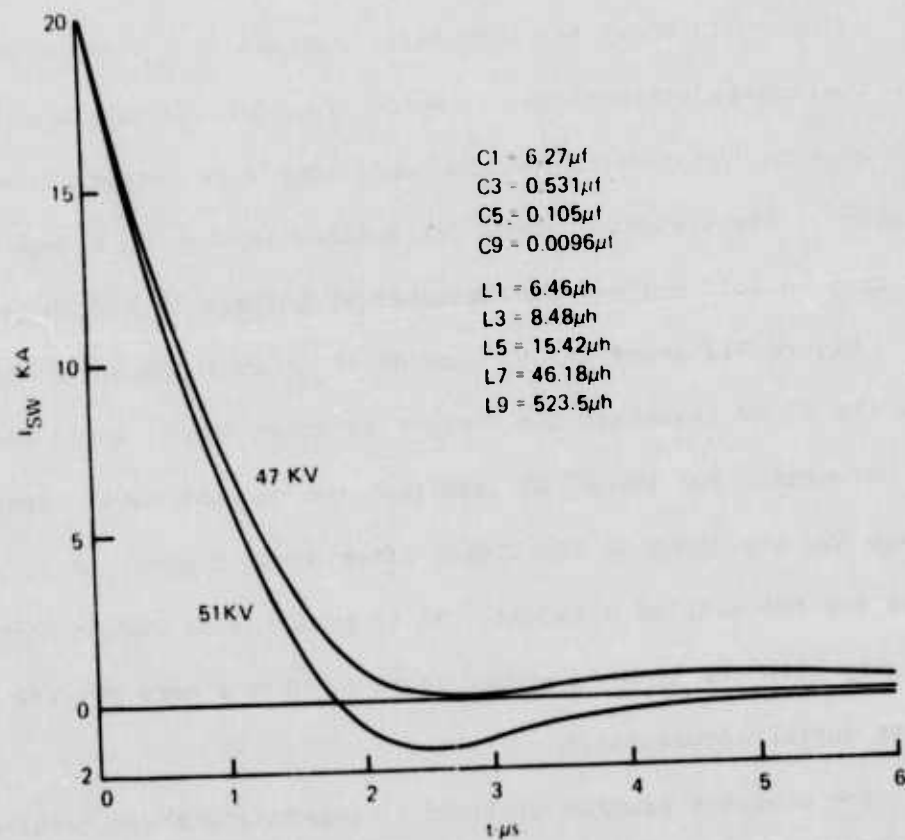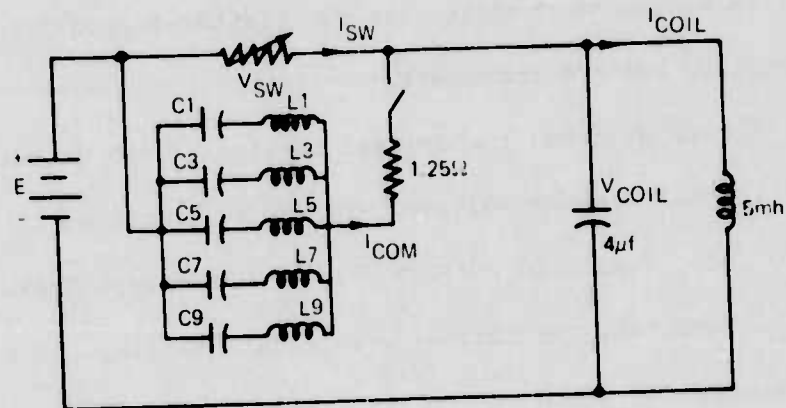
S73-0203-VA-26

Figure B-9. Five-section network switch current vs time.

5-SECTION NETWORK

$$R_{SW} = \frac{E}{I_o} (1 + t^3)$$
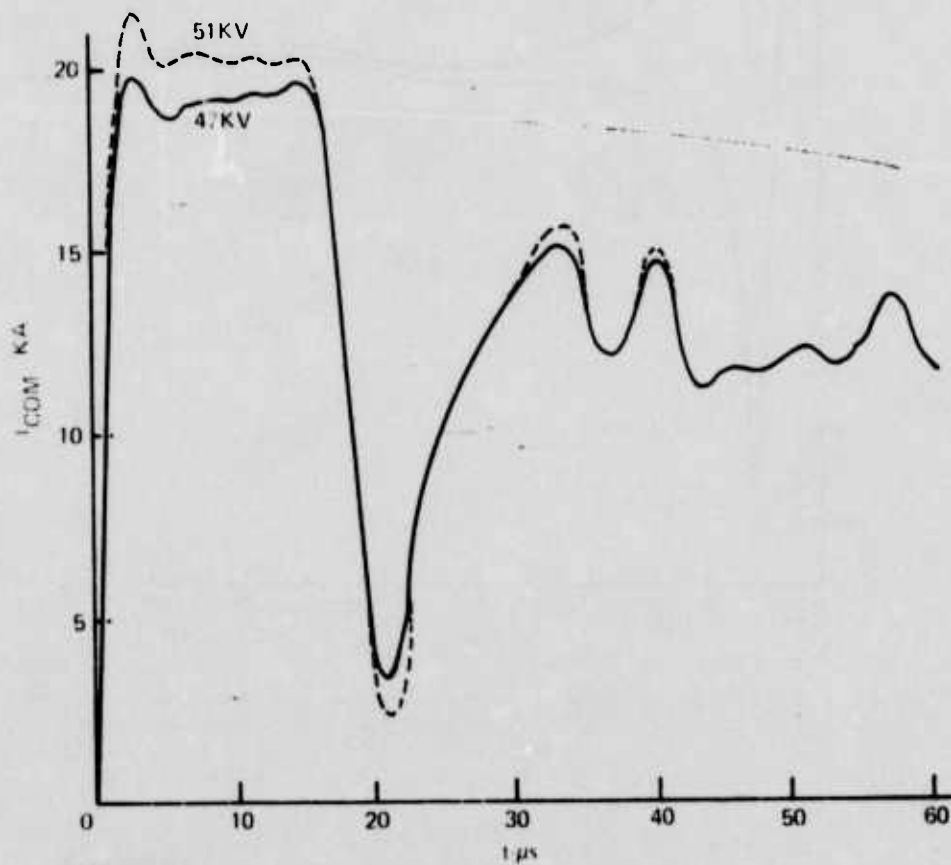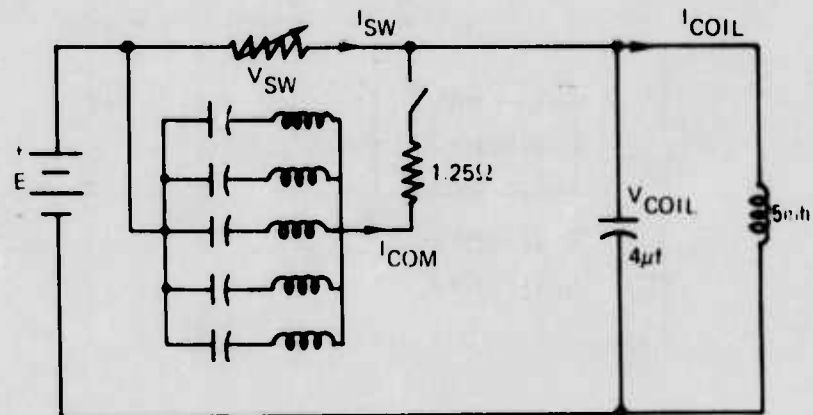
S73-0203-VA-27

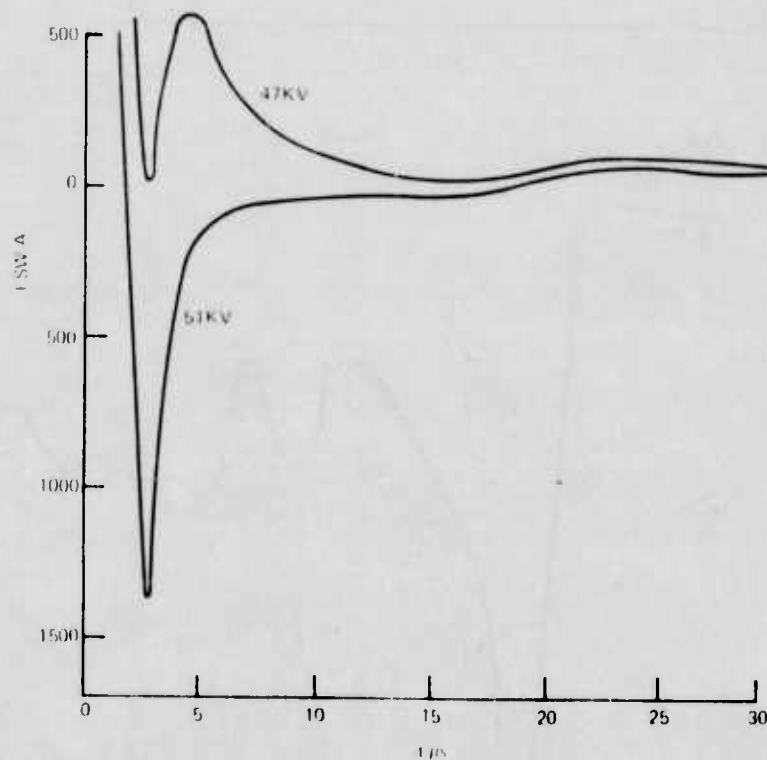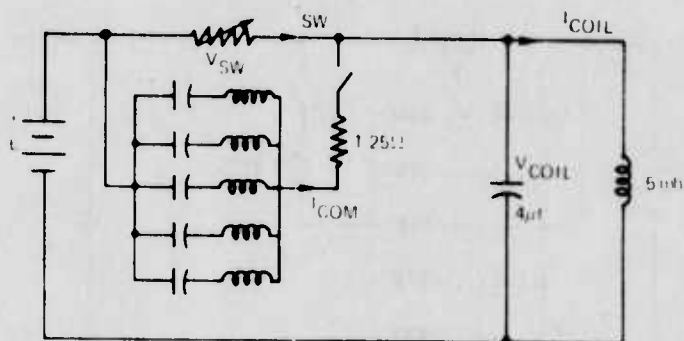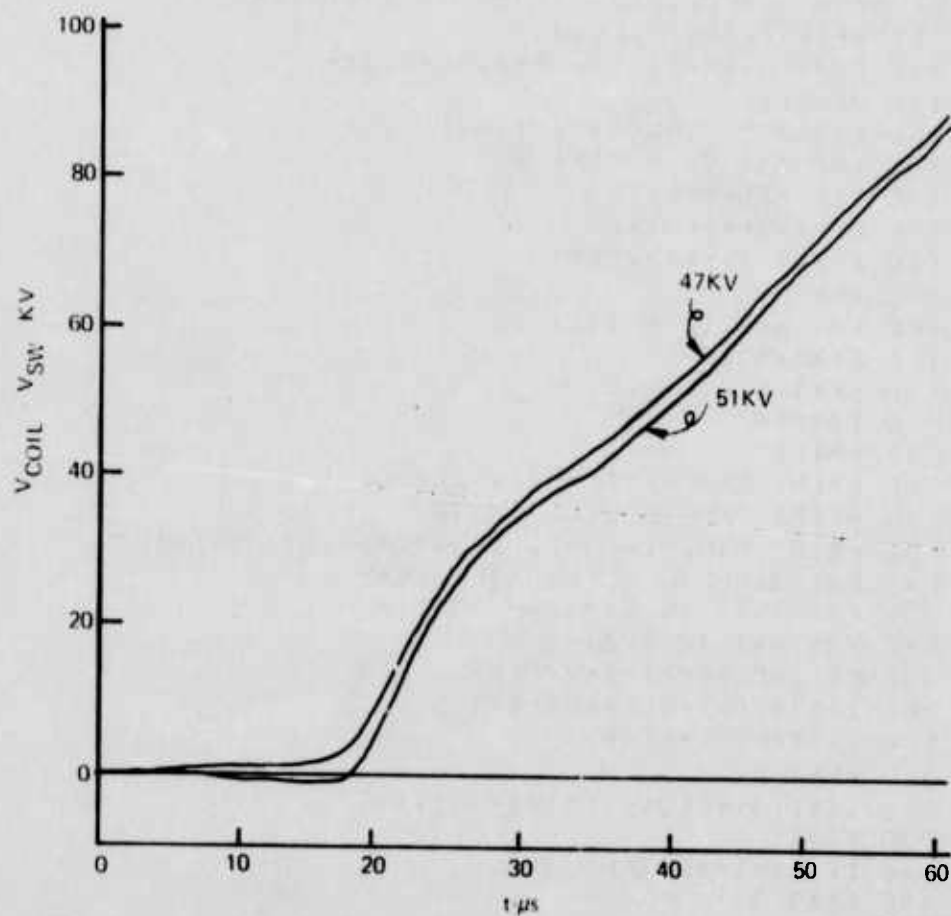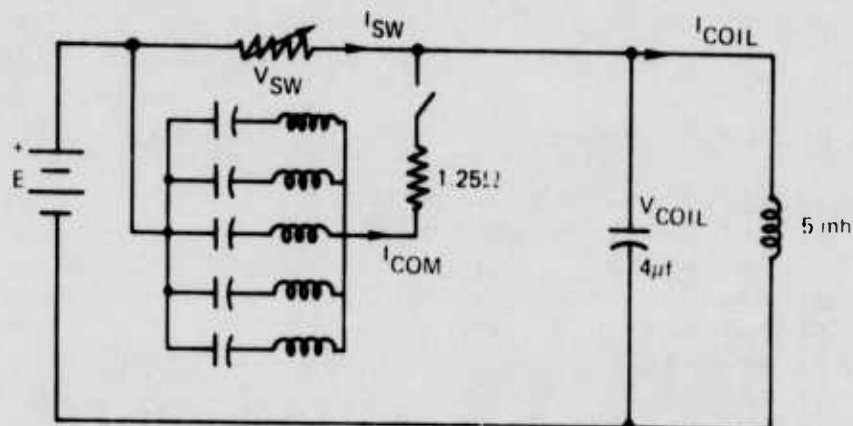Figure B-10. Five-section network commutator current vs time.

153

5 SECTION NETWORK

$$RSW = \frac{E}{I_0} \ (1 + t^3)$$

Figure B-11. Five-section network switch current vs time (compressed scale).

5-SECTION NETWORK

$$R_{SW} = \frac{E}{I_o} \ (1 + t^3)$$

S73-0203-VA-29

Figure B-12.   Five-section network switch and coil voltages vs time.

```
PROGRAM    5SECT

10 PRINT "5-SECTION NETWORK"
20 FOR N=1 TO 9 STEP 2
30 READ L(N)
40 NEXT N
50 FOR N=1 TO 9 STEP 2
60 READ V(N)
70 NEXT N
80 DATA .3981,.03318,.00657,.00112,6E-5
90 DATA .2584,.3393,.6168,1.8472,20.94
100 READ F,TC,CC,LC,R
110 DATA 1.25,2CE-6,3E-6,5E-3,1E-8
115 VC=500
120 PRINT "N","L(N)","C(N)"
130 FOR N=1 TO 9 STEP 2
140 C(N)=TC*U(N)/R
150 L(N)=TC*V(N)*R
160 PRINT N,L(N),C(N)
170 NEXT N
180 FOR N=1 TO 9 STEP 2
190 E(N)=51E3
200 NEXT N
210 I6=2E4
215 PRINT
220 PRINT "R=",R,"CC=",CC,"LC=",LC
225 PRINT "PULSE LENGTH=",TC
230 PRINT "I","I-COM","I-SW","V-SW","V-COIL"
240 FOR T1=0 TO 6CE-6 STEP 5C*R
250 FOR T=T1 TO T1+5C*R STEP R
260 FOR N=1 TO 9 STEP 2
270 E(N)=E(N)-I(N)*R/C(N)
280 I(N)=I(N)+V(N)*R/L(N)
300 V(N)=F(N)-I(*R
310 NEXT N
320 IC=I(1)+I(3)+I(5)+I(7)+I(9)
330 I2=IC
340 IF I2-I6>C THEN 380
350 NEXT T
```

Table B-3

156

```
360  PRINT T,I(,I2-I6,V2,V0
370  NEXT I1
380  T0=T
365  PRINT
390  PRINT T,I(,I2-I6,V2,V0
400  FOR T1=T0 TO I((F-F STEP 50*H
410  FOR T=T1 TO T1+50*H STEP H
420  FC=.(25*(1+(T-T0)*3*1F18)
430  FOR N=1 TO 9 STEP 2
440  F(N)=F(N)-I(N)*H/C(N)
450  I(N)=I(N)+V(N)*H/L(N)
470  V(N)=F(N)-I(*F-V0
480  NEXT N
485  I0=I(1)+I(3)+I(5)+I(7)+I(9)
490  VC=V(+14*H/C0
500  I6=I6+V0*H/L(
510  I4=I8-I6
520  I8=I0-I8
530  I2=V2/R0
540  V2=F(1)-V(1)-I(*F
550  NEXT T
560  PRINT T,I(,I2,V2,V0
570  NEXT T1
999  END
```

Table B-3

157

B-3   Analog Computer Analysis

Analog simulation has the advantage of fast printout in graphic form. With a multi-channel recorder many waveforms of voltages and current can be simultaneously observed. Changes of component values can be rapidly made to find overall circuit effects. Since the analog computer operates in real time with limited amplitude, time scaling and amplitude scaling are necessary for mechanization of the equations. Thus, the programming of the analog simulation is somewhat more involved, but it does allow non-linear, time variation, and step functions to be included.

After simulation of the one section commutation system previously discussed, the analog computer was programmed for the three section network shown in Figure B13, Basically, this is a three section E-type pulse forming network. The network is a lumped constant transmission line used to commutate the current in the interrupter. It has the characteristic of producing an essentially flat-topped current pulse for a given time duration. Unlike a single section capacitor which when discharged would give only one current zero crossing in the vacuum interrupter, the network can produce current zero for a much longer period of time. This provides the interrupter a longer period for deionization and delays application to the interrupter of the high voltage produced by the storage coil.

The network is used in the circuit shown in Figure B14. The sequence of operation of the circuit shown in Figure B14 is as follows. E is the source voltage supplying 20,000 amperes to storage coil L. SW1 is the vacuum
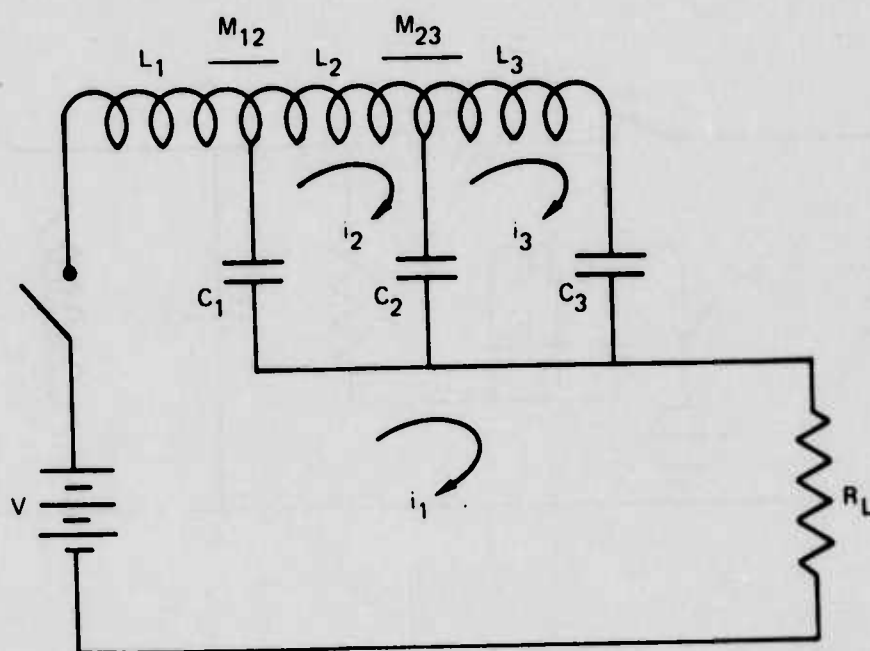
S73-0203-VA-30

NETWORK:

$$L_1 \frac{di_1}{dt} + M_{12} \frac{di_2}{dt} + R_L i_1 + \frac{1}{C_1} \int ((i_1 - i_2)\, dt = V$$

$$L_2 \frac{di_2}{dt} + M_{12} \frac{di_1}{dt} + M_{23} \frac{di_3}{dt} - \frac{1}{C_1} \int (i_1 - i_2)\, dt + \frac{1}{C_2} \int (i_2 - i_3)\, dt = 0$$
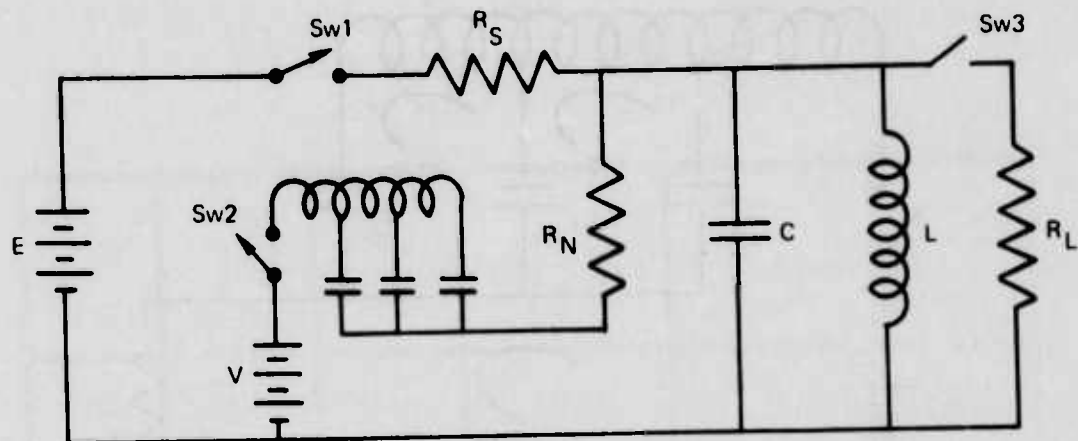
$$L_3 \frac{di_3}{dt} + M_{23} \frac{di_2}{dt} - \frac{1}{C_2} \int (i_2 - i_3)\, dt + \frac{1}{C_3} \int i_3\, dt = 0$$

$$\frac{d\,i_1}{dt} = -\frac{M_{12}}{L_1} \frac{d\,i_2}{dt} - \frac{R_L}{L_1} i_1 - \frac{1/C_1}{L_1} \int (i_1 - i_2)\, dt + \frac{V}{L_1}$$

$$\frac{d\,i_2}{dt} = -\frac{M_{12}}{L_2} \frac{di_1}{dt} - \frac{M_{23}}{L_2} \frac{di_3}{dt} + \frac{1/C_1}{L_2} \int (i_1 - i_2)\, dt - \frac{1/C_2}{L_2} \int (i_2 - i_3)\, dt$$

$$\frac{d\,i_3}{dt} = -\frac{M_{23}}{L_3} \frac{di_2}{dt} + \frac{1/C_2}{L_3} \int (i_2 - i_3)\, dt - \frac{1/C_3}{L_3} \int i_3\, dt$$

Figure B-13.   Three-section E-type pulse forming network.

159

S73-0203-VA-31

Figure B-14   Network Commutator

interrupter which opens, but arcs, at 20,000 A. When SW1 is fully opened,
SW2 (spark gap) is closed discharging the network into the coil. Impedance
and charge voltage V is such that the network supplies 20,000 amperes for a
definite period of time. During this time, current ceases to flow through
the vacuum interrupter, thus allowing the arc to extinguish. At the end of
the current pulse, voltage rises across storage coil L due to the collapsing
magnetic field. At the proper voltage level, SW3 closes and connects the load
R_L. This entire sequence has been simulated on the analog computer for
various network parameters, and the results will be described in detail.

A time period of 20 μsec was assumed to be adequate for arc
extinction and VI plasma decay. Table B4 lists parameters for 20 μsec three
section networks ranging in impedance levels from 0.5 ohm to 2.5 ohms. The
section and total network capacitance are given for each network. It can be
seen that the total capacitance decreases rapidly between 0.5 ohm and 1.5 ohms

160

TABLE B4

THREE-SECTION COMMUTATION NETWORKS

PULSE WIDTH OF 20 µSEC

NETWORK IMPEDANCE (OHM)	SECTION CAPACITANCE (µFD)	TOTAL CAPACITANCE (µFD)	STORAGE VOLTAGE (KV)	ENERGY LOSS PER PULSE (W-SEC)	WATTAGE LOSS 5 PPS (KW)
0.5	6.9	20.7	20	4,000	20
1.0	3.46	10.38	40	8,000	40
1.5	2.3	6.9	60	12,000	60
2.0	1.73	5.19	80	16,000	80
2.5	1.38	4.14	100	20,000	100

and then decreases rather slowly from 1.5 to 2.5 ohms. Storage voltage re-
quired on the network prior to discharge is shown in the next column. Maximum
voltage of 100 KV is required for the 2.5 ohms network. Since, however, all
of the networks must withstand the 100 KV produced by the coil, they all would
require capacitors with the same voltage rating, and the 2.5 ohms network
would have the minimum weight. Stored energy per pulse, and hence total
wattage loss at 5 PPS, is minimum for the 0.5 ohm network. In addition to
the trade-off between minimum weight of capacitors and minimum losses as a
function of network impedance, considerations must also be given to power
supply weight. As shown, there is a five to one difference in losses which
must be supplied. Thus, as the network weight is reduced there is an increase
in power supply weight with additional coolant requirements. For the purposes
of study, the 1.5 ohms network was selected as a compromise.

The 20 µsec schematic and equations are shown in Figure B13. Element

values for the various networks are given in Table B5. Those selected and used are given for the 1.5 ohm, network. In the Figure B13 schematic, L_1, L_2, L_3 represent coil values of inductance with mutual coupling M_{12} and M_{23} as given in Table B5 The three capacitors C_1, C_2, and C_3 have the same value of 2.3 μf each. The equations and element values were mechanized as shown in Figure B15. The output current waveform of the E-type network under a matched load condition is shown in Figure B16. Peak current was 20,000 amperes into a 1.5 ohm resistive load. Approximately 15 sec flat top is available for the commutation period.

TABLE B5

THREE SECTION COMMUTATION NETWORK

PULSE WIDTH OF 20 μSEC

	NETWORK IMPEDANCE				
	.5	1.0	1.5	2.0	2.5
L_1	2.34	4.68	7.02	9.36	11.7 μH
L_2	1.27	2.54	3.81	5.08	6.35 μH
L_3	1.37	2.74	4.11	5.48	6.85 μH
M_{12}	0.158	0.316	0.474	0.632	0.790 μH
M_{23}	0.173	0.346	0.519	0.692	0.865 μH
C	6.9	3.46	2.3	1.73	1.38 μFD

Using the techniques described above, the commutating and interrupter system was simulated on the analog computer. Schematic for this is shown in Figure B17. The current flow is as follows: i_1 is commutating current supplied by the network, i_4 is current in the storage coil L, i_5 is load current
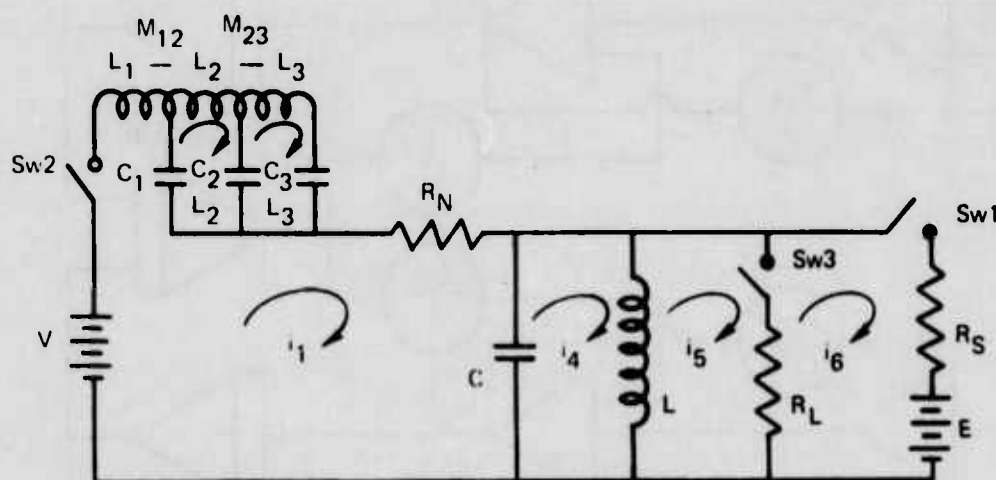
162
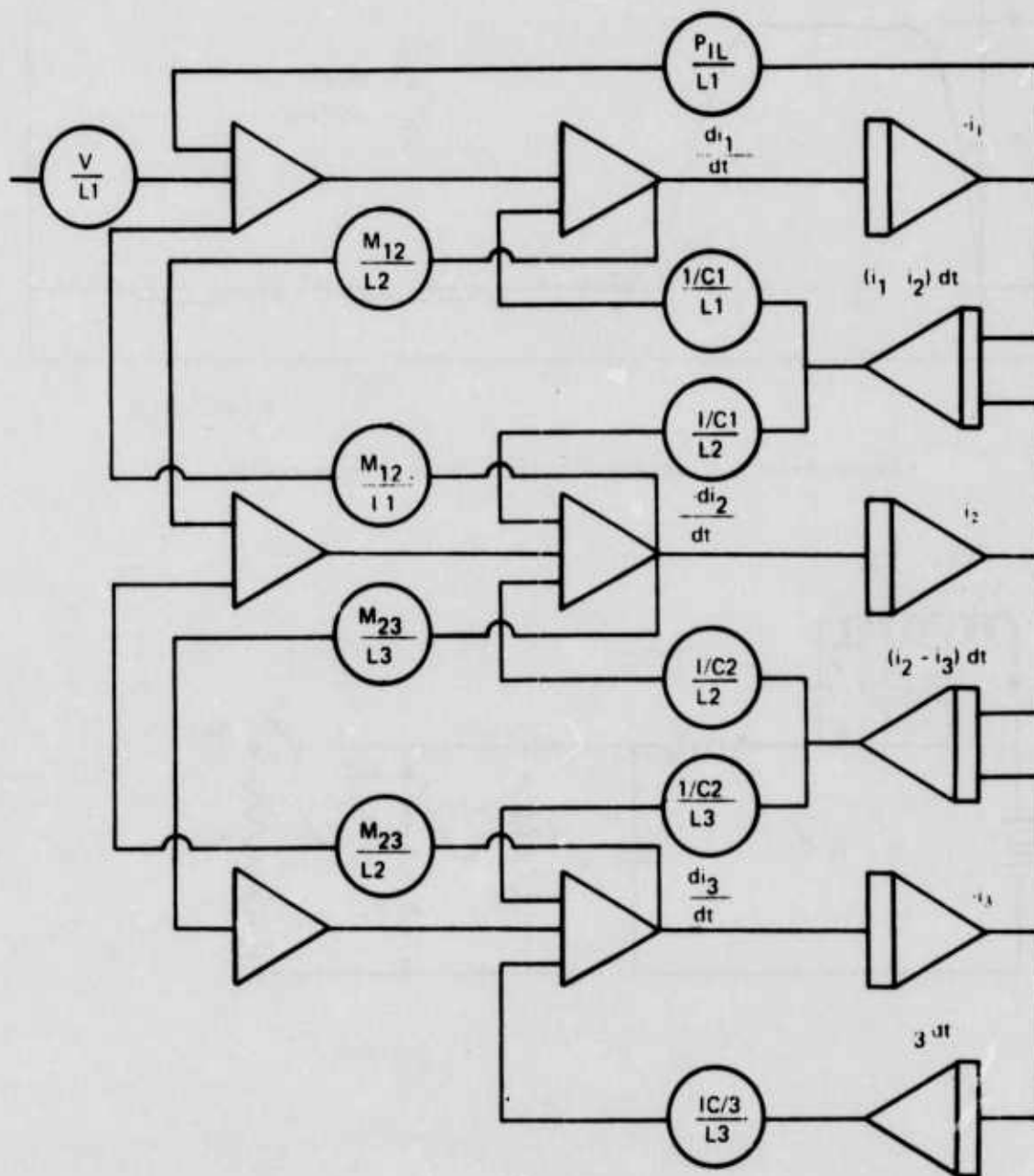
S73-0203-VA-32

Figure B-15. Schematic of Analog Computer Program.

163
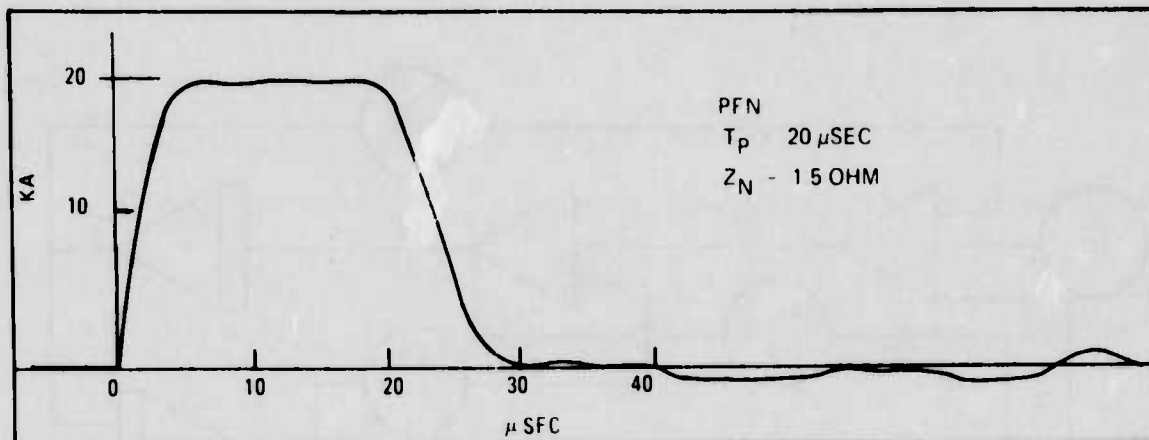
S73-0203-VA-33

Figure B-16. Current waveform of E-type network

L = 5 mh
C = 1 μfd
R_L = 10 ohms
R_S = .05 ohm
R_N = 1.5 ohms
E = 1000 V

S73-0203-VA-34

Figure B-17. Schematic of Commutator and Interrupter Circuit.

164

supplied from storage coil L, and i_6 is current from source voltage E to storage coil L prior to commutation. R_S is the resistance of interrupter plus all connecting cables and contacts and is assumed to be 0.05 ohm total. Mechanization of the interrupter and storage coil equations is shown in Figure B18.

Waveforms of a complete switching cycle are shown in Figure B19. Both zero reference level (0) and initial conditions (I.C.) are given for current i_4 and i_6, where the vertical scale is 5,000 amperes/cm. V_c is the voltage across capacitor C produced by the discharge of energy in the storage coil L, and also the voltage appearing across the load resistor R_L when it is connected. It can be seen that initially i_4 and i_6 have a value of 20,000 amperes at the end of the charge cycle. At time T_o, switch S_2 is closed causing the network to discharge. The discharge current from the network is shown as i_1 which commutates for a period of 15 μsec. During this period of zero current of i_6, the arc is assumed to be quenched and switch 1 (interrupter) recovers. Following the commutation period, voltage rises across the storage coil as shown by V_c. At approximately 70 KV, load resistor R_L is connected by closing switch 3. The voltage continues to rise to approximately 90 KV then decays in an R-L-C transient. It is interesting to note the influence of the network after commutation. After discharge of the network, the voltage build-up across the storage coil causes the network to be charged in the opposite polarity. This can be seen as i_1 continues to flow after network discharge. Interaction of the network and coil causes ripple on the output voltage as shown by V_c. During the output pulse, the coil current i_4 decreases to zero. Figure B20 shows the same cycle except that the load R_L is switched
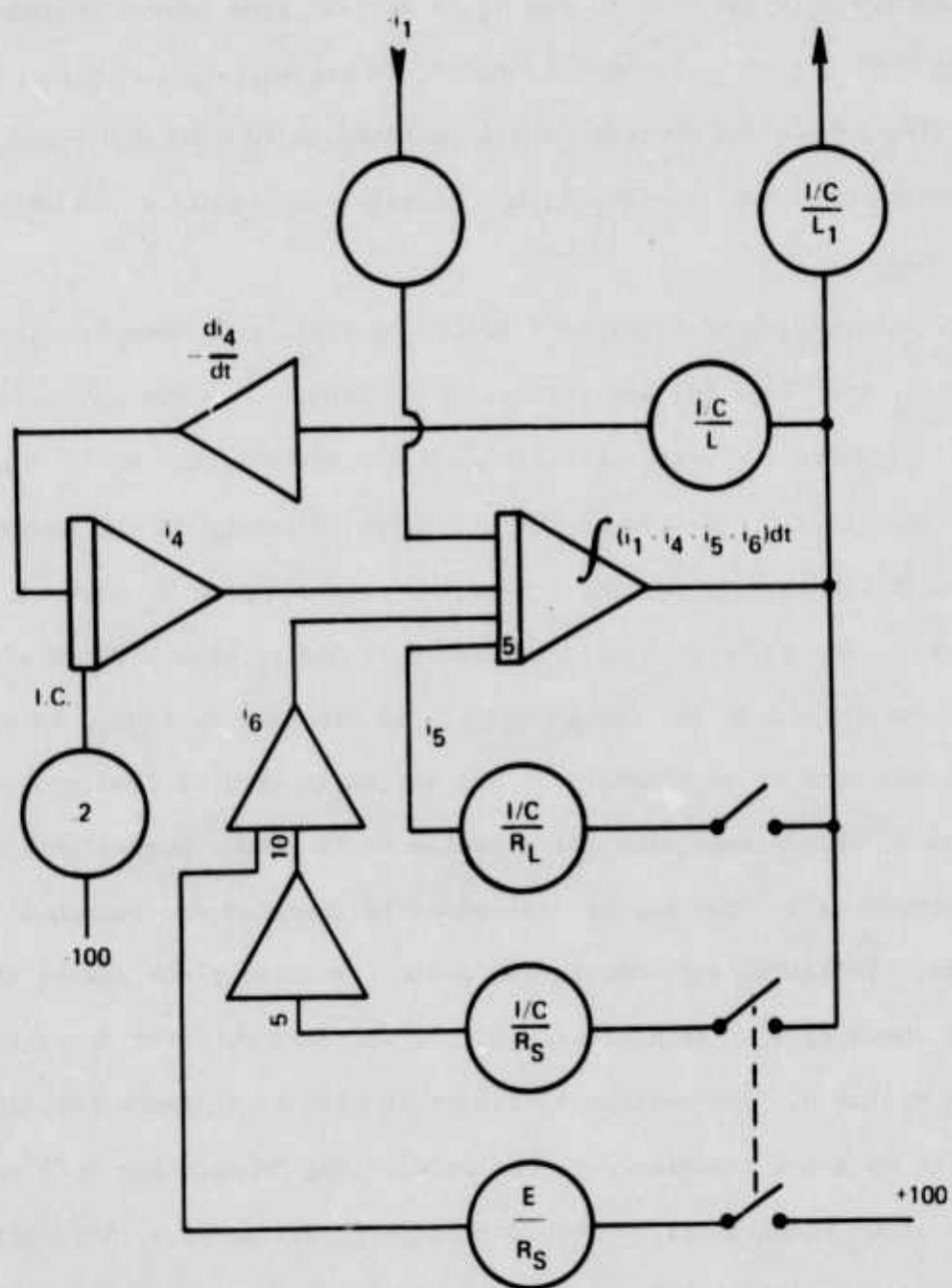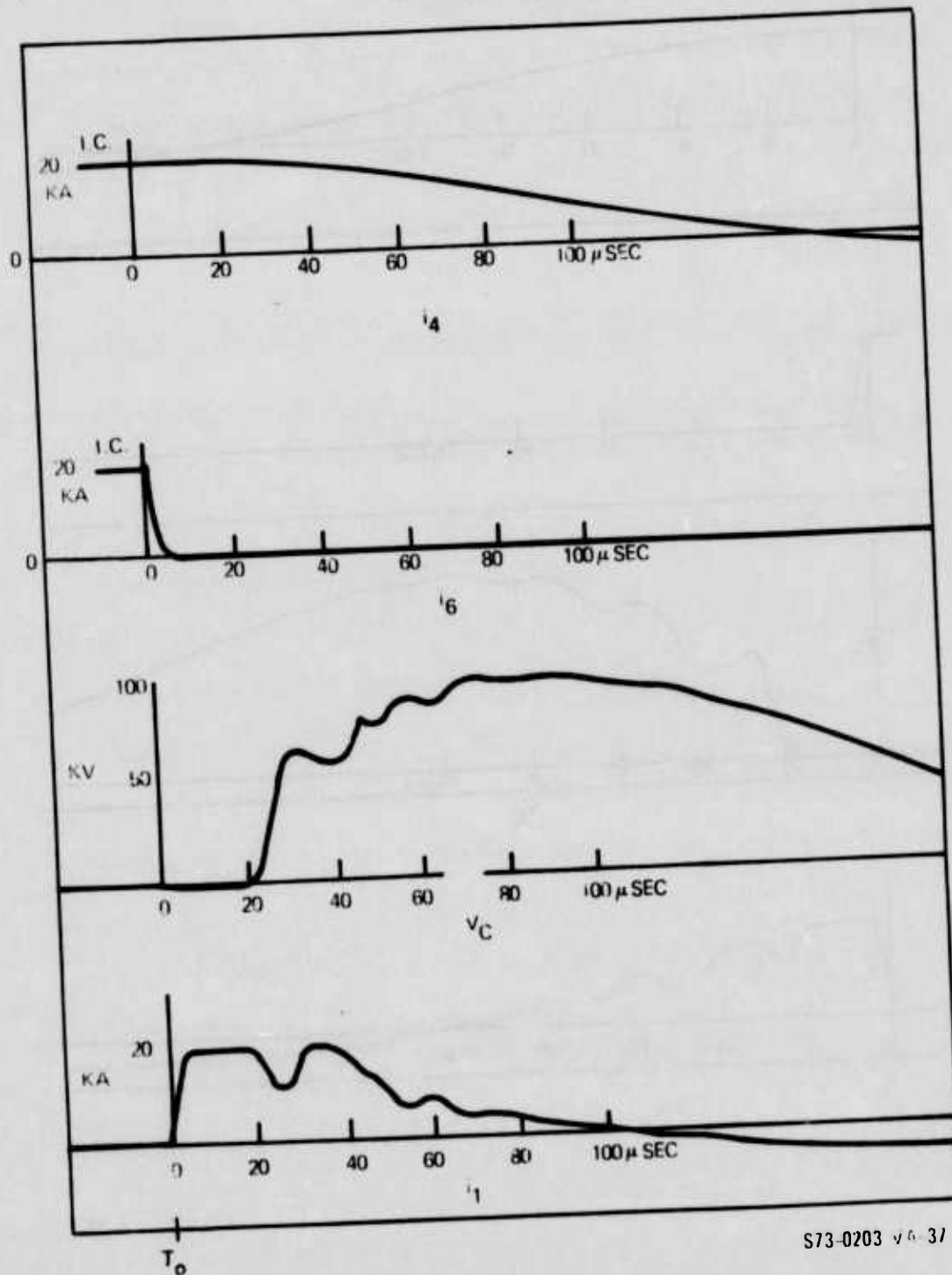
Figure B-18. Mechanization of Interrupter and Storage Coil Equations.
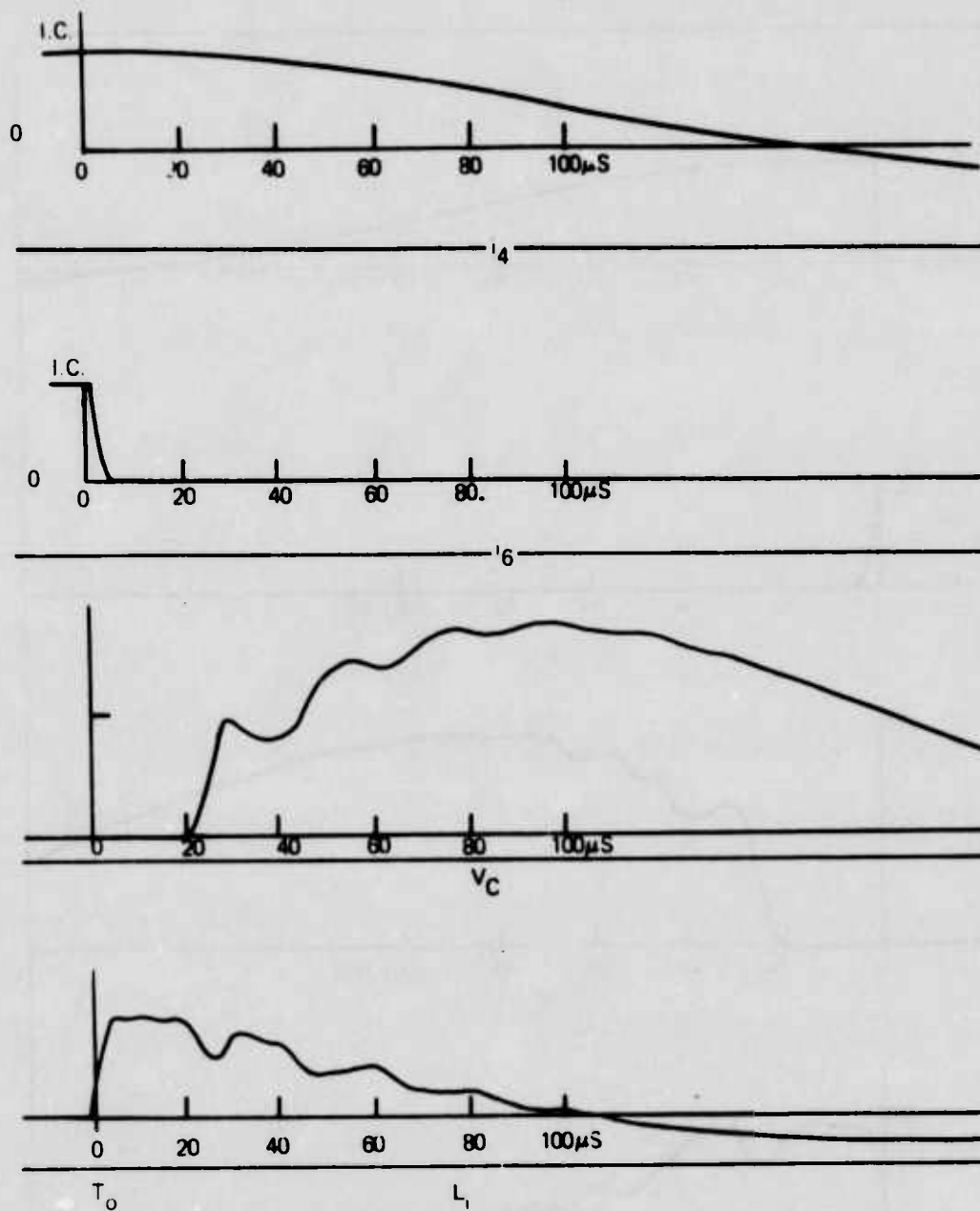
S73-0203-VA-35

166

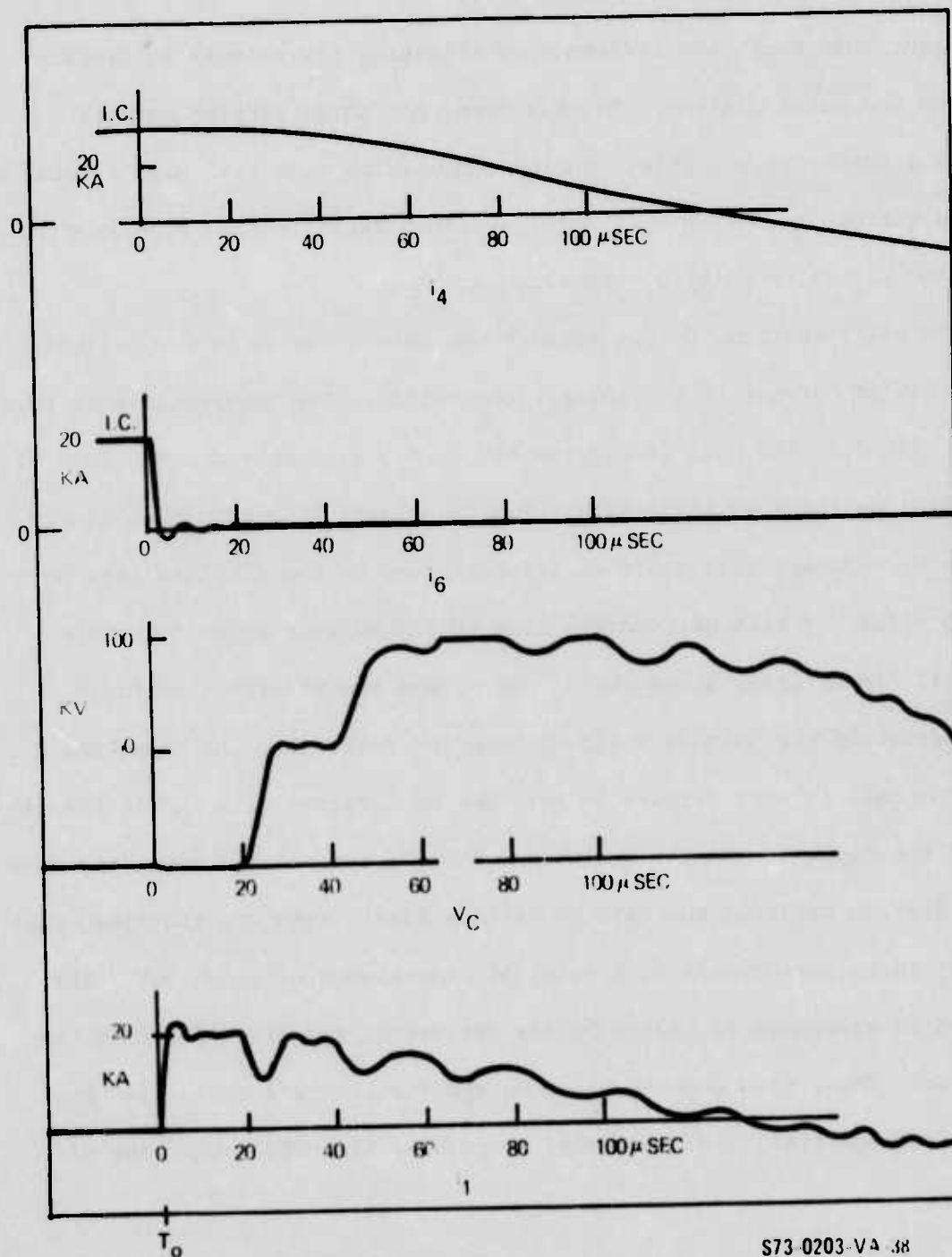Figure B-19. Current and Voltage Waveforms of Complete Switching Cycle. Load connected at voltage of 70 kV.

167

Figure B-20. Current and Voltage Waveforms of Complete Switching Cycle. Load connected at voltage of 80 kV.

168

into the circuit at a higher voltage level.

Figure B21 shows the influence of adjusting the network to produce ripple on the pulse plateau. In this case, the three section network produces a three cycle ripple. During commutation this will give a total of six zero current points in i_6. Multiple zero current points such as this should aid in the commutation and arc quenching.

The multi-section, E-type network has been shown to give excellent commutation of current in the interrupter switch. The apparently more rapid voltage rise from the coil in Figures B19 to B21 as compared with those of the digital analysis is misleading. Two facts must be considered, namely, (a) the VI recovery will start at the beginning of the flat and long commutation pulse. A voltage recovery line at 2.5 kv/μsec drawn from this point will lie entirely above the V_c curve, and the VI will therefore easily withstand the voltage build-up from the coil. (b) The capacitor C across the coil in this circuit is only 1μF as compared with 4μF in the circuits of the digital computer analysis. This capacitor will therefore contribute less in reducing the rate of voltage rise. Even so, the steep part of the V_c curve corresponds to a value of capacitance of about 3μF. The reduction of steepness is caused by the current i, from the PFN after its main pulse. Thus, this network first delays for a considerable time the start of voltage rise, and, secondly, it reduces the subsequent rate of voltage rise.

Figure B- 21. Current and Voltage Waveforms of Complete Switching Cycle.
Network adjusted for ripple on pulse

170

B-4   Circuit Characteristics

The E type network electrical performance characteristics are discussed in Appendix B3. However, to fully describe the circuit, other characteristics require definition.

A particular advantage of the network approach is the flexibility of design factors. By proper choice of the lumped parameters of the network various waveforms may be achieved. That is, the impedance, pulse length, ripple, droop, and rise time can be controlled by element choice. Special waveforms may be generated for a given application. As a general outline, the characteristics of a network are chosen as follows:

Impedance in ohms: $Zo = \sqrt{L/C}$

Pulse Width: $T = 2\sqrt{L\,C}$

Network Capacitance: $C = T/2Zo$

Network Inductance: $L = TZo/2$

Rise Time: $Tr = T/2N$

Number of Sections: N

The general equations, however, do not fully describe what can be done to achieve the desired waveform. By controlling mutual inductance of coil sections, the pulse plateau ripple may be adjusted. Voltage output may be tapered by varying section capacitance or inductance along the network. Other variations may be achieved by using saturable reactors for the coil sections. Therefore, the network may be tailored to compensate for affects such as generator source inductance or storage coil impedance.

Reliability and life are important considerations. As mentioned before, the only component exhibiting limited life is the vacuum gap in the

171

commutating circuit. However, this can be considered an expendable item and replaced as part of routine preventive maintenance. Other components primarily depend upon initial design for a given life expectancy under environmental operating conditions. Since these components are designed to meet specification, the overall reliability will be very high.

The power supply for charging the network may be either of two types. The first - resonant charging - is the most common type used for high pulse repetition rate systems. It offers high efficiency and simplicity of operation. In this system a D.C. power supply is used as the power source. Network charging current is fed through an inductor which resonates with the network capacitance at a predetermined frequency. The transient response of the L-C circuit is such that immediately after network discharge, the network will recharge to approximately twice the D.C. supply voltage. Although highly efficient, this method of network charging is somewhat heavy. Since the P.R.F. of this system is very low, advantage can be made of this fact. A voltage multiplying rectifier such as the 3Ø Cockcraft-Walton will have sized weight advantages. This rectifier can be connected directly to the network without isolation due to the internal impedance of the rectifier. Since the charging current required by the network is lower than the holding current of the gaps, the commutation of the gaps can be accomplished by purposely mismatching the network.

B-5   Breadboard Test

A breadboard circuit of the commutation network was constructed and tested. The circuit schematic is shown in Figure B22. With this circuit a relay issued as the interrupter. As it opens under load an arc initiates and is detected. The detector circuit causes the 2N688 SCR to switch to a conducting state and discharges the commutating network. Figure B23B shows an arc period without commutation. Figure B23A shows the arc quenched by the commutation circuit. In Figure B24A the voltage rise and decay of the storage coil is shown. As shown in Figure B22, the decay is caused by switching the 5 Ω load (RL) across the coil. Figure B24B shows the network discharge current. In general, the waveforms of the circuit are in good agreement with predicted waveforms produced by computer analysis.
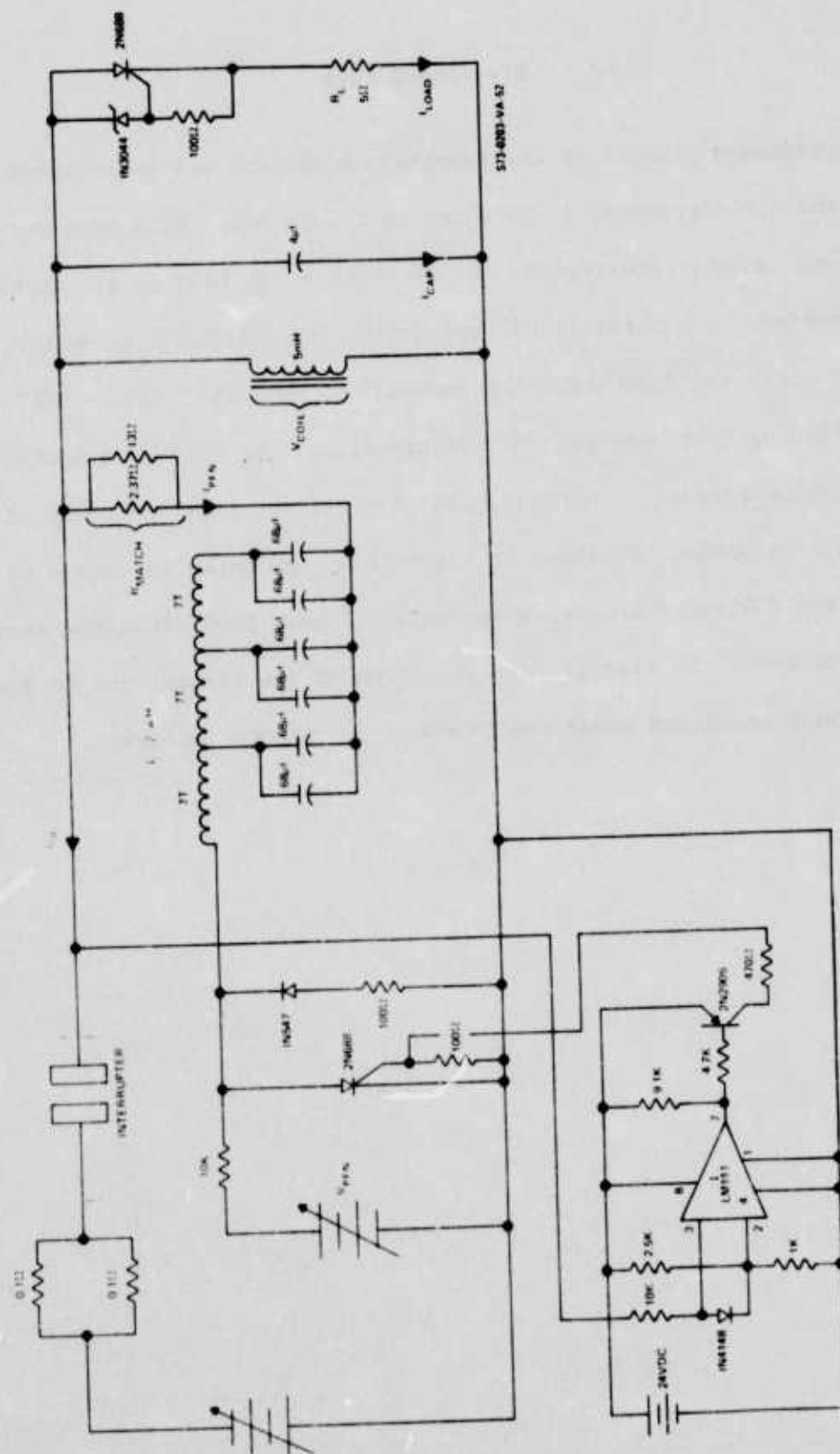
Figure B-22. Schematic of Bread-board test

174

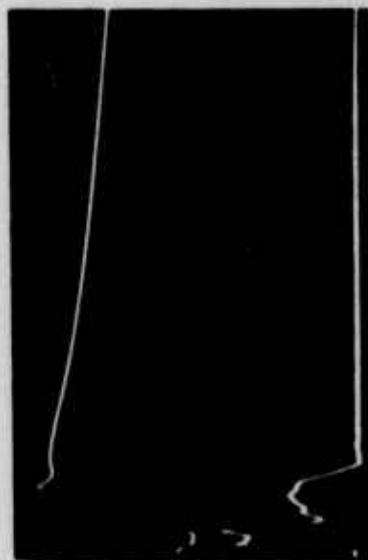Figure B-23

A) Arc quenched with commutation

t = 500 sec/cm

B) Arc period

t = 500 sec/cm

Figure B-24

A) Coil Voltage

B) Network current

APPENDIX C

HYDRAULIC SYSTEM ANALYSIS

C-1   Derivation of Operating Equations For Incompressible Flow, Large
        Signal Transient Response

The basic building block of the hydraulic system is the valve oper-

ated piston where the piston is retarded by Coulomb friction and the valve

flow is proportional to the square root of the pressure drop across the

orifice. The following development will show:

(1) The validity of replacing two series orifices with a single

orifice.

(2) The differential equation for a typical stage including the

square root law orifice, Coulomb friction, and lumped parameter fluid com-

pliance of the entrapped fluid. This differential equation is cumbersome

to solve, and will be replaced by:

(3) The solution of the description of the rise time of a com-

pressible fluid in a blocked load and the load motion solutions assuming an

incompressible fluid. This will yield a description of the basic switching

lag time of each stage and will be followed by:

(4) The incompressible fluid solution for two pistons being driven

by a single orifice as in the actuation stage.

C-1.1   Validity of Replacing Two Series Orifices With a Single Orifice

Schematically, each stage of the valve will be as shown in Figure
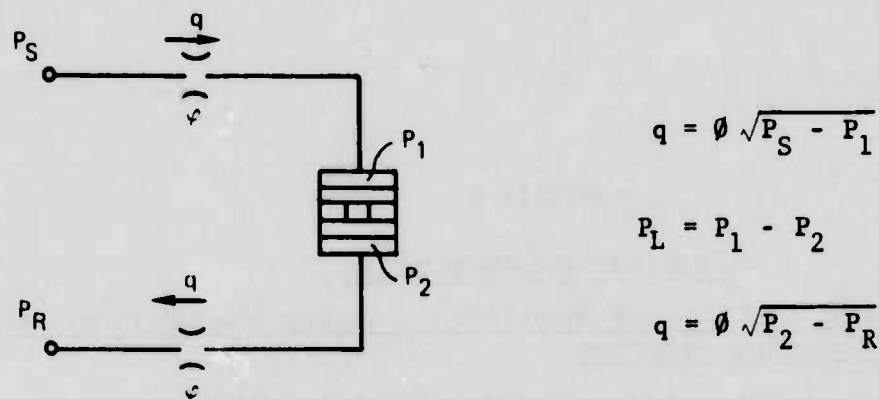
C-1.

$$q = \emptyset \sqrt{P_S - P_1}$$

$$P_L = P_1 - P_2$$

$$q = \emptyset \sqrt{P_2 - P_R}$$

Figure C-1.   Schematic of valve stage.

$$\frac{q^2}{\emptyset^2} = P_S - P_1 = P_2 - P_R \; .$$

Defining $P_R \equiv 0$ leads to

$$P_S = (P_S - P_1) + (P_2) + P_L \; ;$$

$$P_S = \frac{q^2}{\emptyset^2} + \frac{q^2}{\emptyset^2} + P_L = 2 \frac{q^2}{\emptyset^2} + P_L$$

$$P_S - P_L = 2 \frac{q^2}{\emptyset^2}$$

$$q = \frac{\emptyset}{\sqrt{2}} \cdot \sqrt{P_S - P_L} \; . \tag{C-1}$$

Thus, if $\emptyset_o \equiv \dfrac{\emptyset}{\sqrt{2}}$, $q = \emptyset_o \sqrt{P_S - P_L}$ can be represented by a single orifice of the form shown in Figure C-2.

C-1.2   <u>Differential equation for a typical stage including lumped</u>

<u>parameter fluid compliance, square root law orifice, and Coulomb friction.</u>

For the stage represented by Figure C-3 we have
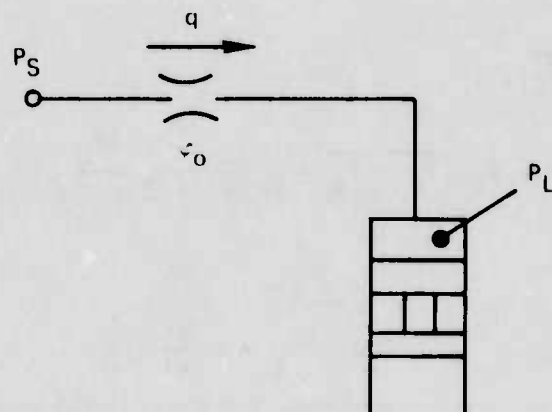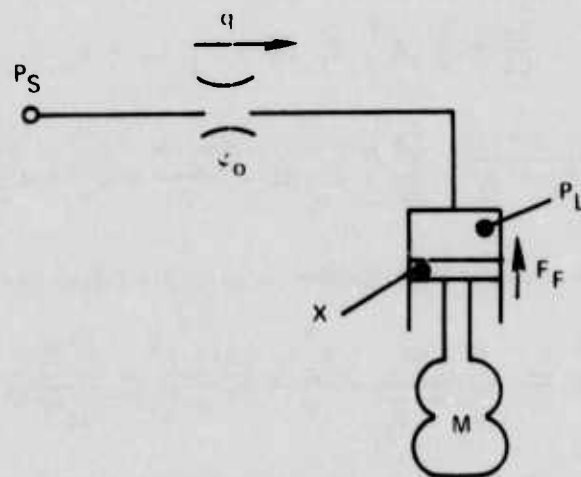
Figure C-2.   Equivalent representation of valve stage.

S73-0203 VA 3

Figure C-3. Stage schematic.

Σ Flow: $q = A \dfrac{dx}{dt} + C_T \dfrac{dP_L}{dt}$ (Piston velocity flow plus compressibility flow with $C_T = v_1/2\beta$.)

Σ Force: $P_L A - F_f = m \dfrac{d^2 x}{dt^2}$.

179

Since $q = \emptyset_o \sqrt{P_S - P_L}$,

$$\emptyset_o \sqrt{P_S - P_L} = A \frac{dx}{dt} + C_T \frac{dP_L}{dt} .$$

Writing $y = \frac{dx}{dt}$ gives

$$P_L A - F_f = m \frac{dy}{dt} ,$$

and integrating gives

$$y = \frac{1}{m} \int (P_L A - F_f)\, dt + C_o = \frac{A}{m} \int P_L\, dt - \frac{F_f t}{m} + C_o .$$

Substituting for y yields

$$\frac{dx}{dt} = \frac{1}{m} \left[A \int P_L\, dt - F_f t \right] + C_o ,$$

so that

$$\emptyset_o \sqrt{P_S - P_L} = \frac{A^2}{m} \int P_L\, dt - \frac{A F_f\, t}{m} + C_o + C_T \frac{dP_L}{dt} .$$

Differentiating this expression gives

$$- \frac{\emptyset_o}{2} \frac{dP_L/dt}{\sqrt{P_S - P_L}} = \frac{A^2 P_L}{m} - \frac{A F_f}{m} + C_T \frac{d^2 P_L}{dt^2} ,$$

so that

$$C_T \frac{d^2 P_L}{dt^2} + \frac{\emptyset_o}{2 \sqrt{P_S - P_L}} \frac{dP_L}{dt} + \frac{A^2 P_L}{m} = \frac{A F_f}{m}$$

and the pressure equation can be written as

$$\text{Pressure Eq.:} \quad C_T \sqrt{P_S - P_L} \frac{d^2 P_L}{dt^2} + \frac{\emptyset_o}{2} \frac{dP_L}{dt} + \frac{A^2 P_L}{m} \sqrt{P_S - P_L} = \frac{A F_f}{m} \sqrt{P_S - P_L} . \qquad (C-2)$$

Rewriting the force equation, we have

180

$$P_L = \frac{F_f}{A} + \frac{m}{A} \frac{d^2 x}{dt^2} \, ,$$

and differentiating with respect to time gives

$$\frac{dP_L}{dt} = \frac{m}{A} \frac{d^3 x}{dt^3} \, .$$

Inserting these into the flow equation gives

$$\frac{C_T m}{A} \frac{d^3 x}{dt^2} + A \frac{dx}{dt} = \emptyset_o \sqrt{P_S - \frac{F_f}{A} - \frac{m}{A} \frac{d^2 x}{dt^2}} \, .$$

Squaring this expression and rearranging allows us to write a displacement equation

$$(\frac{C_T m}{A})^2 (\frac{d^3 x}{dt^3}) \left[\frac{d^3 x}{dt^3} + (\frac{2A^2}{mC_T})(\frac{dx}{dt}) \right] + (\frac{\emptyset_o^2 m}{A})(\frac{d^2 x}{dt^2}) + A^2 (\frac{dx}{dt})^2 = \emptyset_o^2 (P_S - \frac{F_f}{A}) \quad \text{(C-3)}$$

and a velocity equation (again using $y = dx/dt$)

$$(\frac{C_T m}{A})^2 \frac{d^2 y}{dt^2} \left[\frac{d^2 y}{dt^2} + \frac{2A^2}{mC_T} y \right] + \frac{\emptyset_o^2 m}{A} \frac{dy}{dt} + A^2 y^2 = \emptyset_o^2 (P_S - \frac{F_f}{A}) \, . \quad \text{(C-4)}$$

C-1.3 **Appro::imation to solution by addition of pressure rise time lag to the incompressible fluid solution.**

The letter forms of the pressure, displacement, and velocity equations of Section (2) are cumbersome to obtain, but these equations are easily solved if $C_T = 0$ (i.e. $\beta = \infty$) which is the incompressible flow solution. The lag time to charge the cylinder to P_S is also easily calculated for the blocked load case. An acceptable design approach has been to add the lag times for each of these cases taken separately.

181

C-1.3.1   Blocked Load Pressure Rise Time

The flow through the orifice equals the compressibility flow

$$\emptyset_o \sqrt{P_S - P_L} = C_T \frac{dP_L}{dt} \quad .$$

Integrating gives

$$\int \frac{dP_L}{\sqrt{P_S - P_L}} = \frac{\emptyset_o}{C_T} \int dt + C_1 \quad ,$$

or

$$- 2 \sqrt{(P_S - P_L)} = \frac{\emptyset_o}{C_T} t + C_1 \quad .$$

At $t = 0^+$, $P_L = 0$ so that

$$- 2 \sqrt{P_S} = C_1$$

$$\sqrt{P_S - P_L} = \sqrt{P_S} - \frac{\emptyset_o}{2C_T} t \quad .$$

This expression reduces to

$$P_L = (4 \ P_S) \ (\frac{\emptyset_o}{4 \sqrt{P_S} \ C_T}) \ t \ [1 - (\frac{\emptyset_o}{4 \sqrt{P_S} \ C_T}) \ t] \qquad (C-5)$$

If $\tau \equiv \frac{4\sqrt{P_S} \ C_T}{\emptyset_o}$,

$$P_L = 4 \ P_S \ (\frac{t}{\tau}) \ [1 - \frac{t}{\tau}]. \qquad (C-5')$$

Note: the linear time constant at $P_L = 0$ is $\tau_{linear} = \frac{2 \sqrt{P_S} \ C_T}{\emptyset_o} = \frac{1}{2} \tau.$

Now to find t_{max}

$$\frac{\partial P_L}{\partial (t/\tau)} = 0 = 4 P_S \left\{ 1 - 2 \left(\frac{t}{\tau} \right) \right\}$$

$$\frac{t}{\tau} = \frac{1}{2} \; ,$$

$$t_{max} = \frac{1}{2} \, t = \frac{2 \sqrt{P_S} \, C_T}{\phi_o}$$

$$P_L = 4 \, P_S \, (\tfrac{1}{2})(1 - \tfrac{1}{2}) = P_S$$

Thus, P_L rises to P_S in one linear time constant. This is shown in Figure C-4.
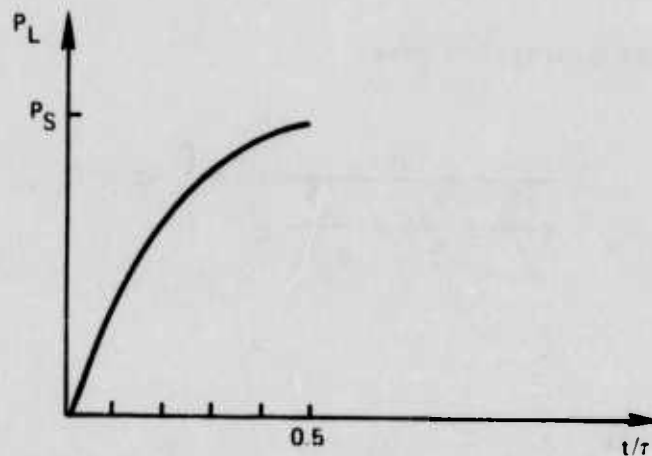
S73-0203-VA-4

Figure C-4. Pressure rise time for massless fluid travelling through a square root law orifice into a blocked load.

This rise time will prove to be small compared to the piston travel time so that the incompressible flow solution will be adequate for sizing the stages.

183

C-1.3.2   <u>Incompressible Flow Solution of a Typical Stage</u>

The equation prev⸱ usly derived for the velocity is

$$\left(\frac{C_T m2}{A}\right) \frac{d^2y}{dt^2} \left[\frac{d^2y}{dt^2} + \frac{2A^2}{mC_T} y\right] + \left(\frac{\phi_o^2 m}{A}\right) \frac{dy}{dt} + A^2 y^2 = \phi_o^2 \left(P_S - \frac{F_f}{A}\right) , \qquad (C\text{-}4)$$

where $C_T = \frac{V_1}{2\beta}$; if $\beta \rightarrow \infty$, $C_T \rightarrow 0$ and the velocity equation becomes

$$\left(\frac{\phi_o^2 m}{A}\right) \frac{dy}{dt} + A^2 y^2 = \phi_o^2 \left(P_S - \frac{F_f}{A}\right)$$

$$\frac{dy}{dt} = \frac{A}{\phi_o^2 m} \left[\phi_o^2 \left(P_S - \frac{F_f}{A}\right) - A^2 y^2\right] = \frac{AP_S}{m} - \frac{F_f}{m} - \frac{A^3}{\phi_o^2 m} y^2 .$$

Integration of this expression gives

$$\int \frac{dy}{\left(\dfrac{AP_S}{m} - \dfrac{F_f}{m}\right) - \dfrac{A^3}{\phi_o^2 m} y^2} = \int dt + C_3 ,$$

$$\frac{m\phi_o^2}{A^3} \int \frac{dy}{\dfrac{\phi_o^2}{A^3}(AP_S - F_f) - y^2} = \int dt + C_3 .$$

Noting that

$$\int \frac{dx}{a^2 - x^2} = \frac{1}{a} \tanh^{-1} \frac{x}{a}$$

gives

184

$$\frac{m\emptyset_o^2}{A^3} \cdot \sqrt{\frac{A^3}{\emptyset_o^2(AP_S - F_f)}} \ \tanh^{-1}\left[y\sqrt{\frac{A^3}{\emptyset_o^2(AP_S - F_f)}}\right] = t + C_3 \ .$$

At $t = t_o^+$, $y = V_o$ and

$$C_3 = \frac{m\emptyset_o^2}{A^3}\sqrt{\frac{A^3}{\emptyset_o^2(AP_S - F_f)}} \ \tanh^{-1}\left[V_o\sqrt{\frac{A^3}{\emptyset_o^2(AP_S - F_f)}}\right] - t_o \ ,$$

$$\tanh^{-1}\left[y\sqrt{\frac{A^3}{\emptyset_o^2(AP_S - F_f)}}\right] = \tanh^{-1}\left[V_o\sqrt{\frac{A^3}{\emptyset_o^2(AP_S - F_f)}}\right] +$$

$$+ \frac{A^3}{m\emptyset_o^2}\sqrt{\frac{\emptyset_o^2(AP_S - F_f)}{A^3}} \ (t - t_o) \ .$$

Substitution for y gives

$$\frac{dx}{dt} = y = \sqrt{\frac{\emptyset_o^2(AP_S - F_f)}{A^3}} \ \tanh\left[\frac{A^3}{m\emptyset_o^2}\sqrt{\frac{\emptyset_o^2(AP_S - F_f)}{A^3}} \ (t - t_o) + \right.$$

$$\left. + \tanh^{-1}\left[V_o\sqrt{\frac{A^3}{\emptyset_o^2(AP_S - F_f)}}\right]\right] \ . \tag{C-6}$$

To solve for x

$$x = \int y \ dt + C_4 \ ,$$

and

$$\int \tanh(at + b) \ dt = \frac{1}{a} \log \cosh(at + b) \ .$$

Thus,

185

$$X = \frac{m\phi_o^2}{A^3} \log \cosh \left[\frac{A^3}{m\phi_o^2} \sqrt{\frac{\phi_o^2(AP_S - F_f)}{A^3}} \ (t - t_o) + \right.$$

$$\left. + \tanh^{-1} \left[V_o \sqrt{\frac{A^3}{\phi_o^2(AP_S - F_f)}} \right] \right] + C_4 \ .$$

At $t = t_o$, $X = \overline{X}_o$ and

$$\overline{X}_o = \frac{m\phi_o^2}{A^3} \log \cosh \left[\frac{A^3}{m\phi_o^2} \sqrt{\frac{\phi_o^2(AP_S - F_f)}{A^3}} \ (t_o - t_o) + \right.$$

$$\left. + \tanh^{-1} \left[V_o \sqrt{\frac{A^3}{\phi_o^2(AP_S - F_f)}} \right] \right] + C_4 \ ,$$

or

$$C_4 = \overline{X}_o - \frac{m\phi_o^2}{A^3} \log \cosh \tanh^{-1} \left[V_o \sqrt{\frac{A^3}{\phi_o^2(AP_S - F_f)}} \right] \ .$$

Thus, the expression for displacement is

$$X = \frac{m\phi_o^2}{A^3} \log \left\{ \frac{\cosh \left[\frac{A^3}{m\phi_o^2} \sqrt{\frac{\phi_o^2(AP_S - F_f)}{A^3}} (t - t_o) + \tanh^{-1} \left[V_o \sqrt{\frac{A^3}{\phi_o^2(AP_S - F_f)}} \right] \right]}{\cosh \left[\tanh^{-1} \left[V_o \sqrt{\frac{A^3}{\phi_o^2(AP_S - F_f)}} \right] \right]} \right\} + \overline{X}_o \qquad \text{(C-7)}$$

(c) Switching Time Lag

If we let $t_o = 0$, $\overline{X}_o = 0$, $V_o = 0$, Equation C-7 becomes

$$X = \frac{m\phi_o^2}{A^3} \log \cosh \left[\frac{A^3}{m\phi_o^2} \sqrt{\frac{\phi_o^2(AP_S - F_f)}{A^3}} \ t \right] \ .$$

186

At $X = X_L$ and $t = t_s$, where X_L = travel of a spool and t_s = switching time lag

$$X_L = \frac{m\emptyset_o^2}{A^3} \log \cosh \left[\frac{A^3}{m\emptyset_o^2} \sqrt{\frac{\emptyset_o^2 (AP_S - F_f)}{A^3}} \, t_s \right] ,$$

or

$$e^{\left(\frac{A^3 X_2}{m\emptyset_o^2} \right)} = \cosh \left[\frac{A^3}{m\emptyset_o^2} \sqrt{\frac{\emptyset_o^2 (AP_S - F_f)}{A^3}} \, t_s \right]$$

and

$$t_s = \frac{m\emptyset_o^2}{A^3} \sqrt{\frac{A^3}{\emptyset_o^2 (AP_S - F_f)}} \cosh^{-1} \left[e^{\frac{A^3 X_L}{m\emptyset_o^2}} \right] . \tag{C-8}$$

To give these expressions a clearer physical meaning, $\emptyset_o$ and A will be eliminated

$$q = \emptyset_o \sqrt{P_S - P_L}$$

$$q_o \equiv \text{no load flow}$$

If $P_L = 0$, $q \equiv q_o = \emptyset_o \sqrt{P_S}$, $\emptyset_o = q_o / \sqrt{P_S}$, and $\emptyset_o^2 = q_o^2 / P_S$, so that

$$\bar{F}_S = P_S A ,$$

where $F_S \equiv$ stall force, and

$$A = F_S / P_S .$$

The terms in Equation (C-8) involving A become

187

$$\frac{m\emptyset_o^2}{A^3} \sqrt{\frac{A^3}{\emptyset_o^2 (AP_S - F_f)}} = \frac{m\, q_o\, P_S}{F_S \sqrt{F_S^2 - F_S F_f}}$$

and

$$\frac{A^3\, X_L}{m\,\emptyset_o^2} = \frac{F_S^3\, X_L}{P_S^2\, m\, q_o^2} \, .$$

Those in Equation (C-7) become

$$\sqrt{\frac{\emptyset_o^2 (A_S P_S - F_f)}{A^3}} = \frac{q_o P_S}{F_S} \sqrt{\left(1 - \frac{F_f}{F_S}\right)} \quad ,$$

$$\frac{A^3}{m\emptyset_o^2} = \frac{F_S^3}{mP_S^2 q_o^2} \; ;$$

$$\frac{m\emptyset_o^2}{A^3} = \frac{mP_S^2 q_o^2}{F_S^3} \, ,$$

$$\frac{A^3}{m\emptyset_o^2} \sqrt{\frac{\emptyset_o^2 (AP_S - F_f)}{A^3}} = \frac{F_S^2 \sqrt{1 - F_f/F_S}}{m\, P_S\, q_o} \, ,$$

$$V_o \sqrt{\frac{A^3}{\emptyset_o^2 (AP_S - F_f)}} = \frac{V_o\, F_S}{q_o\, P_S} \sqrt{1 - F_f/F_S} \, .$$

188

Rewriting

$$\frac{dx}{dt} = \frac{q_o P_S}{F_S} \sqrt{1 - \frac{F_f}{F_S}} \tanh \left\{ \frac{F_S^2 \sqrt{1 - \frac{F_f}{F_S}}}{m P_S q_o} (t-t_o) + \tanh^{-1}(\frac{V_o F_S}{q_o P_S} \sqrt{1 - \frac{F_f}{F_S}}) \right\} \qquad (C-9)$$

$$X = \frac{m q_o^2 P_S^2}{F_S^2} \log \left\{ \frac{\cosh \left(\frac{F_S^2 \sqrt{1 - F_f/F_S}}{m P_S q_o} (t-t_o) + \tanh^{-1}(\frac{V_o F_S}{q_o P_S} \sqrt{1 - F_f/F_S}) \right)}{\cosh \tanh^{-1} (\frac{V_o F_S}{q_o P_S} \sqrt{1 - F_f/F_S})} \right\} + \overline{X}_o \qquad (C-10)$$

$$t_s = \frac{m q_o P_S}{F_S^2 \sqrt{1 - \frac{F_f}{F_S}}} \cosh^{-1} \left\{ e^{\left(\frac{F_S^3 X_L}{P_S^2 m q_o^2} \right)} \right\} \qquad (C-11)$$

$$t_{rise} = \frac{2 \sqrt{P_S} \, C_T}{\emptyset_o} = \frac{F_S X_L}{\beta \, q_o} \qquad (C-12)$$

$$t_s = \frac{F_S X_L}{P_S q_o \sqrt{1 - F_f/F_S}} \cdot \frac{1}{\gamma} \cosh^{-1} \left\{ e^\gamma \right\} , \qquad (C-13)$$

$$\gamma \equiv \frac{F_S^3 X_L}{P_S^2 m q_o^2} \qquad (C-14)$$

$$\frac{t_s}{t_{rise}} = \frac{\dfrac{F_S X_L}{P_S q_o \sqrt{1 - F_f/F_S}} \cdot \dfrac{1}{\gamma} \cosh^{-1} \left\{ e^\gamma \right\}}{\dfrac{F_S X_L}{\beta \, q_o}} = \frac{\beta}{P_S} \cdot \frac{1}{\gamma} \cosh^{-1} \left\{ e^\gamma \right\} \qquad (C-15)$$

189

The function $F(\gamma) = \frac{1}{\gamma} \cosh^{-1} \{e^{\gamma}\}$ in Equation C-15 is dimensionless, so computation of t_s is simplified. This allows rapid sizing of a valve once the desired t_s is known. Values of $F(\gamma)$ for γ ranging from 0.01 to 50 are tabulated below.

EVALUATION OF F(GAMMA)

GAMMA	F(GAMMA)
.01	14.1657
.02	10.0334
.03	8.20535
.04	7.1183
.05	6.37739
.06	5.83141
.07	5.4073
.08	5.06693
.09	4.78506
.1	4.54703
.11	4.3426
.12	4.1646
.13	4.00783
.14	3.86842
.15	3.74342
.16	3.63053
.17	3.52793
.18	3.43417
.19	3.34805
.2	3.26866
.21	3.19513
.22	3.12679
.23	3.06307
.24	3.00349
.25	2.94762
.26	2.8951
.27	2.84562
.28	2.7989
.29	2.75471
.3	2.71281
.31	2.67304
.32	2.63522
.33	2.5992
.34	2.56484
.35	2.53203
.36	2.50066
.37	2.47062
.38	2.44183
.39	2.41421
.4	2.38769

EVALUATION OF F(GAMMA)

GAMMA	F(GAMMA)
.5	2.17008
.6	2.0126
.7	1.89266
.8	1.79795
.9	1.72111
1.	1.65745
1.1	1.60384
1.2	1.55805
1.3	1.51849
1.4	1.48399
1.5	1.45364
1.6	1.42675
1.7	1.40276
1.8	1.38125
1.9	1.36185
2.	1.34427
2.1	1.32827
2.2	1.31367
2.3	1.30027
2.4	1.28795
2.5	1.27658
2.6	1.26606
2.7	1.2563
2.8	1.24722
2.9	1.23875
3.	1.23084
3.1	1.22343
3.2	1.21648
3.3	1.20994
3.4	1.20378
3.5	1.19798
3.6	1.19249
3.7	1.1873
3.8	1.18237
3.9	1.1777
4.	1.17327
4.1	1.16904
4.2	1.16502
4.3	1.16119
4.4	1.15752
4.5	1.15403
4.6	1.15068
4.7	1.14747
4.8	1.1444
4.9	1.14146
5.	1.13863

EVALUATION OF F(GAMMA)

GAMMA	F(GAMMA)
6	1.11552
8	1.08664
10	1.06931
12	1.05776
14	1.04951
16	1.04332
18	1.03351
20	1.03466
22	1.03151
24	1.02888
26	1.02666
28	1.02476
30	1.0231
32	1.02166
34	1.02039
36	1.01925
38	1.01824
40	1.01733
42	1.0165
44	1.01575
46	1.01507
48	1.01444
50	1.01386

C-1.4 <u>Incompressible fluid solution for two pistons driven through a single orifice (without Coulomb friction)</u>.

For the case illustrated in Figure C-5 we can write

$$P_L A_1 = M_1 \frac{d^2 x_1}{dt^2} = M_1 \frac{dy_1}{dt} ,$$

$$P_L A_2 = M_2 \frac{d^2 x_2}{dt^2} = M_2 \frac{dy_2}{dt} ,$$

and

$$q = \emptyset_o \sqrt{P_S P_L} = A_1 \frac{dx_1}{dt} + A_2 \frac{dx_2}{dt} .$$

Differentiating with respect to time gives

192

$$-\frac{\phi_o}{2} \cdot \frac{1}{\sqrt{P_S - P_L}} \frac{dP_L}{dt} = A_1 \frac{d^2 X_1}{dt^2} + A_2 \frac{d^2 X_2}{dt^2} = (\frac{A_1^2}{M_1} + \frac{A_2^2}{M_2}) P_L$$
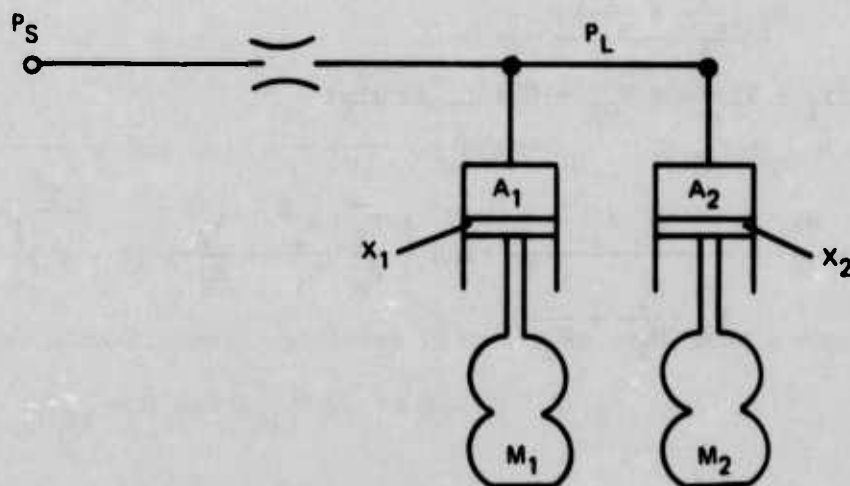
or

$$\frac{dP_L}{dt} = -\frac{2}{\phi_o} (\frac{A_1^2}{M_1} + \frac{A_2^2}{M_2}) P_L \sqrt{P_S - P_L} .$$

Integrating this expression gives

$$\int \frac{d P_L}{P_L \sqrt{P_S - P_L}} = -\frac{2}{\phi_o} (\frac{A_1^2}{M_1} + \frac{A_2^2}{M_2}) \int dt + C_6 ,$$

$$-\frac{2}{\sqrt{P_S}} \tanh^{-1} \sqrt{\frac{P_S - P_L}{P_S}} = -\frac{2}{\phi_o} (\frac{A_1^2}{M_1} + \frac{A_2^2}{M_2}) t + C_6 ,$$

$$\tanh^{-1} \sqrt{\frac{P_S - P_L}{P_S}} = \frac{\sqrt{P_S}}{\phi_o} (\frac{A_1^2}{M_1} + \frac{A_2^2}{M_2}) t + C_6^1 .$$

S73-0203-V1-5

Figure C-5. Schematic of two pistons driven by single orifice.

193

At $t = t_o{}^+$, $P_L = P_S$ and $C_6{}^1 = - \dfrac{\sqrt{P_S}}{\emptyset_o}$ $(A_1{}^2/M_2 + A_2{}^2/M_2)$ t_c, so that

$$\frac{P_S - P_L}{P_S} = \tanh^2 \left\{ \frac{\sqrt{P_S}}{\emptyset_o} \left(\frac{A_1{}^2}{M_2} + \frac{A_2{}^2}{M_2} \right) (t - t_o) \right\} ,$$

or

$$P_L = P_S \left[1 - \tanh^2 \left\{ \frac{\sqrt{P_S}}{\emptyset_o} \left(\frac{A_1{}^2}{M_1} + \frac{A_2{}^2}{M_2} \right) (t - t_o) \right\} \right] . \tag{C-16}$$

To solve for the y's, we have

$$\frac{dy_1}{dt} = \frac{P_S A_1}{M_1} \left[1 - \tanh^2 \left\{ \frac{\sqrt{P_S}}{\emptyset_o} \left(\frac{A_1{}^2}{M_1} + \frac{A_2{}^2}{M_2} \right) (t - t_o) \right\} \right]$$

or

$$y_1 = \frac{P_S A_1}{M_1} \left[\int dt - \int \tanh^2 \left\{ \frac{\sqrt{P_S}}{\emptyset_o} \left(\frac{A_1{}^2}{M_1} + \frac{A_2{}^2}{M_2} \right) (t - t_o) \right\} dt \right] + C_7$$

Integrating this gives

$$y_1 = \frac{\emptyset_o \sqrt{P_S} A_1}{M_1 \left(\dfrac{A_1{}^2}{M_1} + \dfrac{A_2{}^2}{M_2} \right)} \tanh \left\{ \frac{\sqrt{P_S}}{\emptyset_o} \left(\frac{A_1{}^2}{M_1} + \frac{A_2{}^2}{M_2} \right) (t - t_o) \right\} + C_7 .$$

At $t = t_o$, $y_1 = V_{01}$ and $V_{01} = 0 + C_7$ so that

$$y_1 = \frac{dx_1}{dt} = \frac{q_o A_1}{M_1 \left(\dfrac{A_1{}^2}{M_1} + \dfrac{A_2{}^2}{M_2} \right)} \tanh \left\{ \frac{\sqrt{P_S}}{\emptyset_o} \left(\frac{A_1{}^2}{M_1} + \frac{A_2{}^2}{M_2} \right) (t - t_o) \right\} + V_{01}. \tag{C-17}$$

Likewise

$$y_2 = \frac{dx_2}{dt} = \frac{q_o A_2}{M_2 \left(\dfrac{A_1{}^2}{M_1} + \dfrac{A_2{}^2}{M_2} \right)} \tanh \left\{ \frac{\sqrt{P_S}}{\emptyset_o} \left(\frac{A_1{}^2}{M_2} + \frac{A_2{}^2}{M_2} \right) (t - t_o) \right\} + V_{02}. \tag{C-18}$$

194

The displacements then become

$$X_1 = \frac{q_0 A_1}{M_1 \left(\frac{A_1^2}{M_1} + \frac{A_2^2}{M_2}\right)} \int \tanh\left\{\frac{\sqrt{P_S}}{\phi_0}\left(\frac{A_1^2}{M_1} + \frac{A_2^2}{M_2}\right)(t - t_0)\right\} dt + \int V_{01} dt + C_3$$

$$X_1 = \frac{q_0 A_1}{M_1 \left(\frac{A_1^2}{M_1} + \frac{A_2^2}{M_2}\right)^2} \times \frac{\phi_0 \cdot \sqrt{P_S}}{\sqrt{P_S} \cdot \sqrt{P_S}} \left[\log \cosh\left\{\frac{\sqrt{P_S}}{\phi_0}\left(\frac{A_1^2}{M_1} + \frac{A_2^2}{M_2}\right)\right\}\right]$$

$$+ V_{01} t + C_8$$

At $t = t_0$, $X = X_{01}$ and $C_8 = X_{01} - V_{01} t_0$, so that

$$X_1 = \frac{q_0^2 A_1}{P_S M_1 \left(\frac{A_1^2}{M_1} + \frac{A_2^2}{M_2}\right)^2} \log \cosh\left\{\frac{P_S}{q_0}\left(\frac{A_1^2}{M_1} + \frac{A_2^2}{M_2}\right)(t-t_0)\right\} + V_{01}(t-t_0) + X_{01} \qquad \text{(C-19)}$$

Likewise

$$X_2 = \frac{q_0^2 A_2}{P_S M_2 \left(\frac{A_1^2}{M_1} + \frac{A_2^2}{M_2}\right)^2} \log \cosh\left\{\frac{P_S}{q_0}\left(\frac{A_1^2}{M_1} + \frac{A_2^2}{M_2}\right)(t-t_0)\right\} + V_{02}(t-t_0) + X_{02} \qquad \text{(C-20)}$$

To find the time when Piston 1 overtakes Piston 2 we must find t when $X_1 = X_2$.

At $t_0 = 0$, $V_{01} = V_{02} = 0$ and $X_{01} = 0$, so that

$$X_1 = \frac{q_0^2 A_1}{P_S M_1 \left(\frac{A_1^2}{M_1} + \frac{A_2^2}{M_2}\right)^2} \log \cosh\left\{\frac{P_S}{q_0}\left(\frac{A_1^2}{M_1} + \frac{A_2^2}{M_2}\right) t\right\}$$

and

$$X_2 = \frac{q_o^2 A_2}{P_S M_2 \left(\frac{A_1^2}{M_1} + \frac{A_2^2}{M_2}\right)^2} \log \cosh \left\{\frac{P_S}{q_o} \left(\frac{A_1^2}{M_1} + \frac{A_2^2}{M_2}\right) t\right\} + X_{02} \ .$$

Equating these and solving for t gives

$$t_c = \frac{q_o}{P_S \left(\frac{A_1^2}{M_1} + \frac{A_2^2}{M_2}\right)} \cosh^{-1} \left\{ e^{\dfrac{X_{02} \ P_S \left(\frac{A_1^2}{M_1} + \frac{A_2^2}{M_2}\right)^2}{q_o^2 \left(\frac{A_1}{M_1} + \frac{A_2}{M_2}\right)}} \right\} \qquad (C\text{-}21)$$

$$X_1 = X_2 = X_{02} \ \frac{A_1}{A_1 - \frac{M_1}{M_2} A_2} \qquad (C\text{-}22)$$

Equation C-21 gives the time for the large piston to overtake the small one with the large mass.

Summary of Displacement Equations:

$$X_i = \frac{m_i \ q_{opi}^2 P_S^2}{F_{si}^3} \log \left\{ \frac{\cosh \left\lfloor \left(\dfrac{F_{si}^2 \sqrt{1 - F_i/F_{\varepsilon i}}}{m_i \ P_S \ q_{opi}}\right)(t - t_p) \right.}{1} \right\} \ ,$$

$$, \ (t_p + t_{ri}) < t < (t_p + t_{ri} + t_{si})$$

$$t_{ri} = \frac{F_{si} \ X_{ii}}{\beta \ q_{opi}}$$

$$t_{si} = \frac{m_i \ q_{opi} \ P_S}{F_{si}^2 \sqrt{1 - F_i/F_{si}}} \cosh^{-1} \left\{ e^{\dfrac{F_{si}^3 X_{io}}{P_S^2 \ m_i q_{opi}^2}} \right\} = \frac{F_{si} \ X_{io}}{P_S \ q_{opi} \sqrt{1 - F_f/F_{si}}} X$$

$$X \ \frac{1}{\gamma_i} \cosh^{-1} \left\{ e^{\gamma_i} \right\} \ , \ \gamma_i \equiv \frac{F_{si}^3 X_{ii}}{P_S^2 \ m_i \ q_{opi}^2}$$

196

$$X_p = \frac{m_p \, q_{oi}^2 \, P_S^2}{F_{Sp}^3} \log \cosh \left\{ \left(\frac{F_{Sp}^2 \sqrt{1 - F_P/F_{SP}}}{m_p \, P_S \, q_{oi}} \right) (t - [t_p + t_{ri} + t_{si} + t_{rp}]) \right\},$$

$$(t_p + t_{ri} + t_{si} + t_{rp}) < t < (t_p + t_{ri} + t_{si} + t_{rp} + t_{sp})$$

$$t_{rp} = \frac{F_{Sp} \, X_{ip}}{\beta \, q_{oi}}$$

$$t_{sp} = \frac{m_p \, q_{oi} \, P_S}{F_{sp}^2 \sqrt{1 - F_P/F_{Sp}}} \cosh^{-1} \left\{ e^{\gamma_p} \right\} = \frac{F_{Sp} \, X_{Lp}}{P_S \, q_{oi} \sqrt{1 - F_P/F_{Sp}}} X$$

$$X \frac{1}{\gamma_p} \cosh^{-1} (e^{\gamma_P}), \quad \gamma_p \equiv \frac{F_{Sp}^3 \, X_{Lp}}{P_S^2 \, m_p \, q_{oi}^2}$$

$$X_1 = \frac{q_{op}^2 \, A_1}{P_S M_1 \, \left(\frac{A_1^2}{M_1} + \frac{A_2^2}{M_2} \right)^2} \log \cosh \left\{ \frac{P_S}{q_o} \left(\frac{A_1^2}{M_1} + \frac{A_2^2}{M_2} \right) (t - [t_p + t_{ri} + t_{si} + t_{rp} + t_{sp} + t_{ra}]) \right\}$$

$$X_2 = X_{02} + \frac{q_{op}^2 \, A_2}{P_S M_2 \, \left(\frac{A_1^2}{M_1} + \frac{A_2^2}{M_2} \right)^2} \log \cosh \left\{ \frac{P_S}{q_o} \left(\frac{A_1^2}{M_1} + \frac{A_2^2}{M_2} \right) (t - [t_p + t_{ri} + t_{si} + t_{rp} + t_{sp} + t_{12}]) \right\}$$

$$(t_p + t_{ri} + t_{si} + t_{sp} + t_{ra}) < t < (t_p + t_{ri} + t_{si} + t_{rp} + t_{sp} + t_{ra} + t_c)$$

Also, for the same time span

197

$$\frac{dX_1}{dt} = \frac{q_o A_1}{M_1 \left(\frac{A_1^2}{M_1} + \frac{A_2^2}{M_2}\right)} \tanh\left\{\frac{P_S}{q_o} \left(\frac{A_1^2}{M_1} + \frac{A_2^2}{M_2}\right) (t - [t_p + t_{ri} + t_{si} + t_{rp} + t_{sp} + t_{ra}])\right\}$$

$$\frac{dX_2}{dt} = \frac{q_o A_2}{M_2 \left(\frac{A_1^2}{M_1} + \frac{A_2^2}{M_2}\right)} \tanh\left\{\frac{P_S}{q_o} \left(\frac{A_1^2}{M_1} + \frac{A_2^2}{M_2}\right) (t - [t_p + t_{ri} + t_{si} + t_{rp} + t_{sp} + t_{ra}])\right\}$$

At $t = (t_p + t_{ri} + t_{si} + t_{rp} + t_{sp} + t_{ra} + t_c) = t_{A_1}$,

where:

$$t_c = \frac{q_{op}}{P_S \left(\frac{A_1^2}{M_1} + \frac{A_2^2}{M_2}\right)} \cosh^{-1}\left\{e^{\dfrac{X_{02} P_S (A_1^2/M_1 + A_2^2/M_2)^2}{q_{op}^2 \left(\frac{A_1}{M_1} - \frac{A_2}{M_2}\right)}}\right\}\Bigg]\,,$$

the two masses, M_1 & M_2 coalesce and

$$V_0 {}_{1\&2} = \frac{d X_{1\&2}}{dt} = \frac{M_1}{M_1 + M_2} \frac{dX_1}{dt}\Bigg|_{t=t_{A_1}} + \frac{M_2}{M_1 + M_2} \frac{dX_2}{dt}\Bigg|_{t=t_{A_1}}$$

$$X_0 {}_{1\&2} = X_1\Bigg|_{t=T_{A_1}} = X_2\Bigg|_{t=t_{A_1}}$$

So, while the two travel together,

198

$$X_{1\&2} = \frac{(M_1 + M_2)\, q_{op}^2}{P_S\,(A_1 + A_2)^3} \cdot$$

$$\log\left\{ \frac{\cosh\left[\dfrac{[P_S(A_1+A_2)]^2\,\sqrt{1-F/F_S}}{(M_1+M_2)\,P_S\,q_{op}}\,(t-t_{A_1}) + \tanh^{-1}\left(\dfrac{V_0\,F_S}{q_o\,P_S}\sqrt{1-F_f/F_S}\right)\right]}{\cosh\tanh^{-1}\left(\dfrac{V_0\,F_S}{q_o\,P_S}\sqrt{1-F_f/F_S}\right)} \right\} + X_{0_{1\&2}}$$

and

$$\frac{dX_{1\&2}}{dt} = \frac{q_{op}\,P_S}{F_S}\sqrt{1 - \frac{F_F}{F_S}}\ \tanh\left\{ \frac{F_S^2\sqrt{1 - F_F/F_S}}{(M_1+M_2)P_S q_{op}}\,(t-t_{A_1}) + \right.$$

$$\left. + \tanh^{-1}\left(\frac{V_0\,F_S}{q_o\,P_S}\sqrt{1 - F_F/F_S}\right) \right\} \ ,$$

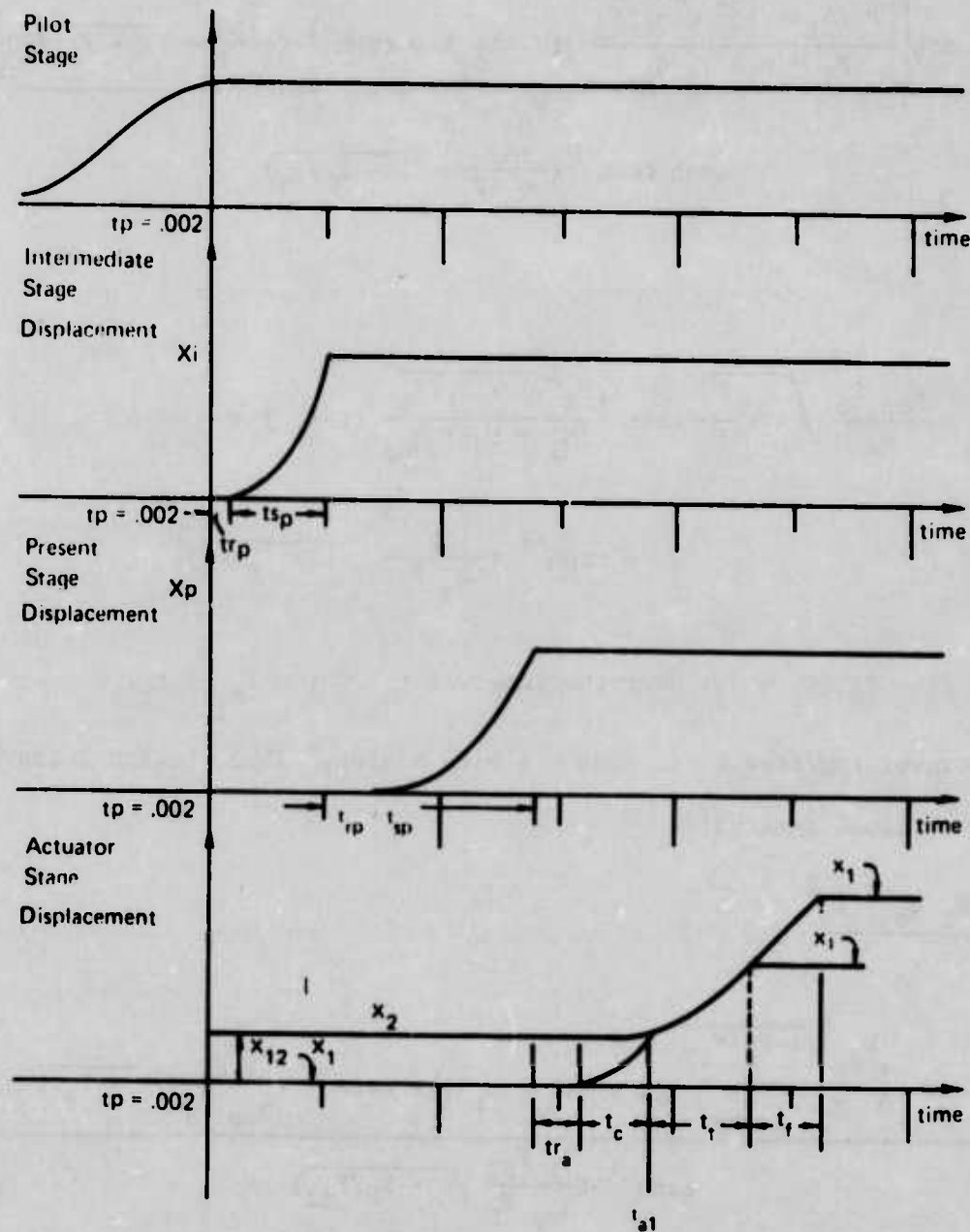where $F_S = P_S\,(A_1 + A_2)$ over the interval $t_{A_1} < t < t_{A_1} + t_t$.

They travel together until Piston 1 hits a stop. Then, Piston 2 travels alone over the final interval.

$$X_2 = \frac{M_2\,q_{op}^2\,P_S^2}{F_{S_2}^3} \cdot$$

$$\log\left\{ \frac{\cosh\left(\dfrac{F_{S_2}^3\sqrt{1-F_f/F_{S2}}}{M_2\,P_S\,q_{op}}\,(t - (t_{A_1} + t_t)) + \tanh^{-1}\left(\dfrac{V_1 F_{S2}}{q_{op}\,P_S}\sqrt{1 - F_F/F_S}\right)\right)}{\tanh^{-1}\left(\dfrac{V_1\,F_{S2}}{q_{op}\,P_S}\sqrt{1 - F_F/F_{S2}}\right)} \right\} + X_1 \,,$$

where $X_1 = X_{1\&2}\Big|_{t=t_{A_1}+t_t}$ and $V_1 = \dfrac{dX_{1\&2}}{dt}\Big|_{t=t_{A_1}+t_t}$

The displacements of the various stages are shown in Figure C-6.

S73-0203-VA-6

Figure C-6. Displacements of stages vs. time

200

C-2   Factors Relating to Configuration of Valve-Actuator Mechanism

C-2.1   Actuator Configuration

The features included in the actuator design necessary to accomplish the overall task are:

(1) Minimum power input.

(2) Low holding force during the 190 msec contact time (400 lbs).

(3) Automatic compensation for electrode wear.

The topics to be pursued in this section deal with the considerations made in the selection of the final actuator configuration. These considerations are:

(1) Kinematics of motion.

(2) Design for proper holding force and minimum power used.

C-2.2   Mechanics of Actuator Motion

The ideal kinematic arrangement for the minimum switching time with the minimum loading caused by acceleration is shown in Figure C-7. The graphs in Figure C-7 are the elementary kinematics of a constant force acting on a mass. The actual equations to be used are the equations for $\frac{dx}{dt}$ and x from Section C-1.3.2. A further derivative of $\frac{dx}{dt}$ would be needed for acceleration.

One difficulty encountered in the kinematics of Figure C-7 is that the peak velocity is higher than any that has been used to date in any bellows testing. Also, these kinematics imply a piston directly attached to the load. The piston peak force is
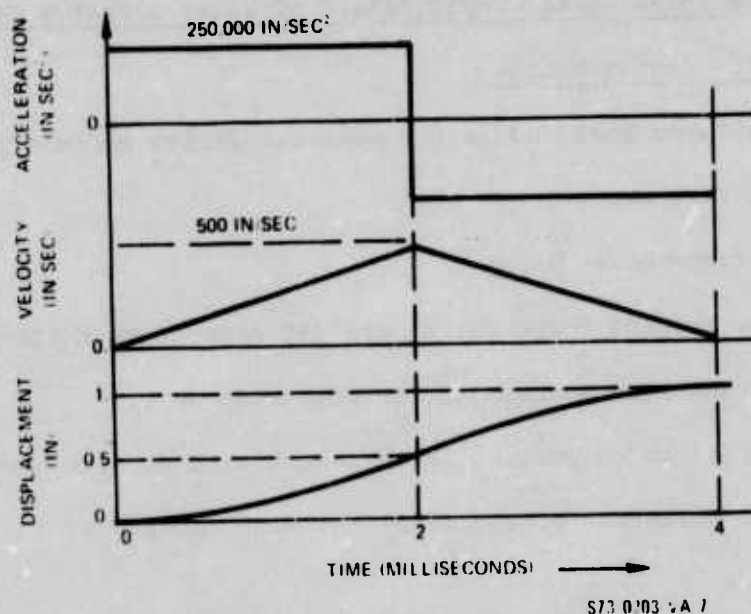
Figure C-7

$$F_{peak} = \frac{10}{386.4} \times 250,000 = 6480 \text{ lbs.}$$

For a binary switching valve, the peak force would be acting as the holding force during the   time   that the contacts are closed. This load is simply too great for the contactors to withstand. Nevertheless, the efficiency will be computed for comparison with other piston arrangements.

$$\eta = \frac{\dfrac{\Delta W_{out}}{\Delta t}}{\dfrac{\Delta W_{in}}{\Delta t}} \approx \frac{\Delta W_{out}}{\Delta W_{in}}$$

for the same time interval. The ΔW_{out} will be defined as the useful work out or the work done during the opening acceleration. The net work done during acceleration and deceleration is zero for the kinematics in Figure C-7. The

202

ΔW_{in} will be determined for the same half stroke. For a real actuator

$$\Delta W_{out} = \int_0^{x_t/2} \overline{F} \cdot \overline{dx} \,,$$

where

$$F = m \frac{d^2 x}{dt^2} = m \cdot \frac{F_s - F_t}{m} \operatorname{Sech}^2 \left\{ \frac{F_S^2 \sqrt{1 - F_t/F_S}}{m\, P_S\, q_o} (t - t_o) \right.$$

$$\left. + \tanh^{-1} \left[\frac{V_o F_S}{q_o P_S} \sqrt{1 - \frac{F_t}{F_S}} \right] \right\}$$

$$dX = \frac{q_o P_S}{F_S} \sqrt{1 - \frac{F_t}{F_S}} \tanh \left\{ \frac{F_S^2 \sqrt{1 - F_t/F_S}}{m\, P_S\, q_o} (t - t_o) + \tanh^{-1} \left[\frac{V_o F_s}{q_o P_s} \sqrt{1 - \frac{F_t}{F_S}} \right] \right\} dt$$

Upon substituting and performing the integration:

$$\Delta W_{out} = \left(1 - \frac{F_t}{F_S}\right)^{3/2} P_S q_o \int_0^{t_s} \operatorname{Sech}^2 (at + b) \tanh (at + b)\, dt$$

Note: $V_o = 0$, $t_o = 0$

Thus: $b = 0$, $a = F_S^2 \sqrt{1 - F_t/F_S}/m\, P_s\, q_o$

$$\int \operatorname{Sech}^2 at \tanh at \, dt = \int (\tanh at - \tanh^3 at)\, dt$$

$$= \frac{1}{a} \left\{ \log \cosh at + \frac{\tanh^2 at}{2} - \log \cosh at \right\} = \frac{\tanh^2 at}{2a}$$

203

$$\Delta W_{out} = \frac{(1 - \frac{F_t}{F_S}) \, m \, P_S{}^2 q_o{}^2}{2 \, F_S{}^2} \, \tanh^2 \, (\frac{F_S{}^2 \sqrt{1 - \frac{F_t}{F_S}}}{m \, P_S \, q_o} \, t) \Bigg|_o^{t_s}$$

$$\Delta W_{out} = \frac{(1 - \frac{F_t}{F_S}) \, m \, P_S{}^2 q_o{}^2}{2 \, F_S{}^2} \, \tanh^2 \, (\frac{F_S{}^2 \sqrt{1 - \frac{F_t}{F_S}}}{m \, P_S \, q_o} \, t_s) \tag{C-23}$$

$$\Delta W_{in} = \frac{F_S \cdot X_T}{2} \tag{C-24}$$

C-2.2.1   <u>Unlimited Velocity Case</u>

For the case:

F_f = 20 lbs P_S = 4500 lbs/in^2

F_S = 7000 lbs q_o = 1800 in^3/sec

m_g = 10 lbs t_s = .002

$$\Delta W_{out} = 3250 \text{ in-lb}$$

$$\Delta W_{in} = 7000 \times .5 = 3500 \text{ in-lb}$$

$$\eta = \frac{3250}{3500} = .93 \quad (\text{Note: } HP_{hyd.in} = 31.68 \text{ hp.})$$

This high efficiency means that most of the energy in the fluid is used to accelerate the load, and little is lost across the power stage orifices.

204

C-2.2.2   Limited Velocity Case

But, the above kinematics cause some potential problems with the

bellows. So consideration will now be made of the case where the velocity

is limited. The diagram of the elementary kinematics is shown in Figure C-8.
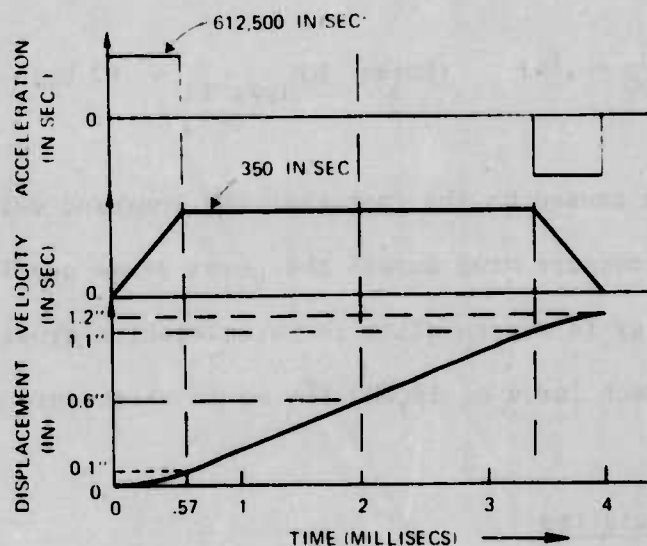
Figure C-8

For the case in Figure C-8,

$$F = \frac{10}{386.9} \times 612,500 = 15,700 \text{ lbs.}$$

For the first 2 millisec, the work done is actually completed in .57 millisec.

205

So, for the case

$$F_S = 18{,}000 \text{ lbs.} \qquad P_S = 4500 \text{ lb/in}^2$$

$$F_t = 50 \text{ lbs.} \qquad q_o = 1400$$

$$m_g = 10 \text{ lbs.}$$

$$\Delta W_{out} = 1590 \text{ in-lb}$$

$$\Delta W_{in} = 18{,}000 \times .6 = 10{,}800 \text{ in-lb}$$

$$\eta = \frac{1590}{10{,}800} = .147 \qquad (\text{Note: } HP_{hyd. \text{ in}} = 82 \text{ hp})$$

This low efficiency is caused by the fact that the constant velocity condition is maintained by the pressure drop across the power stage spool valve, and nearly all of the energy is wasted after the acceleration drops to a low level. Also, the contact force of 18,000 lbs would obliterate a vacuum interrupter.

C-2.3   Final Configuration

An insight giving plot can be made by substituting $t = g(x)$ into the equation for ΔW_{out}. The expression for $t = g(x)$ is the switching time lag and can be found as Eq. (C-11). This produces an equation with $\Delta W_{out} = W(x)$. A plot of this for the two cases is shown in Figure C-9.

A large piston completes most of its work in a short distance, while a small piston with a large power stage continually applies a force over this distance. A staged actuator is suggested by this. That is to say
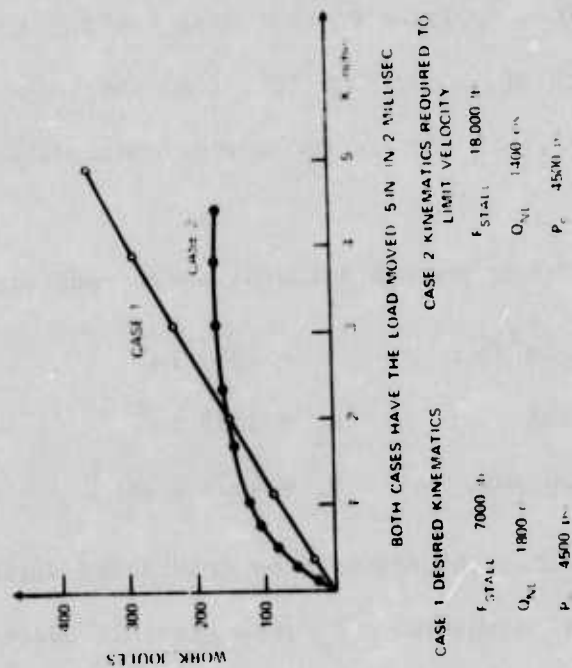
206

Figure C-9. Hydraulic system work for
unlimited (case 1) and limited (case 2) velocity.

an actuator with a large piston to accelerate the load and then stop while a smaller one continues with the load. A bonus feature is that the small piston can be sized to provide the correct contactor holding force when the switch is closed.

The piston peak forces for the large and small pistons currently under investigation are 15000 lbs and 400 lbs respectively. The exact travel of the small piston will vary due to electrode wear, so the worst case will be considered. The equations applying to this case are Eq. (C-9), (C-10), (C-17), (C-18), (C-19), (C-20), (C-21), (C-22). The travel of the large piston is .2 in. This is to provide .1 in for electrode wear compensation and .1 in for acceleration travel.

The parameters of the 2-stage actuator under consideration are:

$$q_o = 1800 \text{ in}^3/\text{sec} \qquad A_1 = .089 \text{ in}^2$$

$$F_{S1} = 400 \text{ lbs} \qquad A_2 = 3.33 \text{ in}^2$$

$$F_{S2} = 15,000 \text{ lbs.} \qquad P_S = 4500 \text{ lb/in}^2$$

There are three different cases to be considered during opening:

(1) After initial exposure to P_S when piston 1 overtakes piston 2.

(2) The period when piston 1 carries piston 2.

(3) The period when piston 1 is stopped and piston 2 "coasts".

Examining each case in detail:

(1) Starting with the piston 1 at X = 0. For the parameters shown:

$$X_1 = 2.49 \log \text{Cosh} [1077 \, t] \, u(t)$$

$$X_2 = .1 + .0133 \log \text{Cosh} [1077 \, t] \, u(t)$$

$$X_1 = X_2 \text{ at } t_c = .28 \text{ millisec}$$

208

$$X_1 = X_2 = .1005 \text{ in}$$

$$\frac{dX_1}{dt} = 540 \tanh (1077 \ t) \ u(t)$$

$$\frac{dX_2}{dt} \approx 0$$

$$\left.\frac{dX_1}{dt}\right|_{t=t_c} = 210 \text{ in/sec.}$$

The velocity of the coalesced assembly is

$$V_o = \frac{10}{12} \cdot 210 + \frac{2}{12} \cdot 0 = 175 \text{ in/sec}$$

(2) Coalesced Assembly

$$V_o = 175 \text{ in/sec} \quad , \quad X_o = .1005 \text{ in.}$$

The velocity during this phase is

$$\frac{dX_{1+2}}{dt} = 540 \tanh \left\{ 894 \ (t - .00038) + .325 \right\} u \ (t - .00038)$$

$$X_{1+2} = \left[.1005 + .602 \log \left\{ \frac{\cosh \left[894 \ (t - .00038) + .325 \right]}{\cosh .325} \right\} \right] u(t - .00038)$$

$$X_{1+2} = \left[.1005 + .602 \log \left\{ \frac{\cosh \ (894 \ t - .0147)}{1.052} \right\} \right] u \ (t - .00038)$$

at $t = .00078$ sec $= .78$ millisec ,

209

$$\frac{dX_{1+2}}{dt} \bigg|_{t=.8 \text{ millisec}} = 320 \text{ in/sec}$$

This is an acceptable velocity.

(3) Travel of the small piston alone.

For the final segment, consider

$X_1 = .2$ in $V_1 = 320$ in/sec

$X_1 = .2$

$$\frac{dX_1}{dt} = 0$$

$$X_2 = 1.025 \times 10^7 \log \left\{ \frac{\text{Cosh} \left[.7625 \ (t - .00078) + .017\right]}{\text{Cosh} \ .0209} \right\} u \ (t - .00078)$$

$$X_2 = 1.025 \times 10^7 \log \left\{ \frac{\text{Cosh} \ (.7625 \ t + .016)}{7.0002} \right\}$$

$$\frac{dX_2}{dt} = 20250 \ \tanh \left\{.7625 \ t + .016\right\}$$

$$X_2 \approx .5 \text{ in} \quad \text{at} \quad t \approx 1.7 \text{ millisec.}$$

These results are summarized in Table C-2.1.

The parameters have been put into the simulation. The results are slightly different due to the greater number of effects that are considered in the simulation. The equations shown herein were used to aid in sizing the hardware on the basis of incompressible flow. The lag times will run greater for compressible flow.

210

TABLE C-2.1 - SUMMARY OF ACTUATOR PISTON TRAVEL

	X_1		X_2			$\dfrac{dX_1}{dt}$		$\dfrac{dX_2}{dt}$	
	Begin	End	Begin	End		Begin	End	Begin	End
t = 0	0		.1			0		0	
t = .28 ms		.1005		.1005			210		0
t = .28 ms	.1005		.1005			175		175	
t = .68 ms		.2		.2			320		320
t = .68 ms	.2		.2			0		320	
t = 1.7 ms		.2		.5			0		320

Valve Configuration

The valving segment of the short pulse switch consists of a pilot stage, an intermediate stage and a power stage. The design of the valving segment resolves into a problem of getting enough flow gain in the number of stages. The pilot stage flow rating and power spool flow rating are known, so the problem becomes one of getting an intermediate stage that is adequate. The present configuration has a slow running intermediate stage. This means that the intermediate spool is large and will cause the power spool to move before the intermediate stage is fully open. This can be pre- dicted approximately with the design equations and confirmed on the simulation. The sequence portrayed in Figure C-6 is not the one employed in the final design, but is simply a pessimistic estimate.

The pilot stage is a jet pipe flow control servovalve. This par- ticular servovalve is highly reliable as proven by many years of service in

211

airborne and underseas applications. A conventional valve with a switching time of .002 seconds would have a q_o = 8 cis at 4500 psi. Since q_o = 1800 cis for the power spool, there is a large gap to be closed by the intermediate spool. The intermediate stage is made large, which makes it slow-running, so that a large orifice will be open to drive the power spool. This is important, since in the final analysis the .002 sec opening time begins when the power spool crosses center. At this instant, the holding force begins to be released (although not instantaneously due to fluid mass). This design has been analyzed in detail in the next section via digital simulation.

C-3   Analysis of The Valve Actuator

C-3.1   Assumptions

In order to analyze and verify the transient behavior of the short pulse switch hydraulic drive mechanism, a detailed dynamic simulation of the valve-actuator drive system has been developed. Using this simulation, the switch opening time and travel can be determined, the hydraulic feedline can be adequately sized and the switch closing operation can be shown to be satisfactorily completed prior to the next switch opening command.

The fundamental relationships upon which the dynamic simulation is based are:

(1) The square root orifice law for hydraulic fluid flow through each of the spool valve stages,

(2) The conservation of mass for flow of the compressible hydraulic fluid through the valve stages,

(3) The force balance relationship for accelerating masses (servo-valve spools and actuator pistons), and

(4) The conservation of mass and conservation of momentum relationships for compressible fluid flow through a line.

Basic assumptions which were made in the application of the above relations to the valve-actuator switch are listed below:

(1) Piston and spool drag force are assumed constant.

(2) Fluid bulk modulus is constant.

(3) Damping ratio for elastic metal to metal contact is 0.1.

(4) The impact absorbing fluid interface between the small and large pistons is incompressible.

213

(5) The air in the accumulator is considered to be a perfect gas and its expansion-compression is taken to be isothermal.

(6) There is no frictional resistance to flow in the accumulator.

(7) The feed lines can be adequately represented by a single section lumped parameter simulation.

For convenience of simulation the valve actuator is simulated with a simple, single section lumped parameter model of the hydraulic feedline supplied with a constant pressure source. However a separate more detailed study of the feed system is reported in section C-4. This simulation includes pump dynamics and the dynamics of both the feedline and the return line.

C-3.2   Simulation Results

The valve-actuator opening and closing transient response functions determined from the simulation are shown in Figures C-10 and C-11. These plots show the positions of the intermediate valve spool, the power valve spool, the actuator small piston and the actuator large piston as functions of time. Time zero for the valve opening response curves is taken as the time when the pilot spool has been opened to its full position. Because of a dynamic lag in the pilot stage torque-motor resulting from the inductance of its coil, the pilot valve spool opens approximately 2 milliseconds after the application of a command pulse to the torquer. This effect has not been included in the simulation because it produces a simple delay of 0.002 secs. in the events shown in Figure C-10, but does not affect the form of these response functions.

As soon as the pilot valve is opened the intermediate spool begins to open. As shown in Figure C-10, the intermediate spool quickly attains a
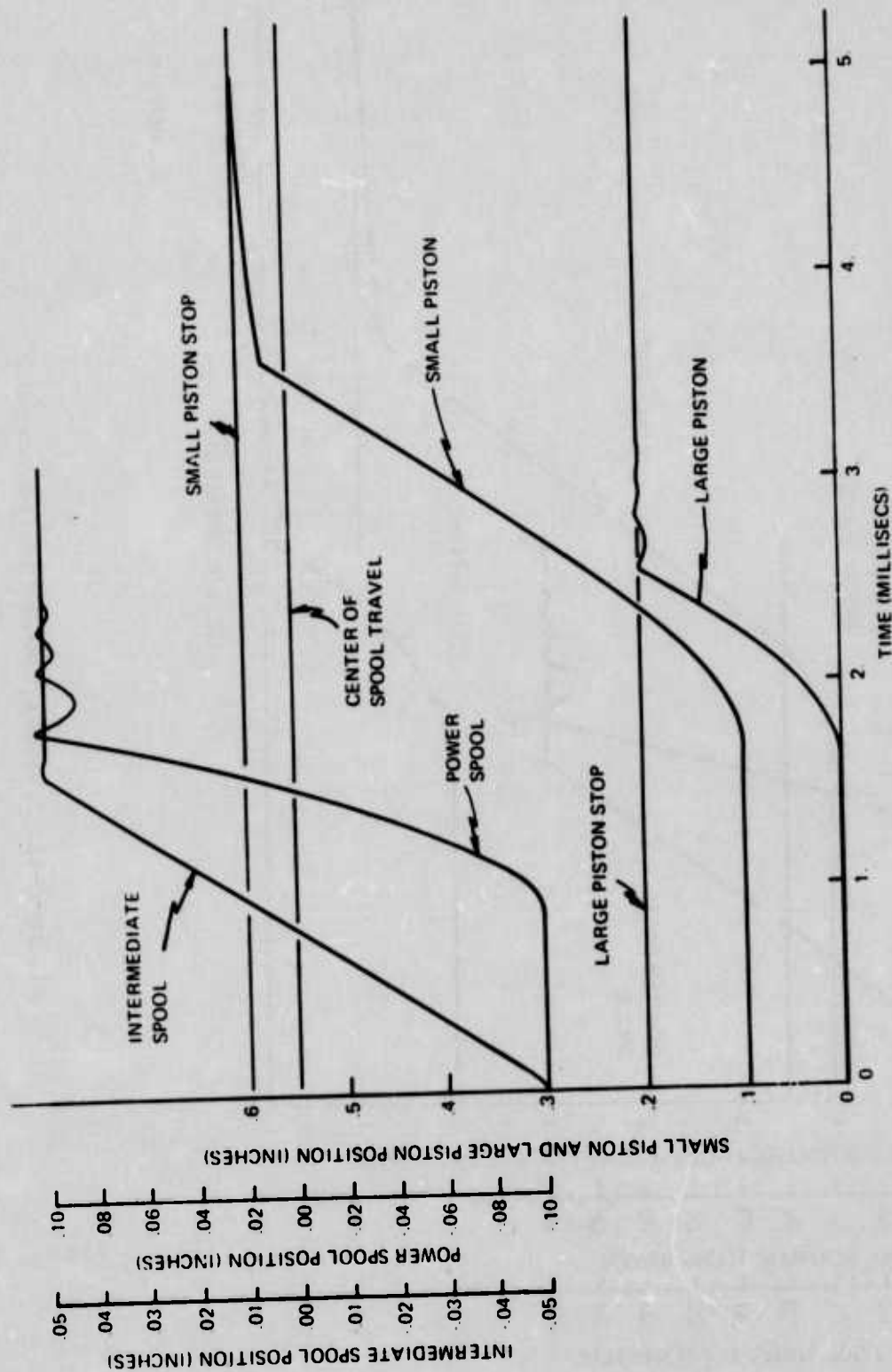
Figure C-10. Valve-Actuator Opening Transient

S73-0203-VA-10

215
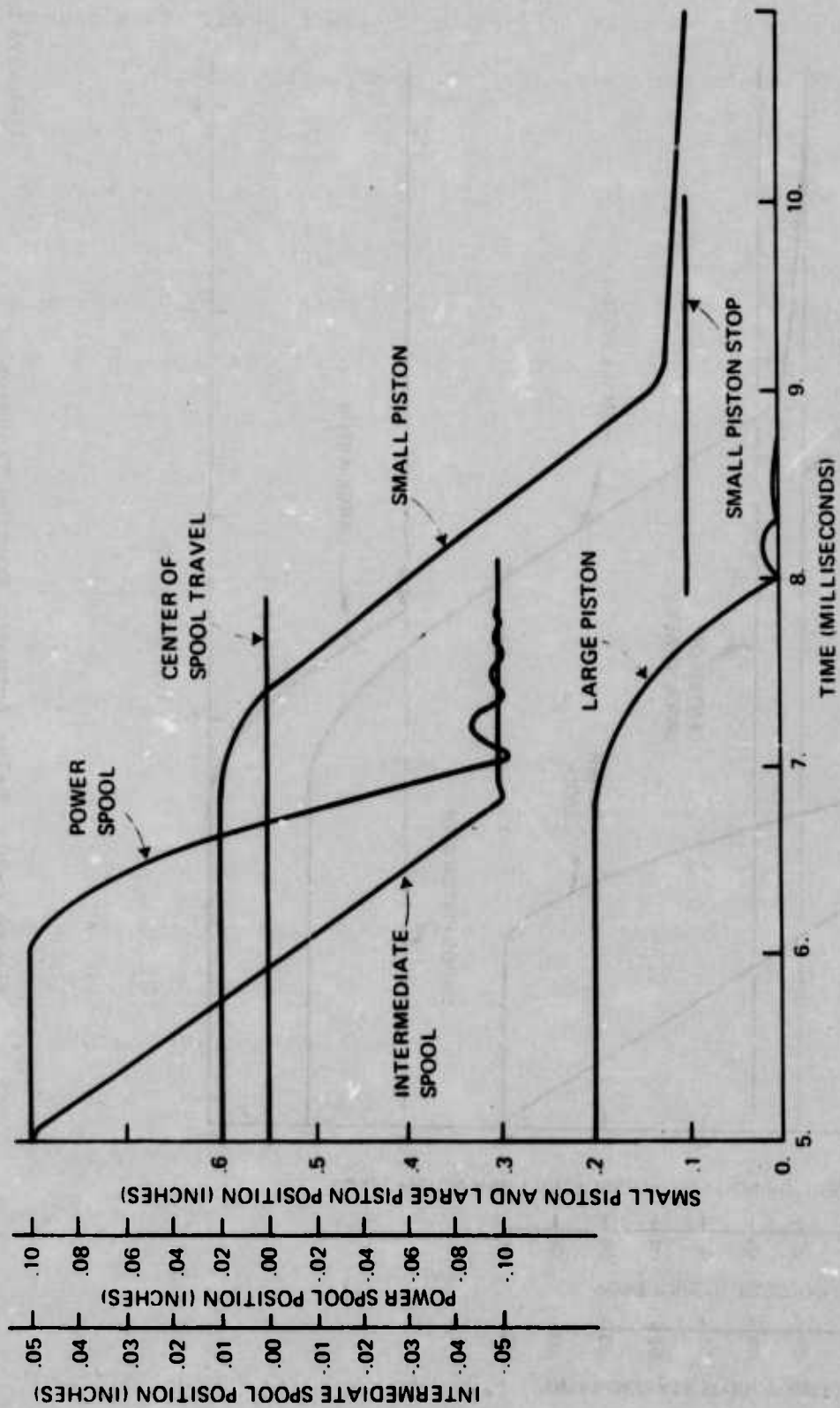
Figure C-11. Valve-Actuator Closing Transient

S73-0203-V4-11

216

steady speed because of its low mass. When it crosses the spool center position, fluid at supply pressure, is applied to the power spool. This causes the power spool to accelerate toward the full open position. When it reaches its stop in this full open position, it bounces back a few times because of its mass and the elasticity of the spool and stop. This will be eliminated in the final design with a "squish" volume. The hydraulic fluid pressure eventually forces it to rest against its stop. When the power spool crosses the spool travel center, fluid at supply pressure is applied to the actuator in a direction to drive both pistons open. The large piston, because of its large area and low mass figure, begins to accelerate. As it does, it tends to compress a trapped volume of fluid between the two pistons. This fluid pressure builds up, developing a force which acts to accelerate the small piston. As the large piston maintains its force against the compressed fluid and the small piston accelerates, fluid is slowly discharged through a specially sized orifice. This prevents the two pistons from a direct, elastic collision.

When the large piston has advanced 0.2", it strikes its stop and comes to rest. The small piston continues at almost constant velocity until it reaches its stop inside the large piston. When it gets to within 0.040" of its stop, the small piston captures a small volume of hydraulic fluid between it and its stop. Further advance of the piston attempts to compress the fluid causing pressure build up. This pressure acts to slow the piston and reduce impact with its stop in the same way as a shock absorbing bumper on an automobile protects against severe impact. A more detailed description of how it is created and simulated is given below. When the small piston has come to rest against its stop inside the large piston, it has moved 0.5" thereby opening the switch contacts the required 0.5 inches.

217

Figure C-11 shows the spool and piston positions during the switch closure transient. Again, this operation is initiated by applying a switch return command to the pilot stage torque motor. Approximately 0.002 sec. later, the pilot spool position is driven to its negative stop. This begins the chain of events shown in Figure C-11. As described before, the intermediate spool and power spool are driven to their full negative positions and supply pressure to the actuator is reversed causing both pistons to return to their initial positions with the switch closed. Again, the "squish" force is utilized to avoid an elastic bounce when the switch closes.

The "squish" force is a force which acts on the small and large pistons when impact between the two is about to occur. It occurs because of a specially designed boss in the small piston which mates with a matching circular counterbore on the large piston. As the two pistons approach each other, the boss and counterbore mate. This creates a small cavity which captures a small volume of hydraulic fluid. A carefully sized orifice located in the small piston groove provides the primary path of discharge for the captured fluid. As the two pistons approach each other, the captured fluid pressure builds up, providing a retarding force which tends to reduce the approach speed of the two pistons. The fluid pressure build-up also increases the rate of fluid discharge through the orifice, resulting in a smooth deceleration of the moving piston thereby eliminating the possibility of a hard impact and an elastic bounce.

Both ends of the small and large pistons are designed to develop the "squish" force as they approach end contact with each other. However, there is a difference between the size of the "squish" zone at each end of the piston.

218

At that end of the large piston which is associated with the switch full open position, the "squish" zone is .040" long. Thus, during the switch opening transient when the small piston is approaching its full open position, it enters the "squish" zone when it is .040" from the stop. However, at the other end of the large piston, the "squish" zone is 0.140" long. This permits the small piston to enter the "squish" zone when it is 0.040" from its stop (switch contact closure). A "squish" zone 0.140" in length is needed here to account for the 0.1" difference in initial position of the two pistons. This 0.1" difference in initial position is designed into the actuator to allow for electrode wear at the point of contact.

In the simulation, logic blocks are used to invoke this "squish" force only when either of the two pairs of piston impact surfaces are (1) sufficiently close together, i.e., within the region where the boss and counterbore mate, and (2) the two impact surfaces are approaching each other. The reason for this feature is that a negative pressure can not exist in the cavities. If the pressure approaches 0 psi, the fluid will cavitate. Negative pressures get generated mathematically when the "squish" pistons seperate. Unless both of these conditions are met, the "squish" force is zero.

Some 10 to 11 milliseconds are required to complete the switch opening and closing operation shown in Figures C-10 and C-11. During this time, the flow requirements to the power spool and particularly the actuator are high. Because of an assumed hydraulic supply line length of 10 feet, the line inertance is rather high. In order to avoid severe pressure drops during the switch opening and closing operation due to the line inertance, an accumulator is placed in the line at the valve actuator. This stores

TABLE C-3.1
NOMENCLATURE, SPS VALVE-ACTUATOR SIMULATION

SUBSCRIPTS		1 - pilot spool	
		2 - intermediate spool	
		3 - power spool	
		4 - actuator, large piston	
		5 - small piston	
PARAMETERS	**GENERAL**	β - fluid bulk modulus	1×10^5 psi
		ρ - fluid density	0.0307 lb/in^3
		g - acceleration of gravity	32.2 ft/sec^2
	INTERMEDIATE STAGE	$X_{2\ max}$ - stroke	$\pm$ 0.05 in.
		A_{S2} - spool x-sect area	0.1257 in^2
		$V_2 = A_{S2} \times X_{2\ max}$ - half stroke displacement	0.00629 in^2
		$C_{f2} = V_2/2\beta$	3.145×10^{-8} in^3/psi
		B_{L2} - leakage coefficient	0.0002 in^3/sec/psi
		m_2 - piston weight	0.138 lb
		K_{S2} - piston/stop spring constant	10^6 lb/in
		F_{B2} - Bernouli flow force coefficient	0.0064 lb/(psi)$^{1/2}$(in^3/sec)
		F_{f2} - piston coulomb friction force	5 lb
		C_{z2} - orifice coefficient	24.4 (in^3/sec)/in(psi)$^{1/2}$
	POWER STAGE	$X_{3\ max}$ - stroke	$\pm$ 0.1 in.
		A_{S3} - spool x-sect area	0.502 in^2
		$V_3 = A_{S3} \times X_3$ - half stroke displacement	0.0502 in^2
		$C_{f3} = V_3/2\beta$	2.51×10^{-7} in^3/psi
		B_{L3} - leakage coefficient	0.0005 in^3/sec/psi
		m_3 - piston weight	0.444 lb
		K_{S3} - piston/stop spring constant	4×10^6 lb/in
		F_{B3} - Bernouli flow force coefficient	0.0064 lb/psi$^{1/2}$(in^3/sec)
		F_{f3} - piston coulomb friction force	10 lb
		C_{e3} - orifice coefficient	59.6 in^3/sec/in(psi)$^{1/2}$
		F_{d3} - damping coefficient-piston & stop in contact	13.57 lb/in/sec
	ACTUATOR	C_{e4} - orifice coefficient	268 in^3/sec/in(psi)$^{1/2}$
		$X_{4\ max}$ - stroke	0 to 0.2 in
		A_{S4} - piston area	3.33 in^2
		m_4 - piston weight	2 lb
		K_{S4} - piston/stop spring constant	32×10^6 lb/in
		F_{f4} - piston coulomb friction force	50 lb
		F_{d4} - damping coefficient-piston & stop in contact	81.2 lb/in/sec
		F_{f45} - coulomb friction force, small piston inside the large	20 lb
		K_{S45} - spring constant - large & small piston in contact	1×10^6 lb/in
		A_{S5} - small piston area	0.089 in^2
		m_5 - small piston weight	10 lb
		X_{m45} - small piston stroke, inside of large piston	0 to .4"
		X_{b5} - small piston stroke lower limit (contact stop position	0.1 in.
		K_{S5} - small piston/contact stop spring contact	1×10^6 lb/in
		β_{eq} - "squish" force orifice coefficient	0.0157 in^3/sec/(psi)$^{1/2}$

TABLE C-3.1   (CONTINUED)

PARAMETERS	**FEEDLINE**	L_f - length of feedline	120 in.
		A_f - cross-sectional area of feedline	0.11 in^2
		L_r - length of return line	120 in.
		A_r - cross-sectional area of return line	0.307 in^2
		R_{fr} - flow resistance of feedline & return line combined	0.105 psi/(in^3/sec)^2
		A_A - accumulator cross-sectional flow area	1.21 in^2
		L_A - accumulator axial length	1.24 in.
		R_A - flow resistance in accumulator	0 psi/(in^3/sec)^2
		P_{A0} - initial accumulator pressure	4500 psi
		V_{A0} - initial air volume in accumulator	1.5 in^3
VARIABLES	**VALVE-ACTUATOR**	X_1 - pilot spool position	inches
		$\emptyset_2$ - flow coefficient controlling drive flow for intermediate spool	in^3/sec/psi$^{1/2}$
		P_2 - drive pressure for intermediate spool	psi
		q_2 - drive flow for intermediate spool	in^3/sec
		X_2 - intermediate spool position	inches
		$\emptyset_3$ - flow coefficient controlling drive flow for power spool	in^3/sec/psi$^{1/2}$
		P_3 - drive pressure for power spool	psi
		q_3 - drive flow for power spool	in^3/sec
		X_3 - power spool position	inches
		$\emptyset_4$ - flow coefficient controlling drive flow for actuator	in^3/sec/psi$^{1/2}$
		P_4 - actuator drive pressure	psi
		q_4 - drive flow for actuator	in^3/sec
		X_4 - large piston position	inches
		X_5 - small piston position	inches
		P_{sq} - fluid pressure associated with "squish" force	psi
		F_{sq} - "squish" force	pounds
	FEEDLINE	P_1 - inlet pressure	psi
		P_S - supply pressure	psi
		P_A - pressure in accumulator	psi
		q_S - flow in feedline from supply toward accumulator	in^3/sec
		q_A - flow into accumulator	in^3/sec
		q_1 - inlet flow to actuator	in^3/sec

221

1.5 cubic inches of fluid at or near supply pressure prior to the opening
transient. It supplies the high flow rates required by the actuator during
the short time of the transient, without a total loss of pressure. The
pressure however does drop during this time even with the accumulator. About
1000 psi reduction in supply pressure occurs during the switch opening and
another 1000 psi reduction occurs during the switch closure. Thus, at the
conclusion of the switch closure, accumulator pressure is roughly 2500 psi.
During the rest time between successive switch openings and closures, the
supply line recharges the accumulator.

SPS Valve-Actuator Simulation Equations

Intermediate Valve - Orifice Coefficient-Pilot Valve:

$$\emptyset_2 = C_{z_2} \; X.$$ (C-25)

Square Root Orifice Law

$$q_2 = Sgn \; (Sgn \; (\emptyset_2) P_i - P_2) \, | \; \emptyset_2 | \; \sqrt{|Sgn(\emptyset_2) P_1 - P_2|}$$ (C-26)

Conservation of Fluid Mass

$$C_{t_2} \frac{d \, P_2}{dt} = - A_{S_2} X_2 + q_2 - B_{L_2} P_2$$ (C-27)

Spool Force Balance

$$\frac{m}{12g} \frac{d \, \dot{X}_2}{dt} = - K_{S_2} \; x \left\{ \begin{array}{l} (X_2 - .05), \; if \; X_2 > .05 \\ \\ 0, \; if \; -.05 < X_2 < .05 \\ \\ (X_2 + .05), \; if \; X_2 < -.05 \end{array} \right\} + P_2 \, A_{S_2} + \emptyset \; (P_1 \; P_2) F_{B_2} - F_{f_2} sgn(\dot{X}_2)$$ (C-28)

Power Valve - Orifice Coefficient - Intermediate Valve

$$\emptyset_3 = C_{z_3} \, X_2$$ (C-29)

Square Root Orifice Law

$$q_3 = \text{Sgn}\,(\text{Sgn}(\emptyset_3)P_i - P_3)\,|\,\emptyset_3\,|\,\sqrt{|\text{Sgn}(\emptyset_3)P_i - P_3|}$$

(C-30)

Conservation of Fluid Mass

$$C_{t_3}\frac{d\,P_3}{dt} = q_3 - A_{S_3}\dot{X}_3 - B_{L_3}P_3$$

(C-31)

Spool Force Balance

$$\frac{m_3}{12g}\frac{d\,\dot{X}_3}{dt} = P_3 A_{S_3} \div \emptyset_3(P_i - P_3)F_{B_3} - K_{S_3} \times \begin{cases} (X_3 - .1) & \text{if } X_3 > .1 \\ 0 & \text{if } -.1 < X_3 < .1 \\ (X_3 + .1) & \text{if } X_3 < -.1 \end{cases} - F_{f_3}\text{sgn}(\dot{X}_3)$$

(C-32)

$$- f_3 \times \begin{cases} \dot{X}_3, \text{if } -.1 > X_3 > .1 \\ 0, \text{if } -.1 < X_3 < .1 \end{cases}$$

Actuator

Square Root Orifice Law

$$q_4 = \text{Sgn}(\text{Sgn}(\emptyset_4)P_i - P_4\,|\emptyset_4|\,\sqrt{|\text{Sgn}(\emptyset_4)P_i - P_4|}$$

(C-33)

Conservation of Fluid Mass

$$C_{t_4} \frac{d\,P_4}{dt} = q_4 - P_4\,B_{L_4} - A_{S_4}\,\dot{X}_4 - A_{S_5}\,\dot{X}_5 \qquad (C\text{-}34)$$

Large Piston Force Balance

$$\frac{m_4}{12g} \frac{d\,\dot{X}_4}{dt} = A_{S_4} P_4 - F_{f_4} \operatorname{sign}(\dot{X}_4) - K_{S_4} \times \begin{cases} (X_4 - .2) & \text{if } X_4 > .2" \\ 0 & \text{if } .2 > X_4 > 0" \\ X_4 & \text{if } X_4 < 0 \end{cases} \qquad (C\text{-}35)$$

$$- F_{d_4} \times \begin{cases} X_4 & \text{if or } X_4 < 0 \\ 0 & \text{if } 0 < X_4 < .2 \end{cases} - K_{S_{45}} \times \begin{cases} X_4 - X_5 & \text{if } (X_4 - X_5) > 0 \\ 0 & \text{if } -.4 < (X_4 - X_5) < 0 \\ (X_4 - X_5 + .4) & \text{if } (X_4 - X_5) < -.4 \end{cases}$$

$$+ F_{f_{45}} \operatorname{sign}(\dot{X}_5 - \dot{X}_4) + \text{"squish" force}$$

Small Piston Force Balance

$$\frac{m_5}{12} \frac{d\,\dot{X}_5}{dt} = A_5\,P_4 + K_{S45} \begin{cases} (X_4 - X_5) & \text{if } (X_4 - X_5) > 0 \\ 0 & \text{if } -.4 < (X_4 - X_5) < 0 \\ (X_4 - X_5 + .4) & \text{if } (X_4 - X_5) < -.4 \end{cases} \qquad (C\text{-}36)$$

$$- F_{f_{45}} \operatorname{sign}(\dot{X}_5 - \dot{X}_4) - K_{S_5} \begin{cases} (X_5 - .1) & \text{if } X_5 < .1" \\ 0 & \text{if } X_5 > .1" \end{cases} - \text{"squish" force}$$

224

<u>"Squish Force"</u>:

$$P_{sq} = \frac{A_{S5}^{2}}{Q_{sq}^{2}} (\dot{X}_5 - \dot{X}_4) \times |\dot{X}_5 - \dot{X}_4| \qquad\qquad \text{(C-37)}$$

$$F_{sq} = P_{sq} A_{S5}$$

<u>Feedline</u>:

<u>Conservation of Momentum in the Feedline</u>:

$$\frac{d\,q_S}{dt} = \left[\frac{12g}{\rho} \frac{1}{(\frac{L_f}{A_f} + \frac{L_r}{A_r})} \right] \left[(P_S - P_i) - R_{fr}\, q_S\, |q_S| \right] \qquad \text{(C-38)}$$

<u>Conservation of Fluid Mass in the Feedline</u>:

$$\frac{d\,P_i}{dt} = \frac{\beta}{(A_f L_f + A_r L_r)} (q_S - q_i - q_A) \qquad\qquad \text{(C-39)}$$

<u>Conservation of Momentum in the Accumulator</u>:

$$\frac{d\,q_A}{dt} = \frac{12g\,A_A}{\rho\,L_A} (P_i - P_A) \qquad\qquad \text{(C-40)}$$

<u>Isothermal Expansion-Compression of Air in Accumulator</u>

$$\frac{d\,P_A}{dt} = \frac{P_A^{2}}{P_{A_0} V_{A_0}} q_A \qquad\qquad \text{(C-41)}$$

C-3.3   <u>Simulation Operation</u>

The program is a listing of the valve-actuator equations as they are provided to the digital computer. In this form, the equations are input to the digital program "COSS" which is available from Comshare Incorporated, a time share computer service company. Each of the lines denotes a specific type of mathematical element. In entering the system to program COSS, each

225

element is listed with the numbers of those connections which feed it. It has been found that an integration interval which is not much larger than 1×10^{-6} sec will yield meaningful results.

C-4   Analysis of The Feedsystem

Operation of the valve-actuator requires adequate supply of hydraulic power. At a pulse rate of 5 pulses per second, an average flow rate of approximately 12 in^3/sec is required. Simulation of the actuator with a crude feedline model (Sec. C-3) indicates that instantaneous flow rates peaking near 1000 in^3/sec are required, and that a pressure loss of 2000 psi can be expected immediately after the actuator is operated through one open-close cycle. Thus it is evident that the feedsystem deserves attention from an analysis standpoint to insure its adequacy in supplying the necessary flow rate and pressure.

For the purposes of this study it is assumed that the hydraulic power supply is located ten feet from the valve actuator, thus requiring 10' long supply and return transmission lines. Such length permits some measure of remote mounting freedom for the valve actuator independent of the power supply. Transmission lines will also prove valuable in isolating the hydraulic power supply from the high electrical potentials at the valve actuator.

In order to examine the question of whether or not transmission lines can adequately supply the valve-actuator hydraulic power requirements, a simulation of the feedsystem was created.

Feedline Accumulators and Feedline Restrictors

Restrictors were found to be necessary as a direct result of the simulation, in order to reduce flow oscillations in the feedline due to interaction between the feedline and the pump.

The approach to the fluid power transmission problem has been to utilize accumulators where necessary to store the necessary volume of fluid

227

required by the actuator, during its operation. After the pulse, the transients are allowed to settle out and the accumulators are replenished before the next pulse occurs. This approach appeared to be satisfactory for the case of 5 pps as the results below will show. However when a pulse rate of 20 pps was examined, the accumulators were found to need enlargement to supply the fluid requirements without excessive pressure loss. This reduced the feedsystem natural frequency to a point close to the 20 pps frequency, making it virtually impossible to achieve steady state conditions before the arrival of the next pulse, as was possible at the 5 pps rate. However, by proper sizing of the two feedline accumulators, it was found that the feedline natural frequency could be adjusted to provide satisfactory pressure recovery in the load accumulator just prior to the arrival of the next pulse. These results are shown below in the section on analysis at the 20 pps rate.

C-4.1   Feedsystem Analysis - 5 Pulses Per Second Operation

System Description - The hydraulic feed system consists of a variable stroke pump capable of delivering a maximum of 12 in^3/sec (approximately 3 gal/min). Its maximum pressure is 4500 psi. The pump discharges through an orifice and then into an accumulator which exists at the upstream end of the 10 ft. long feedline. The ID of this line is considered to be 3/8" and its OD is 5/8". At the downstream or discharge end of the line is a restriction and a second accumulator which stores fluid sufficient for one open-close cycle of the valve-actuator.

The purpose of the accumulators is to store fluid for the short term, high flow demands of the valve-actuator, thereby smoothing the flow requirements of the pump to a much lower, steady value. Restrictors are inserted in the lines as shown to reduce flow oscillations between the accumulators and to decouple the pump dynamics from those of the line.
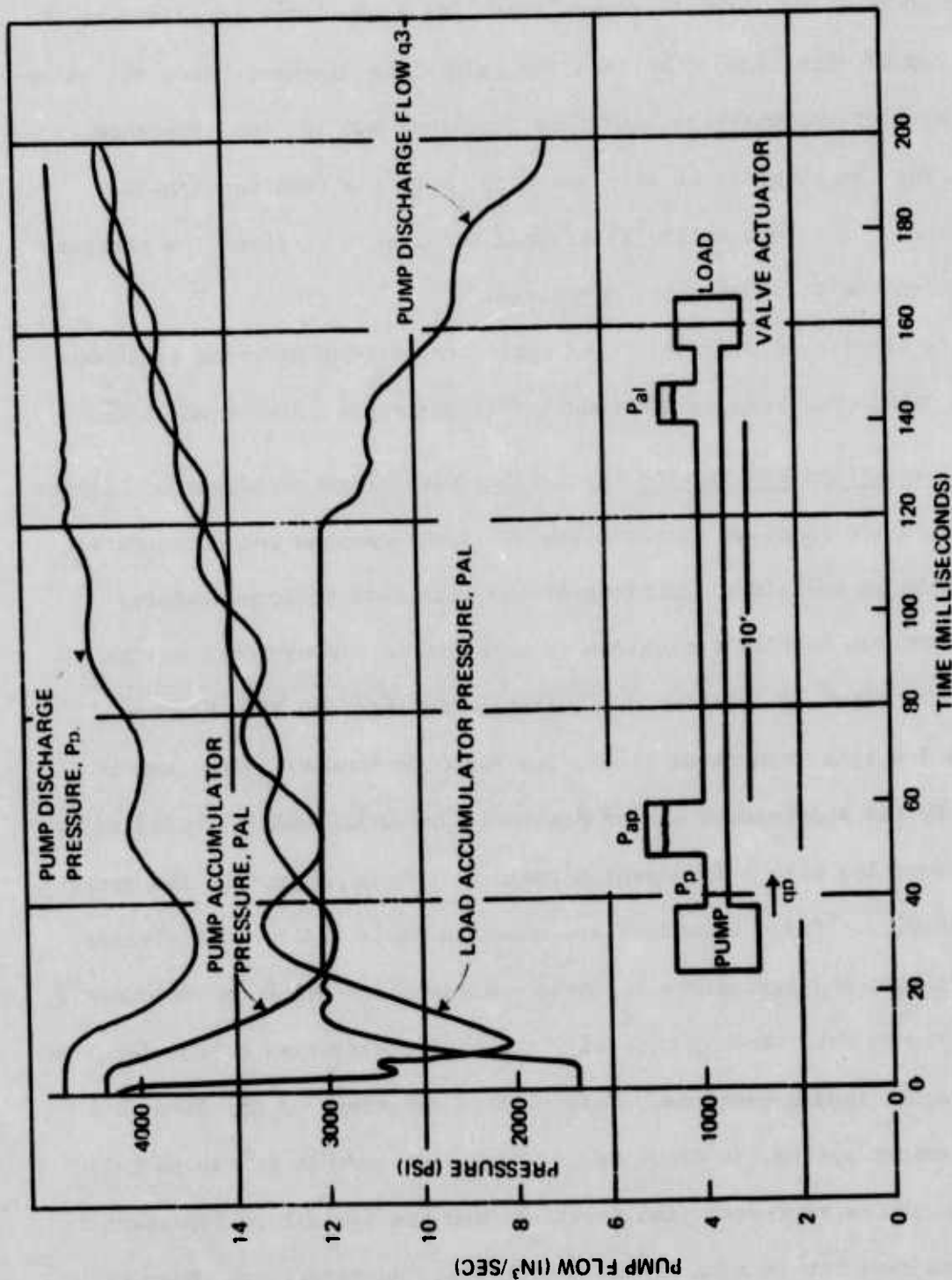
Fluid discharge from the valve-actuator is returned to the pump through a 10 foot long 5/8" ID return line. An accumulator is placed at the upstream end of this line to collect the pulse-like discharge from the valve-actuator without encountering high flow impedance due to line inertance.

For the purposes of this analysis, only the feedline dynamics were examined. The return line is assumed to offer a constant low pressure resistance to the valve-actuator discharge.

A simplified diagram of the system under consideration is shown in Figure C-12. The response curves in this figure are discussed later.
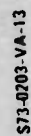
C-4.1.1 <u>Simulation Description</u> - Equations describing the dynamic behavior of the system are based on conservation of fluid momentum and conservation of fluid mass in individual sections of the line and the accumulators. Pressure drop due to flow resistance is taken to be proportional to the square of the flow. This is an approximation in that the flow becomes laminar at low line velocities (i.e., low Reynolds Number). The pump is simulated by its approximate static pressure-flow relationship, modified by a second order lag with a low damping ratio ($\zeta = 0.1$) to provide the proper dynamic behavior. These equations are shown in Table C-4.1. Definitions of the variables and parameters in these equations are given in Table C-4.2.

Figure C-13 shows pictorially the sectionalization of the feedline into four equal length sections. This permits treatment of the line as a lumped parameter system, as shown by the analogous circuit in Figure C-13. Here the inductors represent line inertance and the capacitors represent line storage capacity in each of the 4 sections. Resistors are shown with an arrow to remind that they are non linear elements (square law relationship). The first three sections are handled identically, series inertance

229

Figure C-12. Results of Transient Feedline Analysis

S73-0203 VA-12

Figure C-13. Illustration of The Lumped Parameter Approximation
To The Hydraulic Feedline

S73-0203-VA-13

231

TABLE C-4.1 - EQUATIONS

PUMP:

$$P = 4500. - 14.3\, q_p \qquad 0 \le q_p \le 12$$

$$P = 56269.2 - 4328.4\, q_p \qquad 12 < q_p \le 13$$

$$P = 0. \qquad\qquad\qquad q_p > 13$$

$$\frac{P_p\,(S)}{P\,(S)} = \frac{1}{\dfrac{S^2}{Wn^2} + \dfrac{2\zeta}{W_n} S + 1}$$

UPSTREAM ORIFICE:

$$q_p = S_{gn}(P_p - P_{AP}) \sqrt{(P_p - P_{AP})\, / R_{01}}$$

PUMP ACCUMULATOR:

$$\frac{d}{dt}\, P_{AP} = P_{AP}^2 (q_p - q_1)\, \frac{1}{P_1 V_1}$$

FEED LINE: 1st Section

$$\frac{dq_1}{dt} = \frac{12gA}{\rho\, L/4} \left(P_{A1} - P_1 - R/4\, q_1 |q_1| \right)$$

$$\frac{dP_1}{dt} = \frac{\beta_e}{A\, L/4} \, (q_1 - q_2)$$

2nd Section

$$\frac{dq_2}{dt} = \frac{12gA}{\rho\, L/r} \left(P_1 - P_2 - R/4\, q_2 |q_2| \right)$$

$$\frac{dP_2}{dt} = \frac{\beta_e}{A\, L/4} \left(q_2 - q_3 \right)$$

3rd Section

$$\frac{dq_3}{dt} = \frac{12gA}{\rho\, L/4} \left(P_2 - P_3 - R/4 \; q_3 |q_3| \right)$$

$$\frac{dP_3}{dt} = \frac{\beta_e}{A\, L/4} \left(q_3 - q_{41} \right)$$

4th Section

$$\frac{dq_{41}}{dt} = \frac{12gA}{\rho\, L/8} \left(P_3 - P_{4C} - R/8 \; q_{41}|q_{41}| \right)$$

$$\frac{dP_{4C}}{dt} = \frac{\beta_e}{A\, L/4} \left(q_{41} - q_{42} \right)$$

$$\frac{dq_{42}}{dt} = \frac{12gA}{\rho\, L/8} \left(P_{4C} - P_{AL} - R_{02} \; q_{42}|q_{42}| \right)$$

LOAD ACCUMULATOR:

$$\frac{dP_{AL}}{dt} = \left(q_{42} - q_L \right) P_{AL}^2 \; \frac{1}{P_2 V_2}$$

LOAD:

$$q_2 = f(t)$$

233

TABLE C-4.2 - DEFINITION OF PARAMETERS AND VARIABLES

Parameters

Pump

ζ	Damping Ratio - pump dynamics	0.1
ω_{11}	Natural frequency - pump dynamics	760 rad/sec

Upstream Orifice

R_{01}	Square law orifice resistance - upstream orifice	5 $psi/(in^3/sec)^2$

Pump Accumulator

P_1	initial trapped air pressure	4500 psi
V_1	initial trapped air volume	3.0 in^3

Feed Line

L	line length	120 in
A	line cross sectional flow area	0.11 in^2
R	line square law flow resistance	0.105 $psi/(in^3/sec)^2$

Downstream Orifice

R_{02}	Square law orifice resistance - downstream orifice	0.1 $psi/(in^3/sec)^2$

Load Accumulator

P_2	initial trapped air pressure	4500 psi
V_2	initial trapped airvolume	1.5 in^3

General

ρ	hydraulic fluid density	0.0307 lb/in^3

| g | acceleration of gravity | 32.2 ft/sec^2 |
| β_e | equivalent fluid bulk modulus for line | 10^5 psi |

Variables

| P_p | pump discharge pressure | psi |
P	pump pressure derived from flow	psi
P_{AP}	pump accumulator pressure	psi
P_1	pipe pressure at the end of the first line section	psi
P_2	pressure at the end of the second line section	psi
P_3	pressure at the end of the third line section	psi
P_{4C}	pressure at the center of the fourth line section	psi
P_{AL}	load accumulator pressure	psi
q_p	pump discharge flow	in^3/sec
q_1	flow in the 1st line section	in^3/sec
q_2	flow in the 2nd line section	in^3/sec
q_3	flow in the 3rd line section	in^3/sec
q_{41}	flow in the first half of the 4th line section	in^3/sec
q_{42}	flow in the second half of the 4th line section	in^3/sec
q_L	flow to the load	in^3/sec

first and then shunt capacitance. However, because the last section couples
to the load accumulator which requires a flow input, this section is arranged
such that its series inertance and resistance are distributed upstream and
downstream of the centrally located shunt capacitance. With this arrangement
the output flow of the line, q_{42} is calculated. With q_{42} as the input flow
to the load accumulator simulation, accumulator pressure can be calculated.

Flow out of the accumulator to the load q_1, is developed as a function of time by means of a pair of function generator blocks. This flow
function is shown in Figure C-14. It is an approximation of the flow function calculated from the simulation of the valve-actuator. As Figure C-14
shows, there are two large peaks to the function. The first peak is the flow
required by the valve-actuator during the valve-actuator opening transient.
The second peak is the flow required during the closing transient.

The area under this function represents the volume of hydraulic
fluid required in one opening - closing transient. To be sure that the
approximate flow function sythesized with the function generators represents
an equivalent volume of fluid, the integrals of both the calculated and the
approximate functions were determined. These are reasonably close
(2.107 in^3 for the calculated function and 2.225 in^3 for the approximate
function).

The program is a listing of the feedsystem equations as they have
been provided to the digital computer. While the computations are made
digitally, the format of the program is analog in nature.

C-4.1.2   Simulation Results - The results of the transient feedline analysis
are shown in Figure C-12. It shows pressure in the two accumulators, pump
discharge pressure and flow vs time for a 200 millisecond period. A simple
sketch of the feedsystem is included in the figure for reference purposes.

236
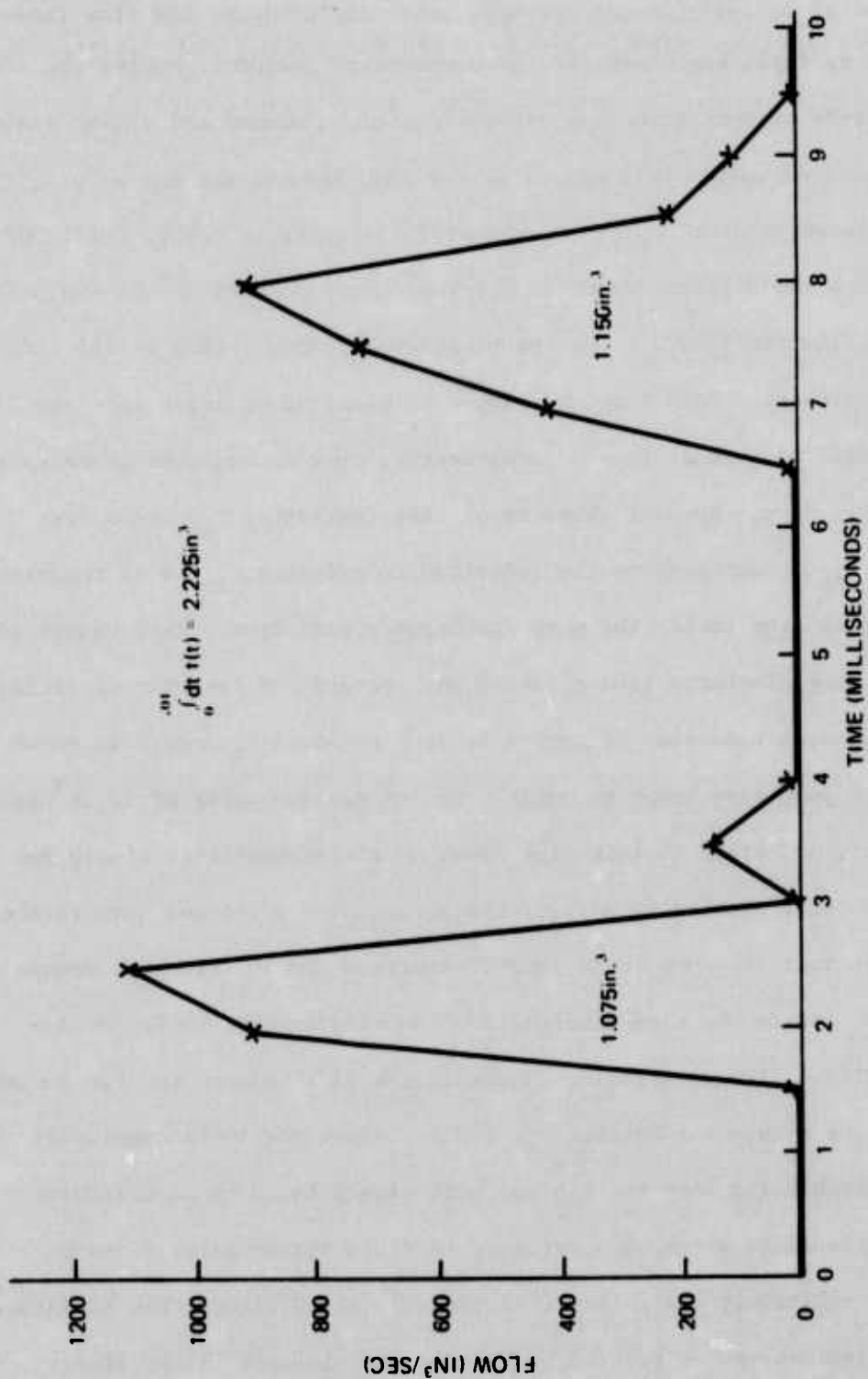
Figure C-14. Load Flow vs Time $(q_2 = f(t))$
For One Open-Close Cycle of The SPS

S73-0203-VA-14

$$\int_0^{.01} dt \; \dot{t}(t) = 2.225 \text{in.}^3$$

1.075in.^{3}

1.150in.^{3}

FLOW (IN^3/SEC)

TIME (MILLISECONDS)

237

These results were obtained by permitting the feedsystem model to operate

through several 200 millisecond periods, until the pressure and flow func-

tions began to duplicate themselves in consecutive periods. During the first

10 milliseconds of operation, the valve-actuator is opened and closed again

depleting the hydraulic fluid stored in the load accumulator and causing the

load accumulator pressure P_{AL} to drop sharply as shown in Figure C-12. Note

that there are two distinct drops in pressure corresponding to the two peaks

in the load flow function q_1. As the pressure P_{AL} drops, flow in the line

begins to increase. Fluid from the pump accumulator discharges into the line

to provide this additional flow. Consequently, pump accumulator pressure P_{AP}

also begins to drop. However because of line inertance, P_{AP} drops more

slowly that P_{AL}. Accompanying the reduction in pressure P_{AP} is an increase

in the pressure drop across the pump discharge restriction. This causes an

increase in pump discharge flow q_p as shown. Because of the pump operating

characteristics, a reduction of pump discharge pressure P_p occurs as shown.

Note that the pump flow jumps up quickly to its maximum value of 12 in^3/sec

(about 3 gpm), and stays at this flow level as the accumulators slowly re-

charge. When sufficiently recharged, the accumulator pressures have climbed

to the extent that the pump is no longer saturated and its flow q_p, begins

to decrease. During the time interval from 30 milliseconds to 200 milli-

seconds, a slight flow oscillation occurs in the line between the two accumu-

lators. As the pressure functions P_{AP} and P_{AL} show, the two accumulators

take turns discharging into the line as both slowly build up in pressure.

Such oscillations are a common occurrence in fluid transmission lines be-

cause of the relatively small flow resistance in these lines. The amplitude

of the oscillations can be reduced by putting restrictions in the line.

Such a restriction has been inserted in this feedline just upstream of the

load accumulator as shown in the system schematic. The size of the restric-

238

tion must be chosen with care. If it is too large an excessive pressure drop will develop across it, causing a reduction of pressure downstream in the load accumulator.

C-4.2   Feedsystem Analysis - 20 pps Operation

Operation of the valve-actuator at a pulse rate of 20 pps places a four fold increase in the demand on average feedsystem flow. For analysis purposes modifications were made in the feedsystem simulation for 20 pps operation. Modifications were made in the pump size (increase by a factor of four) to supply the increased flow requirements of the actuator, the accumulators were enlarged and the restrictions were removed. Figure C-12 illustrates the oscillatory behavior of the load accumulator pressure, P_{AL} at 5 pps operation. A pressure peak occurs some 35 milliseconds after the initiation of the transient. Analysis has shown that a slight reduction of the natural frequency can be obtained by increasing accumulator volumes. This delays the pressure peak in P_{AL} such that it occurs approximately 50 milliseconds after the initiation of the pulse. If this is done and the valve-actuator is operated at a 20 pps switching rate, the load accumulator is then fully charged ready for discharge into the valve-actuator at the next pulse. This "tuning" of line parameters can be effective in providing pulsed hydraulic energy to the switch efficiently. The restrictors utilized in the 5 pps simulation to dampen oscillatory behavior were removed for the 20 pps case to encourage the oscillatory behavior described above.

The dynamic response of the modified feedsystem operating at a 20 pps rate is shown in Figure C-15. This shows a typical cycle near steady state conditions. It shows the reduction of P_{AL} (load accumulator pressure) as the accumulator discharges into the valve-actuator during the first 10

239

milliseconds. Then, as feedline flow builds up, the load accumulator pressure begins to increase as it is recharged. When feedline flow has dropped to about 10 in^3/sec and the load accumulator has built up to about 4300 psi, the next pulse occurs and the cycle repeats itself. The increase in accumulator volume also enables the accumulator to maintain its pressure at a higher level during the period in which the valve-actuator is pulsed.

In addition because of the higher flow rates and pulse rates it was felt necessary to include the dynamics of the return line and the reservoir. The reservoir is equipped with a piston which is double acting as shown in Figure C-16. This piston acts to maintain a pressure ratio in the supply side with respect to the return side of 4500 psi/100 psi. The ratio of its areas is therefore 45/1. Its purpose is to maintain a positive pressure in the reservoir on the suction side of the pump. It was feared that pulsed operation at 20 pps might cause resonant behavior of this piston, and was therefore included in the simulation. Table C-4.3 gives the equations which were added for the 20 pps simulation. Table C-4.4 gives the parameters and variables applicable to these equations.
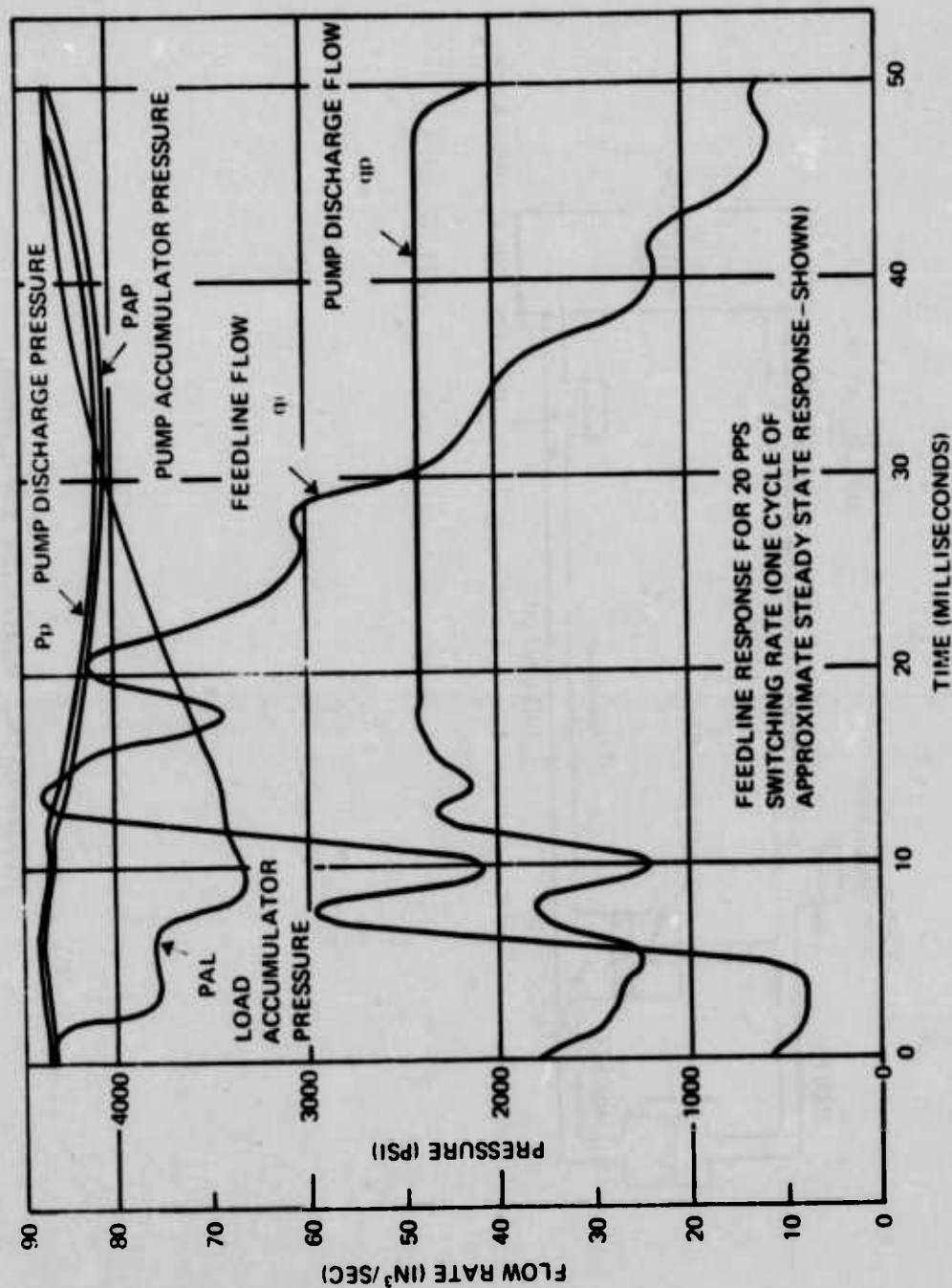
Figure C-15. Dynamic response of modified feed system.

241
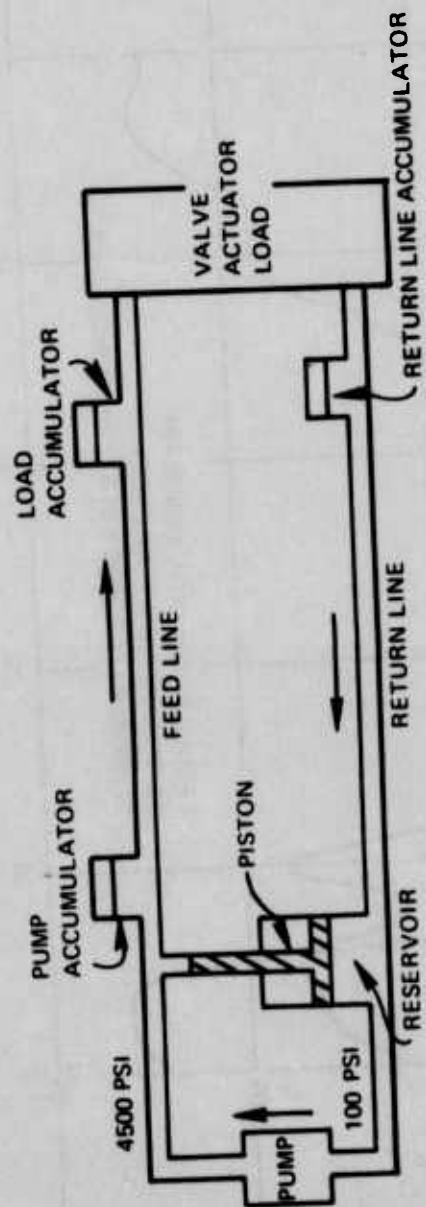
Figure C-16. Hydraulic feedsystem.

TABLE C-4.3. FEEDSYSTEM MODIFICATIONS & ADDITIONS TO EQUATIONS FOR 20 PPS

MODIFICATIONS:

Pump:

$$P = 4500. - 4.17 \, q_P \qquad\qquad 0 < q_P < 48$$

$$P = 55900. - 1075. \, q_P \qquad\qquad 48 < q_P < 52$$

$$P = 0. \qquad\qquad q_P > 52$$

Pump Accumulator:

$$\frac{d}{dt} P_{AP} = \frac{1}{P_{01} V_{01}} \, P_{AP}^{\;2} \, (q_P - q_1 - A_{PS} \dot{X})$$

ADDITIONS:

Return Line Accumulator:

$$\frac{d}{dt} P_{AR} = \frac{1}{P_{03} V_{03}} \, P_{AR}^{\;2} \, (q_L - q_5)$$

Return Line:

1st Section:

$$\frac{dq_5}{dt} = \frac{12 g A_R}{\gamma \, L/4} \, (P_{AR} - P_5 - R_R/4 \, q_5 |q_5|)$$

$$\frac{dP_5}{dt} = \frac{\beta_e}{A_R \, L/4} \, (q_5 - q_6)$$

2nd Section:

$$\frac{dq_6}{dt} = \frac{12 g A_R}{\gamma \, L/4} \, (P_5 - P_6 - R_R/4 \, q_6 |q_6|)$$

243

$$\frac{dP_6}{dt} = \frac{\beta_e}{A_R L/4} \quad (q_6 - q_7)$$

3rd Section:

$$\frac{dq_7}{dt} = \frac{12gA_R}{\rho L/4} \quad (P_6 - P_7 - R_R/4 \; q_7|q_7|)$$

$$\frac{dP_7}{dt} = \frac{\beta_e}{A_R L/4} \quad (q_7 - q_{81})$$

4th Section:

$$\frac{dq_{81}}{dt} = \frac{12gA_R}{\rho L/8} \quad (P_7 - P_{8C} - R_R/8 \; q_{81}|q_{81}|)$$

$$\frac{dP_{8C}}{dt} = \frac{\beta_e}{A_R L/4} \quad (q_{81} - q_{82})$$

$$\frac{dq_{82}}{dt} = \frac{12gA_R}{\rho L/8} \quad (P_{8C} - P_R - R_R/8 \; q_{82}|q_{82}|)$$

Reservoir:

$$\frac{dP_R}{dt} = \frac{\beta_e}{V_R} \quad (q_{82} + A_{PR}\dot{X} - \; _P)$$

Reservoir Piston:

$$\frac{d}{dt} \dot{X} = \frac{12}{m_P} \quad (A_{PS} P_{AP} - A_{PR} P_R + F_P Sign(\dot{X}) + \left\{ \begin{array}{l} KX, \; X < -\frac{S}{2} \text{ or, } X > \frac{S}{2} \\ \\ 0., \; -\frac{S}{2} < X < +\frac{S}{2} \end{array} \right\})$$

$$\frac{d}{dt} X = \dot{X}$$

TABLE C-4.4. FEEDSYSTEM MODIFICATIONS AND ADDITIONS TO
PARAMETERS & VARIABLES FOR 20 PPS SIMULATION

Parameter Modifications:	5 pps	20 pps
Pump (max flow rate)	12 in^3/sec	48 in^3/sec
Pump accumulator air volume	3 in^3	6 in^3
Load accumulator air volume	1.5 in^3	6 in^3
Upstream orifice (restriction)	5 psi/$(in^3$/sec$)^2$	0.
Downstream orifice (restriction)	0.1 psi/$(in^3$/sec$)^2$	0.
Pump natural frequency W_n	760 rad/sec	538 rad/sec
Pump damping ratio f	0.1	0.14
Maximum hydraulic horsepower required	8.18 HP	32.73 HP

Parameter Additions:

Return Line Accumulator:

P_{03}	Initial Trapped Air Pressure	100 psi
V_{03}	Initial Trapped Air Volume	3 in^2

Return Line:

L	Line length	120 in
A_R	Line cross sectional flow area	.307 in^2
R_R	Line square law flow resistance	.0123 psi/$(in^3$/sec$)$

Reservoir:

V_R	Volume	231 in^3
A_{PR}	Return side piston area	34.7 in^2

A_{PS}	Supply side piston area	0.771 in
m_P	Piston mass	.0538 slugs
F_P	Piston coulomb friction	7.5 lb
K	Piston stop spring constant	1×10^6 lb/in
S	Piston stroke	6 in

Variables Added:

P_{AR}	Pressure in the return line accumulator	psi
q_L	Load flow	in^3/sec
q_5	Average flow in 1st return line section	in^3/sec
q_6	" " " 2nd " " "	" "
q_7	" " " 3rd " " "	" "
q_{81}	Average flow in the first half of the 4th return line section	in^3/sec
q_{82}	Average flow in the second half of the 4th return line section	in^3/sec
P_5	Pressure at the end of the first return line section	psi
P_6	Pressure at the end of the second return line section	psi
P_7	Pressure at the end of the third return line section	psi
P_{8C}	Pressure at the center of the fourth return line section	psi
P_R	Pressure in the reservoir	psi
X	Reservoir piston displacement	in

C-5   Mechanical Properties

C-5.1   Mechanical Description

The pilot valve is an ABEX 410 Series servovalve, Figure C-17. It sits atop the intermediate stage (shown with the spool centered). The intermediate stage is a 4 way spool valve and is shown in a 4 band configuration. The porting detail from the pilot stage to the intermediate stage, and from the intermediate stage to the power stage is not shown in detail as it is conventional in nature.

The power spool is shown hard over to the right, which would have the contacts closed. The power stage is also a 4 way spool valve shown in a 5 band configuration. This arrangement permits a better overall flow path design. The center port is at supply pressure while the two outside ports are at return pressure. During operation, fluid flows into the supply port and through the high pressure orifices into the bushing bore. The fluid exits the bore into a rectangular passage and into the actuator, the return flow travels through the opposite rectangular passage, through the return side orifices and out the exhaust port into a header. The header is a V-shaped pipe arrangement attached to the two return ports. This header collects the return flow and directs it to the return side accumulator.

The actuator stage is shown in the closed position. The piston area to supply the 400 lb holding force (.089 in^2) is the differential between the external shaft area and the internal shaft area. All internal sliding seals are attained by close fits between the respective parts. The present plan is to attain an interference fit between the valve bushings and the block by heating the block and cooling the bushing so that they slide together smoothly during assembly. This will eliminate internal elas-

247

tometric static seals consequently permitting seal changes of the system without complete disassembly. The seals are all under end caps and readily accessible (with the exception of seals inside the pilot stage). The details of actuator mounting lugs and load attachment have not been generated yet, and are consequently not shown.

The parameters in the mechanical design are already a little different than those used in the simulation. Fortunately, the numbers used in the simulation appear to be a little pessimistic in the power stage area, but about right in the actuator. The mechanical design to date definitely substantiates the ability to open the contact gap to .5 inches in 1.85 milliseconds.

C-5.2   Weight Summary

The overall weight of this unit is approximately 15 lbs.

Weight breakdown; lb

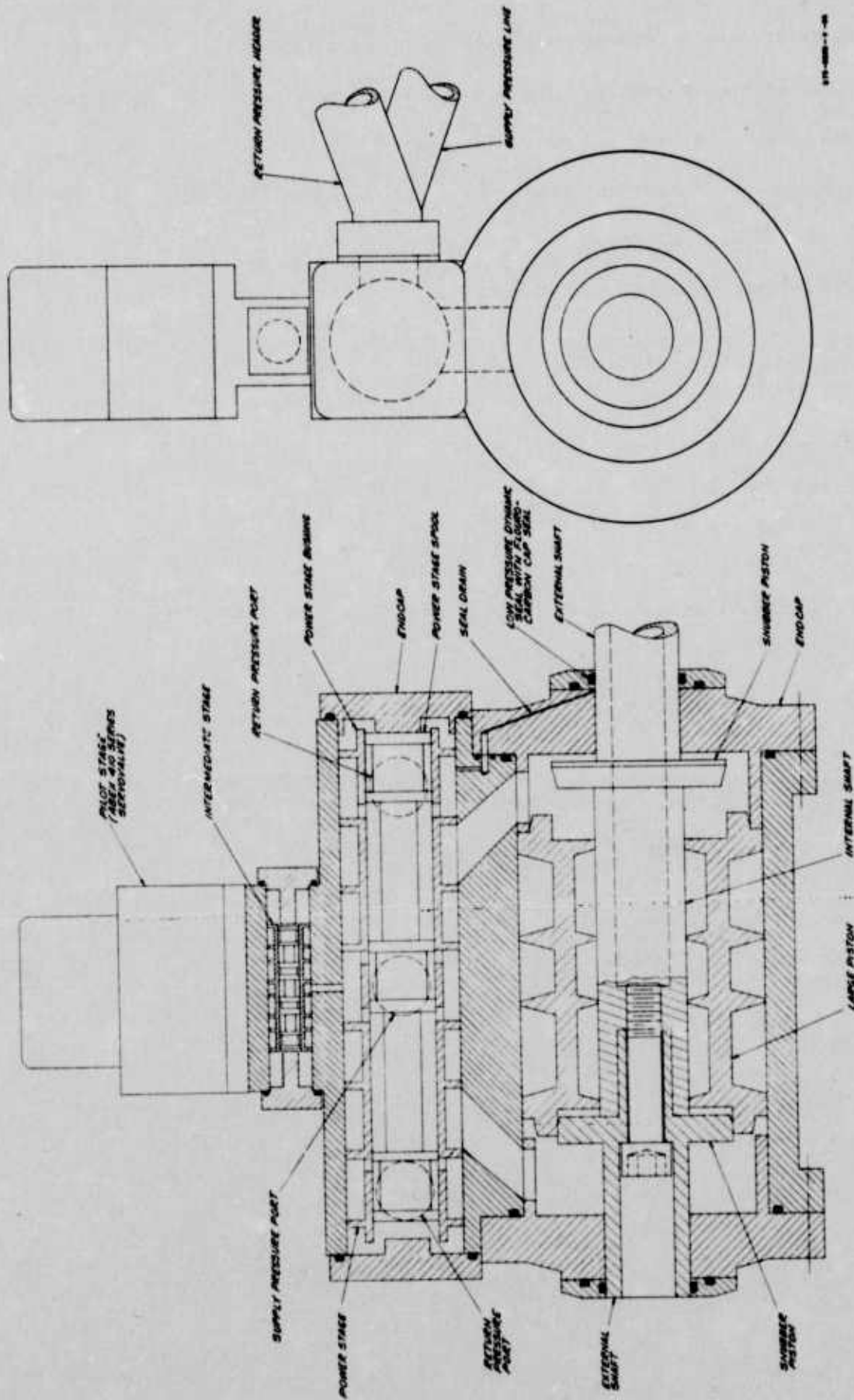|	
Pilot Stage	.75
Valve Actuator Body & Endcaps	9.25
Large Piston	2.2
Internal & External Shafts	1.8
Header Assembly	1.0
	15 lbs

Figure C-17. Short Pulse Switch Hydraulic Actuator

249